A STUDY OF HEAT TRANSFER THROUGH PERIODICALLY CONTACTING SURFACES

by

JACK RALPH HOWARD

A thesis submitted in fulfilment of
the requirements for the degree of
Doctor of Philosophy

Department of Mechanical Engineering
The University of Aston in Birmingham
September 1974

SUMMARY

This thesis describes a theoretical and experimental study of heat transfer through the interface between two solids which make contact and then separate periodically. The cycle of contact and separation is continuous and the quasi-steady state only is considered.

The system chosen as the model for study comprised two identical solid bars, arranged with their longitudinal axes in line and able to make periodic contact at their adjacent ends.

The remote ends of the bars were maintained at fixed but differing temperatures, so that heat was transferred through the interface when the adjacent ends were in contact and ceased when they were separated.

The effects of frequency of contact, thermal contact resistance offered by the interface during the period of contact and the ratio of contact time:periodic time of the cycle on the average thermal resistance of the system were explored theoretically. The results of this study are presented as a set of curves connecting the variables through dimensionless groups. The validity of these results was corroborated by solving the heat diffusion equation by two independent methods, each of which yielded the same result.

Experimental work showed that the theoretical data could be used to obtain a first approximation to the average thermal resistance offered by a pair of periodically contacting surfaces, but large variations (probably due to changes in contact geometry between one cycle and the next) could occur. Tests to establish the effect of impact upon the average thermal resistance were inconclusive and an improved experimental technique is required generally for any future work.

ACKNOWLEDGEMENTS

The author is greatly indebted to his colleague Mr A E Sutton of the Department of Mathematics in the University of Aston in Birmingham for the advice and active assistance given in performing the mathematical work presented in this thesis. The author posed the mathematical problems; Mr Sutton showed him how to solve them. All programming, data processing and analogue computing was performed by the author.

Thanks are due to Mr Norman Moss of the Department of Mechanical Engineering in the University of Aston in Birmingham who built the test apparatus and gave technician assistance when required.

The author is grateful to the University of Aston in Birmingham for allowing him the time and facilities for this study and in particular to Professor A J Ede, Pro Vice-Chancellor and Head of the Department of Mechanical Engineering for the initial reading of the draft manuscript, making many valuable, constructive criticisms and for his encouragement and wise counsel. Similarly thanks are due to Professor D E Elliott of the Department of Mechanical Engineering who supervised the project, and made many suggestions which are incorporated in this thesis.

The author also owes a debt of gratitude to his doctors, Dr D G Craig and Dr A Orwin both of whose professional judgment and treatment restored the author's health during part of the period when this work was being done.

Finally thanks are due to Miss Heather Johnson who typed the manuscript and to Mr Graham Smith who drew the diagrams.

NOMENCLATURE

Equation numbers in text

Equations having numbers prefixed by a number and oblique stroke, will be found in the Appendices. Thus equation (3/7) will be found in Appendix 3.

Equations having no prefix and oblique stroke will be found in consecutive order in the main text of the thesis.

Symbols

(Arabic)

a, a_L	Radius of local contact area
a_n	coefficient equation (4/2) Appendix 4
a_1 and a_2	constants in straight line equation (122)
A	area
A_c	area; sum of local contact areas
A_n	coefficient equation (72); or $\alpha\sqrt{\pi n/\tau}$ eq.(14/39)
b	elemental cylinder radius
b_L	macroscopic heat channel radius
b_n	coefficient equ. (4/3) Appendix 4
B_n	coefficient equation (72)
c	local contact area radius; or specific heat capacity
C	dimensionless constant, equation (5); or length
$C_{m,k}$	see equ. (4/10) in Appendix 4
d_1, d_2	flatness deviation
d_i	$\frac{1}{2}(d_1 + d_2)$
d_t	total flatness deviation
$D(\ )$	$\partial(\ )/\partial t$
$D_{m,k}$	see equ.(4/12) Appendix 4 m and k are integers

e_i	input voltage
e_o	output voltage
E	Youngs modulus of elasticity; or emf.
f	frequency; or defined by equ. (15)
f(t)	function of time
$f_n(x)$	$g_n(x) + h_n(x)$
g( )	function of ( );
$g_n(x)$	see equation (14/40) Appendix 14
h	thermal conductance of single contact area Equ. (14a)
h_c	thermal contact conductance
h_s	thermal conductance of solid-to-solid heat flow path; or microscopic contact conductance
h_L	the macroscopic contact conductance
$h_n(x)$	see equation (14/41) Appendix 14
H	length
i	integer
I	current
j	$\sqrt{-1}$
k	thermal conductivity W/mK
k_f	thermal conductivity of interfacial fluid
k_m	arithmetic mean thermal conductivity; harmonic mean thermal conductivity
k_s	thermal conductivity of solid
k_1	thermal conductivity of solid 1
k_2	thermal conductivity of solid 2
ℓ	length of bar
ℓ_i	length of solid bar equivalent to ½ thermal resistance due to periodic interruption of heat flow

ℓ_T	$\ell_i + \lambda$
L	loss, equation (64)
m	integer, or iteration number
M	Meyer hardness
M_1	constant
n	integer; or number of local contact areas per unit surface area
N	number of local contact area per unit surface area
Þ	mean pressure; potentiometer setting, or $\frac{\alpha . g(f\tau_c)}{\ell^2}$ eq. (70)
Þ_a	mean pressure
Þ_{max}	maximum local pressure
$\text{Þ}_{m,k}(x)$	matrix element equ.(74)
$P_{m,L}(x)$	function of x, with iteration Lth term equ.(14/5)
P	see also overleaf nominal pressure etc.
$q_{m,k}$	matrix element equ.(78)
$q_{m,L}(x)$	function of x, with iteration Lth term equ.(14/5)
Q	heat transfer rate
QAH	axial heat flow through interface (hot bar)
QRH	radial " " " hot bar
QZH	axial heat flow " " " " at any plane
	Symbols QAC, QRC & QZH for cold bar
Q_c	heat transfer rate steady state permanent contact conditions. Zero thermal contact resistance.
r	radius or electrical resistance
r_d	radius of dividing flow line a long way from contact area. Equ. (6).
r_e	contact element radius
R	thermal resistance
R_c	thermal contact resistance

R_r	thermal resistance of radiative heat flow path
R_s	thermal resistance of solid-to-solid heat flow path (constriction resistance)
R_T	total thermal contact conductance
t	time
s	volume of interfacial fluid per unit surface area
T	temperature
$T(x,t)$	temperature at distance x, at time t
T_A	temperature at A
T_n	temperature at x_n
$T_m(x,t)$	temperature at distance x, at time t corresponding to the m th iteration
$T(x)$	time-average temperature at distance x
$T_1(x,t)$	temperature during period 1 equ. (4/2)
$T_2(x,t)$	temperature during period 1 equ. (4/3)
u	uncertainty in ℓ_i, equation (128)
W	load
x	distance or position
x_n	distance of n th node
X	dimensionless distance (x/ℓ); or distance, equ. (42)
z	distance in axial direction

Greek symbols on next page

Greek Symbols

α	thermal diffusivity or angle of intersection between ridges equ. 16, or as in Appendices 14 and 16 $(\text{diffusivity})^{-\frac{1}{2}}$
β	coefficient of thermal expansion; or potentiometer setting Fig.23 equ(97)
β_c	arithmetic mean distance between surfaces fluid gap thickness; or asperity height
δ_1	asperity height on surface 1
δ_2	asperity height on surface 2
δ	depth below surface at which temperature fluctuations are negligibly small; effective fluid gap
$\Delta\Theta_n$	dimensionless temperature difference see equ.(3/5) Appendix 3
ΔT_c	fictitious temperature drop, equ.(1) & (2) and Fig.2
ε	ratio A_c/A; or constant equ. (13) or error equation (131)
ε_1 and ε_2	measuring errors equations (126) and (127)
λ	length of bar equivalent to $\frac{1}{2}$ thermal contact resistance, see section 4.3.2.- and Fig. 19
λ_1	wave length of ridges on surface 1
λ_2	wave length of ridges on surface 2
λ_m	mean value of λ above
η	$1/\sqrt{\alpha}$
ψ	see equation (35)
$\psi(\ )$	function of ( )
ρ	density; or electrical resistivity
σ	surface roughness
Θ	dimensionless temperature T/T_A

Θ_n	dimensionless temperature at position x_n
Θ_{n_s}	dimensionless temperature at node n, in steady state permanent contact condition equ. (3/5) and Fig. 3-2
Θ_ℓ	temperature drop in length ℓ of bar
Θ_λ	temperature drop due to ½ thermal contact resistance
τ	periodic time
τ_c, τ_2	contact time
τ_o, τ_1	non-contact time
ξ	elastic conformity modulus $\frac{P_a b_L}{E_m d_t}$
ϕ	Temperature see Appendices 14 and 16
$\bar{\phi}$	Laplace transform of ϕ

CONTENTS

Page Numbers

Page Numbers

Page Numbers

Page Numbers

Page Numbers

Page Numbers

APPENDICES

Page Numbers

APPENDICES CONT.

Page Numbers

APPENDICES CONT.

LIST OF TABLES

LIST OF TABLES cont.

List of figures overleaf

List of Figures

Page Numbers

Page Numbers

Page Numbers

Page Numbers

Figures in Appendices

Page Numbers

1. INTRODUCTION

1.1 Preliminary Remarks

An engineering designer may have to consider a system in which heat is transferred through two solid surfaces which are periodically brought into contact and then separated. An example of this kind of process is to be found in the internal combusion engine; the head of the exhaust valve is brought into contact with the relatively cooler valve seat and then separated from it each working cycle. In repetetive hot metal-forging processes, the die or hammer is brought into contact with and separated from the hot work-piece periodically. Heat input to the die influences the wear of the die.[1]

1.2 Statement of the Design Problem

Knowing the thermal resistance offered by the interface of two solids in permanent contact, a designer would have to try to predict the effect of periodic contact and separation of the solids on heat flow.

1.3 Object of Investigation

Faced with the problem 1.2 above the object of the investigation described in this thesis was:

(i) To derive a simple theory which could be used to predict the effect of periodic contact and separation of the solids on heat flow.

(ii) To devise and perform experiments which would:

  (a) show how far the theoretical predictions were applicable to an actual system.

  (b) indicate some effects not considered in the theory.

2. HEAT TRANSFER BETWEEN CONTACTING SOLIDS

2.1 General State of Knowledge

A simple qualitative explanation of how heat is transferred, in the steady state, through the interface between two solids, in permanent contact with each other, is well established. References [35], [92] and [108] are typical of the papers in which an explanation may be found. For convenience of reference, however, an account of the mechanism of steady state, heat transfer through the interface between two permanently contacting solids will be given in section 2.2.

Prediction of the magnitude of the thermal resistance offered by the general type of contact interface met in everday engineering practice is however tedious and less certain, despite the large research effort made over the years. Recent attempts to obtain a better correlation of the thermal resistance of a contact interface with various important parameters have been more encouraging. However, the behaviour of a contact interface under transient heating is not fully understood and very little research appears to have been done on heat transfer under non-permanent contact conditions. These and other aspects of the subject are discussed in more detail in section 3.

2.2 Mechanism of Steady State Heat Transfer Between Permanently Contacting Solids

The surface of all solids, even those apparently smooth to the naked eye, can be revealed under magnification to appear as an irregular array of "hills" and "valleys", so that when two surfaces are pressed together they make contact at only a few discrete areas as shown in Fig. 1. If the

fluid which fills the space between these areas is of low thermal conductivity compared with that of the solid, heat will flow more readily through the contact areas and the heat flux lines will be constricted as shown in Fig.1. This constriction causes a resistance to heat flow additional to that due to the bulk solid material.

Fig. 2 shows the temperature distribution along the axis of two solid bars, insulated over their curved outer surfaces to prevent transverse heat losses and with adjacent ends butted together. In the regions some distance upstream and downstream of the contacting end of each bar the heat flow is one-dimensional. Near the contact region however, the heat flow in the bars becomes three-dimensional. There is no temperature discontinuity at the contact areas, but the temperature distribution is decidedly non-uniform across any section of the bars at and near the contact areas. Extrapolation of the temperature distribution in each bar from the region remote from the contacting surfaces, where the heat flux lines are parallel, to the contact interface reveals an apparent temperature drop ΔT_c, see Fig. 2. This is a fictitious temperature drop because temperature continuity must exist everywhere. However it allows thermal contact resistance and conductance to be defined in a practical way. Thus:

Thermal contact resistance $R_c = \frac{\Delta T_c}{Q}$ (1)

Thermal contact conductance $h_c = \frac{Q}{A.\Delta T_c}$ (2)

Contact resistance as discussed above may be thought of as a sum of two resistances in series, due respectively to macroscopic and microscopic constrictions. The macroscopic constrictions arise from large-scale flatness deviations, (waviness), of the surfaces, see Fig. 1a. The

microscopic constrictions are produced by local surface roughnesses which are superimposed on the flatness deviation, see Fig. 1b. The term "constriction resistance" arises naturally from the above and is used often in the literature.

The heat flow at the interface between the contacting surfaces will take up different modes, namely

(a) Conduction through the actual solid-to-solid contact areas.

(b) Heat flow through the fluid filled gaps surrounding the contact areas. If the distance between the non-contacting parts of each solid is small, as is commonly the case, fluid convection is suppressed and heat is transferred through the fluid by conduction alone.

(c) Radiative heat transfer is usually small; with interface temperatures as high as 600°C, it has been reported that heat transfer by radiation is less than 1% of the total amount,[37].

For analytical purposes, it is commonly assumed that the above modes of heat transfer are independent of each other and that there are three separate paths for the heat flow. The total resistance to heat flow arising from the presence of the interface is then given by:-

$$\frac{1}{R_t} = \frac{1}{R_s} + \frac{1}{R_f} + \frac{1}{R_r} \qquad (3)$$

where R_t = total thermal contact resistance

R_s = thermal resistance of solid-solid heat flow path, (constriction resistance)

R_f = thermal resistance of heat flow path through interfacial fluid

R_r = thermal resistance of radiative heat flow path

When oxide or other surface films are present their thermal resistance must be added to those quoted above. With metal surfaces, such films are caused by chemical reaction of the metal with some constituents of the surrounding atmosphere or by adsorption. In normal engineering circumstances they are always present. Surface films are also often present with plastic surfaces, but plastics are not generally chemically reactive with the atmosphere; such films arise from use of plasticizers during processing which are liable to produce a "bloom" on the surface. With plastics the thermal conductivity of the film material is higher than the plastic whereas with metal oxides the converse is the case. A detailed discussion of the effects of surface films is regarded as beyond the scope of this present work. However, a useful, brief appraisal may be found in reference (111)

As distinct from films it is well known that if a thin shim of high conductivity, easily deformed material (e.g. soft copper) is placed between the contact surfaces and a load applied, the material flows into the gaps between the surface asperities and assists heat flow through what would otherwise be fluid filled gaps. Reference (63) analyses the effect of plating surfaces with high conductivity materials.

3. REVIEW OF LITERATURE

3.1 Preliminary Remarks

The number of publications concerned with heat transfer between periodically contacting surfaces is now very large. In contrast heat transfer between solids which make intermittent contact has received scant attention. For these reasons much of this review will deal only with a selection of papers concerned with permanent contact heat transfer which are felt to give a broad indication of the state of knowledge.

Selection was determined by picking out those papers which are:-

(a) Referred to in past literature surveys as being of fundamental importance and which frequently appear in the list of references in other papers.

(b) Basic studies published subsequent to those above in various journals of heat transfer.

(c) Found to be relevant among papers not necessarily concerned with heat transfer at the outset but in which contact heat transfer has emerged as an important consideration.

3.2 Heat Transfer Through Surfaces In Permanent Contact

3.2.1 Bibliographies and surveys

Bibliographies have appeared from time to time but they consist of lists of published papers only, arranged in alphabetical order of authors. References (4),(54),(69),(99) are typical. They contain no comment on the papers listed although the bibliography compiled by Moore, Atkins and Blum (69) presents a list of references tabulated by topic.

Surveys have been written or contained within papers by such authors as Wong[108],[110],[111] Thomas and Probert[92] Fletcher and Gyorog[41], Moore[70], Bloom[20] and Putnaerglis[113]. Each explains the mechanism of contact heat transfer, examines factors which influence it in some detail and comments on the state of knowledge at the time of writing. References [108],[111],[92] and [70] contain literature references on permanent contact heat transfer in both the steady and transient states, but only Wong[108], [111] and Moore[70] discuss the effects of an interface on thermal transients.

All the surveys quoted above indicate that considerable progress has been made towards a better understanding of steady state heat transfer through the interface between two contacting solids. However, at the time they were written, and indeed now, no simple or satisfactory method for accurate prediction of the resistance to heat transfer offered by the general type of interface met in everyday engineering practice exists. The biggest difficulty is that of characteristing the roughness of a surface in a meaningful way[70,108,110]. This situation has meant that studies have had to be made using mathematical models on the one hand or carefully prepared and controlled surfaces[25,27,35,36,37,61,79,110] on the other. Subsequent to these surveys however, some attempts at correlation of experimental data[41,90] have met with more success than hitherto and are discussed in section 3.2.2.4.

The surveys above also show that relatively little work has been published on temperature transients within a system where two solids are in permanent contact and such that have appeared e.g.[1,88,12,22] only reveal the complexity of the matter. An assessment of some papers published subsequent to these surveys is also included in this review.

3.2.2 Steady state, permanent contact heat transfer.

3.2.2.1 Basic studies involving mathematical models. Holm and Roess

In view of the similarity between the flow of electric current and the flow of heat in conductors, various workers [17],[18],[23] have made reference to it and used it to assist theoretical study. A simple expression for the constriction resistance of a single local contact area on the "flat" surface of two contacting semi-infinite bodies is due to Holm [57]

$$R = \frac{1}{2ak} \qquad (4)$$

where a = radius of contact area

k = thermal conductivity

No surface films are present in the above case, and the entire heat flow passes through the contact spot and the two contacting bodies are of the same material.

The restriction of equation (4) to conductors of semi-infinite extent was removed by Roess [77] and others, see [92] and [58], who analysed axial heat flow through two identical cylinders of radius b, whose axes are in line and which make contact through a single, centrally placed contact area of radius a. Equation (4) then becomes modified to

$$R = \frac{c}{2ak} \qquad (5)$$

where c is dimensionless and a power series in $(\frac{a}{b})$ [58]. The values of c are $1 > c > 0.1$, for $0 < \frac{a}{b} < 0.75$, [92]

As with Holm's model the entire heat transfer passed through the local contact area.

Cetinkale and Fishenden

In 1951 Cetinkale and Fishenden [25] analysed a contact model composed of an array of elementary cylinders which make contact at a local contact area. The contact area is raised from the surface and is surrounded by an annulus of conducting fluid as shown in Fig. 3. Heat passed through the fluid as well as the contact area. However, there was no heat flow transversely between contact elements. The heat flow lines at a large axial distance from the contact area were assumed to be parallel. They introduced a "dividing flow line" which separated the heat flow through the contact spot from that conducted through the fluid.

Isothermal surfaces near the contact spot were assumed to be ellipses having their focii where the fluid meets the contact spot. To satisfy Laplace's equation the flow lines were hyperbolae. The thermal resistance of an elementary shell formed between two adjacent ellipsoids was integrated to give an expression for the resistance of the solid-to-solid heat flow path. The resulting expression contained a single unknown parameter w. This unknown parameter w, was eliminated using the results of the relaxation method used to obtain the steady state temperature distribution. The solid-to-solid component R_s of the total contact resistance of the two surfaces, then became

$$\tfrac{1}{2}R_s = \frac{1}{2\pi a k_m} \tan^{-1}\left\{\frac{r_d - r}{r}\right\} \qquad (6)$$

where r = a = radius of local contact area

r_d = radius of dividing flow line a long way from contact area (Fig. 3)

k_m = arimethmetic mean thermal conductivity

which reduces to Holm's expression, equation (4) when a is very small

compared with r_d.

Heat flow through the fluid was linear and this, combined with the results of the relaxation method used to obtain temperature distribution, yielded the fluid conduction component, R_f, of the total contact resistance as

$$\tfrac{1}{2}R_f = \frac{\delta}{\pi r_e^2 k_f} \qquad (7)$$

where δ = asperity height, see Fig. 3.

r_e = contact element radius

The total contact resistance R_T (R_c in the notation in the paper) is given by

$$\frac{1}{R_T} = \frac{1}{R_f} + \frac{1}{R_s} \qquad (8)$$

The expression resulting from equation (8) is then

$$\frac{1}{R_f} = \frac{\pi r_e^2 k_f}{\delta} + \frac{2\pi r k_m}{\tan^{-1}\left\{\frac{r_d - r}{r}\right\}} \qquad (9)$$

Determination of R_c depends on known values of the ~~5~~ 6 variables k_f, k_m, δ, r_d, r_e and r. r_d was eliminated by equating the flux density on one side of the flow dividing line a long way upstream from the contact spot to the average flux density. The authors suggest that

(i) k_m is the harmonic mean of the thermal conductivities k_1 and k_2

(ii). k_f includes allowance for radiation and an accomodation effect[122]

(iii) The ratio $\frac{r}{r_e}$ can be obtained from the relation between pressure p and Meyer hardness M, dependent on whether the local deformation of the contact is plastic or elastic.

For plastic flow $\frac{r}{r_e} = \sqrt{\frac{p}{M}}$ (10)

For elastic flow $\frac{r}{r_e} = \sqrt{\frac{p_{max}^{1/3} \; p^{2/3}}{M}}$ (11)

(iv) Fluid thickness δ obtained from joint conditions; e.g. for rough surfaces

$$\delta = \varepsilon\beta_c \tag{12}$$

where β_c = arithmetic mean distance between surfaces and $\varepsilon < 1$

(v) Heat channel radius r would be found from a relation between the wavelength of surface roughness λ_c, and the constriction ratio r/r_e, thus

$$r_e = \psi \lambda_c \left(\frac{r}{r_e}\right)^{\zeta} \tag{13}$$

where ψ and ζ are constants which have to be found from heat transfer experiments.

Equation (9) was not used in the final analysis. Some manipulations were performed and thermal contact conductance was introduced, the ultimate expression being in dimensionless form.

Cetinkale and Fishenden conducted heat transfer experiments using ground surfaces whose roughness had been determined by "Talysurf" profilometer and determined values for constants ε, ψ and ζ. These constants were found to be independent of the nature of the metal or fluid, but were constant for a given type of surface roughness.

Fenech, Rohsenow and Henry

Fenech and Rohsenow[35,36,37] and Henry[48] analysed a contact model consisting of an array of contact spots formed from elementary cylinders of

the kind shown in Fig. 4. However, unlike Cetinkale and Fishenden they did not introduce a "flow dividing line" in each element.

Due to physical shape of the boundary and the numerous conditions to be satisfied, an exact analysis to obtain the temperature distribution was considered far too complex a problem to solve. However, Fenech and Rohsenow obtained an exact solution of Laplace's equation (in two dimensions r and z) for an approximate set of boundary conditions. A resulting expression for thermal contact conductance is,

$$h_c = \frac{\dfrac{k_f}{\delta_1 + \delta_2}\left[(1-\varepsilon^2)\left(\dfrac{4.25\sqrt{n}\,\frac{\delta_1}{\varepsilon}+1}{k_1} + \dfrac{4.26\sqrt{n}\,\frac{\delta_2}{\varepsilon}+1}{k_2}\right) + 1.1\varepsilon\left(\dfrac{1}{k_1}+\dfrac{1}{k_2}\right)\right] + 4.26\varepsilon\sqrt{n}}{(1-\varepsilon^2)\left[1 - \dfrac{k_f}{\delta_1+\delta_2}\left(\dfrac{\delta_1}{k_1}+\dfrac{\delta_2}{k_2}\right)\right]\left[\dfrac{4.26\sqrt{n}\,\frac{\delta_1}{\varepsilon}+1}{k_1} + \dfrac{4.26\sqrt{n}\,\frac{\delta_2}{\varepsilon}+1}{k_2}\right]} \quad ..(12)$$

where c = contact radius

a = radius of cylinder

n = number of contacts per unit surface area

k = thermal conductivity δ = asperity height

$$\varepsilon = \frac{c}{a} \tag{13}$$

and

$$n\pi a^2 = 1 \tag{14}$$

The first fraction, with square brackets, in the numerator represents the heat flow through the interfacial fluid while the second fraction represents the heat flow through the solid-to-solid contact area.

When applying equation (12) to real surfaces, the surface profiles must be

analysed to obtain the button-model equivalent values of δ_1. δ_2, n, and ε^2. Two separate surface profile tracings with the directions of the stylus movement at right angles are required from each surface. The profiles were recorded on transparent paper, the traces of corresponding profiles being superpositioned until they were translated in a direction perpendicular to the plane of contact by small increments, bringing further zones into contact. The volume average thickness of the voids was determined with a planimeter. An actual count of contact areas was made to determine n. The actual contact area was measured from the amount of interference between the surface profiles so that $\varepsilon^2 = \frac{A_c}{A}$ can be obtained. The profiles were then shifted laterally a small distance and the process repeated. Finally the data ~~was~~ were averaged to give "better" values for the required parameters.

The above procedure is clearly very tedious and lengthy, but more sophisticated methods of establishing contact parameters from surface profiles have been investigated e.g. (93),(49) employing random process theory.

However, experimental determination of thermal contact conductance of surfaces whose profiles were measured and whose contact parameters were determined using the above procedure agreed well with the predictions of equation (12).

Laming

Laming (58) analysed the same kind of basic contact model as Fenech and Rohsenow(37) and Cetinkale and Fishenden(25). He assumed that the pressure over each contact spot can be determined from the Meyer Hardness of the material. If the contact consists of two different

materials, the softer material will yield plastically until the pressure over each contact spot equals the Meyer hardness. The relationship between the local contact area radius, a, number of contact areas per unit nominal area N, nominal pressure P and Meyer Hardness M is

$$a = \left(\frac{1}{N\pi} \cdot \frac{P}{M}\right)^{\frac{1}{2}} \tag{13a}$$

Laming then uses Roess's modification of Holm's [51] expression for thermal contact conductance to allow for "constriction alleviation effect" and writes down the conductance of a single contact area in the form.

$$h = \frac{2ak}{1-f} \tag{14a}$$

The (1-f) term is Roess's series described earlier in this review. For most practical purposes Laming takes f as

$$f = 1.41\,\frac{a}{b} \tag{15}$$

where b = radius of heat channel

To estimate the number of contact areas per unit area of surface, Laming assumes the two surfaces to have regularly pitched ridging or waviness and the number of potential contact spots is the number of ridge intersections available. The thermal conductance, h_s, of the solid-to-solid heat flow path is then

$$h_s = \frac{2k_m}{1-f}\left(\frac{\sin\alpha}{\pi\lambda_1\lambda_2}\,\frac{P}{M}\right)^{\frac{1}{2}} \tag{16}$$

where k_m is the harmonic mean thermal conductivity, λ_1 and λ_2 the wavelengths of the two sets of surface ridges and α is the angle of intersection between the directions of the ridges.

The thermal conductance, h_f, of the fluid gap is

$$h_f = \frac{k_f}{\delta} \tag{17}$$

where δ = the effective fluid gap

k_f = thermal conductivity of fluid.

The total thermal contact conductance, h, is:

$$h = \frac{k_f}{\delta} + \frac{2k_m}{(1-f)} \left(\frac{\sin \alpha}{\lambda_1 \lambda_2} \frac{P}{M} \right)^{\frac{1}{2}} \tag{18}$$

To evaluate (18), the effective fluid film thickness δ had to be determined. It proved possible to establish a correlation between h and δ experimentally. Inspection of equation (18) shows that the fluid conductance term k_f/δ can be determined by measuring the thermal contact conductance at P = 0 or ~~obtain it~~ obtained by extrapolation. This procedure gave badly scattered results. The zero load conductance was then obtained by measuring the total contact conductance at each load using interfacial fluids of different thermal conductivities. Equation (19) was used to evaluate k_f/δ

$$\frac{k_f}{\delta} = k_f \frac{(h' - h)}{k_f' - k_f} \tag{19}$$

where h' and h are the fluid conductances with different fluids.

A second method of obtaining the fluid conductance involved linearisation of the total contact conductance-pressure curves. The fluid conductance was correlated with the volume of the interfacial fluid per unit area, S, obtained from surface roughness data. The effective fluid film thickness δ was found to be:

$$\delta = \frac{2}{3} S \tag{20}$$

Determination of f in equation (18) requires a/b (see equation (15)) to be found. It was shown from the ratio of heat flow through solid-to-solid paths to total heat flow that

$$\frac{a}{b} = \left(\frac{P}{M} \frac{h}{h_s}\right)^{\frac{1}{2}} \tag{21}$$

Dividing equation (18) by (16) gives

$$\frac{h}{h_s} = 1 + \frac{k_f}{\delta h_s} \tag{22}$$

and substituting for $\frac{h}{h_s}$ in (21) and using the result in (15) gives

$$f = 1.41 \frac{P}{M}\left(1 + \frac{k_f}{\delta h_s}\right)^{\frac{1}{2}} \tag{23}$$

An iterative process is therefore required to determine h from equation (18). In practice though, the ratio of heat flow through the fluid to that through the solid-to-solid path ($k_f/\delta h_s$) is small and f is taken as $1.41 \left(\frac{P}{M}\right)^{\frac{1}{2}}$. Thus in Laming's work thermal contact conductance can be predicted from knowledge of Meyer hardness, thermal properties of the fluid and solids and the waviness and roughness of the surfaces.

Clausing and Chao

Clausing and Chao [27] made a study of thermal contact resistance in a vacuum environment thus eliminating the component of conductance due to interstitial fluid. A new contact model was analysed. This is shown in Fig. 5. For purposes of analysis the apparent contact area was considered to be divided into two regions. The non-contact region was the proportion of the contact surface containing few or no microscopic contact areas. The contact region was defined as that portion of the

contact surface where the number of microcontacts per unit area is high. This model differs from that employed by Centikale and Fishenden [25] Fenech and Rohsenow [37] and Laming [58] in that they assumed uniformly distributed microscopic contact areas. In passing through the model the heat flow was constricted to the macroscopic area of contact and then further constricted to pass through the microscopic contact areas. Flatness deviation was simulated by the spherical caps on the end of the contacting cylinders.

The authors applied Roess's [77] solution in dimensionless form to arrive at the thermal contact conductance, h_L, of the macroscopic constriction.

$$\frac{h_L b_L}{k_m} = \frac{2\left(\frac{a_L}{b_L}\right)}{\pi g\left(\frac{a_L}{b_L}\right)} \tag{24}$$

a_L = macroscopic contact area radius

b_L = heat channel radius (macroscopic)

k_m = harmonic mean thermal conductivity

$$g\left(\frac{a_L}{b_L}\right) = \text{Roess's series} = 1 - 1.40925\left(\frac{a_L}{b_L}\right) + 0.29591\left(\frac{a_L}{b_L}\right)^3 + 0.05254\left(\frac{a_L}{b_L}\right)^5 + 0.02105\left(\frac{a_L}{b_L}\right)^7 + 0.01108\left(\frac{a_L}{b_L}\right)^9 + \ldots\ldots$$

They then used Hertz's [50] equation to determine the radius, a, of the contact area between the hemispherical ends of the heat channel cylinders. Hertz [50] assumes elastic deformation and yields

$$\frac{a_L}{b_L} = 1.285\left[\left(\frac{p_a}{E}\right)\left(\frac{b_L}{d_i}\right)\right]^{1/3} \tag{25}$$

where d_i = equivalent flatness deviation $\frac{1}{2}(d_1 + d_2)$, see Fig. 5.

and p_a = apparent contact pressure. After some manipulation, equation

(24) is quoted as a series of the form

$$\frac{h_L b_L}{k_m} = A_1 p_a^{1/3} + A_2 p_a^{2/3} + A_3 p_a + \ldots\ldots \qquad (26)$$

where A_1, A_2 etc. are independent of p_a. Equation (26) explains the highly non-linear variation of conductance with load with small loads.

The microscopic constriction areas are assumed to be uniformly distributed within the macroscopic area. The microscopic contact conductance h_s, of n microscopic contact areas each of radius a_s, and at centre distances $2b_s$ is

$$h_s = \frac{2p_a k_m}{H\pi\xi a_s g(\frac{a_s}{b_s})} \qquad (27)$$

where H = microhardness

ξ = elastic conformity modulus = $\frac{p_a b_L}{E_m d_t}$

d_t = total flatness deviation

and

$$\frac{h_s}{h_L} = \frac{2p_a}{\pi H} \cdot \frac{1}{\phi(\xi) a_s} \cdot \frac{b}{\xi g(\frac{a_s}{b_s})} \qquad (28)$$

where $g\,(\frac{a_s}{b_s})$ is Roess's series $1 - 1.40925\,(\frac{a_s}{b_s}) + 0.2591\,(\frac{a_s}{b_s})^2$ etc.

$\phi\,(\xi) = 2.1285\xi \;/\; \pi g(1.285\xi^{1/3})$

In evaluating equation (28) it was assumed that a_s was independent of load and the average size of microscopic contact areas were of the same order of magnitude as the surface roughness. Thus a value could be assigned to $a_s\ \xi\ g\,(\frac{a_s}{b_s})$ and hence $\frac{h_s}{h_L}$ can be calculated. Results of this calculation show that macroscopic constriction resistance was about two orders of magnitude larger than the microscopic constriction

resistance.

Experiments were performed on several different specimens of various materials and various spherical ends to match their model. Most experimental results showed good agreement with the theory and demonstrated that the macroscopic contriction resistance was dominant, except for smooth aluminium surfaces, when the disagreement was attributed to either the presence of a surface oxide film or microscopic constriction resistance was operative.

The major difficulty arising in attempting to apply Clausing and Chao's work to practical engineering surfaces is the difficulty in selecting an appropriate value for surface flatness deviation d_i (equation (25)) and macroscopic heat channel radius b_L.

However, their work does show the importance of macroscopic effects which are bound to arise in some cases.

Wong

In a very careful treatment of thermal conductance of metallic contacts Wong [110] analysed the "button" contact model of Fenech and Rohsenow [37] and developed a different expression for contact conductance. Wong then proposed a model of different geometry, arguing that the shape of the asperities on a surface are better represented by a conic frustum than by the spigot formed by a circular cylinder used in the models of Fenech and Rohshenhow et al [25],[37],[77] In the new model shown in Fig. 6, there is a constriction of flow lines within the main body of the model to the base of the asperity and unlike the earlier models, an additional constriction within the asperity itself. The resulting expression for

thermal contact resistance is more complicated than those of earlier workers. The contact conductance for Wong's new model will follow the same trend as the "button" model provided that the assumption for no heat transfer between the solid spots and the fluid is valid. However, when the apex angle of the conic frusta is large as in the case of the very smooth surfaces, contact heat transfer will take place between the solid junctions and the fluid. The boundary conditions at the solid-fluid interface would be too complex for mathematical solution and a simplified method was proposed to make an approximate solution possible.

Carefully performed experiments were conducted with artificial metallic junctions between the contact members. Small steel balls or aluminium discs were inserted between two highly finished flat surfaces, so that the number, size and distribution of the contact spots was controlled; supplementary experiments being needed to establish contact areas. Thermal contact conductance measurements over a wide range of conditions were made and the results compared with prediction based on the mathematical models studied. Test results obtained with steel balls between the surfaces showed the same kind of variation with load as predicted from the model equations during the first increase in load, but the measured conductances were generally higherthan predicted and rose with load more steeply. The high values of measured thermal contact conductance was attributed to the value of thermal conductivity of the steel of the balls used in the prediction formulae. However, the more rapid rise of contact conductance with load was thought to be caused by a reduction of metal hardness with time causing an increase in contact area and reduction of the mean fluid gap.

The tests also revealed the presence of a hysteresis phenomenon; as the load is decreased the contact conductance is higher than during loading.

This phenomenon has been reported by other workers[37][102] and is discussed in a later section of this literature review.

Rominger

Rominger [79] pointed out that previous work on thermal contact resistance was limited in scope and that no general method of predicting thermal contact resistance existed. The object of his work was to develop a procedure for calculating thermal contact conductance that would be applicable to a wide range of situations. No experimental work is reported in this work.

Macroscopic and microscopic contact models as used by Clausing and Chao[27] but without the restriction of being in a vacuum were investigated. The Laplace equations governing heat transfer in these two basic models were solved using the Monte-Carlo technique. The isotherm patterns found by this means were then used to determine the contact resistance. The macroscopic contact resistance, so found, was compared with results obtained from the equations developed by Holm[51] and Roess[77]. Rominger's values of macroscopic contact resistance were in good agreement with the Holm and Roess values. Similarly the microscopic resistances found by Rominger were compared with the equation and experimental data of Fenech and Rohsenow[36]. Rominger's predictions seemed to show better agreement with the experimental data than the equation developed by Fenech and Rohsenow. Most of the discrepancies would appear to be due to using a small number of walkers to reduce computer time.

McMillan et al

McMillan[61] considers thermal contact resistance in a vacuum of rough,

spherically wavy surfaces. The heat transfer across the interface is modelled in three different ways.

1. Assuming constant temperature over the contour area.
2. Assuming constant flux over the contour area.
3. Assuming that the flux through any point on the contour area is proportional to the microscopic conductance, which in turn is a function of local contact pressure between the surfaces.

The equations for constriction resistance were developed by Cooper, Mikic and Yovanovitch[28] for 1 and 2 above and by Mikic[65] for case 3, where contact resistance is a function of pressure distribution. The work evaluates numerically the pressure distribution curves for rough, wavy surfaces in contact, which are required to calculate contact resistance by Mikic [65] equations.

To determine the interface pressure distribution, three equations are set up (a) from surface-height distribution theory and the assumption of plastic deformation of surface asperities, (b) from geometry and an assumed elastic deformation of the spherical waviness and (c) a force balance equation. These equations are solved iteratively until the three equations are simultaneously satisfied. The resulting pressure distributions show the regions under which roughness causes pressure distributions to differ significantly from Herzian[50] predictions. These regions are given by:

$$\frac{F}{H\sigma R_1} < 12.8\,(P1)^{1.25}, \text{ for } 0 < P1 < 0.01 \qquad (29)$$

and

$$\frac{F}{H\sigma R_1} < 11.7\,(P1) - 0.25 \text{ for } 0.1 < P1 < 0.6 \qquad (30)$$

Where E = Youngs Modulus

$$\bar{E} = \left(\frac{1-\nu_1^2}{\pi E_1} + \frac{1-\nu_2^2}{\pi E_2} \right)^{-1}$$

F = Force

H = Microhardness of softer of two materials in contact

R_1 = Undeformed radius of curvature

Pl = Plasticity index $(\bar{E}/H)(\sigma/R_i)^{\frac{1}{2}}$

σ = r.m.s. deviation radius of curvature

ν = Poisson's ratio

The contour area is substantially larger than that obtained from Hertzian theory.

Experiments were performed in the above ranges and the results compared with the predictions of the three different ways of modelling the process. It was found that the method assuming constant flux over the contour area using contour radii predicted by the methods developed by McMillan showed best agreement (within 25%) with the experimental results.

McMillan substantiates that in certain ranges of parameters, a wavy surface will yield higher thermal contact conductance if it is roughened. This being due to the engagement of two surfaces covering a large area when roughened.

3.2.2.2 Measurement of thermal contact resistance

O'Callaghan and Probert[74] investigated heat leaks in systems through which heat flows longitudinally. For simplicity the effects of heat leaks through thermocouple leads was analysed in detail using an equivalent thermal network. An analogous analysis could be devised to account for the effects of radiant or conductive heat leaks by considering them to occur through nodes located at the

cont....

thermocouple sites. The temperature indicated by the thermocouple is lower than the true temperature at its location in the absence of heat leaks. The higher the temperature the greater the error. This leads to large errors in the apparent interfacial temperature drop. The error in thermal contact resistance determination due to transverse heat leaks can therefore be extremely large.

Where dissimilar metals are in contact, a negative apparent interfacial temperature drop can be indicated when the high conductivity material is the cooler of the two. Also if the thermal contact resistance is determined with the direction of heat flow being first in one direction and then reversed, two different values of thermal contact resistance can be indicated but these indications may be caused by transverse heat leaks.

Where the bars are used as their own flux meters, the temperature measurement errors cause large errors in temperature gradient or flux determination which combined with errors in the apparent interfacial temperature drop, gives large errors in thermal contact resistance determination. In such cases, the indicated temperature gradient or heat flux in the cooler bar will be greater than in the hotter bar. Yet both such temperature distributions are linear, showing that an indicated linear temperature distribution does not mean that transverse heat leaks are absent; a point made elsewhere in a different context in reference[59]. However the indicated gradient or heat flux in the cooler bar will be more accurate than in the hotter bar.

O'Callaghan and Probert suggest an improved technique for thermal contact resistance determination, employing only two thermocouples to reduce heat leaks from this source. However the method relies on accurate determination of heat flux and thermal conductivity of each bar material.

An apparatus in which transverse heat leaks are reduced is described in reference (136). The length : diameter ratio of the specimens is considered; this has to be sufficiently small to minimise transverse heat leaks, but must be sufficiently large so that thermocouples are not placed in the region near the contact interface where the heat flow is three-dimensional due to constrictions at the contact interface. This leads to an optimal length:diameter ratio for particular assembly of specimens. A single thin disc was used for one of the contacting specimens.

The test apparatus was designed with tests for directional effects in mind so that the direction of heat flow could be reversed. Tests were to be conducted in vacuum of 2×10^{-5} torr. Matched pairs of heaters, water in cooled sinks and invar fluxmeters were used. Although it was planned to use only two thermocouples as recommended in reference (74), each fluxmeter had four thermocouples installed. Linear extrapolation of the temperature distribution in the invar fluxmeters was used to calculate the interface temperature drop. Exterior surfaces of components were highly polished to reduced emissity.

Performance of the rig was such that an overall error in measurement of thermal contact resistance was less than ten per cent.

3.2.2.3 Directional effect

It has sometimes been reported(9),(78),(91) that thermal contact resistance between dissimilar metals depends upon the direction of heat flow. Various explanations(74)(78)(114)(26)(107) have been advanced to account for it. Some very careful experimental work by Thomas and Probert(91) in which "thermal rectification" was observed with similar metals in contact as well as dissimilar metals, was however, challenged by Barber(115) but repeatable results were obtained in reference(91) and the matter is

not fully resolved. Thomas and Probert[91] attributed thermal rectification in part to potential barriers produced by interfacial films as proposed by Moon and Keeler[114].

O'Callaghan and Probert[74] demonstrated that a directional effect could be indicated where none may exist due to the effect of transverse heat leaks on the observed temperature distributions. Indeed reference[74] shows that negative apparent interfacial temperature drop can be indicated when the material of lower thermal conductivity is the hotter of the two materials in contact. The apparent heat flow against a negative temperature difference of course conflicts with the second law of thermodynamics.

Mathematical investigations by Veziroglu and Chandra[101] and Barber[7] have shed further light on the matter. Veziroglu & Chandra[101] analysed a model developed by combining the double constriction model of Clausing and Chao[25] for study of thermal contact resistance in vacuum with the single constriction model used by Cetinkale and Fishenden[25] for contact with fluid present in the spaced between local contact areas. Barber analysed semi-infinite solids having rotational symmetry. Both papers showed that the explanation suggested earlier by Clausing[26], namely, that it was due to the effect of thermal strain on the local contact area would be one reason for dependence of thermal contact resistance on direction of heat flow. But Barber[7] goes further and suggests that at least two independent mechanisms, namely thermal strain and potential barriers due to surface films suggested by Rogers[78] are involved. Barber concludes among other things that there is "experimental evidence that the direction of rectification can be reversed when the contact surfaces are nearly flat" and challenges the suggestion of Lewis and Perkins[129] that with certain special surface geometries thermal strain could account for this.

Further work on directional effect was recently published[135] in which the thermal contact resistance and directional effects of very smooth non-wavy surfaces were investigated experimentally. A direction in-dex $\nabla = (R_{max} - R_{min})/R_{max}$ is defined for correlation purposes. Directional effects between dissimilar materials occurred in all but one of the cases investigated. Repeated cycling of the direction of heat flow removed the directional effect but subsequent increase in load on the surfaces could cause a directional effect to reappear and it was concluded that the most probable cause of diredional effect is relative thermoelastic distortion of the contact surfaces, investigations into which are being continued by the authors of reference [135].

It is clear that further investigation of this is required as well as of reported evidence of thermal rectification between solids of similar materials which cannot be attributed to thermal distortion.

3.2.2.4 Hysteresis

A hysteresis phenomenon has been reported by various workers e.g.[102][37][110]. If a contact is loaded progressively the thermal contact conductance will increase with load. If the contact is then progressively unloaded the thermal contact conductance will be higher at each load than when the contact was being progressively loaded. This phenomenon is attributed firstly to modes of deformation; when the load is reduced, recoveryof deformation at the interface is elastic, with contact area proportion to $(\text{load})^{2/3}$. Secondly it was also attributed to cold welding of the metals at the actual metal-to-metal contact areas, causing in some cases very little reduction in thermal contact conductance as the load is removed[37][110].

Molgaard and Smeltzer[67] in experiments to determine thermal contact resistance at gold foil surfaces, found that the initial loading produced a permanent reduction in thermal contact resistance but when the pressure was cycled between the maximum of about $8 \times 10^7 N/m^2$ and $4 \times 10^7 N/m^2$ the

pressure - contact resistance relationship was reversible suggesting elastic deformation at the interface.

3.2.2.5 Reduction in thermal contact resistance

It is well known that a significant reduction in thermal contact resistance can often be achieved by inserting a piece of ductile, high thermal conductivity foil between the two contact surface and then re-establishing contact again[102][9][10][42]. This is attributed to the foil material flowing into the interstitial spaces and creating a larger area of contact and the replacement of the interstitial fluid, usually of low thermal conductivity, with a substance of higher thermal conductivity.

A reduction in thermal contact resistance would also be achieved by plating the two surfaces with a high conducting, more ductile material. Mikic and Carnascali[63] analysed the situation mathematically when one or both surfaces are plated. They argued that since the thermal contact resistance through one half of an elemental "button" contact in vacuum is given by

$$R = \frac{1}{4ka} \psi\left(\frac{a}{b}\right) \qquad (31)$$

(where $\psi\left(\frac{a}{b}\right)$ is a geometrical factor depending on the ratio of contact spot radius, a, to the elementary channel radius, b.), it follows from equation (31) that an increase in the thermal conductivity, k, of the material in the near vicinity of the contact spot will reduce the thermal contact resistance for fixed geometry $\psi(a/b)$. Plating alone with a material of high conductivity should achieve this by providing a layer where part of the heat flux line constriction takes place. An entirely separate effect of plating the surface would be to alter the geometry of contact because of the different yield strength of the plating material.

Mikic and Carnascali pointed out that plating of only one surface would have limited effect because the whole constriction of flux lines on the unplated side of the contact takes place in low thermal conductivity material. Thus when both surfaces are plated the reduction in thermal contact resistance is due to the combined effect of a change in thermal conductivity and an improved contact geometry.

An approximate solution of the equation of the mathematical model used to simulate the contacts showed that for cases where microscopic constriction is the dominant resistance in the system, a reduction in thermal contact resistance of an order of magnitude could arise.

Experiments in which care was taken to produce the same kind of model as the mathematical one verified the predictions adequately.

3.2.2.6 Correlations

Very large variations in experimental results obtained with ostensibly similar surfaces have been observed by many authors. A large collection of examples of this are to be found in reference[92] in 1966 and no general correlation then seemed possible. Other attempts have been made [43] [58][116] to correlate a large range of experimental data. Three recent papers are reviewed here.

Thomas and Probert

Thomas and Probert[90] discuss earlier attempts at correlation of thermal contact conductance data. They point out that although theory for the special case of plastic contact between flat and isotropically rough surfaces whose heights are distributed normally about a mean plane, is in fair agreement with experimental data; contacts between surfaces in common engineering practice are less amenable to mathematical analysis.

The physical basis of a correlation for thermal contact conductance measurement in vacuum by Holm[52] is deduced using dimensional analysis and is modified by including surface roughness and ignoring nominal contact area. This yields that dimensionless conductance C* is a function of dimensionless load W*

where

$$C^* = \frac{c}{\sigma k} \tag{32}$$

$$W^* = \frac{W}{\sigma^2 M} \tag{33}$$

where σ = rms surface roughness, k = thermal conductivity

c = thermal contact conductance M = surface hardness N/m^2

350 data points from literature for aluminium and stainless steel in vacuum showed C* to be proportional to $W^{*0.73}$ with correlation coefficients better than 0.9. The correlation for the two materials, however, did not coincide so that there is likely to be one or more variables missing from the dimensional analysis. Interface temperature, elastic modulus and surface slope are among variables which might be included if the published data quotes these.

Fletcher and Gyorog

Fletcher and Gyorog[41] attempted a correlation for prediction of thermal contact conductance in vacuo. Their expression was formulated from experimental results obtained with contacts from aluminium, brass, stainless steel and magnesium with a wide range of test variables e.g. mean junction temperature, apparent interface pressure, surface flatness deviation and surface roughness. Their correlation expression was

$$\psi = (5.22 \times 10^{-6} \delta_c^* + 0.36\ P^*T^*)^{0.56} \tag{34}$$

Where $\psi = \frac{h_c \delta}{k_m}$ (dimensionless thermal conductance) (35)

where δ = Equivalent gap thickness or surface parameter

and $\delta_c^* = \frac{\delta}{b}$ dimensionless surface parameter (36)

b = elementary cylinder or specimen radius

$P^* = \frac{P_a}{E}$ (dimensionless pressure) (37)

where P_a = apparent pressure

E = modulus of elasticity

$T^* = \beta T_m$ (dimensionless temperature) (38)

where β = coefficient of thermal expansion

T_m = mean interface temperature (^oF)

The most important elements in expressions (34)(37)(38) above are interface pressure, mean interface temperature and surface parameter. Published experimental data correlated with the above exression within an average overall r.m.s. error of 24%. Fletcher and Gyorog's inclusion of interface temperature in the correlation above is likely to lead to an improved correlation while their use of elastic modulus (rather than surface hardness as used by Thomas and Probert[90]) might possibly lead to better correlation.

O'Callaghan and Probert

Further very recent work on dimensionlesss correlations is included in reference [135] which corroborates the findings of reference [90]. The most useful correlation was found to be

$$\frac{1}{R^*} = 3.73\ (W^*)^{0.66} \qquad (38a)$$

where $R^* = 1/C^*$ where C^* is defined by equation (32)

W^* = see equation (33)

For elastic deformations only the authors suggest that surface hardness M in equation (33) is replaced by the effective elastic modulus E^* defined by

$$\frac{1}{E^*} = \frac{1 - \nu_1^2}{E_1} + \frac{1 - \nu_2^2}{E_2} \qquad (38b)$$

where ν_1 and ν_2, E_1 and E_2 are respectively Poisson ratios and elastic modullii of the contact materials. However, the use of E^* in place of M in equation (33) was found to increase the scatter of the data, which is attributed to the effects of loading history, tranverse heat flows etc. which had not been considered in the analysis.

3.2.2.7 Summary of section 3.2.2

Research into heat transfer through the interface between two solids in permanent contact has gradually improved understanding of the process under steady state conditions. Prediction of thermal contact resistance of any given interface remains a tedious and uncertain task, which is hampered by the difficulty of determining the size, number and distribution of local areas of contact under load and the determination of the heat transfer area and thickness of the interstitial fluid. Although tedious, some techniques (35)(49) have been developed whereby these parameters have been

estimated from surface profile measurements and then used to predict the thermal resistance with some assurance when the surfaces are held in contact under load. An alternative means of estimating thermal contact resistance of a given pair of surfaces is to attempt to make use of approximate correlations, e.g. reference (41)(135) and (90), of thermal contact resistance with surface geometrical parameters, load and physical properties. Where applicable these correlations give probable values of thermal contact resistance.

Dennis and Fuggle(30) displayed photgraphs of various metal surfaces, obtained by scanning electron microscope , after their surface roughness had been determined by "Talysurf" profilometer. The photographs showed considerable damage to the surfaces of copper and mild steel due to the stylus passing over the surface. In the case of copper and mild steel, the stylus had ploughed through the "peaks" and did not touch the bottom of many "valleys", leading to a low value of surface roughness being indicated. It appears that unless the surface is very hard(600 V.P.N.) and the stylus is very small the true profile will not be indicated. Clearly the softer the metal the greater the error in surface roughness, with attendant effect on precision of those parameters used for correlations(41)(90)(134) in which surface roughness appears.

Transverse heat leaks have always been a source of inaccuracy in thermal contact resistance determination and much published data must be of uncertain accuracy. However, the measurement technique suggested by O'Callaghan and Probert(74) seems to be the best yet advanced.

The phenomena of hysteresis and directional effect serve to complicate the problem of predicting what the thermal contact resistance of a

particular interface would be. More detailed knowledge of the changes in surface geometry as the load is reduced is required to improve understanding of hysteresis. The phenomenon of directional effect is better understood now than in the past and is thought to be due sometimes to thermal distortion and sometime to surface films acting as potential barriers, while in other cases transverse heat leaks could cause a directional effect to be indicated. Clearly this matter requires further investigation.

The reasons for significant reductions in thermal contact resistance brought about by introducing ductile, high conductivity foil between two surfaces in contact or plating the surfaces with such a material are now more clearly understood; being due to increased contact area and the lowering of constriction resistance by the presence of high conductivity material near local contact areas. But knowledge of properties of surface films and their precise effects on thermal contact resistance, directional effect etc. is lacking.

3.2.3 Non-steady State Permanent Contact Heat Transfer

3.2.3.1 Selected papers

Barzelay and Holloway

Barzelay and Holloway[8][12] appear to be the first to publish work on the effects of thermal contact conductance in systems undergoing transient heating. Several aircraft structural joints were tested under conditions in which aerodynamic heating of the structure was simulated. Thermal contact conductance was found to vary widely from specimen to specimen. But generally the presence of an interface had a large effect on the time-temperature history at a given point in the structure

Aaron and Blum

Aaron and Blum[1] made a theoretical study, to try to establish what effects would arise when the ambient pressure of the gas surrounding two surfaces in contact was changed. A change in the ambient pressure would cause the gas to flow into (or out of) the voids surrounding the local solid-to-solid contact areas. From appropriate fluid flow equations they showed that for most practical cases, the time taken to fill (or empty) the voids by a sudden change in ambient pressure was very small.

Using as an example, one of the metallic joints investigated by Fenech and Rohsenow, in which conduction through the voids (air filled) accounted for 58% of the total heat transfer, Aaron and Blum demonstrated that the thermal contact conductance is unaffected by reducing the ambient air pressure until the pressure has fallen to a certain threshold value (21mm Hg). But thereafter the thermal contact conductance falls linearly with ambient pressure. Investigation of other joints showed that the threshold pressure depended on the gas, its temperature and the void thickness.

The effect of sudden and gradual changes in ambient pressure on the axial temperature distribution in two bars whose axes were in line with adjacent ends in contact and remote ends at different, fixed temperatures was also calculated using numerical methods. The time required for the temperature distribution to stabilise after the ambient pressure was changed from below the threshold value, varied according to the system from 28s - 267s. Stabilisation times increased at slow rates of pressure change, magnitude of pressure change, heat flow rates and temperature, and with lower thermal diffusivity.

In a later paper[2] describing a computer study of transients in a one-dimensional system, Aaron and Blum reported on the effect of a sudden change of temperature at one end of the system described in the above paragraph, and also a change in thermal contact conductance at the interface. The time required to reach a steady state is plotted as a function of thermal contact conductance. When a sudden change is imposed on the system, the temperature drop across the interface overshoots the final steady value when the higher conductivity material is on the hotter side of the contact interface.

Blum and Moore

Blum and Moore[22] considered theoretically two types of transient situations when heat flows across an interface.

(i) Response of a system having constant thermal contact conductance to a change in the temperature. The initial condition is one of uniform temperature throughout the system. One end of the system was subjected to a different temperature which is held constant until steady conditions were obtained.

(ii) Response of a system with fixed end temperatures subjected to a sudden change in contact conductance. The initial condition was one of steady state temperature distribution.

The one dimensional heat-diffusion equation was used to represent the problem.

Numerical and analytical methods were used to solve each case, the analytical method providing a check on the accuracy of the numerical method. The two methods showed excellent agreement with each other. The information obtained from the solutions were temperature-distance data at various times. This information was correlated in such a way that it

is possible to estimate the time taken to reach a steady state when subjected to a sudden temperature change. A series of graphs for each set of materials was compiled, plotting " dimensionless time" Θ against dimensionless "time constant ratios" τ, at various values of "inverse Biot number" β, where

$$\tau = \frac{b}{a}\sqrt{\frac{\alpha_1}{\alpha_2}} \tag{39}$$

$$\Theta = \theta\left[\frac{\alpha_1}{a^2} + \frac{\alpha_2}{b^2}\right] \tag{40}$$

$$\beta = \frac{k_1}{h_c a} \tag{41}$$

where a = length of region 1 of bar

b = length of region 2 of bar

α = thermal diffusivity

h_c = contact conductance

k = thermal conductivity

θ = time

When the material on both sides of the interface was the same, the time taken to reach steady state was found to be independent of the overall temperature difference. Furthermore, the minimum time taken (for such an assembly of a fixed overall length) to reach steady state occurred when the interface was midway between extreme ends of the system. The study indicated the existence of an "overshoot" phenomenon, where the temperature drop across the contact interface during the transient period exceeds the steady state value. The criteria for "overshoot" is that

$$\tau > 1 \tag{42}$$

regardless of whether the materials were the same or not.

It would seem possible that the graphs could be used to determine thermal contact conductance for a given system from experimental data by measuring the time taken to reach a steady state.

A more detailed version of Blum and Moore's paper[22] is given in reference[70] which also gives an account of experiments performed to check the applicability of the analysis. Transient temperature distributions were observed for various combinations of materials.

Analysis of this data showed that contact conductance varied with time, commencing with a steep rise followed by a sharp reduction to a near steady value. The reason for the initial rise and fall is attributed to the calculation method employed but the calculation method is satisfactory for the later times.

Beck's work on optimising of transient experiments[15] may be of relevance here, although Moore checked his results using a program written by Beck, details of which were not given. However, Beck's program gave the same results.

It was concluded however that the theoretical solutions obtained could be used to predict the transient response of systems with sufficient accuracy for engineering purposes.

Schauer and Giedt

Schauer and Giedt[84] derived some equations and conducted transient experiments to determine thermal contact conductance between two thin plates during heating.

The plates were of dissimilar metals. A near step difference in

temperature between two parallel plates in contact was produced by discharging a capacitor bank through the two plates.

The emfs of a thermocouple installed in each surface were fed via a protecting circuit to an oscilloscope. Instantaneous heat flux was determined from the measured surface temperature history.

The results indicated that with stainless steel-aluminium contact, thermal conductance rose sharply with time and gradually levelled out to a near steady value after about 100ms. Stainless steel-ceramic contacts produced a sharp rise of thermal contact conductance with time to reach a peak and then gradually reduced to some near steady value after about 100ms. The latter type of result was displayed by Moore[70] who attributed the sudden rise to the calculation method employed rather than being a real phenomenon. Since the surface thermocouples could not indicate an instantaneous rise in temperature due to their being embedded in epoxy resin, the temperature difference between the surfaces at time zero had to be obtained by extrapolation. It is likely that this may have led to errors in calculation. A later paper by Beck[13] suggests a method for determining thermal contact conductance and claims that it can be extended for determining thermal contact conductance as a function of time. The method involves minimising the sum of the squares of the difference between calculated and measured temperatures; the calculated temperatures being determined by a numerical solution of the problem.

Heasley

A mathematical analysis of transient heat transfer between contacting solids was carried out by Heasley[47] in the course of a study of heat transfer in glass forming processes, where heat is transferred to a colder mould. An analysis of transient heat flow through a single contact spot between two semi-infinite bodies is made. The

response of an array of contact spots is analysed and it is shown that the contact spots act as both heat flow resistances and capacitances.

If the capacitance is negligible the usual convection boundary condition is used for each body at the contact surface thus

$$k_1 \frac{\delta T_1}{\delta X} = k_2 \frac{\delta T_2}{\delta X} = H(T_1 - T_2) \tag{42}$$

where the conductance H includes constriction resistance and any other surface barrier present.

For short values of time the capacitance is not negligible and each boundary condition takes the form

$$\frac{\partial T_1}{\partial X} - \frac{H}{K}(T_1 - T_2) - \frac{w}{\alpha_1}\frac{\partial T_1}{\partial t} = 0 \tag{43}$$

where $$w = \frac{2 - \sqrt{NA_o} - NA_o}{6\gamma\sqrt{N}} \tag{44}$$

and N = N^o of contact areas per cm^2 of surface

A_o = Area per contact cm^2

γ = dimensionless constant

and accounts for the heat capacity of the restrictions.

Baklastov and Gorbenko

Baklastov and Gorbenko[6] considered the problem of determining how to calculate the thermal contact resistance between two bodies when one of them was heated at one end at some rate q. The heat flow was assumed one-dimensional everywhere. They postulated the contact zone to be a body of finite thickness and having its own finite thermo-physical properties. The equations they developed showed that thermal contact

resistance depended mainly on the ratio q/b where

$$b = \alpha \frac{\partial^2 T}{\partial x^2}$$

for the body which was heated via the contact interface, but do not discuss the matter further. Tharmalingham's work[89] (commented on in this thesis) studies a similar problem but in a more practical way.

Tharmalingham

Tharmalingham[89] developed a method to determine thermal contact conductance between metal to plastic surfaces from measurements of temperature transients. The transients were set up in two aluminimum bars with a disc of plastic sandwiched between them. Initially the rods and plastic were all insulated to reduce radial heat loss and also at one remote end. The other end of the system was then exposed to a constant radiant heat flux.

The temperature-time variation predicted from appropriate solutions to the one-dimensional heat-diffusion equations, (which depend on the values of thermal contact conductance h_c and thermal conductivity k_p of plastic) was compared with the temperature-time variation observed experimentally. An optimisation technique was employed to determine those values of h_c and k_p which gave the minimum sum of squares of the difference between predicted and measured temperatures. Some difficulty was encountered in that the values of h_c and k_p so found were dependent on the initial starting value of the optimisation procedure. It was found that the least squares function had no unique minimum point but a line ~~of~~ minimum. This result required k_p to be measured independently of h_c. This was done by obtaining k_p from transient experiments where h_c was made very large by increasing the contact pressure and filling the interstitial spaces with glycerine. The value of k_p so found was used to evaluate

h_c in other experiments.

The major source of error arose in estimation of the radiant heat flux rather than in the calculation procedure. The results of experiments to determine how h_c varied with contact pressure P are of the form

$$h_c = AP^2 + BP + C \qquad (44a)$$

which suggests that the explanation of how heat is transferred across the interface between two contacting metals may not be applicable to metal-to-plastic contacts.

3.2.3.2 Summary of section 3.2.3

In the non-steady state, the behaviour of the interface between two contacting solids and its influence on heat transfer is not properly understood. Some experimental work with two metals in contact appears to indicate that the thermal contact resistance changes considerably with time[70][84]. However, in some cases it has been shown to be likely that this apparent change in thermal contact resistance is not real but the result of the method used to calculate it from experimentally obtained temperature distributions. It is worth commenting that for simplicity of calculation, it was assumed that the heat flow was one-dimensional everywhere, whereas in the regions near the contact interface, the heat flow is three-dimensional. Extrapolation of temperature distributions within those regions where the heat flow is substantially one-dimensional to the contact interface when the heat flow is non-steady, could lead to errors in the estimation of space-average heat flux and temperature at the contact interface. However, if the thermal contact resistance arose through the contact surfaces being coated with a thin, low conductivity solid film with solid-to-solid contact everywhere across the interface, instead of by constriction of the heat flow lines to pass through dispersed, local solid-to-solid contact areas,

the one-dimensional representation of the problem would be valid.

3.3 Non-Permanent Contact Heat Transfer

3.3.1 Mathematical Studies

Baillie and Fan

Baillie and Fan[5] calculated the temperature transients in a system comprising two finite bars, initially at uniform, but different temperatures and entirely insulated from the surroundings. The insulation was removed from one end of each bar and the ends brought into perfect thermal contact for a definite period of time, at the end of which the insulation was replaced. No attempt to include the effects of thermal contact resistance between the bars when held in contact was made.

Reed and Mullineux

Towards the end of the work described in this thesis and subsequent to publications[57] and [123], my colleagues J R Reed of the Department of Mathematics, University of Aston in Birmingham and G Mullineux, after discussion with the writer, considered the same mathematical problem posed in section 4.3.2 of this thesis; namely solution of the heat diffusion equation subject to boundary conditions $x=0,\ T=T_A=\text{constant};\ x=\ell,\ n(\tau_0+\tau_c)<t<n(\tau_0+\tau_c)+\tau_0;\ \partial T/\partial x=0;\ x=\ell\ n(\tau_0+\tau_c)+\tau_0<t<(n+1)(\tau_0+\tau_c),\ \partial T/\partial x=-T(\ell,t)/\lambda$ in section 4.3.2.3. They used a different method to solve the problem from those described in this thesis. The result of their work was published towards the end of 1973 in reference [124].

Finite integral transforms were used to obtain expressions for temperature distribution due to one-dimensional heat flow in a bar, one end of which was held at a fixed temperature. The other end made periodic contact with a body at a lower temperature through a film which presents a thermal resistance. The temperature distributions

sought initially were:

(a) at the instant of contact

(b) at the instant of separation

Once these were known the temperature distribution at any instant in the cycle could be computed after the necessary inversion process. Temperature distributions (a) and (b) were used to determine the length of bar ℓ_i used to represent the thermal resistance due to periodic interruption of the heat flow. (The same ℓ_i as in this thesis, section 4.3.2 and Fig.21)

To determine temperature distributions (a) and (b), two systems of linear simultaneous equations were required to be constructed, from whose solution values of temperature at each position along the bar at instants (a) and (b) could be found. The amount of computation involved was similar to that required for sections 4.3.4 and 4.2.7 of this thesis, but the amount of algebraic work was less. The result of computation of ℓ_i at a single chosen test condition agreed closely with that obtained by the methods described in this thesis and references[53] and[123] which are discussed next in this section of this thesis.

The method is applicable to the case where perfect thermal contact is made at the contact end of the bar during the contact period. The new boundary condition during the contact period will be as quoted in this thesis section 4.2.4. A new integral transform would then be required for the contact period.

Howard and Sutton

Part of the work described in this thesis was published in references[53]

and[123]. A copy of each paper accompanies each of this thesis.

Reference[53] considers the problem of one-dimensional heat flow along two bars of identical conducting material whose remote ends are held at a fixed temperature and whose adjacent ends meet and separate cyclically. The contact interface assumes a fixed temperature when the adjacent ends meet and no heat is transferred when they are separated. Finite differences were used to approximate to the heat diffusion equation and the boundary conditions. An analogue computer was used to solve the problem The relationship between the thermal resistance due to periodic interruption of the heat flow, represented by length l_i of bar material, frequency f, ratio of contact:periodic time ($f\tau_c$) and thermal diffusivity α, is shown to be

$$\left(\frac{f l_i^2}{\alpha}\right) = g\,(f\,\tau_c)$$

for a sufficiently large length of bar. The results suggest that in practice at sufficiently high values of ($f\tau_c$), thermal contact resistance at the contact interface will exert a more significant effect on heat flow than the periodic interruption.

Reference[123] considers the effect of thermal contact resistance at the contact interface and uses the same technique as reference[53] but with a derivative type of boundary condition during the contact period. The results complement those of reference[53] and shows the degree to which thermal contact resistance affects heat flow under periodic contact conditions.

Dyehouse

Dyehouse[31] formulated a mathematical model to calculate the temperature distribution in hot-forging dies. Finite difference methods of solving the heat diffusion equation were used. The results of this study show that

sub-surface temperature prediction by the model are in good agreement with experimental measurements performed by Demidov[32]. But die surface temperatures predicted by the model are significantly lower than surface temperatures measured by Kellow et al[56]. It is suggested that the model should be modified to permit the thermal contact conductance at the die-workpiece interface to be time variable.

3.3.2 Exhaust valves

Mogford and Ball

Mogford and Ball[68] asserted that most of the heat removed from exhaust valves travelled via the seat. Increasing of the valve seat width reduced the valve operating temperature up to a certain width, beyond which the valve operating temperature rose again. This was attributed to the valve requiring a certain minimum impact pressure to give good thermal contact.

Bedale and Graham

Bedale and Graham[16] presented the temperature contours obtained on an exhaust valve by hardness relaxation method but did not analyse them to see how much heat passed via the valve seat and via the valve guide.

Cowley, Robinson and Flack

Some years later, Cowley, Robinson and Flack[29] also showed temperature contours on an exhaust valve and point to the development of new alloys as the approach to alleviating the problems brought about by high exhaust valve temperatures.

Stotter, Woolley and Ip

An investigation into diesel engine exhaust valve temperature is reported in reference[87]. The temperature distribution in the valve, valve seat,

cylinder head and valve guide was calculated using an electrolytic tank analogue. Experiments were carried out on an engine which had thermocouples installed at selected positions in the valve and its surrounding components. Laplace's equation was solved using the electrolytic tank of geometrically similar shape to that of the valve and cylinder head with electrolyte of various resistivities to represent the different component materials. The boundary conditions at the interface of valve and seat were expressed as an equivalent steady state heat transfer coefficient, calculated from empirical data in reference.[43] Using these values, the predicted temperature at the valve seat was higher than that measured on the test engine. The resistance units used to simulate the heat transfer coefficients (thermal contact conductance) were then adjusted until the temperature at the valve seat agreed with that measured on the engine and the new value of heat transfer coefficient was noted.

The authors realised that assumptions made in evaluating boundary conditions merited further investigation; in particular valve seat roughness.

Bertodo and Sivakumaran

In a paper[19] covering a wide range of factors influencing diesel engine exhaust valve performance Bertodo and Sivakumaran assert that for an optimised design of valve, 2/3 of the heat input to the valve is rejected through the valve seat.

3.2.3 Hot forging processes

Continuous hot forging processes involve cyclic heat transfer from the workpiece to the tools or dies and the transient heat input to the die has a marked effect on die life[3],[56].

Kellow, Bramley and Bannister

Kellow, Bramley and Bannister[56] measured temperatures in forging dies, developing a suitable thermocouple for measuring die surface temperatures. The dies were used to reduce the height of a hot cylindrical billet of typical forging steel, initially at 1100C, in a high energy rate forming machine.

The results indicated that, during forging, internal heat generation and convection within the billet, brought about by the deformation of the billet, are significant in causing die surface temperatures to be some 50 °C higher than the mean of the initial temperatures of billet and die. Measurements of contact area showed that after a strain of about 20% the real area of contact is about 70% of the nominal, leading to a heat flow across the interface of about 95% of the maximum possible. In addition, the presence of oxide films on the billet led to reduced transient surface temperature rise.

3.3.4 Summary of section 3.3

Apart from the references reviewed in section 3.3.1 there appears to be no mathematical study published on heat transfer under non-permanent contact conditions. Reference[53], being part of the work of this thesis, established the minimum thermal resistance to be expected by periodic interruption of the heat flow.

Reference[123] also being part of this thesis gives an approximate representation of the effects brought about by thermal contact resistance. Reference[124] tackles the problem posed in (123) by a different method and seems to support the findings of reference[123].

Such experimental work that has been published has been concerned with development work or observations of temperatures in engineering components and no systematic study seems to have been made.

3.4 Overall Review

Despite a great deal of research into steady-state heat transfer through the interface between two solids in permanent contact with each other, the process is still not sufficiently understood in detail for accurate predictions of thermal contact resistance of the kinds of interface met generally in everyday engineering. Tedious and somewhat uncertain methods or incomplete empirical correlations of experimental data are the only means at present available for estimating probable values of thermal contact resistance. These estimates may be made more uncertain by the possible occurrence of the directional effect, or, if the load on the interface fluctuates, by hysteresis effects.

Under transient heat transfer, permanent contact conditions, the physical and geometrical changes that take place at the contact interface are not known. Although valuable theoretical studies of some non-steady state situations have been made,[1,2,22,117,118] the problem was idealised so that the heat flow within the solids was one-dimensional, even at and near to the contact interface, presumably because of the magnitude of the task of solving the three-dimensional heat diffusion equation.

Little appears to have been published on the subject of heat transfer between solids which make non-permanent contact, i.e. intermittent periodic or non-periodic. Apart from references[53] and[123] (in which the writer of this thesis is joint author and which arose out of the

work described in this thesis), and[124] (which appeared when this thesis was nearing completion and has been reviewed in section 3.3.1) no basic theoretical studies seem to have been made.

It would appear that a study of heat transfer through surfaces which make regular, period contact would be the starting point from which to advance knowledge in this field.

4. THEORETICAL STUDY

4.1 Preliminary Remarks

In processes such as those described in section 1, the heat transfer through the contact interface will depend upon:-

1. the frequency of contact
2. the proportion of cycle time spent in actual contact
3. conditions at the contact interface.

A complete specification of item 3 above requires information on:-

(a) conditions at the contact interface during the time the surfaces are in contact

(b) conditions during the time the surfaces are separated

(c) the manner in which transition from contact to separation, (and vice-versa) takes place

(d) the physical properties of the solids and any interfacial fluids, surface films or other deposits present

(e) the interface temperature and adjacent temperature differences.

4.2 Ideal Contact Condition

4.2.1 Description of system

For simplicity consider a system comprising two bars of conducting material arranged with their axes in line and able to make or break contact at adjacent ends as shown in Fig. 7(a). The bars are insulated around their outer curved surface to prevent transverse heat loss and the remote ends A and B of the bar are at different but fixed temperatures T_A and T_B. If the adjacent ends (H and C) are brought into

permanent contact heat will flow continuously across the interface. Under ideal conditions of contact there will be no interfacial films present, but solid-to-solid contact at every point on the two contact faces and hence no constriction of the heat flux lines at the interface. If the two bars are of identical material and its thermal conductivity is constant the axial temperature distribution will be linear. When contact between ends H and C is broken by separating them slightly then the heat flow across the interface will be greatly reduced and under steady state conditions the temperature distribution in each bar would be near uniform, giving a large temperature drop across the small gap between the ends H and C.

If ends H and C are brought into contact and separated according to a regular cycle, then the time-average,quasi - steady state temperature distribution would be between the permanent contact and non-contact distributions as shown in Fig. 7b by lines $T_A, T'_{0_H}, T'_{0_C}, T_B$.
The temperature in each bar fluctuates cyclically everywhere but the amplitude near the fixed temperature end of the bar is very small.

The performance of this simple system under periodic contact conditions, when a quasi-steady state has been attained will now be investigated.

4.2.2 Assumptions

Considering the system shown in Fig.7a, the following assumptions are made:

(i) only one dimensional heat flow along the axis of the bars is possible

(ii) the two bars are of identical material and cross sectional area

(iii) when the ends H and C of the bars are in contact, ideal thermal contact is established. (Under these conditions, the moment that the two surfaces make contact the temperature of each surface will change instantaneously [46] to the mean of the surface temperatures immediately prior to contact

(iv) when the ends H and C of the bars are separated, it will be assumed that no heat is transferred into or across the gap

(v) Temperatures at ends A and B are fixed for all time at T_A and T_B respectively.

Instantaneous temperature distributions during the period of contact and during the period of separation are shown in Fig.8. Note that during the non-contact period, the temperature gradient at the contact surfaces is assumed zero.

4.2.3 Formulation

The heat diffusion equation

$$\frac{\partial T}{\partial t} = \alpha \frac{\partial^2 T}{\partial x^2} \tag{45}$$

has to be satisfied throughout the system at all times. Under periodic contact conditions, separate boundary conditions at the contact interface will be required for each part of the contact-separation cycle

(see boundary condition 2 below).

Since the two bars in Fig 7a are assumed to be of identical material, events in only one bar need be considered. Furthermore, it is shown in Appendix 1, that the heat flow through the system is unaffected by the axial location of the contact interface, provided that, with the shortest bar, the temperature fluctuations due to cyclic interruption of heat flow at the contact interface are not detectable at the opposite end of the bar. The solution for the temperature distribution in a semi-infinite solid, whose surface temperature is periodic shows that the temperature oscillations will have decayed to a negligible amplitude when (see reference[33])

$$\frac{x}{2\sqrt{\frac{\pi\alpha}{f}}} \simeq 0.8 \qquad (46)$$

where x = depth below the surface

f = frequency of oscillations

α = diffusivity

The problem can then be reduced to finding the quasi-steady state temperature distribution in a bar of length ℓ such that (from equation (46))

$$\ell > 1.6\sqrt{\frac{\pi\alpha}{f}} \qquad (47)$$

4.2.4 Boundary and initial conditions

Choosing the hotter of the two bars in Fig 7a, let the temperature at the contact interface during the period of contact now be taken as zero

and let the temperature at the other end of the bar be fixed at T_A. Let both bar lengths be sufficiently large to satisfy equation (47). Let the origin of distance measurements be located at the hottest end of the bar and take the zero of time at the moment when contact is broken. The boundary conditions then become:-

1. At $x = 0$, $T(0,t) = T_A = \text{(constant)}$
2. At $x = \ell$

   (i) During the non-contact period when

   $$n(\tau_o + \tau_c) < t < n(\tau_o + \tau_c) + \tau_o$$

   where $n = 0,1,2,3 \ldots\ldots$

   $$\frac{\partial T}{\partial x} = 0$$

   (ii) During the period of contact when

   $$n(\tau_o + \tau_c) + \tau_o < t < (n+1)(\tau_o + \tau_c)$$

   where $n = 0,1,2,3 \ldots\ldots$

   $$T(\ell,t) = 0$$

Initial condition

In order to reduce the time taken for the system to reach the quasi-steady state, the initial condition was chosen as the steady state, permanent contact temperature distribution, i.e.

$$T(x,o) = T_A(1 - \frac{x}{\ell}) \tag{48}$$

4.2.5 Dimensional analysis

Consider the heat flow through the system depicted in Fig.7, when the contact faces at H and C are undergoing a continuous cycle of contact

and separation, and a quasi-steady state is reached. If each bar is sufficiently long for temperature fluctuations due to the periodic interruption of heat flow to be sufficiently small at ends H and C, (i.e. equation (47) is satisfied), then the total thermal resistance of the system is made up of the solid resistance of the material of the two bars, R_s, and an additional resistance, R_i, due to periodic interruption of the heat flow. R_s and R_i are then independent of each other and may be represented by appropriate lengths of the material of the bars (of the same cross-sectional area). Events in only one bar, say the hotter bar, need be studied; the appropriate bar lengths are ℓ, for the solid resistance, and ℓ_i, for that due to periodic interruption of the heat flow as shown in Fig.9 (Note that ℓ_i is determined by extrapolation of the time-average temperature distribution when in the quasi-steady state to the zero of temperature).

Provided that the length of the bar is sufficiently long, (see equation (47)), length ℓ_i will depend on the frequency, f, ratio of contact time: periodic time ($f\tau_c$) and the thermal properties of the bar material, k, ρ and c. The four primary dimensions are length,L, mass, M, or heat quantity H, time,t, and temperature T. The number of dimensionless groups arising will be two. Writing diffusivity, α in place of $\frac{k}{\rho c}$ yields the relationship

$$\left(\frac{f\ell_i^2}{\alpha}\right) = g\left[(f\tau_c)\right] \qquad (50)$$

Equation (47) may be transposed to give the dimensionless group

$$\left(\frac{f\ell^2}{\alpha}\right) > 2.56\,\pi \tag{51}$$

as the condition for validity of equation (50), otherwise

$$\left(\frac{f\ell_i^2}{\alpha}\right) = g\left[(f\tau_c),\ \left(\frac{f\ell}{\alpha}\right)^2\right] \tag{52}$$

It is shown later, (see section 4.2.7.6), that $\left(\frac{f\ell_i^2}{\alpha}\right)$ is not sensitive to changes in $\left(\frac{f\ell^2}{\alpha}\right)$ when $\left(\frac{f\ell^2}{\alpha}\right)$ is greater than about 2. It can be shown, (see Appendix 2) that for a given value of $(f\tau_c)$,

$$\lim_{\left(\frac{f\ell^2}{\alpha}\right)\to 0} \left(\frac{f\ell_i^2}{\alpha}\right) = \left(\frac{f\ell^2}{\alpha}\right)\left[\frac{1-(f\tau_c)}{(f\tau_c)}\right]^2 \tag{53}$$

It should be noted, see Appendix 1, that if the overall length of the system of two bars is unchanged but the length of the shorter bar is such that equation (51) is not satisfied, the thermal resistance due to periodic interruption of the heat flow will be less than when equation (51) is satisfied. When the shorter bar is of zero length this thermal resistance becomes half that when the length of the shorter bar is greater than that given by equation (51).

4.2.6 Analogue computer Solution

4.2.6.1 Simulation

The heat diffusion equation (45) and boundary conditions were written in finite-difference form in which temperature and distance were expressed as dimensionless quantities. An E.A.L Limited PACE analogue computer was

used to solve these finite-difference equations. Their derivation is given in Appendix 3.

4.2.6.2 Finite-difference equations

A non-uniform mesh was used, in which the elemental distances were shortest in the region nearest to the contact interface, in an attempt to gain accuracy. The elemental distances expressed in dimensionless form ($X = x/\ell$) are shown in Fig. 3.2 of Appendix 3. The steady state permanent contact temperature distribution was employed as an initial condition and as the datum from which temperature measurements were made. Temperature measured from this datum was expressed in dimensionless form ($\Delta\Theta_n = \Delta T_n/T_A$), the finite-difference equations in which $D = \frac{\partial}{\partial t}$, being:-

$$D(\Delta\Theta_1) = (0.089\Delta\Theta_2 - 0.098\Delta\Theta_1) \quad s^{-1} \quad (3/14)$$

$$D(\Delta\Theta_2) = (0.488\Delta\Theta_3 - 0.976\Delta\Theta_2 + 0.488\Delta\Theta_1) \quad s^{-1} \quad (3/9)$$

$$D(\Delta\Theta_3) = (6.95\Delta\Theta_4 - 7.82\Delta\Theta_3 + 0.87\Delta\Theta_2) \quad s^{-1} \quad (3/10)$$

$$D(\Delta\Theta_4) = (31.25\Delta\Theta_5 - 62.5\Delta\Theta_4 + 31.25\Delta\Theta_3) \quad s^{-1} \quad (3/11)$$

$$D(\Delta\Theta_5) = (31.25\Delta\Theta_6 - 62.5\Delta\Theta_5 + 31.25\Delta\Theta_4) \quad s^{-1} \quad (3/12)$$

$$D(\Delta\Theta_6) = (31.25\Delta\Theta_7 - 62.5\Delta\Theta_6 + 31.25\Delta\Theta_5) \quad s^{-1} \quad (3/13)$$

During the contact period:

$$\Delta\Theta_7 = 0 \quad (3/15)$$

During the non-contact period:-

$$D(\Delta\Theta_7) = (0.625 - 62.5\Delta\Theta_7 + 62.5\Delta\Theta_6) \quad s^{-1} \quad (3/19)$$

Fig 10 shows the dimensionless temperature Θ plotted against dimensionless distance X in the steady state permanent contact condition, the steady state non-contact condition and the time-average temperature when in the quasi-steady state. Measurement of the $\Delta\Theta_n$ shown in Fig 10 i.e. temperature difference at any node n, between the quasi-steady permanent contact line is required to evaluate $\frac{\ell i}{\ell}$.

4.2.6.3 Circuitry

An EAL Limited PACE TR - 20 analogue computer was used to solve the finite-difference equations (3/9) to (3/15) and (3/19) in section 4.2.6.2 and Appendix 3. A diagram of the circuit employed is shown in Fig.11. Contact and separation of the two bars at the contact face was simulated by the opening and closing of the switch across amplifier 4, Fig.11. The switch, which was solenoid operated, formed part of the "relay comparator" of the analogue computer. The "relay comparator" comprised a high gain amplifier and a relay (solenoid operated switch). The inputs to the amplifier was a reference voltage and the output of an oscillator generating a sinusoidal output with a steady d.c. bias. The relay was energised and hence the switch across amplifier 4, Fig.11 was opened when these inputs produced a negative voltage at the summing junction of the amplifier. When the polarity of the summing junction was positive (or when no inputs were applied) the relay was not energised and switch across amplifier 4, Fig.11 returned to its original position. Alteration of the steady d.c. bias of the oscillator output allowed the ratio of contact time: periodic time, ($f\tau_c$) to be

varied as indicated in Fig.12.

For a given input voltage, Δv_i (t), to each amplifier, the output voltage, $\Delta v_o(t)$, will be given by

$$\Delta v_o(t) = -\frac{1}{RC} \int \Delta v_i(t)dt + \Delta v_o(o) \tag{53a}$$

where $\Delta v_o(o)$ is the initial condition. The initial condition chosen was the steady state, permanent contact temperature distribution given by equation (48) which was used as the datum for the dimensionless temperature changes $\Delta\Theta_n$,(see Appendix 3). In this case the initial condition term $\Delta v_o(0)$ is zero. The output voltages of the amplifiers shown in Fig.11 have been defined as Δv_1, $-\Delta v_2$, Δv_3, $-\Delta v_4$, Δv_5, $-\Delta v_6$, and Δv_7, to eliminate the need for sign reversal amplifiers in series with the feed-back resistors at each stage. The relationship between input and output voltage to each amplifier shown in Fig.11 is given by:

$$D(\Delta v_1) = (0.089\Delta v_2 - 0.098\Delta v_1) \quad Vs^{-1} \tag{54}$$

$$D(\Delta v_2) = (0.488\ \Delta v_3 - 0.976\ \Delta v_2 + 0.488\Delta v_1) \quad Vs^{-1} \tag{55}$$

$$D(\Delta v_3) = (6.95\Delta v_4 - 7.82\Delta v_3 + 0.87\Delta v_2) \quad Vs^{-1} \tag{56}$$

$$D(\Delta v_4) = (31.25\Delta v_5 - 62.5\Delta v_4 + 31.25\Delta v_3) \quad Vs^{-1} \tag{57}$$

$$D(\Delta v_5) = (31.25\Delta v_6 - 62.5\Delta v_5 + 31.25\Delta v_4) \quad Vs^{-1} \tag{58}$$

$$D(\Delta v_6) = (31.25\Delta v_7 - 62.5\Delta v_6 + 31.25\Delta v_5) \quad Vs^{-1} \tag{59}$$

During the contact period

$$\Delta v_7 = 0 \tag{60}$$

During the non-contact period and referring to Fig. 11 and the potentiometer

at the top left hand corner, if some voltage E is applied to the input end of the potentiometer set at some proportion p, then

$$D\ (\Delta v_7) \ = \ -100\ (Ep + 0.625\Delta v_7 - 0.625\Delta v_6) \qquad Vs^{-1} \qquad (61)$$

Comparison of equations (54) to (60) with equations (3/14), (3/9) to (3/13) and (3/15) in section 4.2.6.2 and Appendix 3, reveals that the two sets of equations are identical, with $\Delta v_n = \Delta\Theta_n$. Equation (61) is identical to equation (3/19) if the product Ep = -0.00625; the amplitude scale would then be 1V = 1. A stabilised supply of $\pm$ 10V was available on the analogue computer. Putting E = -10V a potentiometer setting p = 0.000625 is required for equations (3/19) and (61) to be identical. This value is not practicable if only a single potentiometer is used because discrimination in setting to 0.0001 is not possible. The setting actually used (approx 0.00625) gave an amplitude scale of approximately 10V = 1.

A block diagram of the layout of the analogue computer and its peripheral equipment is shown in Fig. 13. The output of amplifier 4, namely Δv_7, was displayed on a cathode ray oscilloscope and could also be displayed on an ultra-violet (u.v.) recorder. Fig. 14 shows a typical trace of Δv_7 recorded by the u.v. recorder. The frequency of contact, f, and ratio of contact:periodic time, ($f\tau_c$) was determined from the trace of Δv_7. The outputs of amplifiers 15 and 11, namely Δv_1 and Δv_2 were measured with a digital voltmeter, since at frequencies other than the lowest they did not fluctuate. At the lowest frequencies these outputs were switched to the u.v. recorder and their time-average values were determined from the traces.

4.2.6.4 <u>Procedure</u>

Preliminary Setting

After wiring the circuit shown in Fig. 11 and setting the potentiometers against the reference "helipot" on the analogue computer facia, the circuit was energised from the -10V stabilised supply with the switch across amplifier 4 open continuously. When the output voltages of the amplifiers became steady, this state simulated the steady state, non-contact condition; the temperature distribution being shown by the horizontal line in Fig. 10. The dimensionless temperature, $\Delta\Theta_n$, at the various nodes should be the solutions obtained when the $D(\Delta\Theta_n)$ in equations (3/14), (3/9) to (3/13) and (3/19) are all zero. These solutions are shown in Table 1. It will be observed that the values of the $\Delta\Theta_{n_s}$ are all between 0.01003 and 0.01026 smaller than those expected from the steady state, non-contact temperature distribution in Fig. 10. This is of course due to replacing the heat diffusion equation (45) by finite-difference equations.

The amplifier output voltages Δv_{n_s} (and hence $\Delta\Theta_{n_s}$) showed deviations from the values quoted in Table 1. It turned out that the finite-difference equations (3/14), (3/9) to (3/13) and (3/19) are not particularly well conditioned. The effect of a small change in coefficients of the $\Delta\Theta_n$ on the solutions of these equations when $D(\Delta\Theta_n) = 0$, is shown in Appendix 12. Thus the analogue could be sensitive to inaccuracies in the potentiometer settings. Some amplifier drift was also encountered. Clearly a judgement had to be made as to when the setting of the potentiometers was such that tests under quasi-steady state conditions could proceed, consistent with the time taken for the analogue to reach the steady state. A rough rule used was that the ratio $\Delta v_{2_s}/\Delta v_{1_s} \simeq 1.1$ and that other Δv_{n_s} when plotted against $(\frac{x_n}{\ell})$ were not too widely scattered about a straight line drawn among the points.

This was admittedly crude but it seemed, at the time, the best that could be done.

Quasi-steady state tests

To verify the validity of equation (50) trials at fixed frequency, f, but varying the contact time:periodic time ($f\tau_c$) were carried out. These trials were then repeated at other fixed frequencies.

Once the quasi-steady state had been reached, the output voltages of the amplifiers Δv_7, Δv_1 and Δv_2 (Fig.11) were observed. The frequency and ratio of contact time:periodic time were obtained from the trace of Δv_7 recorded by the U.V. recorder (see Fig. 14), representing temperature fluctuation at the contact interface. Mean values of Δv_1 and Δv_2 (which at most frequencies were steady and observed with a digital voltmeter) were used to calculate the value of ℓ_i required for computing the dimensionless group$\left(\frac{f\ell_i^2}{\alpha}\right)$. Referring to Fig. 10 and writing $\overline{\Delta\Theta}_n$ for the time-average values of $\Delta\Theta_n$ and remembering that $\Delta\Theta_n$ = scale factor x Δv_n it will be seen that

$$\frac{\overline{\Delta\Theta 7}}{(\ell_i/\ell)} = \frac{1}{1 + (\ell_i/\ell)} \tag{63}$$

and writing

$$\overline{\Delta\Theta}_7 = \frac{\overline{\Delta\Theta}_1}{\Delta\Theta_{2_s}} = \frac{\overline{\Delta\Theta}_2}{\Delta\Theta_{2_s}} = L \tag{64}$$

and hence

$$\ell_i = \frac{\ell L}{1-L} \tag{65}$$

(Note that L is the proportion of the heat flow under steady state permanent contact condition which is lost due to periodic interruption of the heat flow). The observed values of $\frac{\overline{\Delta v}_1}{\Delta v_{1_s}}$ and $\frac{\overline{\Delta v}_2}{\Delta v_{2_s}}$ agreed closely.

4.2.6.5 Results of analogue computer study

The results are tabulated in Tables 2 and a plot of $\left(\frac{f\ell_i^2}{\alpha}\right)$ against $(f\tau_c)$ is shown in Fig. 15.

4.2.6.6 Discussion of results of analogue computerstudy

The plot of $\left(\frac{f\ell_i^2}{\alpha}\right)$ against $(f\tau_c)$, Fig. 15 shows that all the points lie very close indeed to one single curve drawn among them, thus verifying the relationship given by equation (50).

From equation (65) it will be seen that for small values of heat flow loss, L,

$$L \simeq \frac{\ell_i}{\ell} \tag{66}$$

Since

$$\frac{\ell_i}{\ell} = \left[\left(\frac{f\ell_i^2}{\alpha}\right)\left(\frac{\alpha}{f\ell^2}\right)\right]^{\frac{1}{2}} \tag{67}$$

and

$$\left(\frac{f\ell_i^2}{\alpha}\right) = g(f\tau_c) \tag{67}$$

(obtainable from the graph, Fig. 15) it follows that the loss of heat flow L tends to

$$L = \left(\frac{f\ell^2}{\alpha}\right)^{-\frac{1}{2}} \left[g(f\tau_c)\right]^{\frac{1}{2}} \tag{68}$$

If the frequency of contact f, is varied for a given system (fixed ℓ and α) maintaining $(f\tau_c)$ constant, then from equations (50) and (65)

$$\frac{L}{1-L} = \left[\left(\frac{f\ell_i^2}{\alpha}\right)\left(\frac{\alpha}{f\ell^2}\right)\right]^{\frac{1}{2}}$$

$$= g(f\tau_c)^{\frac{1}{2}}\left(\frac{\alpha}{f\ell^2}\right)^{\frac{1}{2}} \tag{69}$$

and since L cannot be negative or exceed unity, only the positive root of the right hand side of equation (69) is admissible. Writing p for

$\left[\frac{\alpha\, g(f\tau_c)}{\ell^2}\right]$ and transposing equation (69) leads to

$$L = \frac{(p/f)^{\frac{1}{2}}}{1 + (p/f)^{\frac{1}{2}}} \qquad (70)$$

Thus at fixed p,as f increases, so loss of heat flow L falls. For sufficiently large, fixed values of $(f\tau_c)$, which means small $g(f\tau_c)$, the loss of heat flow brought about by the periodic interruption of heat flow, will be small.

It should be emphasised that the analogue does not solve the partial differential equation (45) but only the finite-difference approximations to it, equations (54)-(61); which includes the boundary condition that the temperature at the hottest end of the bar is fixed i.e. $\Delta\Theta_0 = 0$,

In practical cases the amplitude of temperature fluctuation within the rod will decay exponentially [34] with distance from the contact planes. At the lowest frequency investigated, 0.0145 Hz, the amplitude at the hottest end of the bar would only amount to 2.2% of that at the contact plane, thus approximating to the boundary condition.

Since a non-uniform division of the model was employed, it is difficult to estimate the error due to the finite-difference approximation. Later a numerical method of solution, described in section 4.2.6, was developed and the analogue computer solutions were found to be in close agreement with it.

It is emphasised that the data obtained is applicable only to the case where both hot and cold members are of identical material and perfect contact and separation occurs at the plane of contact. Cases where thermal contact resistance is present are reported in section 4.3.

Clearly the results suggest that in practical cases, at sufficiently high

values of $(f\tau_c)$ and frequency, thermal contact resistance at the contact plane will exert a more significant effect on heat flow than the periodic interruption at the contact plane.

4.2.7 Numerical matrix inversion method of solution

4.2.7.1 Preamble

It was feared that the results of the analogue computer solution of the periodic contact problem described in section 4.2.4 might be in serious error due to the finite-difference approximations and the non-uniform mesh employed. Rather than try to estimate the errors, an alternative method of solution was sought, which did not depend on finite-difference approximations.

4.2.7.2 Formulation

A solution of the heat diffusion equation (45), subject to the boundary conditions given in section 4.2.4 when the quasi-steady state has been reached, is required. It is shown in Appendix 4 that the temperature $T_1(x,t)$ during the non-contact period can be expressed as:-

$$T_1(x,t) = T_A + \sum_{n=1}^{\infty} A_n \exp\left\{-\left(\frac{n\pi}{2\ell}\right)^2 \alpha t\right\} \sin\left(\frac{n\pi}{2}\,\frac{x}{\ell}\right) \qquad (71)$$

$$n = \text{odd} \qquad 0 < t < \tau_1$$

where t is measured from the instant the bars are separated and the A_n are real constants to be determined.

Likewise the temperature $T_2(x,t)$ during the contact period can be expressed as:-

$$T_2(x,t) = T_A\left(1 - \frac{x}{\ell}\right) + \sum_{n=2}^{\infty} B_n \exp\left\{-\left(\frac{n\pi}{2\ell}\right)^2 \alpha t\right\} \sin\left(\frac{n\pi}{2}\,\frac{x}{\ell}\right)$$

$$n = \text{even} \qquad 0 < t < \tau_2 \qquad (72)$$

where t is measured from the instant the bars make contact, and the A_n and B_n are real constants to be determined.

4.2.7.3 Method of solution; determination of the A_n and B_n

Appendix 4 deals with the derivation of equations from which the A_n and B_n in equation (71) and (72) can be determined. Equations (4/13) and (4/14), (which are repeated below for convenience of reference) have to be solved to determine the A_n and B_n.

For odd values of m > 0 and odd values of k

$$\frac{\pi^2}{16}(-1)^{(m+1)/2} A_m + \sum_{k=1}^{\infty}(-1)^{\frac{k-1}{2}} C_{m,k} \exp\left\{-\left(\frac{k\pi}{2\ell}\right)^2 \alpha\tau_1\right\}$$

$$= \frac{T_A}{2m^2} - T_A\, C_{m,o} \qquad (4/13)$$

$$\text{where } C_{m,k} = \sum_{\substack{n=2 \\ n \text{ even}}}^{\infty} \frac{n^2}{(n^2-m^2)(n^2-k^2)} \exp\left\{-\left(\frac{n\pi}{2\ell}\right)^2 \alpha\tau_2\right\} \qquad (4/10)$$

(m,k odd)

For even values of m > 0 and even values of k

$$\frac{\pi^2}{16m}(-1)^{m/2} B_m + \sum_{k=2}^{\infty}(-1)^{k/2} k\, D_{m,k} \exp\left\{-\left(\frac{k\pi}{2\ell}\right)^2 \alpha\tau_2\right\}$$

$$= 2\frac{T_A}{\pi} D_{m,o} + \frac{\pi T_A}{4m^2} \qquad (4/14)$$

$$\text{where} \quad D_{m,k} = \sum_{\substack{n=1 \\ n \text{ odd}}}^{\infty} \frac{\exp\left\{-\left(\frac{n\pi}{2\ell}\right)^2 \alpha\tau_1\right\}}{(n^2-k^2)(n^2-m^2)} \qquad (4/12)$$

(m,k even)

Equations (4/13) and (4/14) above are, for a given set of values for α, ℓ, τ_1, τ_2 and T_A, two systems of linear simultaneous equations in A_n and B_n respectively. The number of unknowns and equations in each system are both infinite. An approximation was made by truncating equations (4/13) and (4/14) to a finite number of terms and then solving each truncated system for the A_n and B_n. Equations (73) and (77) below are equations (4/13) and (4/14) truncated to 20 terms. The truncation to 20 terms was set by the available computer program for solving linear simultaneous equations.

$$
\begin{array}{c|c}
 & k \longrightarrow 1 \quad 3 \quad 5 \quad \cdots \quad 39 \\
m \downarrow & \\
\begin{array}{c} 1 \\ 3 \\ 5 \\ \vdots \\ 39 \end{array} &
\begin{bmatrix}
P_{1,1} & P_{1,3} & P_{1,5} & \cdots & \\
P_{3,1} & P_{3,3} & \cdots & & \\
P_{5,1} & \cdots & & & \\
\vdots & & \cdots & P_{37,37} & P_{37,39} \\
 & & \cdots & P_{39,37} & P_{39,39}
\end{bmatrix}
\cdot
\begin{bmatrix} A_1 \\ A_3 \\ \vdots \\ \vdots \\ A_{39} \end{bmatrix}
=
\begin{bmatrix} R_1 \\ R_3 \\ \vdots \\ \vdots \\ R_{39} \end{bmatrix}
\end{array}
\tag{73}
$$

where, when $m \neq k$

$$
p_{m,k} = (-1)^{(k-1)/2} C_{m,k} \exp\left\{-\left(\frac{k\pi}{2\ell}\right)^2 \alpha\, \tau_1\right\} \tag{74}
$$

($C_{m,k}$ from equation (4/10) in Appendix 4)

On the leading diagonal where m = k

$$p_{m,m} = (-1)^{\frac{m-1}{2}} C_{m,m} \exp\left\{-\left(\frac{m\pi}{2\ell}\right) \alpha \tau_1\right\} + (-1)^{\frac{m+1}{2}} \frac{\pi^2}{16} \tag{75}$$

and $$R_m = \frac{T_A}{2m^2} - T_A C_{m,o} \tag{76}$$

$$\begin{array}{c|c} & k \longrightarrow 2 \quad 4 \quad 6 \quad \ldots \quad 40 \\ \hline m \downarrow & \end{array}$$

$$\begin{array}{c} 2 \\ 4 \\ 6 \\ \\ 40 \end{array} \begin{bmatrix} q_{2,2} & q_{2,4} & \cdots & & \\ q_{2,4} & q_{4,4} & \cdots & & \\ \vdots & & & & \\ & & & \cdots & q_{38,40} \\ & & \cdots & q_{40,38} & q_{40,40} \end{bmatrix} \cdot \begin{bmatrix} B_2 \\ B_4 \\ B_6 \\ \vdots \\ B_{40} \end{bmatrix} = \begin{bmatrix} S_2 \\ S_4 \\ S_6 \\ \vdots \\ S_{40} \end{bmatrix} \tag{77}$$

where $m \neq k$

$$q_{m,k} = (-1)^{k/2} k D_{m,k} \exp\left\{-\left(\frac{k\pi}{2\ell}\right)^2 \alpha \tau_2\right\} \tag{78}$$

($D_{m,k}$ from equation (4/10) in Appendix 4)

On the leading diagonal where m = k

$$q_{m,m} = (-1)^{m/2} m D_{m,m} \exp\left\{-\left(\frac{m\pi}{2\ell}\right)^2 \alpha \tau_2\right\} - (-1)^{m/2} \frac{\pi^2}{16m} \tag{79}$$

and $$S_m = \frac{2T_A}{\pi} \cdot D_{m,o} + \frac{\pi T_A}{4m^2} \qquad (80)$$

Computer programs CAS1 and CBS1, shown in Appendices 8 and 9 were written to generate the elements of the coefficient matrix and vector of equations (73) and (77). The University ICL 1905E computer processed the data. An existing applications program, UA08, was used to solve the systems of linear simultaneous equations (73) and (77) to obtain A_n and B_n. The maximum number of simultaneous equations which could be handled by UA0 8 was 20. Appendices 8 and 9 each show a specimen input, the output coefficient matrix and vector generated by CAS1 and CBS1 and the solutions of equations (73) and (77).

In order to reduce the error due to truncation of equations (4/13) and (4/14), the value of ($\alpha\tau_1/\ell^2$) and ($\alpha\tau_2/\ell^2$) were made large, so as to cause the exponential component of the elements of the coefficient matrix of equations (73) and (77) to decay rapidly with m and k. Elements on the leading diagonal of these matrices, however, contain an additional term which is non-exponential, see equations (75) and (79). The values of α, ℓ, τ_1, and τ_2 which were used initially were

$$\alpha = 5 \times 10^6 \ \frac{m^2}{s} \qquad \ell = 0.04m$$

$$\tau_1 = \tau_2 = 10s$$

Errors due to truncation of equations (4/13) and (4/14) (see Appendix 4) were shown to be small by progressively increasing the coefficient matrix size (increasing m and k) and showing that the solutions for A_n and B_n are not sensitive to matrix size. Appendix 5 which shows solutions of equations (4/13) and (4/14) when truncated to 5,10,15 and 20 terms using the above values of α, ℓ, τ_1 and τ_2 verifies this.

4.2.7.4 Determination of temperature-time data and dimensionless group $\left(\frac{fl_i^2}{\alpha}\right)$

The values of A_n and B_n have to be substituted into equations (71) and (72) to obtain the temperature. Convergence of the series in (71) and (72) is ensured by the exponential term except when t = 0, when the exponential term becomes unity. The series in this case is still convergent, due to the A_n and B_n each decreasing with n with alternating sign, but convergence is less rapid. A method of finding the sum of each series when t = 0 is shown in Appendix 6. Specimen temperature-time data at various positions, $(\frac{x}{\ell})$, in the bar are shown in Tables 4-13 and Fig. 17 and are discussed in section 4.2.7.7.

In order to determine the thermal resistance offered by periodic interruption of the heat flow (represented by length ℓ_i of bar material see Figure 9, the time-average temperature, $\overline{T}(x)$ at any point, $(\frac{x}{\ell})$ in the bar has to be found. Equation (81) below gives an expression for $\overline{T}(x)$. Initially however since temperature-time data had already been calculated T(x) was found by alternative means, namely by averaging the temperature-time data calculated from equations (71) and (72) over a period $(\tau_1 + \tau_2)$ using numerical integration by Simpson's rule.

$$\overline{T}(x) = \left(\frac{1}{\tau_1 + \tau_2}\right) \left\{ T_A\tau_1 + \sum_{\substack{n=1 \\ n \text{ odd}}}^{\infty} \left\{ \frac{A_n}{\left(\frac{n\pi}{2\ell}\right)^2 \alpha} \left[1 - \exp\left\{-\left(\frac{n}{2}\right)^2 \alpha\tau_1\right\}\right] \sin\left(\frac{n\pi x}{2\ell}\right)\right\} \right.$$

$$\left. + T_A\tau_2 - \frac{T_A x}{\ell}\tau_2 + \sum_{\substack{n=2 \\ n \text{ even}}}^{\infty} \left\{ \frac{B_n}{\left(\frac{n\pi}{2\ell}\right)^2 \alpha} \left[1 - \exp\left\{-\left(\frac{n\pi}{2\ell}\right)^2 \alpha\tau_2\right\}\right] \sin\left(\frac{n\pi x}{2\ell}\right)\right\}\right\} \tag{81}$$

It was realised later that when the periodic time τ was large, Simpson's rule was insufficiently accurate using only 20 ordinates and the results

were re-worked using equation (81). The program used is shown in Appendix 18. The length ℓ_i was determined from T(x) by Equation (83) below. Considering Fig. 9; by similar triangles

$$\frac{T_A - \overline{T}(x)}{x} = \frac{\overline{T}(x)}{\ell + \ell_i - x} \tag{82}$$

and hence

$$\ell_i = \ell \left[\frac{\overline{T}(x)(\frac{x}{\ell})}{(T_A - \overline{T}(x))} - 1 + \frac{x}{\ell} \right] \tag{83}$$

For computing purposes T_A was assigned a value of 100K and $\frac{x}{\ell} = 1.0$. Appendix 7 shows the stages of computation from the initial input of data to the output of temperature-time data and dimensionless groups. Individual programs are given in Appendices 8 - 10.

Appendix 18 shows the program for computing dimensionless groups using equation (81).

4.2.7.5 Range of application

Dimensional analysis of the problem in section 4.2.5 led to the relationships between dimensionless groups described by equations (50) to (53). Solutions of the heat diffusion equation (45) by the numerical matrix inversion method of the present section (4.2.7), should be consistent with this. Equation (50) is limited in range of application by the requirement that the bar shall be sufficiently long for the temperature oscillations at the contact interface to be undetectable at the opposite end of the bar. Equation (51), derived from a solution of the heat diffusion equation specifies a minimum value of the dimensionless group $(\frac{f\ell^2}{\alpha})$ above which equation (50) is applicable.

With the matrix inversion method of solution, truncation of the series in equations (4/13) and (4/14), Appendix 4 sets a maximum value of $(\frac{f\ell^2}{\alpha})$ above which calculation of $(\frac{f\ell_i^2}{\alpha})$ would not be sufficiently accurate. This maximum value of $(\frac{f\ell^2}{\alpha})$ depends on the number of terms to which the series are truncated. In this present investigation the number of terms was limited to 20 due to the size of matrix which the available computing facilities could handle.

Appendix 5 shows the effect of truncating equations (4/13) and (4/14) on the solutions A_n and B_n when $\tau_1 = \tau_2 = 10s$.

To establish the above maximum and minimum of $(\frac{f\ell^2}{\alpha})$, the input data to the computer program in Appendices 8,9 and 10 covered the range $0.008 < (\frac{f\ell^2}{\alpha}) < 160$ with the ratio of contact to periodic time, $(f\tau_c)$ held constant. Three fixed values of $(f\tau_c)$ were chosen. The lower values chosen for $(\frac{f\ell^2}{\alpha})$ were also well outside the range of $(\frac{f\ell^2}{\alpha})$ where $(\frac{f\ell_i^2}{\alpha})$ was a function of $(f\tau_c)$ alone, see equations (50) to (52). The results are shown in Tables 3 (a), (b) and (c) and Fig. 16(a) and (b) are discussed in section 4.2.7.7.

4.2.7.6 Results of numerical matrix inversion method of solution

Additional to the results in Tables 3 (a), (b) and (c) and Fig.16(a) and (b), specimen temperature-time data at various positions in the bar are shown in Tables 4 to 13 and some cases are plotted in Fig.17.

Table 14 shows computed values of $(\frac{f\ell_i^2}{\alpha})$ at various $(f\tau_c)$ at a value of $(\frac{f\ell^2}{\alpha})$ fixed at 16; a value sufficiently large for $(\frac{f\ell_i^2}{\alpha})$ to be a function of $(f\tau_c)$ alone. c.f. Fig. 16(a). The data from Table 14 is plotted in Fig.18. Appendix 11 shows a spot test to verify that the heat diffusion equation is satisfied numerically.

4.2.7.7 Discussion of results of matrix inversion method of solution

Scrutiny of Tables 3(a) (b) and (c) and Fig.16(a) shows that at any fixed value of the dimensionless group $(f\tau_c)$, the dimensionless group $(\frac{f\ell_i^2}{\alpha})$ is insensitive to changes in $(\frac{f\ell^2}{\alpha})$ when $(\frac{f\ell^2}{\alpha}) > 2$ approx. This is as expected, the $(\frac{f\ell^2}{\alpha})$ being of the same order of magnitude as that estimated from temperature fluctuations in a semi-infinite body, equation (51) and reference[33]. The largest value of $(\frac{f\ell^2}{\alpha})$ at which $(\frac{f\ell_i^2}{\alpha})$ was calculated was 160, (Table 3(b)) and the corresponding value of $(\frac{f\ell_i^2}{\alpha})$ differed very little from other values of $(\frac{f\ell_i^2}{\alpha})$ when $(\frac{f\ell^2}{\alpha}) > 2$. Calculation of $(\frac{f\ell_i^2}{\alpha})$ when $(\frac{f\ell^2}{\alpha})$ increases beyond 160 would be progressively less accurate due to truncation of equations (4/13) and (4/14), to 20 terms, see Appendix 4.

Furthermore, Table 14 and Fig. 18 show the values of $(\frac{f\ell_i^2}{\alpha})$ obtained from the analogue computer solution to be in very good agreement with those calculated by the numerical matrix inversion method. The error in the analogue computer solution based on finite-differences is thus small.

Considering further the data plotted in Fig. 16 (a) and (b) it will be notes that as $(\frac{f\ell^2}{\alpha}) \rightarrow 0$, $(\frac{f\ell_i^2}{\alpha})$ tends as expected to be asymptotic to straight lines given by equation (2/4) below, taken from Appendix 2.

$$\text{i.e.} \quad \lim_{(\frac{f\ell^2}{\alpha}) \rightarrow 0} (\frac{f\ell_i^2}{\alpha}) = \frac{f\ell^2}{\alpha} \left\{ \frac{1 - (f\tau_c)}{(f\tau_c)} \right\}^2 \qquad (2/4)$$

Tables 4-13 and Fig. 17 shows the dimensionless temperatures T/T_A fluctuates with time at various positions, $(\frac{x}{\ell})$ in the bar when $(\frac{f\ell^2}{\alpha}) = 16$. The temperature-time curves in Fig. 17 are of the shape observed in the analogue computer study, section 4.2.6. and Fig. 14. In Tables 4 - 13

it should be noted that continuity is preserved at the ends of the two separate periods, i.e. equations (4/6a) and (4/6b) Appendix 4, hold to a high degree of accuracy. Thus in Table 6 for example

$$\frac{T_1\ (x,\tau_1)}{T_A} = 0.23460861 \tag{84}$$

compared with

$$\frac{T_2(x,0)}{T_A} = 0.23467114 \tag{85}$$

and

$$\frac{T_1(x,0)}{T_A} = 0.6192917 \tag{86}$$

compared with

$$\frac{T_2(x,\tau_2)}{T_A} = 0.6193004 \tag{87}$$

The data in Tables 7-9 were also used to make a spot check that the temperature-time-distance output from the digital computer satisfied the heat-diffusion equation numerically. This was found to be so using finite differences, see Appendix 11. Additionally the data in Table 13 shows the temperature fluctuation at $\frac{x}{\ell} = 0.05$ to be very small.

4.3 Imperfect Thermal Contact Condition

4.3.1 Description of problem

Heat transfer through a system similar to that described in the opening paragraphs of section 4.2.1 and Fig. 7a is to be studied. The difference between the two systems lies in the conditions of contact between adjacent ends of the bars, (H and C in Fig. 7a), during the period of contact. With the system of section 4.2.1 and Fig. 7a, during the period of contact, actual solid-to-solid contact occurs at every point on the contact surfaces. Thus under steady state permanent contact conditions, the thermal contact resistance, (see equation (1)), is zero.

In the system to be studied now, under steady state permanent contact conditions, the thermal contact resistance will be finite.

It was shown in section 2 that thermal contact resistance arises when actual solid-to-solid contact occurs only at a number of discrete areas of the surfaces which are nominally in contact. The heat flux lines then become constricted, to pass preferentially through these discrete areas as shown in Fig. 1(a) and 1(b). Extrapolation of the steady state, permanent contact, axial temperature distribution of the bars, from a region remote from the contact surfaces reveals an apparent temperature drop ΔT_c as shown in Fig. 2, leading to the definition of thermal contact resistance given by equation (1). In the regions near the contact surfaces, since the pattern of heat flux lines, (Figs 1(a) and (b)), is three-dimensional, a calculation of thermal contact resistance under steady state, permanent contact conditions required that the Laplace equation in three-dimensions, equation (88) below must be solved.

$$\nabla^2 T = 0 \tag{88}$$

As remarked in section 3, solutions of the Laplace equation (89) have been attempted only in cases where the assumed geometrical shape of the contacting surfaces has been greatly simplified, leading to a reduction in the number of dimensions of the Laplace equation from 3 to 2. e.g. equation (89), in cylindrical co-ordinates [25],[35][37][110]

$$\frac{\partial^2 T}{\partial r^2} + \frac{1}{r}\frac{\partial T}{\partial r} + \frac{\partial^2 T}{\partial z^2} = 0 \tag{89}$$

Further simplification was made by using average boundary conditions.[35][37] These solutions required major amounts of effort and time to obtain.

Cases where periodic, solid-to-solid contact occurs only at isolated,

discrete areas of the nominally contacting surfaces, requires solution of the heat-diffusion equation in three space dimensions and time, (see equation (90) below),

$$\frac{\partial T}{\partial t} = \alpha \nabla^2 T \tag{90}$$

and hence correspondingly more mathematical and computational effort than the steady state permanent contact case.

In order to avoid this difficulty and yet to gain some kind of insight into the matter, it was decided to try to make a more readily soluble, approximate representation of the problem.

4.3.2 Approximate representation of the problem

A soluble, approximate representation of the problem of heat transfer through surfaces which make periodic contact only at isolated, discrete areas of the nominally contacting surfaces is possible using the one-dimensional heat diffusion equation (45), with appropriate boundary conditions.

4.3.2.1 Description of system

Consider such a system comprising two identical solid bars, as shown in Fig. 19 insulated to prevent transverse heat loss, whose remote ends A and B are held at different, but fixed temperatures and whose adjacent ends H and C make periodic solid-to-solid contact only at isolated, discrete areas of the end faces at H and C. Under steady state, permanent contact conditions, the temperature distribution will be as shown by the full lines in Fig. 19, (except in the region near to contact interface). The thermal contact resistance may be represented by some length, 2λ, of the bar material (of the same cross-sectional area). When the

adjacent ends H and C undergo a continuous, regular cycle of contact and separation and the quasi-steady state is reached, the time-average temperature distribution will be as shown by the chain dotted lines in Fig. 19 and the thermal resistance of the system will have increased due to the periodic interruption of the heat flow. Let this additional thermal resistance be represented by a length, $2\ell_i$, of bar material (of the same cross-sectional area of the bar).

4.3.2.2. Assumptions

(1) Events in only one of the two bars, say the hotter one, need be considered and the bar must be sufficiently long for temperature fluctuations not to be detected at the fixed temperature end of the bar; thus the length of bar ℓ should satisfy equation (47).

(2) Fig. 20 shows a temperature distribution within the bars at any time, t, when the ends H and C are making a continuous, regular cycle of contact and separation. The temperature distribution shown in Fig. 20 is at a time t, when ends H and C are in contact and the heat flow is quasi-steady.

In the region ~~of~~ near the contact interface the heat flow pattern will be three-dimensional, due to solid-to-solid contact occurring only at isolated, discrete areas of the contact interface. The temperature distribution across any cross-section of the bar, in the region near the contact interface, will be non-uniform. The temperature shown dotted in Fig. 20 represents the average temperature across the cross-section at any time, t, and is some curved extrapolation from the temperature distribution in the region where the heat flow is one-dimensional. This extrapolation leads to there being an apparent temperature drop ΔT_c across the contact interface at any time t. If it is assumed for simplicity that the interface has no heat capacity, then at the contact

interface,

$$k \frac{\partial T}{\partial x} = h \Delta T_c \tag{91}$$

where k = thermal conductivity of the bar material

h = a suitable heat transfer coefficient

(3) For simplicity let it be assumed that h is constant during the period of contact and equal to the thermal contact conductance, h_c, (see equation (2)). h_c could be found from experiments in which contact is permanent and the heat flow is steady; or, alternatively from correlated data. Likewise, the thermal contact resistance may be similarly obtained and may be expressed as a length 2λ of the bar material. The temperature gradient at the contact interface may then be expressed as

$$\frac{\partial T}{\partial x} = \frac{\Delta T_c}{2\lambda} \tag{92}$$

During the non-contact period of the cycle, let it be assumed that there is no heat transfer through the contact surfaces.

4.3.2.3. Boundary and initial conditions

Events in only one bar, the hotter one, are being considered. Let the zero of temperature now be at the mean interface temperature, T_m, shown on Fig. 20. The boundary conditions then become:-

Fig. 21 shows the steady state and quasi-steady state time average temperature distributions

1. At $x = 0$, $T(0,t) = T_A$ = constant

2. At $x = \ell$,

(i) During the non-contact period when

$$n(\tau_o + \tau_c) < t < n(\tau_o + \tau_c) + \tau_o$$

where n = 1,2,3 ..... etc.

$$\frac{\partial T}{\partial x} = 0$$

(ii) During the period of contact when

$$n(\tau_o + \tau_c) + \tau_o < t < (n+1)(\tau_o + \tau_c)$$

when n = 1,2,3 .... etc.

$$\frac{\partial T}{\partial x} = -\frac{T(\ell,t)}{\lambda}$$

Initial condition

In order to reduce the time taken for the system to reach the quasi-steady state, the initial condition was chosen as the steady-state, permanent contact temperature distribution.

$$T(x,0) = T_A\left(\frac{\ell + \lambda - x}{\ell + \lambda}\right) \tag{93}$$

4.3.2.4 Dimensional analysis

It was shown in section 4.2.5 that the thermal resistance of the system of two solid bars whose adjacent ends made periodic contact could be considered as being made up of two independent thermal resistances, namely the thermal resistance of the length, ℓ, of each bar and the thermal resistance due to periodic interruption of the heat flow. It was also shown that the relationship between the thermal resistance (expressed as length ℓ_i of bar), frequency of contact, f, and ratio of contact:periodic time ($f\tau_c$) was given by equation (50). It was assumed that when the adjacent bar ends were in contact there was solid-to-solid contact everywhere across the contact interface and hence the thermal contact resistance was zero. In the case of imperfect thermal contact during the contact period an additional variable, the thermal contact

resistance, is present and the relationship given by equation (50) has to be modified to include an additional dimensionless group.

Using the momenclature on Fig. 21, the relationship becomes:-

$$\left(\frac{f\ell_i^2}{\alpha}\right) = g\left[(f\tau_c),\left(\frac{f\lambda^2}{\alpha}\right)\right] \qquad (94)$$

for sufficiently large values of ℓ_i, given by equation (47)

4.3.3. Analogue computer solution

4.3.3.1 Simulation

The heat diffusion equation (45) was written in finite-difference form in which temperature and distance were expressed as dimensionless quantities and the E.A.L PACE analogue computer was used to solve these equations.

4.3.3.2 Finite-difference equations

The identical mesh to that used for solution of the ideal contact case, section 4.2.6.2 was employed. Except for the finite-difference equation (3/15) which expressed the boundary condition at the contact interface during the period of contact, the identical finite-difference equations to those in section 4.2.6.2 and/or Appendix 3 had to be solved. (see equations (3/9) to (3/13) and (3/19)). The finite-difference equation appropriate to the imperfect contact boundary condition, 2(ii) in section 4.3.2.3 is derived in Appendix 13 and is repeated below.

$$D(\Delta\Theta_7) = 62.5\,\Delta\Theta_6 - 62.5\Delta\Theta_7\left(1 + \frac{\Theta_\ell}{100\,\Theta_\lambda}\right) \qquad s^{-1} \qquad (13/9)$$

As in section 4.2.6.2 the steady state permanent contact temperature distribution was used as the datum from which temperature measurements

were made. Fig. 22 shows the dimensionless temperature Θ plotted against dimensionless distance X in the steady state permanent contact and steady state non-contact condition together with the time-average temperature when in the quasi-steady state.

4.3.3.3. Circuitry

The EAL Limited PACE analogue computer was used to solve the relevant finite-difference equations. The circuitry and instrumentation used was identical to that described in section 4.2.6.3 and Fig. 11 except that part required to simulate the new boundary condition given by equation (13/9). The modified circuit employed is shown in Fig. 23. The switch in the input to amplifier 4 was magnetically operated and its frequency and ratio of closed time:open time could be varied as in section 4.2.6.3.

Setting of thermal contact resistance

When the switch in the input to amplifier 4 is in the closed position the output of amplifier 4 will be given by

$$D(\Delta v_7) = -100((0.625 + \beta)\,\Delta v_7 - 0.625\,\Delta v_6) \qquad Vs^{-1} \tag{95}$$

where β is the proportion of the voltage Δv_7 tapped off potentiometer 19 and corresponds to equation (13/9). When a steady state is reached $D(\Delta v_7) = 0$ and hence

$$\Delta v_7 = \frac{0.625\,\Delta v_6}{(0.625 + \beta)} \tag{96}$$

comparison of equation (96) with equation (13/9) with $D(\Delta\Theta_7) = 0$ shows that

$$\beta = \frac{0.625\Theta_\ell}{100\,\Theta_\lambda} = \frac{0.625}{100}\,\frac{\ell}{\lambda} \tag{97}$$

Thus the setting of potentiometer 19 fixes the ratio of the length of

solid bar ℓ, to the length of solid bar λ equivalent to the thermal contact resistance. The setting, β, of potentiometer 19 was made with the switch in the closed position and isolating amplifier 4 from the rest of the circuit by removing the input lead to it from amplifier 3. This part of the input to amplifier 4 was replaced by an input, e_i, of 10V fed to the summing junction via a 200 kΩ resistor. The output, e_o of amplifier 4 is then given by

$$e_o = \frac{-e_i}{2(0.625 + \beta)} \tag{98}$$

The value of ℓ/λ ($=100\beta/0.625$) was set by adjusting potentiometer 19 until the required value of e_o was reached.

4.3.3.4 Procedure

With the switch in the input to amplifier 4, Fig. 23 in the open position, setting procedure described in section 4.2.6.4 was carried out. The thermal contact resistance was set as described in section 4.3.3.3. Tests in the quasi-steady state, similar to those described in section 4.2.6.4 were then conducted to obtain the value of the dimensionless group $(\frac{f\ell_i^2}{\alpha})$ at various $(f\tau_c)$ at various fixed values of $(\frac{f\lambda^2}{\alpha})$. Each test involved measurement of the amplifier outputs Δv_7, Δv_1 and Δv_2. The latter two outputs did not fluctuate except when the frequency of contact was low and were observed with a digital voltmeter; mean values Δv_1 and Δv_2 were therefore observed. Δv_7 was recorded on a U.V. recorder to determine the frequency of switching and ratio of contact tine: periodic time, $(f\tau_c)$. Fig. 24(a) shows a typical trace of Δv_7, representing temperature fluctuation at the contact interface.

Determination of ℓ_i

Referring to Fig. 22 it will be seen that by similar triangles

$$\frac{\Theta_\lambda + \Theta_\ell}{(1 + \frac{\lambda}{\ell} + \frac{\ell_i}{\ell})} = \frac{0.2\Theta_\ell + \Theta_\lambda + \overline{\Delta\Theta}_1}{(0.2 + \frac{\lambda}{\ell} + \frac{\ell_i}{\ell})} \tag{99}$$

and since

$$\frac{\Theta_\lambda}{\lambda} = \frac{\Theta_\ell}{\ell} \tag{100}$$

equation (99) reduces to

$$\ell_i = \frac{\ell(1 + \frac{\lambda}{\ell})\ \overline{\Delta\Theta}_1}{0.8\Theta_\ell - \overline{\Delta\Theta}_1} \tag{101}$$

$\overline{\Delta\Theta}_1$ being determined from the measured voltages $\overline{\Delta v}_1$, Δv_{1_s} and the set thermal contact resistance.

4.3.3.5 Results

The results are tabulated in Tables 15-22 and are plotted out in Fig.24(b).

4.3.3.6 Discussion of Results

Fig. 24(b) demonstrates the validity of the relationship given by equation (94). A measure of the importance of thermal contact resistance on heat flow may be illustrated by reference to Fig. 25 which is derived from Fig. 24(b). Heat flow through the system of two bars of conducting material whose adjacent ends are brought into contact and separated cyclically may be expressed by the ratio (Q/Q_c) where Q = heat transfer rate under periodic contact conditions (quasi-steady state) and Q_c = heat transfer rate under permanent contact conditions in the steady state when the thermal contact resistance is zero.

(Q/Q_c) is given by

$$\frac{Q}{Q_c} = \frac{\ell}{\ell + \lambda + \ell_i} \tag{102}$$

Tables 23 - 25 shows the tabulated data for Fig. 25 which illustrates the way in which the heat flow through the system alters with the ratio of contact time:periodic time ($f\tau_c$). As ($f\tau_c$) falls the reduction in heat flow becomes more marked as the thermal contact resistance increases, being as much as a 30% reduction when ($f\tau_c$) changes from 1.0 to 0.5 with a contact resistance equivalent to a 28.3mm length of bar.

Estimation of the error in the solution of the finite-difference equations due to the use of a non-uniform mesh was not attempted. It was feared that the error might be appreciable, so an attempt to develop an iterative method of solution which did not rely on finite-difference approximations to the heat diffusion equation was made. This method and its results are described in section 4.3.4.

4.3.4 Iterative method of solution

4.3.4.1 Formulation

A solution of the diffusion equation (45), subject to the boundary conditions given in section 4.3.2.3 is required. Only the solution for the quasi-steady state is needed. Boundary conditions 2(i) and 2(ii) at the contact interface $x = \ell$ may alternatively be combined and expressed as

$$\left.\frac{\partial T(x,t)}{\partial x}\right|_{x=\ell} = f(t).T(\ell,t) \qquad (103)$$

where f(t) is a periodic function of time t alone. Fig. 26 shows the function f(t) appropriate to the present case, f(t) being zero during the non-contact period and some fixed value, μ,

$$\mu = -\frac{1}{\lambda} \qquad (104)$$

during the contact period.

4.3.4.2 Basis of the method

Fig. 27 shows a series of bars of conducting material each of length, ℓ The temperature within each bar and at the ends are those which occur at each stage of an iterative process. Thus $T_i(x,t)$ is the temperature after the ith iteration.

Conditions at commencement of iterations are as shown in the uppermost figure in Fig. 27. Thus the temperature within the bar $T_o(x,t)$ is uniform at value T_A. The boundary conditions are:

At x = o,

$$T_o\ (o,t) = T_A \tag{105}$$

At x = ℓ,

$$\left.\frac{\partial\ _o(x,t)}{\partial x}\right|_{x=\ell} = o \tag{106}$$

The next figure in Fig. 27 shows the conditions after the first iteration; the temperature within the bar being $T_1(x,t)$ with boundary conditions:

At x = o,

$$T_1(0,t) = 0 \tag{107}$$

At x = ℓ,

$$\left.\frac{\partial T_1(x,t)}{\partial t}\right|_{x=\ell} = f(t)\ \ T_o(\ell,t) \tag{108}$$

where f(t) is a function of time. The remaining figures in Fig. 27 show the conditions after each successive iteration.

Summation of the temperatures $T_i(x,t)$ after "m" iterations with $m \rightarrow \infty$, leads to the temperature T(x,t) within the bar being:-

$$T(x,t) = \sum_{m=o}^{\infty} T_m(x,t) \tag{109}$$

Summation of the boundary conditions at x = o is

$$T(0,t) = \sum_{m=0}^{\infty} T_m(0,t) = T_A \qquad (110)$$

Summation of boundary conditions at $x = \ell$ is

$$\left.\frac{\partial T(x,t)}{\partial x}\right|_{x=\ell} = f(t).\sum_{m=1}^{\infty} T_{m-1}(\ell,t)$$

$$= f(t).\ T(\ell,t) \qquad (111)$$

Equation (110) is boundary condition 1 in section 4.2.3.1. If in equation (111), the function f(t) is periodic, being zero when $n(\tau_o + \tau_c) < t < n(\tau_o + \tau_c) + \tau_o$, (where n = 0,1,2 ...), and being $-\frac{1}{\lambda}$ when $n(\tau_o + \tau_c) + \tau_o < t < (n+1)(\tau_o + \tau_c)$, (where n=0,1,2...), then equation (111) expresses boundary condition 2 in section 4.2.3.1.

Provided that the summations are convergent, the required temperature T(x,t) in the quasi-steady state may be found.

The iterative process is explained in detail and the equations of iteration are developed in Appendix 14. The required series for f(t) is derived in Appendix 15 and derivation of an important function used in Appendix 14 is given in Appendix 16.

4.3.4.3 Execution of the process

A complete temperature-time history at various points in the system was not attempted. For purposes of comparison of the results of the iterative solution with those of the analogue computer solution, section 4.3.3, the time-average temperature at a given point was found and from this the dimensionless group $(\frac{f\ell_i^2}{\alpha})$ was evaluated.

Determination of ℓ_i and λ

The expression used to determined the instantaneous temperature at any point was the sum of a steady component and a fluctuating component, see equation (14/48) in Appendix 14.

The steady or time-average component could be found from the equations gathered together in Appendix 14 i.e. equation of iteration listed on page 322

The computer program for doing this is shown in Appendix 17.

Referring to Fig. 21 which shows the steady state permanent contact and the time-average quasi-steady state temperature distributions. If the time-average temperature, $\overline{T}(\ell)$ at distance $x = \ell$ from the heated end of the system is known then

$$\ell_i = \left\{ \frac{T(\ell)}{T_A - T(\ell)} \right\} \ell - \lambda \qquad (112)$$

The value of λ, see boundary condition 2 in section 4.3.2.3 is related to the value of f(t) see equation (111) by

$$f(t) = -\frac{1}{\lambda} \qquad (113)$$

for $n(\tau_0 + \tau_c) + \tau_0 < t < (n+1)(\tau_0 + \tau_c)$ (with n = 0,1,2...)
see Fig. 26 where $\mu = -\frac{1}{\lambda}$

In the series for f(t) derived in Appendix 15, values of μ_1 and μ_2 were required in equations (15/9) and (15/10) in order to obtain the values of the terms of the series. The values appropriate to the boundary conditions at $x = \ell$ are

$$\mu_1 = 0 \qquad (114)$$

$$\mu_2 = -\frac{1}{\lambda} \qquad (115)$$

Computation

The input data required for the computer program, Appendix 17 was periodic time, τ, of the cycle of contact and separation, $(1/\sqrt{\text{diffusivity}})$ length of the bar ℓ, μ_1, and μ_2 equations (114) and (115), period of contact τ_c, and distance, x, along the bar from the fixed temperature end. The principal part of the output from the program was the dimensionless groups $(\frac{f\ell_i^2}{\alpha})$, $(\frac{f\lambda^2}{\alpha})$, $(\frac{f\ell^2}{\alpha})$ and $(f\tau_c)$. Variation in the input data was made in order that the output could be compared with the results of the analogue computer study, see Fig. 24. The value of $(\frac{f\ell^2}{\alpha})$ was greater than the minimum required for $(\frac{f\ell_i^2}{\alpha})$ to be a function of $(f\tau_c)$ and $(\frac{f\lambda^2}{\alpha})$ alone; see equation (94), section 4.3.2.4.

4.3.4.4 Results of iterative method

Effect of varying $(f\tau_c)$ at fixed $(\frac{f\lambda^2}{\alpha})$

As a start the input data was chosen with periodic time τ, $(1/\sqrt{\text{diffusivity}})$, bar length ℓ, μ_1, μ_2 and distance x fixed and with contact period τ_c variable. This gave a fixed value for each of the dimensionless groups $(\frac{f\ell^2}{\alpha})$ and $(\frac{f\lambda^2}{\alpha})$

The results of this are shown in Table 26 and are plotted in Fig. 28 against the background of the results obtained from the analogue computer solution of the problem. These and other results reported below are discussed in section 4.3.4.5.

Because of increasingly slow convergence of the series $\sum_{m=1}^{\infty} T_m(\ell,t)$ with $(f\tau_c)$, the values of $(\frac{f\ell_i^2}{\alpha})$ was not determined for values of $(f\tau_c) \geqslant 0.5$. In order to do this the periodic time τ and μ_2 $(=-\frac{1}{\lambda})$ were altered simultaneously to maintain $(\frac{f\lambda^2}{\alpha})$ unchanged. Slow convergence and

divergence of the series $\sum_{m=0}^{\infty} T_m(\ell,t)$ occurs in some instances. These results are plotted in Fig. 29 .

Some results are shown in Table 29 and where possible have been plotted against a background of the analogue computer results, Fig. 29.

4.3.4.5 Discussion of results of iterative method

Where convergence of the series $\sum_{m=0}^{\infty} T_m(\ell,t)$ is sufficiently rapid for calculation of the dimensionless group $(\frac{f\ell_i^2}{\alpha})$ to be made, Figs. 28 and 29 shows the results of the analogue computer solution to be in good agreement with the iterative method. In such cases, the error due to the particular finite-difference approximation used on the analogue computer would thus appear to be small.

Inspection of the values of $(\frac{f\ell_i^2}{\alpha})$ in Table 28 shows that over the range $0.3 < \frac{f\ell^2}{\alpha} < 100$, the $(\frac{f\ell_i^2}{\alpha})$ are not very sensitive to changes in $(\frac{f\ell^2}{\alpha})$ and thus equation (94) holds.

The cases where the summation $T_m(\ell,t)$ is divergent could be dealt with by modifying the iteration process at $x = \ell$ into the form

$$\frac{\partial T_m(\ell,t)}{\partial x} = f(t)\left\{\beta T_{m-1}(\ell,t) + \gamma T_{m-2}(\ell,t)\right\} \qquad \text{for } m > 3, \qquad (116)$$

and where $\beta + \gamma = 1$ (117)

see Fig.30, provided that when $\beta = 1$ and $\gamma = 0$, (i.e. the original case), successive values of $T_m(\ell,t)$ alternate in sign. This is the case for the last entry in table 28 and the first in table 29.

$\left.\frac{\partial T_m(x,t)}{\partial x}\right|_{x=\ell}$ when $m \geqslant 0$ will be as shown at the

upper stages of Fig. 30. Referring to Fig. 30, the boundary conditions and temperature will be given by:-

Boundary condition at x = 0

$$T(0,t) = \lim_{r \to \infty} \sum_{m=0}^{r} T_m(0,t) = T_A \tag{118}$$

The temperature at any point x at time t:-

$$T(x,t) = \lim_{r \to \infty} \sum_{m=0}^{r} T_m(x,t) \tag{119}$$

Boundary condition at x = ℓ

$$\left.\frac{\partial T(x,t)}{\partial x}\right|_{x=\ell} = \lim_{r \to \infty} \sum_{m=0}^{r} \left.\frac{\partial T_m(x,t)}{\partial x}\right|_{x=\ell}$$

$$= \lim_{r \to \infty} \left[f(t) \left\{ \beta T_{r-1}(\ell,t) + \sum_{m=0}^{r-2} T_m(\ell,t) \right\} \right] \tag{120}$$

5. EXPERIMENTAL WORK

5.1. Object

The object of the experimental work was:

(a) To try to establish the extent to which data obtained from theoretical study ~~was~~ were applicable to a real system in which heat was transferred through periodically contacting surfaces.

(b) To consider some effects not included in the theoretical study which might be expected to influence heat transfer in the above system. The effects considered were contact geometry, surface wear and impact.

5.2 Test Apparatus

Two separate pieces of test apparatus were made. Experience with the first test apparatus, termed "test rig No. 1" indicated that transverse heat flows could not be sufficiently well controlled for sufficiently reliable estimates of thermal resistance to be made. A second apparatus termed "test rig No. 2" was made in an attempt to overcome this problem.

5.2.1 Test rig No. 1

This test rig is shown schematically in Fig 31(a). The rig contained a heated bar and a cooled bar; one end of the former could be brought into contact with or separated from the latter by angular motion of a rocker arm which was operated by a rotating cam. The cam shaft was belt driven from a d.c. motor whose speed could be varied. When in contact, the bar ends were kept together by the force exerted by a spring; the self-aligning bearing permitted slight movement so that the contact faces of the two bars could seat squarely together. The heated bar

was screwed for a length of 40 mm at its coupling end for fixing its coupling flange and to provide location for insulated heater wire which was wound on it.

The two bars, in each of which 5 thermocouples were located were made of steel to specification EN52(c) BS970 - 1955; their dimensions being as shown in Fig.31(b). Each bar was insulated with felt of thermal conductivity 0.0655 W/mK outside which a thin-walled mild steel guard tube with 5 thermocouples located in it was fitted over the insulation. Guard heaters were wound over the outside of each tube.

Determination of the ratio contact time:periodic time ($f\tau_c$) was by measuring the angle through which the camshaft drive pulley rotated while the bars were in contact. Frequency of contact was determined by measuring the time taken for a given member of revolutions of the pulley with a stop watch.

5.2.2 Instrumentation

5.2.2.1 Thermocouples and temperature recording equivalent

Chromel-alumel thermocouples made from twin insulated thermocouple wire 0.122 mm (0.0045 in) diameter supplied by Saxonia Electrical Wire Co. Limited, Greenwich were used throughout. They were soft-soldered into their locations in the bars and the guard tubes, as indicated in Fig. 31(b) and (c). Each thermocouple lead was wrapped once around the outer surface of the bar or guard tube in the neighbourhood of its hot junctions and thence to the cold junctions located in melting ice.

The outputs of the thermocouples, were recorded by a 24 channel

potentiometer type recorder made by Honeywell Controls Limited whose designation for the recorder was type 15305825 - 24 - 0 - 000 - 002 - 10. This recorder printed the output from each channel at the rate of 1 channel every 18 s. The range was 0 - 6 mV with a specification accuracy of $\mp$ 20 μV and reproducibility to within 5μV. With the thermocouple materials used, (chromel-alumel), this represented $\mp$0.5K and 0.125K respectively.

5.2.2.2 Calibration of thermcouples

All the thermocouples were made from the same batch of thermocouple wire and calibrated individually in an NPL pattern calibration tank of the kind described in reference[127], against small range, mercury-in-glass thermometers having a certified accuracy of $\mp$ 0.02K. The temperature range of the thermocouple calibration tests was 20 - 120°C.

5.2.2.3 Contact surface preparation

Each bar had its contact end faced off square to its axis in a lathe using a fine feed of the facing tool. No further preparation was carried out. The surface roughness and hardness of each surface was:-

Surface roughness:

Heated bar	1.5 μm C.L.A.
Cooled bar	0.5 μm C.L.A.

Vickers hardness:

Heated bar	271 kg/m.m^2 2659 N/mm^2
Cooled bar	277 kg/mm^2 2171 N/mm^2

5.3. Test Procedure

5.3 Test procedure - test rig No. 1

5.3.1 Determination of steady and quasi-steady states

Referring to the diagram of test rig No. 1, Fig. 31(a), when the heated bar was in contact with the cooled bar, the force on the contact surfaces was 178N, (40 lbf), this being determined by measuring the force required to just separate the contact faces using a spring balance.

Initially tests were conducted with the bars permanently in contact. Tests under periodic contact conditions followed these. The test procedure at each condition was as follows:-

With the heaters energised, cooling water flowing, and the chart drive of the 24 channel temperature recorder running continuously, the thermocouple outputs were recorded one at a time at 18 second intervals. Thus the recorder took 7 minutes 12 seconds to record the 24 outputs necessary to obtain a complete temperature distribution in the bars and guard tubes. Even after many hours of continuous operation at one condition of contact, successive temperature distributions were not absolutely identical. Instead the temperatures tended to oscillate slowly and irregularly about a mean value, the periodic time being 2 - 6 hours. The amplitude of these oscillations was about 1.25K at the hottest position on the heated bar, but about 0.5K at the coolest position in the cooled bar.

5.3.2 Temperature distributions

The temperature distributions in the bars and guard tubes were non-linear, and particularly with the heated bar and its guard tube, the temperature distribution in the guard tube was very poorly matched to that in the bar. The best that could be done was to try to adjust

the guard heater current to make the temperature near the contact interface end similar to that of the corresponding position in the bar.

These latter shortcomings led to the replacement of test rig No. 1 by test rig No. 2. Some results from test rig No. 1 were obtained by selecting the extremes of the temperature distributions at each test condition and computing the required dimensionless groups from them. These are presented and commented upon in sections 5.4 and 5.5.

5.3.3. Determination of thermal resistance from temperature distributions

In order to compare experimental data with theoretical predictions shown by Fig. 24 (b), thermal resistance was required to be expressed as an equivalent length of bar.

A computer program for finding the equation to a curve of best fit among experimental data points, was used to find a quadratic expression for the temperature distribution in each bar and each guard tube. The heat flux through the contact interface was computed from these quadratic temperature distributions thus:

Consider Fig. 32 which shows temperature distribution in each bar and guard tube. In the heated bar the axial heat flow rate QZH at a given position x is

$$QZH = k_b A(a_1 + 2a_2 x) \qquad (120(a))$$

where k_b = thermal conductivity of bar material, A = cross-sectional area. The transverse heat flow QRH over the length x is

$$QRH = \frac{2\pi k_i x \, \Delta T_m}{\log \frac{r_2}{r_1}} \qquad (120(b))$$

where k_i = thermal conductivity of insulation

r_1 and r_2 = inner and outer radii of insulation

ΔT_m = mean temperature difference between bar and guard tube over length x.

The axial heat flow through the contact interface QAH is then

$$QAH = QZH - QRH \qquad (120(c))$$

This was calculated for various values of x. Temperature distribution in the cooled bar and its guard heater were similarly processed to determine the heat flow through the interface QAC for various values of x. The heat flow Q used for calculation of thermal resistance offered by the interface was that when QAH = QAC.

Since the origin for all the equations of temperature distribution was the contact interface, the interface temperature drop was $(a_o - a_3)$. The length of bar β, equivalent to the thermal resistance offered by the contact interface was given by

$$\beta = \frac{k_b A (a_o - a_3)}{Q} \qquad (120(d))$$

5.3.4 <u>Determination of thermal resistance due to periodic interruption of the heat flow</u>

In order to compare experimental data with that predicted theoretically shown by Fig. 24(b), thermal resistance is required to be expressed as an equivalent length of bar. The relevant lengths are those due to:

(a) Thermal contact resistance

(b) Periodic interruption of the heat flow

The length appropriate to (a) in Fig. 24(b) is λ, (this is half the value due to thermal contact resistance, because in the theoretical work, events in only one bar were studied). Similarly the length appropriate to (b) in Fig. 24(b) is ℓ_i. Thus in the experimental work, under steady state, permanent contact conditions,

$$\beta_{ss} = 2\lambda \qquad (120(e))$$

where β_{ss} = length of bar equivalent to thermal contact resistance
Under quasi-steady, periodic contact conditions

$$\beta_{qs} = 2(\lambda + \ell_i) \qquad (120(f))$$

where β_{qs} = length of bar due to thermal resistance in quasi-steady state. Thus

$$\ell_i = \tfrac{1}{2}(\beta_{qs} - \bar{\beta}_{ss}) \qquad (120(g))$$

Tests in the steady state permanent contact condition were performed several times to establish a mean value of β_{ss}, since it was found that if the surfaces were separated and then brought into contact again after each determination of β_{ss} the value of β_{ss} was not reproducible.

ℓ_i for each test in the quasi-steady state was found from

$$\ell_i = \tfrac{1}{2}(\beta_{qs} - \bar{\beta}_{ss}) \qquad (120(h))$$

where $\bar{\beta}_{ss}$ = mean value of β_{ss}.

Serious errors in ℓ_i could arise if β_{qs} and β_{ss} are not accurately measured.

5.3.5 Dimensionless groups

From section 4.3.2.4 relevant dimensionless groups are $(\frac{f\ell_i}{\alpha})^2$, $(f\tau_c)$ and $(\frac{f\lambda^2}{\alpha})$; (where $\lambda = \frac{1}{2}\bar{\beta}_{ss}$ above). In evaluating these groups the value of thermal conductivity k_b and k_i and thermal diffusivity were obtained from tests from samples of bar material and insulation. The tests were carried out by Brown-Firth Research Laboratories, Altercliffe Road, Sheffield 4 and the Department of Building, University of Aston. The results were

Bar material: $k_b = 15.73 + 5.2 \times 10^{-3}T + 1.093 \times 10^{-4}T^2$

where T = temperature in ^oC

$$\text{Diffusivity } \alpha = \frac{k_b}{7630(456 + 0.562T)} \quad \frac{m^2}{s}$$

The expression for diffusivity was obtained from British Iron and Steel Research Association.

Thermal insulation $k_i = 0.0655$ W/mK

5.4 Results of Tests with Test Rig No.1

Contacting materials:- EN 52(c) B.S. 970 1955 steel

Contact surface roughness Heated member 1.5μm C.L.A. , Cooled member 0.5μm C.L.A.

Contact surface hardness (Vickers) Heated member 2659 N/mm^2, Cooled member 2717 N/mm^2

Static Load on contact surface - 178N (40lbf) Contact gap 0.76mm (0.030 in)

Thermal contact resistance (equivalent length of bar) Mean value 15.8 mm range of variation from 5.0 to 25.4 mm
Standard deviation 3.9 mm

Set No.	$\left(\frac{f\lambda_m^2}{\alpha}\right)$	Table No.	Fig. No.	Comparison of $\left(\frac{f\ell_i^2}{\alpha}\right)$ with theory
1	0.4 - 0.8	30(a)	33(a)	Scattered about theoretical values (0.2 to 10) x theoretical value
2	0.8 - 1.0	30(b)	33(b)	Scattered about theoretical values (0.3 to 8) x theoretical value
3	1.6	30(c)	33(c)	Good agreement 0.8 x theoretical value
4	1.8 - 2.0	30(d)	33(d)	Good agreement 0.9 x theoretical value
5	3.2 - 4.4	30(e)	33(e)	Scattered about theoretical values (0.1 to 1) x theoretical value; mostly low
6	6.2 - 7.6	30(f)	33(f)	Scattered about theoretical values (0.15 -10) x theoretical value; mostly low.
7	11.0 - 15.5	30(g)	33(g)	Scattered about theoretical values (0.2 to 3) x theoretical value
8	21 - 30	30(h)	33(h)	Higher than theoretical values (1 to 3) x theoretical value

TABLE I SUMMARY OF RESULTS: TEST RIG NO. 1

5.4 Results of Tests with Test Rig No.1

84 values of the dimensionless group $(\frac{f\ell_i^2}{\alpha})$ obtained experimentally are presented in Table I. The quantities varied independently were frequency of contact, f and ratio of contact time:periodic time $(f\tau_c)$. The highest temperatures in the heated bars ranged from 110 to 130°C, while the lowest temperatures in the cooled bar was 25 to 30°C.

5.5 Discussion of Results obtained with Test Rig. No.1

Experiments, the results of which are summarised in Table I, section 5.4 and plotted in Figs. 33(a) to (h), show that a real system in which heat is transferred through periodically contacting surface, behaves in a similar manner to that predicted by theoretical study, section 4.3.

Faced with the design problem stated in section 1.2, the plot of the non-dimensional groups $(\frac{f\ell_i^2}{\alpha})$ against $(f\tau_c)$ at various fixed $(\frac{f\lambda^2}{\alpha})$ shown in Fig. 24(b) can be used to obtain a first order approximation of the average thermal resistance due to periodic interruption of the heat flow at the contact interface. However, the experimental results suggest that wide variations, as much as $\mp$ 1 order of magnitude about the average theoretical value of $(\frac{f\ell_i^2}{\alpha})$ can be expected.

This is due at least in part to variation in thermal contact resistance between successive meetings of the surfaces causing the temperature distributions to vary so that the system was never in a truly quasi

steady state. The mean value and range of thermal contact resistance recorded are given above, Table I in section 5.4.

However, more important with test rig No. 1 was the fact that the guard heaters on test rig No. 1, fig 31(a), particularly that guarding the heated bar, could not be adjusted satisfactorily to reduce transverse heat flow to a level at which the correction for transverse heat flow would be small. (Transverse heat flows of the order of 30% of the axial heat flow were often encountered). Since the component of thermal resistance due to periodic interruption of the axial heat flow, (characterised by bar length ℓ_i) is calculated from the difference between two thermal resistances, (see equation 120(h)), the experimental error in ℓ_i could be large and the error in the dimensionless group $\left(\frac{f\ell_i^2}{\alpha}\right)$ would be larger still because of the squaring of ℓ_i.

In view of these thermal resistance determination difficulties, it was decided to build a second test apparatus, test rig No. 2, in which an attempt would be made to make transverse heat flows significantly smaller.

5.6 Redesigned Test Apparatus

5.6.1 Test rig No. 2

Fig 34(a) shows schematically test rig No. 2 and Fig. 34(b) shows a photograph of it. Referring to Fig. 34(a) the rig contained two copper bars 25.4 mm (1 in) diameter arranged vertically. The lower end of the upper copper bar could be brought into contact or separated from the upper end of the lower bar by the motion of the piston of the pneumatic cylinder at the top of the rig. When compressed air

was supplied to the pneumatic cylinder, the upper copper bar was lifted upwards and out of contact with the lower bar, the stroke of the cylinder being limited by a stop. When the air pressure was released the upper bar moved downwards under gravity and the force of the return spring until its lower end made contact with the upper end of the lower copper bar. The coupling was arranged so that when the bars were in contact the force on the contact surfaces was due solely to the weight of the upper copper bars, steel extension bar and insulation, this force amounting to 33.4N (7.5 lbf).

The frequency of contact, f, and ratio of contact time:periodic time($f\tau_c$) could be varied by the opening and closing of electrical solenoid-operated air valves, one in the compressed air supply line and the other in the exhaust line. The valve operation was controlled by the opening and closing of a cam-operated micro-switch. The camshaft was driven via a reduction gear box by a small electric motor whose speed could be varied. The cam dwell angle could be adjusted.

The upper end of the upper copper bar was maintained in firm contact with an electric heater, by the steel extension bar screwed to the bar. The lower copper bar had a cooling jacket screwed on to its lower end; the cooling jacket was mounted on a ball seating so that the contact faces of the copper bars could seat squarely together when in contact.

The two copper bars were surrounded by a copper tube 32.41 mm (1.276 in) bore x 35.05 mm (1.38 in) outside diameter which was fixed in firm contact over the lower end of the steel extension bar, but was free to slide over a collar surrounding the lower copper bar near the cooling jacket. The copper tube was surrounded by "sil-o-cel" thermal

insulation 7.62 ~~mm~~ cm (3 in) diameter and of thermal conductivity 0.044 W/mK.

5.6.2 Instrumentation

5.6.2.1 Thermocouples and temperature measuring equipment

Chromel-alumel thermocouples made from twin insulated wire 0.122 mm (0.0048 in) diameter were located in the bars in the positions shown in Fig. 35(a). Each bar had four radial drillings 0.814 mm (0.032 in) diameter and 12.7 mm (½in) deep at the bottom of which a thermo junction was positioned, each junction being held in place with "Araldite" and epoxy resin. The leads emerging from these holes were wrapped around the outer surface of the bar in the neighbourhood of each drilling and then brought out axially along each bar to the cold junctions located in melting ice. In addition to these four thermocouples each bar had a thermocouple located at the outer surface of the bar diametrically opposite the entrance to each hole making, so far, eight thermocouples in each bar. The thermocouples junctions located on the outer surface were held in contact with the bar by silver-impregnated epoxy resin, of the kind used to improve electrical contact, made by Johnson Matthey and Co. Limited. Each insulated thermocouple lead was wrapped around the bar and then led axially away to the cold junction. Two further thermocouples were installed in each bar making a total of ten per bar. These latter thermocouples were located on the outer surface of the bar at two diametrically opposite positions, both being close to the contact end of the bar as shown in Fig. 35(a). Fig. 35(b) is a photograph of the two copper bars and cooling jacket with the thermocouples installed in them.

Thermocouple outputs were indicated on a Solartron type LM 1420.2 digital voltmeter whose digital display could discriminate to the nearest 2.5 μv. The accuracy of the digital volmeter over the range

used was $\mp$ 2.5 μv . Reproducibility, according to the manufacturers specification should be $\mp$ 0.01 per cent over one year, with a drift of 0.05 per cent/^{o}C temperature change. With the thermocouple materials used, 2.5 μV corresponded to a temperature change of about 0.0625K.

5.6.2.2 Calibration of thermocouples

24 thermocouples were made from the same batch of thermocouple wire and calibrated individually in an NPL pattern calibration tank, of the kind described in reference[127], against small range, mercury-in-glass thermometers having a certified accuracy of $\mp$0.02K. The temperature range of the thermocouple calibration tests was 19 - 110°C. The individual thermocouple calibrations were found to be almost identical and a common calibration table was produced.

5.6.2.3 Detection of contact and separation periods

Initially the frequency of the cycle of contact and separation of the copper bars was determined by timing, with a stop watch, a known number of cycles which were determined by listening to the noise emitted by the test rig when running. The ratio of contact time:separation time was deduced from the profile of the cam which operated the micro-switch controlling the operation of the pneumatic cylinder. These methods were later refined as described below.

First refinement

With the first refinement, the instants of contact and separation were detected using a photocell and shutter arrangement shown in Fig. 36. A light beam from a lamp mounted in a tube made of "Tufnol" passed through a pin-hole in a disc supported in the tube. A sheet metal

shutter attached to the extension bar connected to the upper copper bar and moving with it, passed through a transverse slot in the supporting tube, allowing the light beam to impinge on the photocell when the contact faces of the two copper bars in Fig. 34(a) were separated and interrupting the beam when the bars were in contact. The output of the photocell was connected to the galvanometer of an ultra-violet (U.V.) recorder. The periods of contact and separation produced a "stepped" trace when the U.V. recorder paper feed was switched on from which the ratio of contact time:periodic time ($f\tau_c$) could be determined from measurements of the trace. Frequency of contact was determined by comparing the length of trace for several cycles with the time marks recorded by the automatic time marker of the U.V. recorder.

Second refinement

In later tests, the photocell was replaced by a simple electrical resistance network which was used to observe the electrical resistance of the contact interface during the period of contact as well as the instants of contact and separation. The circuit is shown in Fig. 37. Modifications were made to render the upper copper bar (Fig.34(a)) electrically separate from the main part of the apparatus.

The resistor R_2 in Fig. 37 was of similar value to the resistance of the two copper bars (plus the electrical resistance of the contact interface when the bars were in contact). R_2 was connected in parallel with the copper bars. A resistor, R_1, connected in series with this parallel network was of high value (20Ω) compared with that of the network, so that current drawn from the 2V cell was hardly altered by the contact and separation of the copper bars. The p.d. across

resistor R_2 when the copper bars were separated was about twice that when the bars were in contact. This p.d. was applied to the U.V. recorder galvanometer so that the periods of contact and separation could be detected.

5.6.2.4 Contact surface preparation

Lapped surfaces

With the test rig partly assembled; i.e. referring to Fig. 34(a), but with the pneumatic cylinder, its mounting and the coupling removed, the contact faces were lapped together in situ using a fine carborundum paste. The grade used was Grade W made by Flexible Abrasives Limited, Portsmouth. The lapping motion was effected by rotating the upper copper bar about its longitudinal axis in alternating directions with its lower face in contact, (via the carborundum paste), with the upper face of the stationary lower copper bar. During the lapping process the sub-assembly comprising the upper copper bar, copper tube and insulating jacket were lifted clear of the lower copper bar, so that both contact faces could be inspected to assess visually progress of the lapping. Since the copper tube was not separated from its fixing to the upper copper bar, the contact face of this bar was viewed by shining a light down the inside of the tube to illuminate it.

When it was judged that the lapping marks showed over the whole contact area of each bar, the carborundum was removed from each surface which were then washed off with ethanol. (Wipers on the end of a length of tube were used to reach the contact face of the upper copper bar since it was located about half-way along the axis of its enclosing copper tube, see Fig. 34(a). When the surfaces were cleaned and without disturbing the fixing of the copper tube to the upper copper

bar, the test apparatus was completely assembled and ready for test.

No attempt was made to measure the profile of the lapped surface because dismantling to enable the copper bars to be passed to the profilometer would have disturbed the relative position of the contact surfaces. However, the surface roughness and hardness of two other pieces of copper bar which had been lapped together with the same lapping compound used for the above surface preparation was found to be:

Surface roughness	1.2 - 1.6 μm C.L.A.
Vickers hardness	97.7 to 102 kg/mm^2
	958 to 1000 N/mm^2

It should be remarked however that the surface was badly damaged by the stylus, as found by Dennis and Fuggle[30], section 3.2.2.7.

Surfaces coated with silver-impregnated epoxy resin

In later tests, in order to reduce thermal contact resistance, the contact surfaces were coated with silver-impregnated epoxy resin of the kind used to improve electrical contact. It was type FSP 49R made by Johnson Matthey & Co Limited. No hardener was added to the resin to maintain the coating in a plastic state.

5.7 Test Procedure with Test Rig No. 2

Referring to Fig. 34(a) the force on the contact surfaces, when the upper copper bar was in contact with the lower copper bar was determined by observing the force required to separate the surfaces using a spring balance. This force amounted to 33.4N (7lbf). The length of stroke of the pneumatic cylinder was such that the contact surfaces

were 2.54 mm (0.1 in) apart when fully separated. Prior to thermal tests the copper bars were separated and brought together many times to test for satisfactory mechanical operation.

The first tests were conducted with the upper and lower copper bars (Fig. 34(a)) permanently in contact. Tests under periodic contact conditions followed these interspersed with further tests when the bars were in permanent contact. The test procedure as follows.

5.7.1 Determination of steady or quasi-steady state

The test apparatus was left running continuously with the copper bars permanently separated, the temperature distribution being observed on a temporarily connected temperature recorder until the temperatures appeared to be steady. The two copper bars were then brought into contact and it was found that after about 2 hours the temperatures appeared to be steady, but there was a slow oscillation in temperatures of periodic time about 2 hours and the amplitude was equivalent to about 0.4K.

When changing test conditions no alterations in frequency or ratio of contact time:periodic time ($f\tau_c$) was made once it had been altered. No temperature observations were made using the digital voltmeter for at least 2 hours. The thermocouple outputs were then observed and recorded. About 5 minutes later the thermocouple outputs were observed again to confirm that they were within 5μV equivalent to $\mp$ 0.125K of their previous values. About 30 minutes later the outputs were observed and recorded again.

5.7.2 Variation of thermal contact resistance from cycle to cycle

Several successive tests with the copper bars in permanent contact were

made. After each test the pneumatic cylinder (Fig. 34(a)) was operated once to break the contact between the copper bars and re-establish contact immediately. These tests were performed in an attempt to establish the variation in thermal contact resistance which might be encountered from cycle to cycle during periodic contact conditions. After breaking and remaking contact once, two hours elapsed before observing temperature distributions. Two or three observations were then made at 15 minute intervals.

5.7.3. Transverse heat flow

The thermocouples in the copper bars (Fig. 34(a)) indicated that the outer surface temperature of the heated copper bar was less than that on the centre line at the corresponding axial position, by up to about 0.5K; while in the cooled copper bar, the indicated outer surface temperature was nearly always higher than the corresponding temperature on the centre line by about 0.2K. It had to be accepted that some transverse heat flow would occur in practice, with attendant error in determination of thermal contact resistance of the contact interface.

However, some attempt was made to assess the error in thermal resistance that is likely to arise due to transverse heat flow. A thermal resistance network approximate to the thermal system of test rig No. 2 is analysed in Appendix 19. This analysis suggests that the values of thermal resistance determined with test rig No.2 are lower than the true value by an amount of the order of 10 per cent.

Thereafter only the outputs of the thermocouples on the centre line were recorded.

5.7.4. Determination of thermal resistance from temperature distributions

In order to compare experimental results with the theoretical predictions shown by Fig. 24(b) thermal resistance was required to be expressed as an equivalent length of bar. With test rig No. 2 the temperature distribution in each copper bar was linear. It should be remarked here that in some tests, the temperature gradient in the axis of the cooler copper bar was steeper than that in the hotter bar by amounts up to 10 per cent.

This phenomenon has been observed elsewhere in references cited in reference [74] and arises because of errors in temperature measurement due to transverse heat leaks through thermocouple leads. In such cases the temperature at the thermocouple site indicated by the thermocouple will be lower than that in the absence of such a heat leak. The difference between these two temperatures decreases as the distance from the heated end of the bar. To reduce the error in measuring thermal resistance offered by an interface, reference[74] recommended limiting the number of thermocouples to two, provided that the heat flux and material thermal conductivity are known accurately, (otherwise extra thermocouples would be required). Using this recommendation, the thermal contact resistance, R, at the interface between two bars of length ℓ_a and ℓ_b respectively, made of material of thermal conductivity k_a and k_b respectively shown in Fig. 38 is given by:

$$R = \frac{(T_A - T_B)}{Q} - \left\{ \frac{\ell_a}{k_a A} + \frac{\ell_b}{k_b A} \right\} \qquad (121)$$

where Q = heat flux

T_A and T_B = respectively the measured temperatures at the heated end and cooled end of the system.

In test rig No2 Fig 34(a) the two copper bars were used as their own fluxmeters and the indicated temperature at each thermocouple site in the cooler bar was in less error than those in the hotter bar. In using equation (121) therefore, the value of heat flux used was that indicated by the temperature distribution in the cooler bar.

The equation of the straight line fitted to the measured temperature distribution in the cooler bar of test rig No. 2 was determined by least squares method. The length ℓ_T of bar equivalent to the thermal resistance R in equation (121) then

$$\ell_T = \frac{T_A - T_B}{a_2} - (\ell_a + \ell_b) \qquad (122)$$

where referring to Fig. 38

T_A = measured temperature of the hotter bar at the thermocouple site nearest the contact interface.

ℓ_a = distance from contact interface to thermocouple site T_A

T_B = measured temperature of the cooler bar at thermocouple site nearest the contact interface

ℓ_b = distance from contact interface to thermocouple site T_B

a_2 = temperature gradient in the cooler bar

5.7.5 <u>Determination of thermal resistance due to periodic interruption of heat flow</u>

To compare experimentally observed thermal resistances with the

theoretical predictions shown by Fig 24(b) the value of the thermal resistance due to periodic interruption, expressed as an equivalent length, ℓ_i, of bar must be found.

Prior to tests in the quasi-steady state, periodic contact condition, successive tests in the steady state, permanent contact condition had been carried out to determine values of the length of bar, 2λ, equivalent to the thermal contact resistance. The mean of these values, $2\lambda_m$, was found.

The thermal resistance offered by the contact interface in the quasi-steady state periodic contact condition yielded an equivalent length $2(\ell_i + \lambda)$.

From these tests

$$\ell_i = (\ell_i + \lambda) - \lambda_m \qquad (123)$$

Two comments may be appropriate here,

(i) serious errors in the determination of ℓ_i can arise unless two quantities $(\ell_i + \lambda)$ and λ_m are known to a high degree of accuracy.

(ii) if in the experiments, the thermal contact resistance has a different value each time the bars come into contact, ℓ_i could be expected to vary accordingly.

5.7.6. Dimensionless groups

From section 4.3.2.4 the relevant dimensionless groups are $(\frac{f\ell_i^2}{\alpha})$, $(f\tau_c)$ and $(\frac{f\ell^2}{\alpha})$. In evaluating these groups the mean value λ_m determined as described in section 5.9.1 was used, together with a value of

diffusivity, α, quoted as 115×10^{-6} m^2/s in reference[128].

5.8 Test Results with Test Rig No.2

5.8.1 Table of Results

77 values of the dimensionless group $(\frac{f\ell_i^2}{\alpha})$ were obtained from the experiments. The quantities varied independently were frequency of contact f, ratio of contact time:periodic time $(f\tau_c)$, condition of the contacting surfaces and the impact of the surfaces as they were brought into contact.

The temperature indicated by the thermocouple nearest the heater on the heated copper bar was within the range 40-50°C and that nearest the cooling jacket in the cooled bar was 18 - 25°C.

These experimental results are presented in Table II overleaf and discussed in section 5.9.

The experimentally obtained values of the dimensionless group $(\frac{f\ell_i^2}{\alpha})$ will be compared with those predicted by the theoretical study shown in Fig 24(b). Some other effects are also discussed.

5.9 Discussion of Results with Test Rig No.2

5.9.1 Tests with lapped contact surfaces, test set No.1

Referring to Table II, set No.1 section 5.8.1, Tables 31(a) and (b) give values of the dimensionless groups $(\frac{f\ell_i^2}{\alpha})$ obtained experimentally for various values of $(f\tau_c)$ and $(\frac{f\lambda_m^2}{\alpha})$ with lapped contact surfaces. Values of $(\frac{f\ell_i^2}{\alpha})$ from Tables 31(a) and (b) are plotted in Fig. 39 and 40 for comparison with the curves expressing the theoretical relationship

SUMMARY OF TEST RESULTS WITH TEST RIG NO. 2

TABLE II

Contact materials: Copper

Contact surface roughness when lapped with grade W carborundum 1.2 to 1.6 μm C.L.A.

Contact surface hardness (Vickers) 958 to 1000 N/mm^2

Set No.	Object of tests	No. of data points per set	Discussed in section No.	Table No.	Fig No.	Surface Condition	Static Load N(lbf)	Contact Gap mm (in)	Momentum before impact kg m/s	Range of contact resistance K/W	Test frequency Hz		Comparison of ($f\ell_i^2/\alpha$) with theory and remarks		
											Low	High	Low freq.	High freq.	Remarks
1	To compare experimental data with theoretical predictions	18	5.9.1 5.9.2	31 (a); (b)	39 40	Lapped. Grade W Carborundum	33.4N (7.5 lbf)	2.54mm (0.1in)	0.763	0.523 to 0.88	0.0405 - 0.0575	No Test	Fair	No test	Scattered about theoretical values (0.6 to 2.5) x theoretical value
2	As set 1, but with different surface preparation, giving lower thermal contact resistance	28	5.9.3 5.9.4	32 (a)-(b)	41	Coated with silver-impregnated epoxy resin	33.4N (7.5 lbf)	2.54mm (0.1in)	0.763	0.0507 to 0.217	0.098 - 0.103	1.18 - 1.67	Fair	High	low frequency results (0.6-1.2)x theoretical except 1 value, high frequency result (1.2to5) x theoretical value
3	To see if high values of $(\frac{f\ell_i^2}{\alpha})$ occur at high frequency with surface preparation as in set 1.	12	5.9.5 5.9.6	33	43	Lapped Grade "W" carborundum	33.4N (7.5 lbf)	2.54mm (0.1in)	0.763	0.385 to 0.855	No Test	1.18 - 3.7	No Test	Mostly high some fair some low	Scattered about theorectical value (0.15 to 3) x theoretical value
4	To assess effect of reducing impact (reduced contact gap)	2	5.9.9	34	46	Lapped Grade "W" carborundum	33.4N (7.5 lbf)	0.152mm (0.006 in)	0.187	1.0 to 1.27	No Test	1.96 - 1.98	No test Test	High	3 x theoretical value
5	To assess effect of increasing impact by increasing static load	1	5.9.9	35	47	Lapped Grade "W" carborundum	66.8N (15 lbf)	0.152mm (0.006 in)	0.264	0.81 to 1.31	No Test	2.7	No Test	Low	Inconclusive only one test
6	To assess effect of further increase in impact (increased contact gap)	4	5.9.9	36	49	Damaged during set No.3 to 5 and not re-lapped	66.8N (15 lbf)	1.24mm (0.049 in)	0.755	0.685 to 1.032	No Test	2.6 - 2.74	No Test	Scattered	One value in good agreement with theory. Others 0.5 x theoretical value
7	To assess effect of reduced impact (reduced contact gap)	12	5.9.9	37 38	50 51	As set No.6	66.8N (15 lbf)	0.635mm (0.025 in)	0.539	0.73 to 1.1	0.0823 - 0.176	1.715 - 3.37	Fair	Fair	Scattered about theoretical value (0.4to1.1) x theoretical value

between the dimensionless groups.

It will be seen on Fig.39 that the values of $(\frac{f\ell_i^2}{\alpha})$ determined experimentally varies with $(f\tau_c)$ in the same manner as that predicted theoretically. The greatest discrepancy occurred when $(f\tau_c) = 0.83$, when the experimentally obtained values of $(\frac{f\ell_i^2}{\alpha})$ were 4 - 6 times those predicted by theory. In other cases the experimental results were (0.3 - 2.25) times the theoretical values.

It will be recalled that the value of ℓ_i is obtained by the difference between two quantities $(\ell_i + \lambda)$ and λ_m, see equation (123). The value of λ_m used to compute the experimentally obtained values of $(\frac{f\ell_i^2}{\alpha})$ in Tables 31(a) was obtained from a group of trials when $(f\tau_c) = 1.0$, performed before each group of trials under periodic contact conditions. Thus for example in Table 31(a), λ_m for trials 69-73 was the mean λ of trials 67 and 68. In these particular trials the values of λ are significantly smaller than in others, which would account for a considerable amount of the discrepancy between theoretically and experimentally obtained values of $(\frac{f\ell_i^2}{\alpha})$ at $f\tau_c = 0.63$ and 0.83.

The values of $(\frac{f\ell_i^2}{\alpha})$ for tests ref Nos.69-73 and 76-79 were re-worked using the mean value of λ obtained from tests at $(f\tau_c) = 1.0$ before and after each group of periodic contact tests to determine ℓ_i. These are shown in Table 31(b) and are plotted in Fig. 40. This latter procedure for calculating ℓ_i was adopted for all subsequent tests.

It will be seen that these re-worked experimental results are in better agreement with the theoretical predictions.

Nevertheless the scatter of the experimentally determined values of

$(\frac{f\ell_i^2}{\alpha})$ about the theoretical values would have an upper limit of about 2.5 x theoretical values $(\frac{f\ell_i^2}{\alpha})$ and a lower limit of about 0.6 times theoretical values $(\frac{f\ell_i^2}{\alpha})$.

This is however a much smaller range of variation than was encountered in the experiments with test rig No. 1 where the corresponding limits were 0.1 x theoretical value and 10 x theoretical value. But variation in thermal contact resistance between successive contactings remains.

5.9.2 Condition of contact surfaces after periodic contact tests; set 1

Visual inspection of the contact surfaces by naked eye after the above tests revealed no obvious macroscopic surface damage. The heated copper bar was not disturbed from its location in the surrounding copper tube and thermal insulation so that the surfaces could be re-lapped together in situ. The new lapping marks showed all over the contact surfaces on the first inspection of the surfaces after minimal lapping, suggesting that no alteration in alignment during the preceding tests had occurred.

Since no macroscopic damage to the surfaces was evident, the variation in thermal contact resistance in successive contactings of the surfaces, may have been caused by changes in microscopic constriction or due to the mechanics of the test rig which could not be expected to bring the contact surfaces into this microscopically identical position each time they came together.

5.9.3 Tests with contact surfaces coated with unhardened, silver-impregnated epoxy resin; tests set No. 2

In order to continue the work of comparing experimentally obtained values of $(\frac{f\ell_i^2}{\alpha})$ with theoretical values, it was desired to conduct tests with lower thermal contact resistance due to the contact interface, such that the dimensionless group $(\frac{f\lambda_m^2}{\alpha})$ should have the same values as in tests set No.1 Table II.

The contact faces of the copper bars were re-lapped, then coated with unhardened, silver-impregnated epoxy resin, (type FSP 49R made by Johnson Matthey and Co. Limited) to reduce the thermal contact resistance of the contact interface. After some mechanical operation to provide some settling in of the surfaces, thermal tests were resumed.

The test results are summarised in Table II section 5.8. The individual observations are shown in Tables 32(a)and (b) and these are plotted in Fig 41 respectively. In Tables 32(a) and (b) the value of λ_m, used to calculate ℓ_i, equation (123), is the mean value of λ of the groups of trials immediately before and immediately after the group of tests under periodic contact conditions was used. This method was used to evaluate λ_m in all subsequent tests reported in this thesis.

Comparison of test results with theoretical data

Results from Table 32(a) and (b) are plotted in Fig. 41 and fall into two categories. The experimental values of $(\frac{f\ell_i^2}{\alpha})$ at low frequency where $(\frac{f\lambda^2}{\alpha})$ = 0.1 to 0.26 are in reasonable agreement with theory, ranging from 0.6 to 1.2 times the theoretical values. In contrast, when $(\frac{f\lambda^2}{\alpha})$ was in the region of 1.37 to 2.97 i.e. high frequency, the experimental values of $(\frac{f\ell_i^2}{\alpha})$ are all considerably higher than

theoretical, ranging from 1.2 to 5 times theoretical.

This relatively large comparative change suggested that surface contact phenomena might change with frequency or be different from that assumed by theory. A detailed visual study of the contact surfaces was then made.

5.9.4 Condition of contact surfaces after periodic contact tests (set No.2) with silver-impregnated resin coating on surfaces

Fig. 42 shows a colour photograph of the contact surface of each copper bar after completing the periodic contact tests set No.2, Table II in section 5.8. The blackened areas on each surface are probably a thin film of silver oxide. Some silver may also have been adsorbed into the copper. Metal-to-metal contact appears to have been confined to the small bright area at the centre of the surface. This lighting of the photograph does not show this area as distinctly as the naked eye. This bright area had an appearance of fine pitting as if it had been acid etched. The bright area was about 0.1 in (2.54 mm)diameter.

Steady state permanent contact tests (when f_{τ_c} =1.0) in Tables 32(a) and (b) showed thermal contact resistance to be about 0.132K/W, (since 1in of copper bar 1 in diameter has a thermal resistance of 0.132K/W). This value is compared with the value predicted by the Roess[77] expression for thermal contact between the cylinders of radius b, which make contact through a single, centrally placed contact area of radius a. The entire heat flow is through the contact area. Roess's formula is obtained from reference [58]; thermal contact resistance r is:-

$$r = \frac{1}{2ak}\left[1 - 1.4093\,\frac{a}{b} + 0.296\,\left(\frac{a}{b}\right)^3 + 0.052\left(\frac{a}{b}\right)^5 + \ldots\right] \tag{126}$$

where k = thermal conductivity.

Putting a = 1.252mm (0.05in), b = 12.7mm(½in) and k = 380W/mK yields

$$r = 0.895 \text{ K/W}$$

the length of copper bar 1 in dia, equivalent to this thermal contact resistance is 6.77 in (172mm).

Since the measured thermal contact resistance (about 0.132K/W) is considerably lower than this, it would appear that with the contact surfaces coated with silver impregnated epoxy resin much of the heat flow passed through the macro area outside the middle 0.1 in (2.54 mm) of the nominal (1in (25.4) diameter) contact area.

The theoretical study section 4.3.2.2 assumed heat flow in the bars to be one-dimensional everywhere so that when the bar ends are in contact, it is implicit that heat flows from one bar to the other through a thin film of negligible heat capacity whose thermal resistance is equal to the thermal contact resistance. No constriction of heat flow lines within the bar was assumed. The heat flow lines would be less constricted when the contact surfaces are coated with silver-impregnated epoxy resin, than when uncoated as in tests set nos. 1 and 3 to 7 Table II section 5.8 It should be noted that the thermal contact resistance encountered with the lapped surfaces in tests set No.1, Table 31(a) and (b) was about 0.6K/W. This is not greatly less than the value calculated assuming all heat was transferred through the single centrally placed

contact area. It should be noted however that such a value could arise if negligible solid-to-solid contact had occurred and the entire heat transfer was through a thin film of air about 8×10^{-3}mm (0.3×10^{-3}in) thick. Measurement of electrical resistance of the contact interface in section 5.9.7 suggests that the metal-to-metal contact may have been negligible, but this is uncertain.

It was decided to experiment to see if the high values of $(\frac{f\ell_i^2}{\alpha})$ obtained experimentally at "high" frequency in tests set No.2 were obtained with lapped surfaces.

5.9.5 Tests with lapped contact surfaces at "high" frequency; tests set No.3

The object and summary of results of these tests is in Table II, section 5.8.1. The surfaces were lapped "in situ". The results are plotted in Fig 43 from the data in Table 33. It will be seen from Fig.43 that most of the values of $(\frac{f\ell_i^2}{\alpha})$ are higher than theoretical.

5.9.6. Summary of sections 5.9.1 to 5.9.5

The object of tests set Nos. 1 to 3 Table II section 5.8 was to try to establish how the theoretical predictions of the dimensionless group $(\frac{f\ell_i^2}{\alpha})$ compared with values obtained experimentally.

Although under periodic contact conditions the temperature distributions were never absolutely steady, the tests showed that for lapped surfaces and surfaces coated with silver-impregnated epoxy resin, there was fairly close agreement between the theoretically predicted values of

$(\frac{f\ell_i^2}{\alpha})$ and the average of the experimentally obtained values at frequencies within the range 0.04 - 0.1Hz. However, variations about this average value of $(\frac{f\ell_i^2}{\alpha})$ from 0.6 to 2.5 times the theoretical value occurred.

At frequencies from about 1 to 3.7 Hz, most of the experimental values of $(\frac{f\ell_i^2}{\alpha})$ were considerably higher than theoretical, but there are two experimental values much lower than theoretical. The reason for this is not readily apparent. It was thought that one reason for the discrepancy between the experimental and theoretical value of $(\frac{f\ell_i^2}{\alpha})$ might be because of the assumption in the theory that the heat flux lines within the bars were not constricted. However, the discrepancy was greater when constriction of the heat flux lines was likely to have been least (with silver-impregnated coating on the contact surfaces).

5.9.7. Electrical resistance of the contact interface

In the experiments discussed so far the thermal contact resistance offered by the contact interface was measured a relatively long time after contact had been established. It is not possible to measure instantaneous values of thermal contact resistance, but it was thought that observation of the electrical resistance of the contact interface might indicate whether or not the thermal contact resistance varies during the period of contact. The modifications to the test rig and the circuit used were used in all experiments after set 3 (Table II), section 5.8).

Fig. 44(a) shows a typical trace of the voltage drop across resistor R_2 in Fig.37. The "ripple" on the trace when the bars were in contact is

of frequency 50Hz and was thought to be due to stray magnetic flux which was linked through the closed loop formed when the bars were in contact, see Fig.37. This "ripple" persisted when the bars were permanently in contact. However, it did not appear in later experiments, see Fig.44(b) in which the impact with which the surfaces came together and the static load were larger.

In both cases Figs 44(a) and (b) it will be noticed that immediately at the end of the period when the surfaces were separated (open) the voltage drop across resistor R_2, (Fig.37), which characterises the electrical resistance of the contact interface, falls then rises and falls again to settle to a lower steady value all within a time interval of about 12.5ms. This is a short time relative to the duration of contact (120ms minimum) in the experiments sets 4 to 7. Referring to the circuit diagram Fig 37, the electrical resistance R_2 and that of the copper bars and contact interface, when in permanent contact, are both about the same value, 0.2 Ω. Since they are small compared with resistance R_1, the current through R_1 is little affectedby the contact and separation of the copper rods. Let the current through R_1 be I, then the voltage drop across R_2 will then be IR_2 when the copper bars are separated and $IR_2R_3/(R_2 + R_3)$ when in contact, where R_3 is the electrical resistance offered by the copper bars and contact interface. R_3 can be dtermined by measuring the ratio, r, of the above voltage drops.

$$IR_2 : IR_2R_3/(R_2 + R_3) = r.$$

Thus

$$R_3 = \frac{R_2}{r - 1} \qquad (124)$$

Considering Fig.44(b), during the short time interval between the copper bars being fully separated and fully in contact, the electrical

resistance, R_3 offered by the copper bars and the contact interface fluctuates. The values of R_3 during this transient are inserted on Fig. 44(b), being 0.477 Ω, 2.73Ω and 0.21Ω . The average electrical resistance offered by the copper bars and contact interface from the instant the bars start to come together until they commence separation is higher than the 0.21Ω obtained when the bars are permanently in contact. A rough estimate of the average electrical resistance of the copper bars and interface can be made from a plot of electrical resistance against time. This yielded a value of 0.26Ω .

This result (at a frequency of about 1Hz at which the greatest discrepancy between experimentally determined values of $\frac{f\ell_i^2}{\alpha}$ occurred) suggests that the value of thermal contact resistance, λ_m, used to compute the length ℓ_i, equation (123) should be higher than the thermal contact resistance determined from steady state, permanent contact experiments. Such a procedure would bring the experimentally determined values of $(\frac{f\ell_i^2}{\alpha})$ in tests sets 1 - 3 into better agreement with theoretical values. The higher the frequency and the shorter the duration of contact, the greater the proportion of contact time occupied by the transient.

Electrical resistance of the contact interface appeared to be about 0.2Ω . Using Holm's expression $r = \rho/2a$ for the constriction resistance, r, of an isolated contact area of radius, a, of material of resistivity ρ yields (for copper, of resistivity 1.72 μΩcm) a contact area of diameter only 0.86×10^{-4}mm. One may suspect the validity of this observation, but, if genuine, this would mean either:

(i) there is an electrically insulating surface film present which means the contact area is really greater than 0.86×10^{-4}mm diameter.

(ii) the above contact area is genuine, giving support to the proposition that most of the heat flow across the contact interface is through the interstitial air gap.

The matter is left for future investigation in which it is suggested that continuous electrical resistance measurements should be accompanied by simultaneous measurement of the force on the contact surfaces.

5.9.8 Cyclic temperature variation near the contact surfaces

Fig 44(c) shows amplified outputs of the thermocouples placed in the copper bars near to the contact surfaces. It will be seen that they are of the same form as that shown in the theoretical study using the analogue computer, section 4.3, Fig. 24(a).

5.9.9 Tests to assess the effect of impact on thermal resistance tests sets nos. 4 to 7.

Referring to Table II in section 5.8.1, tests sets Nos 4 to 7, the impact of one contact surface on the other was varied either by altering the static load on the surfaces or by altering the height from which the upper copper bar fell on to the lower copper bar. The impact was quantified by calculating the momentum of the upper copper bar (and everything attached to it) just before impact since the mass and height of fall were known.

In tests Nos 5 to 7, adjustments to the coupling, see Fig. 34(a), were made so that the static load on the contact surfaces was the weight of the upper copper bar, its attachments and the force of the return

spring of the pneumatic cylinder.

The experimentally obtained values of $(\frac{f\ell_i^2}{\alpha})$ are for tests 4 to 7 plotted in Figs 46,47 and 49 to 51.

5.9.9.1 Effect of changes of impact on thermal contact resistance

Fig 45 shows a plot of the average value and upper and lower limits of thermal contact resistance against the value of the momentum of the upper copper bar and its attachments immediately before impact, for tests sets nos 3 to 7. The contact surfaces were lapped together prior to tests set No.3 and not lapped at any subsequent time. It should be observed from Fig.45 that thermal contact resistance is reduced with increase in momentum before impact, although to a much lesser extent when the static load on the contact surfaces is 66.8N, than when it is 33.4N. One would expect the thermal contact resistance to fall with impact since more local areas of contact are likely to be established and maintained (as the force on the surfaces relaxes from its maximum impact value to its final steady value), than would be the case with gradual increase in load up to the final steady value. This matter would merit a more detailed examination in the future, as increasing the impact might afford a method of increasing the heat transfer through periodically contacting surfaces.

5.9.9.2 Comparison of $(\frac{f\ell_i^2}{\alpha})$ obtained experimentally with theoretically determined values under differing impact

The data summarised in Table II section 5.8 is amplified to consider further the effect of impact upon the experimentally obtained values of $(\frac{f\ell_i^2}{\alpha})$. The amplified data is shown in Tables 39 and 40 and is shown plotted in Fig.52. Tests sets Nos 1 and 3 to 7 are considered since the preparation of the contact surfaces was the same, i.e. lapped

with grade W carborundum.

Fig 52 which shows the ratio of experimentally obtained $(\frac{f\ell_i^2}{\alpha})$ to that predicted theoretically plotted against momentum before impact. With tests sets Nos. 5 to 7 in which the static load on the contact surfaces was 66.8N, the experimentally obtained values of $(\frac{f\ell_i^2}{\alpha})$ are significantlysmaller than those values predicted theoretically. However with these three tests, increasing the momentum before impact does not alter the ratio of the experimentally obtained value of $(\frac{f\ell_i^2}{\alpha})$ to that predicted theoretically.

On the other hand with test sets Nos. 1,3 and 4 in which the static load was 33.4kN, increasing the momentum before impact appears to reduce the ratio of experimentally obtained value of $(\frac{f\ell_i^2}{\alpha})$ to that predicted theoretically significantly. In each case the experimentally obtained value of $(\frac{f\ell_i^2}{\alpha})$ is larger than that predicted theoretically.

Clearly there is insufficient experimental data from which to draw firm conclusions. However, reducing both the thermal contact resistance, λ_i and the thermal resistance due to periodic interruption of the heat flow can be effected by increasing the impact of the contacting surfaces on each other. This aspect of the work merits further investigation.

5.9.10 Surface wear

Fig.48 shows the condition of the contact surfaces after tests set No.5. A thin film of dirt or oxide covers the darkened areas. Metal-to-metal contact had occurred near the centre of the surfaces. Elsewhere there is evidence of the surfaces being rotated relative to each other.

The surfaces were not re-lapped prior to tests sets 6 and 7.

Figs. 53 (a) and (b) show the condition of contact surfaces after tests set No.7. There was considerable damage around the centre and towards the outer edge of the surfaces; some of the dirt or oxide formed after tests set No.5 was still present.

Fig. 54 (a)(b)(c) and 55 (a)(b)(c) showed the surface condition at various positions under X27 magnification. Most of the damage near the centre is heavy scoring (Figs 54(a) and 55(a)), some of it due to relative rotation and some probably due to local welding and breaking apart of the local contact areas. Indentation, showed ringed in Figs.54(a) and 55(a) could have been caused by trapped debris from this welding and breaking. The deep scores running radially could have been caused by relative lateral movement allowed by the ball seating of the colder copper bar and cooling jacket.

Figs. 54(b) and 55(b) which are of areas about 6mm (1/4in) away from the centre of the contact surfaces shows no evidence of metal-to-metal contact having occurred, the lapping marks being visible.

Figs.54(c) and 55(c) taken near the outer edges show some pitting and surface film.

Thermal contact resistance measurements, see Tables 33 and 36, suggested that either greater constriction of heat flux lines or an increased mean interstitial air gap occurred with the damaged surfaces of tests set No.6 than with the freshly lapped surfaces of tests set No.3 where the impact was about the same.

5.10 Discussion of Accuracy of Experimental Results with Test Rig No.2

The sensitivity of the experimentally determined values of $(\frac{f\ell_i^2}{\alpha})$ to changes in the value of λ_m was illustrated in section 5.9.1. Errors in the experimental determination of thermal resistance arise due to transverse heat flow. Positioning of the temperature distribution line among the data points would also affect the experimentally obtained thermal resistance. However, in this thesis, the scatter of the data points was small and use of the method of least squares to position the temperature distribution lines ensured consistency.

If λ_m and $(\ell_i + \lambda) = \ell_T$ are each subject to error or uncertainty $\mp\varepsilon_1$ and $\mp\varepsilon_2$ respectively, then from equation (123)

$$\text{Maximum value of } \ell_i = \ell_T(1+\varepsilon_2) - \lambda_m(1 - \varepsilon_1) \tag{125}$$

$$\text{Minimum value of } \ell_i = \ell_T(1-\varepsilon_2) - \lambda_m(1 + \varepsilon_1) \tag{126}$$

Hence the maximum value of $(\frac{f\ell_i^2}{\alpha})$, assuming the error in f and α to be small compared with ε_1 and ε_2, is

$$\text{Maximum } (\frac{f\ell_i^2}{\alpha}) = \left\{\ell_T(1 + \varepsilon_2) - \lambda_m(1 - \varepsilon_1)\right\}^2 \frac{f}{\alpha} \tag{127}$$

$$\text{Minimum } (\frac{f\ell_i^2}{\alpha}) = \left\{\ell_T(1-\varepsilon_2) - \lambda_m(1 + \varepsilon_1)\right\}^2 \frac{f}{\alpha} \tag{128}$$

and the difference δ between maximum and minimum $(\frac{f\ell_i^2}{\alpha})$, is

$$\delta = 4\left\{\ell_T^2\, \varepsilon_2 - \lambda_m\, \ell_T(\varepsilon_2 - \varepsilon_1) - \lambda_m^2 \varepsilon_1\right\} \tag{129}$$

and the percentage uncertainty, P, in $(\frac{f\ell_i^2}{\alpha})$ is

$$p = \frac{100\delta}{(\ell_T - \lambda_m)^2} = \frac{4\left\{\ell_T^{\,2}\varepsilon_2 - \lambda_m \ell_T(\varepsilon_2 - \varepsilon_1) - \lambda_m^{\,2}\varepsilon_1\right\}}{(\ell_T - \lambda_m)^2} \qquad (130)$$

If for example $\varepsilon_2 = \varepsilon_1 = \varepsilon$ and $\ell_T = 2\lambda_m$, a condition met with $(f\tau_c) \simeq 0.5$ then the percentage uncertainty, p, would be

$$p = 12\varepsilon \qquad (131)$$

Thus a given value of $\left(\frac{f\ell_i^{\,2}}{\alpha}\right)$ would be subject to a tolerance of $\mp 6\varepsilon \left(\frac{f\ell_i^{\,2}}{\alpha}\right)$.

In a given observation, ε_2 in equations (126) and (127) arises from temperature distribution measuring errors due to transverse heat flows, unless accurately corrected, and to scatter among the data points making possible a range of possible straight lines drawn among the data points. Known methods of measuring thermal contact resistance are not precise as pointed out in reference[74]. Appendix 19, suggests that an error of (-11) percent is quite likely, leading to very large uncertainty, p, in equation[131].

Error, ε_1, in equations (125) and (127) is compounded from the errors resulting from temperature distribution measurement and more important the uncertainty as to whether λ_m is the true mean of the values of λ, which alters each time the surfaces make contact.

Despite these probable errors it is clear that the manner in which $\left(\frac{f\ell_i^{\,2}}{\alpha}\right)$ varies with $(f\tau_c)$ and $\left(\frac{f\lambda^2}{\alpha}\right)$ is in agreement with that suggested by the theoretical study.

6. OVERALL DISCUSSION

6.1 General

A theoretical and experimental study of heat transfer through periodically contacting surfaces has been made, in which the variables considered have been frequency of contact, f, ratio of contact time:periodic time ($f\tau_c$) and thermal contact resistance (expressed for convenience as an equivalent length λ, of solid bar). An attempt was also made to assess the effect of impact upon heat transfer in such a system.

It is clear from both studies that at a given frequency, f, and ratio of contact time: periodic time, thermal contact resistance, λ, exerts a major effect on thermal resistance caused by periodic interruption of the heat flow. This is additional to its effect on heat flow in the steady state, permanent contact case.

The experimental work showed that the dimensionless group $(\frac{f\ell_i^2}{\alpha})$ which represents thermal resistance due to periodic interruption in heat flow at the contact interface varies with $(f\tau_c)$ and $(\frac{f\lambda^2}{\alpha})$ in a similar manner to that predicted by the theoretical study, but the numerical values did not always agree.

Observation of electrical resistance of the contact interface suggested that when the contact surfaces were brought into contact a transient of short duration occurred before the electrical resistance reached its steady value. As the frequency of contact increases, the transient would occupy an increasing proportion of the contact period, suggesting that the average thermal contact resistance during the contact period might be higher than the value obtained from steady state experiments.

The experimental work on the effect of impact showed that at the smallest of the two static loads used, both thermal contact resistance and $(\frac{f\ell_i^2}{\alpha})$ were reduced significantly by increasing the impact with which the surfaces came together. At the higher static load, however, the reduction in thermal contact resistance was less marked but in every case experimental values of $(\frac{f\ell_i^2}{\alpha})$ was considerably less than the theoretical value. The effect of impact requires future investigation.

Examination of the copper contact surfaces showed that metal-to-metal contact had been confined to the central 2.54mm (0.1in) of the nominal contact surface. With lapped contact surfaces electrical resistance measurements suggested that the actual metal-to-metal contact area was much smaller than the damaged area suggesting that most of the heat flow might have passed through the interstitial air gap between the surfaces when in contact.

With lapped contact surfaces the thermal contact resistance increased as the surfaces became damaged. Future experiments with surface materials more resistant to damage than copper, would in view of their low thermal conductivity need the bars to be within a vacuum chamber in order to keep transverse heat losses small.

Changes in thermal contact resistance between successive meetings of the surfaces might be explained by changes in the microscopic areas of contact which could be produced by the alignment of the surfaces being different each time they came into contact. In view of this and the difficulty of obtaining a truly quasi-steady state, a statistical approach seems essential in future experiments.

6.2 Mathematical Modelling

The theoretical study was concerned with trying to establish quantitatively the effects of requency of contact, f, ratio of contact time:periodic time, ($f\tau_c$) and thermal contact resistance, (expressed as an equivalent length, λ, of bar), on heat flow. The results were expressed in non-dimensional form and presented in Fig.24(b).

By solving the heat diffusion equation by two different methods and finding the same result from each, it has been established that the data presented in Fig 24(b) has no significant errors. Convergence difficulties with the iterative method used to solve the imperfect thermal contact case, section 4.3.4 allowed comparison with the analogue computer solution over a limited range of ($f\tau_c$) and ($\frac{f\lambda^2}{\alpha}$). These results were in extremely close agreement with the analogue computer solution, see Fig.28 and the investigation was taken no further. These results are supported by the work of Reed and Mullineux[124] who used yet another method for solution.

The relationship

$$\left(\frac{f\ell_i^2}{\alpha}\right) = g(f\tau_c) \qquad (50)$$

for sufficiently large $\left(\frac{f\ell^2}{\alpha}\right)$, obtained when $\lambda = 0$, is important as it represents a limiting condition; since if the surfaces make solid-to-solid contact at every point over their area,(no thermal contact resistance),then the reduction of heat flow due to periodic interruption is the minimum which can occur. In practical situations however the contact will occur at discrete areas and the thermal contact resistance will always be finite. The numerical matrix inversion method section 4.2.7 provided some data outside the range of the analogue

computer study, namely at $(\frac{f\ell^2}{\alpha})$ below the value required for equation (50) to hold good. This is presented in Fig 16(a).

No constriction of the heat flux lines in the region adjacent to the contact interface was assumed in the mathematical model. The analysis of a contact model similar to that analysed by Cetinkale and Fishenden[25] and Fenech and Rohsenow[37],[38] shown in Figs 3 and 4, where periodic contact was made at the junction of the surface asperities in contact, was not attempted for reasons of complexity.

However, the model studied could be a reasonable representation of the case where local contact areas were numerous, of negligible heat capacity, and uniformly distributed over the contact surface; or cases where (a) most of the heat passes through the interfacial fluid, (b) the surfaces are completely covered with a thin, film of material having low conductivity and heat capacity, which is never penetrated by asperities.

7. CONCLUSIONS

In this thesis the author has developed a theory from which a designer could predict the heat flow in a system in which two solids, made of identical materials, are brought into contact and separated periodically; the cycle being repeated continuously. The designer would know the frequency, f, of contact, the ratio contact time:periodic time ($f\tau_c$), the length, ℓ, of material on either side of the contact interface, the thermal contact resistance offered by the interface,* and the thermal diffusivity, α, of the materials.

A theoretical model of heat transfer between periodically contacting surfaces has been developed and its accuracy has been confirmed by two independent methods of solving the relevant equations. The results of this study are presented as a graphical data sheet Fig24(b) and is applicable for $(\frac{f\ell^2}{\alpha})$ > about 4. This data illustrates the major effect on heat transfer exerted by the contact interface. The case when $(\frac{f\ell^2}{\alpha})$ < 4 has been partly explored, but only in the case where thermal contact resistance is zero. The result is shown in Fig 16(a) and (b).

Experimental work was performed in an attempt to establish the validity of the theoretical study. This showed that the heat flow characteristics of a process where heat is transferred through periodically contacting surfaces is similar to that predicted from the above theory, so that Fig 24(b) provides data from which at least a first approximation to thermal resistance due to periodic interruption of the heat flow can be made.

However, the thermal contact resistance does not have the same value

* Thermal contact resistance, R, is related to λ on Fig 24(b) by $R = \frac{2\lambda}{k}$

each time the surfaces make contact. This is probably due to changes in contact geometry each time contact is made. These changes could be due to the size and distribution of local solid-to-solid contact areas, and to the mean air gap between the surfaces when in contact. When copper contact surfaces were used, they suffered considerable damage on a macroscopic scale and the thermal contact resistance varied by about $\mp$ 45 per cent.

The experimental work on the effect of impact was inconclusive but suggested that increasing the impact with which the surfaces came together considerably reduces thermal contact resistance which in turn reduces the thermal resistance due to periodic interruption of heat flow.

8. RECOMMENDATIONS FOR FURTHER WORK

Statistically-orientated experimental work of higher precision is required to test fully how far the theoretical results are applicable to practical cases. The conditions of contact must be known in greater detail to establish the proportions of the heat transferred during contact which passes through metal-to-metal contact areas and through interfacial gas in each case.

In addition to surface roughness and hardness measurements, the contact surfaces might be examined visually by scanning electron microscope to show more clearly the changes to asperities after successive cycles of contact and separation. The specimens used so far were too large to be accommodated on an electron microscope stage. Materials less susceptible to surface damage should be investigated. In view of the lower thermal conductivity of such materials compared with copper, tests would have to be conducted in vacuum using equipment and techniques similar to those described in references[136][135] and [90] in order to minimise the effects of transverse heat flows. Such vacuum experiments would also give information about the air gap heat transfer.

The effects of velocities of impact and separation, static load, alignment of surfaces or deposits, ~~and~~ periodic contact of dissimilar materials and surface films are factors which might be investigated.

Theoretical analysis of contact models similar to those analysed by Cetinkale and Fishenden[25] and Fenech and Rohsenow[37][38], see Figs 3 and 4, which make periodic contact at the junction of surface asperities

may be worth while but would undoubtedly be a major exercise. However, this would yield valuable information on the performance of a "constriction model" relative to the "film model" analysed in this thesis.

TABLE 1 ANALOGUE COMPUTER STUDY

Effect of finite mesh on solutions for temperature distribution in non-contact condition.

	Solution of finite difference equations when $D(\Delta\Theta_n) = 0$	Values expected from steady state non-contact temperature distribution, Fig.10
$\Delta\Theta_{1_s}$	0.78997	0.80
$\Delta\Theta_{2_s}$	0.86986	0.88
$\Delta\Theta_{3_s}$	0.94974	0.96
$\Delta\Theta_{4_s}$	0.95974	0.97
$\Delta\Theta_{5_s}$	0.96974	0.98
$\Delta\Theta_{6_s}$	0.97974	0.99
$\Delta\Theta_{7_s}$	0.98974	1.0

TABLE 1

TABLE 2 ANALOGUE COMPUTER STUDY RESULTS (PERFECT THERMAL CONTACT)

Frequency, Hz 0.0145			0.073			0.18			0.585		
$(f\tau_c)$	L	$(f\ell_i^2/\alpha)$	$(f\tau_c)$	L	$(f\ell_i^2/\alpha)$	$(f\tau_c)$	L	$(f\ell_i^2/\alpha)$	$(f\tau_c)$	L	$(f\ell_i^2/\alpha)$
0.0828	0.51	5.05	0.0327	0.472	18.7	0.0372	0.343	15.7	0.0612	0.170	7.86
0.0204	0.325	1.08	0.0871	0.303	4.44	0.061	0.272	8.05	0.105	0.127	4.06
0.403	0.176	0.212	0.126	0.244	2.43	0.115	0.191	3.22	0.167	0.0937	2.00
0.515	0.125	0.0945	0.182	0.205	1.56	0.18	0.138	1.48	0.378	0.038	0.292
0.667	0.072	0.0279	0.234	0.168	0.945	0.304	0.085	0.498	0.467	0.0275	0.149
0.786	0.034	0.00575	0.313	0.126	0.482	0.43	0.054	0.188	0.595	0.0163	0.0515
			0.509	0.067	0.122	0.50	0.042	0.111	0.672	0.0111	0.0234
			0.726	0.023	0.0129	0.612	0.0272	0.0451	0.765	0.0067	0.0085
			0.778	0.016	0.00615	0.723	0.0159	0.0151			
						0.844	0.0065	0.00247			

Frequency Hz 0.99			4.07			8.13			16.4		
$(f\tau_c)$	L	$(f\ell_i^2/\alpha)$	$(f\tau_c)$	L	$(f\ell_i^2/\alpha)$	$(f\tau_c)$	L	$(f\ell_i^2/\alpha)$	$(f\tau_c)$	L	$(f\ell_i^2/\alpha)$
0.0446	0.154	10.5	0.0311	0.0895	12.6	0.0518	0.046	6.05	0.0525	0.0267	3.78
0.0857	0.121	6.0	0.0117	0.0461	3.04	0.1165	0.0284	2.23	0.137	0.0171	1.52
0.1075	0.100	3.92	0.176	0.0340	1.62	0.223	0.0178	0.855	0.184	0.0149	1.15
0.164	0.0752	2.09	0.265	0.0225	0.690	0.328	0.0123	0.403	0.242	0.0120	0.740
0.214	0.0602	1.30	0.37	0.0156	0.327	0.43	0.00875	0.193	0.337	0.00872	0.389
0.284	0.0438	0.665	0.472	0.0109	0.158	0.523	0.00586	0.0906	0.479	0.00494	0.124
0.385	0.0295	0.293	0.600	0.00625	0.0515	0.596	0.0043	0.0485	0.579	0.00310	0.0486
0.496	0.0183	0.110	0.730	0.0032	0.0134	0.688	0.00263	0.0181	0.683	0.00192	0.0186
0.585	0.0135	0.0595	0.838	0.00137	0.00245	0.749	0.0018	0.00845	0.790	0.00089	0.004
0.68	0.0079	0.0201				0.870	0.0006	0.00095			
0.772	0.00444	0.00630									
0.833	0.00301	0.00289									
0.895	0.00099	0.000311									

Tables 3(a)-(c) Numerical Matrix Inversion Method Solutions

$(f\tau_c) = 0.1$

Periodic Time s	$(\frac{f\ell^2}{\alpha})$	$(\frac{f\ell_i^2}{\alpha})$	$\frac{\ell_i}{\ell}$
10	32	3.8168	0.3454
100	3.2	3.8148	1.0918
200	1.6	3.7930	1.5397
500	0.64	4.2038	2.5629
1000	0.32	4.8967	3.9118
2000	0.16	4.8826	5.5242
5000	0.064	3.3544	7.2396
10000	0.032	2.0650	8.0331
40000	0.008	0.61059	8.7376

TABLE 3(a)

$f\tau_c = (0.5)$

Periodic time s	$(\frac{f\ell^2}{\alpha})$	$(\frac{f\ell_i^2}{\alpha})$	$\frac{\ell_i}{\ell}$
2	160	0.11774	0.02713
6	53.3	0.11679	0.04681
20	16	0.11652	0.08534
60	5.33	0.11651	0.1478
180	1.776	0.11686	0.2565
500	0.64	0.13826	0.4648
1000	0.32	0.13702	0.6544
2000	0.16	0.10422	0.8071
5000	0.064	0.053910	0.9178
10000	0.032	0.029357	0.9578
40000	0.008	0.0078238	0.9889

TABLE 3(b)

$(f\tau_c) = 0.9$

Period time s	$(\frac{f\ell^2}{\alpha})$	$(\frac{f\ell_i^2}{\alpha})$	$\frac{\ell_i}{\ell}$
10	32	0.59427×10^{-3}	0.004309
20	16	0.58926×10^{-3}	0.006069
50	6.4	0.58748×10^{-3}	0.009581
200	1.6	0.58860×10^{-3}	0.01918
500	0.64	0.60110×10^{-3}	0.03065
1000	0.32	0.61419×10^{-3}	0.04381
2000	0.16	0.60453×10^{-3}	0.06147
5000	0.064	0.47212×10^{-3}	0.08589
10000	0.032	0.30775×10^{-3}	0.09807
40000	0.008	0.92933×10^{-4}	0.1078

TABLE 3(c)

TABLES 4 - 13 VARIATION OF TEMPERATURE WITH TIME AT VARIOUS POSITIONS.

$(\frac{x}{\ell})$, ALONG THE BAR

* Taking $T(o,t) = T_A = 100^oC$, length = 0.04 m and $\alpha = 5 \times 10^{-6} \frac{m^2}{s}$

Frequency, f = 0.05 Hz, $(f\tau_c) = 0.5$, $(\frac{f\ell^2}{\alpha}) = 16$

$\frac{x}{\ell} = 1.0$

TIME s		Dimensionless Temperature T/T_A	
0	Bar separated	-0.00001270	$= T_1(x,o)/T_A$
1		0.07749025	
2		0.10852447	
3		0.13176079	
4		0.15095255	
5		0.16756913	
6		0.18236887	
7		0.19580357	
8		0.20816768	
9		0.21966534	
10		0.23044472	$= T_1(x,\tau)/T_A$
0	Bars in contact	0.000000	$= T_2(x,o)/T_A$
1		↓	
2			
3			
4			
5			
6			
7			
8			
9			
10			$= T_2(x,\tau_2)/T_A$

TABLE 4

VARIATION OF TEMPERATURE WITH TIME AT VARIOUS POSITIONS, $(\frac{x}{\ell})$, ALONG THE BAR

* Taking $T(o,t) = T_A = 100^oC$, length = 0.04m and $\alpha = 5 \times 10^{-6} \frac{m^2}{s}$

frequency, f = 0.05 Hz, $(f\tau_c) = 0.5$, $(\frac{f\ell^2}{\alpha}) = 16$

$$\frac{x}{\ell} = 0.95$$

TIME s		Dimensionless Temperature T/T_A	
0	Bars separated	0.06192917	$= T_1(x,o)/T_A$
1		0.09213969	
2		0.11878058	
3		0.13999871	
4		0.15797508	
5		0.17376161	
6		0.18795098	
7		0.20091427	
8		0.21290125	
9		0.22408909	
10		0.23460861	$= T_1(x,t_1)/T_A$
0	Bars in contact	0.23467114	$= T_2(x,o)/T_A$
1		0.11972309	
2		0.09383287	
3		0.08244110	
4		0.07589624	
5		0.07160938	
6		0.06856891	
7		0.06629275	
8		0.06452044	
9		0.06309840	
10		0.06193004	$= T_2(x,\tau_2)/T_A$

TABLE 5

VARIATION OF TEMPERATURE WITH TIME AT VARIOUS POSITIONS, $(\frac{x}{\ell})$, ALONG THE BAR

* Taking $T(o,t) = T_A = 100^oC$, length = 0.04m and $\alpha = 5 \times 10^{-6} \frac{m^2}{s}$

frequency, f = 0.05 Hz, $(f\tau_c) = 0.5$, $(\frac{f\ell^2}{\alpha}) = 16$

$$\frac{x}{\ell} = 0.910$$

TIME s		Dimensionless Temperature $T/_A$	
0	Bars separated	0.11090350	$= T_1(x,o)/T_A$
1		0.12165550	
2		0.14048059	
3		0.15773903	
4		0.17323838	
5		0.18729811	
6		0.20020111	
7		0.21216192	
8		0.22334160	
9		0.23386285	
10		0.24382095	$= T_1(x,\tau_1)/T_A$
0	Bars in contact	0.24380719	$= T_2(x,o)/T_A$
1		0.19336039	
2		0.16068767	
3		0.14402483	
4		0.13387536	
5		0.12701068	
6		0.12204090	
7		0.11826658	
8		0.11529624	
9		0.11289321	
10		0.11090581	$= T_2(x,\tau_2)/T_A$

TABLE 6

VARIATION OF TEMPERATURE WITH TIME AT VARIOUS POSITIONS, $(\frac{x}{\ell})$, ALONG THE BAR

* Taking $T(o,t) = T_A = 100^oC$, length = 0.04m and $\alpha = 5 \times 10^{-6} \frac{m^2}{s}$

frequency, f = 0.05 Hz, $(f\tau_c) = 0.5$, $(\frac{f\ell^2}{\alpha}) = 16$

$$\frac{x}{\ell} = 0.900 \quad .$$

TIME s		Dimensionless Temperature T/T_A	
0	Bars separated	0.12301679	$= T_1(x,o)/T_A$
1		0.13077864	
2		0.14747289	
3		0.16354570	
4		0.17827601	
5		0.19178909	
6		0.20427983	
7		0.21591664	
8		0.22683376	
9		0.23713718	
10		0.24691111	$= T_1(x,\tau_1)/T_A$
0	Bars in contact	0.24690987	$= T_2(x,o)/T_A$
1		0.20788827	
2		0.17573190	
3		0.15848684	
4		0.14776977	
5		0.14044089	
6		0.13509754	
7		0.13101950	
8		0.12779839	
9		0.12518513	
10		0.12301900	$= T_2(x,\tau_2)/T_A$

TABLE 7

VARIATION OF TEMPERATURE WITH TIME AT VARIOUS POSITIONS, $(\frac{x}{\ell})$, ALONG THE BAR

* Taking $T(o,t) = T_A = 100^oC$, length = 0.04m and $\alpha = 5 \times 10^{-6} \frac{m^2}{s}$

frequency, f = 0.05 Hz, $(f\tau_c) = 0.5$, $(\frac{f\ell^2}{\alpha}) = 16$

$$\frac{x}{\ell} = 0.89$$

TIME s		Dimensionless Temperature T/T_A	
0	Bars separated	0.13506646	$= T_1(x,o)/T_A$
1		0.14040634	
2		0.15499857	
3		0.16984457	
4		0.18376394	
5		0.19669464	
6		0.20874335	
7		0.22003118	
8		0.23006458	
9		0.24073200	
10		0.25030601	$= T_1(x,\tau_1)/T_A$
0	Bars in contact	0.25031860	$= T_2(x,o)/T_A$
1		0.22097156	
2		0.19005750	
3		0.17252701	
4		0.16138635	
5		0.15367377	
6		0.14800647	
7		0.14365745	
8		0.14020837	
9		0.13740138	
10		0.13506885	$= T_2(x,\tau_2)/T_A$

TABLE 8

VARIATION OF TEMPERATURE WITH TIME AT VARIOUS POSITIONS, $(\frac{x}{\ell})$, ALONG THE BAR

* Taking $T(o,t) = T_A = 100^oC$, length = 0.04m and $\alpha = 5 \times 10^{-6} \frac{m^2}{s}$

frequency, f = 0.05 Hz, $(f\tau_c) = 0.5$, $(\frac{f\ell^2}{\alpha}) = 16$

$$\frac{x}{\ell} = 0.810$$

TIME s		Dimensionless Temperature T/T_A	
0	Bars separated	0.22866848	$= T_1(x,o)/T_A$
1		0.22647048	
2		0.22861019	
3		0.23410741	
4		0.24112757	
5		0.24878719	
6		0.25667223	
7		0.26457974	
8		0.27240720	
9		0.28010280	
10		0.28764154	$= T_1(x,\tau_1)/T_A$
0	Bars in contact	0.28764818	$= T_2(x,o)/T_A$
1		0.29123479	
2		0.28107277	
3		0.26929558	
4		0.25943185	
5		0.25150679	
6		0.24570896	
7		0.23986865	
8		0.23550833	
9		0.23182632	
10		0.22867569	$= T_1(x,\tau_2)/T_A$

TABLE 9

VARIATION OF TEMPERATURE WITH TIME AT VARIOUS POSITIONS, $(\frac{x}{\ell})$, ALONG THE BAR

* Taking $T(o,t) = T_A = 100^oC$, length = 0.04m and $\alpha = 5 \times 10^{-6} \frac{m^2}{s}$

frequency, f = 0.05 Hz, $(f\tau_c) = 0.5$, $(\frac{f\ell^2}{\alpha}) = 16$

$$\frac{x}{\ell} = 0.800$$

TIME s		Dimensionless Temperature T/T_A	
0	Bars separated	0.23997281	$= T_1(x,o)/T_A$
1		0.23756375	
2		0.23882933	
3		0.24339421	
4		0.24962037	
5		0.25662470	
6		0.26396664	
7		0.27141792	
8		0.27885748	
9		0.28621900	
10		0.29346680	$= T_1(x,\tau_1)/T_A$
0	Bars in contact	0.29347762	$= T_2(x,o)/T_A$
1		0.29793273	
2		0.29013441	
3		0.27961446	
4		0.27034514	
5		0.26269912	
6		0.25642515	
7		0.25122865	
8		0.24686944	
9		0.24316539	
10		0.23998030	$= T_2(x,\tau_2)/T_A$

TABLE 10

VARIATION OF TEMPERATURE WITH TIME AT VARIOUS POSITIONS, $(\frac{x}{\ell})$, ALONG THE BAR

* Taking $T(o,t) = T_A = 100^oC$, length = 0.04m and $\alpha = 5 \times 10^{-6} \frac{m^2}{s}$

frequency, f = 0.05 Hz, $(f\tau_c) = 0.5$, $(\frac{f\ell^2}{\alpha}) = 16$

$$\frac{x}{\ell} = 0.790$$

TIME s		Dimensionless Temperature T/T_A	
0	Bars separated	0.25118344	$= T_1(x,o)/T_A$
1		0.24862571	
2		0.24915277	
3		0.25286009	
4		0.25832790	
5		0.26469317	
6		0.27149799	
7		0.27849460	
8		0.28554461	
9		0.29256886	
10		0.29952171	$= T_1(x,\tau_1)/T_A$
0	Bars in contact	0.29953677	$= T_2(x,o)/T_A$
1		0.30454683	
2		0.29886137	
3		0.28961123	
4		0.28098900	
5		0.27367072	
6		0.26755952	
7		0.26243709	
8		0.25810254	
9		0.25439500	
10		0.25119024	$= T_2(x,\tau_2)/T_A$

TABLE 11

VARIATION OF TEMPERATURE WITH TIME AT VARIOUS POSITIONS, $(\frac{x}{\ell})$, ALONG THE BAR

* Taking $T(o,t) = T_A = 100^oC$, length = 0.04m and $\alpha = 5 \times 10^{-6} \frac{m^2}{s}$

frequency, f = 0.05 Hz, $(f\tau_c) = 0.5$, $(\frac{f\ell^2}{\alpha}) = 16$

$\frac{x}{\ell} = 0.500$

TIME s		Dimensionless Temperature T/T_A	
0	Bars separated	0.54125654	$= T_1(x,o)/T_A$
1		0.54050186	
2		0.53965096	
3		0.53874491	
4		0.53785910	
5		0.53709500	
6		0.53653814	
7		0.53624038	
8		0.53622338	
9		0.53648791	
10		0.53702228	$= T_1(x,\tau_1)/T_A$
0	Bars in contact	0.53703183	$= T_2(x,o)/T_A$
1		0.53781840	
2		0.53883276	
3		0.53999780	
4		0.54109958	
5		0.54192929	
6		0.54239817	
7		0.54251233	
8		0.54232179	
9		0.54188806	
10		0.54126913	$= T_2(x,\tau_2)/T_A$

TABLE 12

VARIATION OF TEMPERATURE WITH TIME AT VARIOUS POSITIONS, $(\frac{x}{\ell})$, ALONG THE BAR

* Taking $T(o,t) = T_A = 100^oC$, length = 0.04m and $\alpha = 5 \times 10^{-6} \frac{m^2}{s}$

frequency, f = 0.05 Hz, $(f\tau_c) = 0.5$, $(\frac{f\ell^2}{\alpha}) = 16$

$$\frac{x}{\ell} = 0.05$$

TIME s	Dimensionless Temperature T/T_A	
0	0.95390207	$= T_1(x,o)/T_A$
1	0.95393185	
2	0.95396050	
3	0.95398556	
4	0.95400494	
5	0.95401710	
6	0.95402113	
7	0.95401670	
8	0.95400419	
9	0.95398469	
10	0.95395998	$= T_1(x,\tau_1)/T_A$
0	0.95396317	$= T_2(x,o)/T_A$
1	0.95393473	
2	0.95390633	
3	0.95388029	
4	0.95385905	
5	0.95384482	
6	0.95383936	
7	0.95384361	
8	0.95385731	
9	0.95387887	
10	0.95390572	$= T_2(x,\tau_2)/T_A$

TABLE 13

NUMERICAL MATRIX INVERSION METHOD SOLUTION

Periodic time = 20s

$\ell = 0.04\text{m}, \alpha = 5 \times 10^{-6} \frac{m^2}{s}, (\frac{f\ell^2}{\alpha}) = 16$

$f\tau_c$	$(\frac{f\ell_i^2}{\alpha})$
0.05	9.7628
0.1	3.8245
0.2	1.2402
0.32	0.45909
0.4	0.25058
0.5	0.11652
0.6	0.050515
0.7	0.018741
0.8	0.0050918
0.9	0.58926×10^{-3}
0.95	0.72586×10^{-4}

TABLE 14

TABLES 15 - 22 Analogue computer study results (Imperfect Contact)

$\frac{f.\lambda^2}{\alpha} = 0.016$

Frequency Hz →	0.02		0.2		2.0	
	$f\tau_c$	$\frac{f\ell^2_i}{\alpha}$	$f\tau_c$	$\frac{f\ell^2_i}{\alpha}$	$f\tau_c$	$\frac{f\ell^2_i}{\alpha}$
	0.097	11.0	0.067	14.2	0.192	2.38
	0.174	3.98	0.04	32.6	0.307	0.81
	0.354	0.742	0.134	3.98	0.485	0.22
	0.519	0.154	0.232	1.24	0.609	0.081
	0.597	0.100	0.371	0.435	0.692	0.026
	0.705	0.034	0.605	0.071	0.88	0.0023
	0.824	0.0065	0.71	0.025	0.933	0.0004
	0.933	0.0004	0.795	0.0092		
			0.878	0.0031		
			0.52	0.137		

TABLE 15

$$\frac{f.\lambda^2}{\alpha} = 0.16$$

Frequency Hz →	0.02		0.2		2.0	
	$f\tau_c$	$\frac{f\ell^2_i}{\alpha}$	$f\tau_c$	$\frac{f\ell^2_i}{\alpha}$	$f\tau_c$	$\frac{f\ell_i^2}{\alpha}$
			0.108	21.0	0.77	30.4
	0.134	14.0	0.062	43.9	0.173	8.72
	0.238	3.4	0.188	6.7	0.277	2.41
	0.334	1.72	0.300	2.07	0.408	0.952
	0.434	0.761	0.400	0.95	0.55	0.362
	0.565	0.28	0.523	0.346	0.66	0.107
	0.66	0.115	0.607	0.175	0.808	0.024
	0.725	0.0602	0.710	0.0701	0.95	0.0008
	0.858	0.0203	0.825	0.0164		
			0.905	0.0031		

TABLE 16

$$\frac{f.\lambda^2}{\alpha} = 0.295$$

Frequency Hz →	0.187		0.187		1.46		16.4	
	$f\tau_c$	$\frac{f\ell_i^2}{\alpha}$	$f\tau_c$	$\frac{f\ell_i^2}{\alpha}$	$f\tau_c$	$\frac{f\ell_i^2}{\alpha}$	$f\tau_c$	$\frac{f\ell_i^2}{\alpha}$
	0.065	98.6	0.086	53.1	0.048	126	0.079	81.9
	0.220	6.9	0.163	13.4	0.124	21.1	0.089	40.5
	0.357	1.85	0.129	22.0	0.089	52.5	0.137	13.5
	0.558	0.445	0.283	3.71	0.209	7.84	0.261	3.30
	0.686	0.119	0.428	1.13	0.316	3.0	0.400	1.05
	0.802	0.037	0.527	0.516	0.465	1.1	0.523	0.336
	0.907	0.0033	0.675	0.144	0.605	0.28	0.75	0.050
			0.795	0.041	0.73	0.087		
			0.893	0.0075	0.815	0.0301		

Table 17

$$\frac{f\lambda^2}{\alpha} = 1.6$$

Frequency Hz	0.02		0.2		2.0		20	
	$f\tau_c$	$\frac{f\ell_i^2}{\alpha}$	$f\tau_c$	$\frac{f\ell_i^2}{\alpha}$	$f\tau_c$	$\frac{f\ell_i^2}{\alpha}$	$f\tau_c$	$\frac{f\ell_i^2}{\alpha}$
	0.275	17.0	0.090	190	0.071	383	0.107	173
	0.162	53.6	0.188	35.8	0.142	66.9	0.194	26.4
	0.109	131	0.311	10.6	0.236	24.6	0.327	5.91
	0.297	12.5	0.485	2.35	0.308	10.2	0.500	1.63
	0.420	4.38	0.640	0.679	0.480	2.51	0.73	0.221
	0.559	1.40	0.760	0.196	0.62	1.03	0.873	0.033
	0.688	0.466	0.87	0.0423	0.77	0.185	0.615	0.645
	0.867	0.052			0.935	0.025		

Table 18

$$\frac{f.\lambda^2}{\alpha} = 16$$

Frequency Hz	0.0794		0.81	
	$f\tau_c$	$\frac{f\ell_i^2}{\alpha}$	$f\tau_c$	$\frac{f\ell_i^2}{\alpha}$
	0.182	342	0.858	0.366
	0.091	1770	0.744	1.99
	0.318	64.0	0.989	0.193
	0.477	23.4	0.616	6.60
	0.618	7.10	0.497	17.1
	0.767	1.64	0.390	43.0
			0.222	211
			0.113	957
			0.058	3540

Table 19

$$\frac{f.\lambda^2}{\alpha} = 160$$

Frequency Hz →	0.0807		0.80		8.0	
	$f\tau_c$	$\frac{f\ell_i^2}{\alpha}$	$f_{\tau c}$	$\frac{f\ell_i^2}{\alpha}$	$f\tau_c$	$\frac{f\ell_i^2}{\alpha}$
	0.0912	1.74×10^4	0.08	2.1×10^4	0.081	2.78×10^4
	0.203	2360	0.134	5910	0.211	3150
	0.295	936	0.062	2.9×10^4	0.383	654
	0.451	241	0.225	1850	0.689	42.8
	0.580	45.8	0.34	53.8	0.797	13.2
	0.710	26.1	0.512	139	0.918	1.41
	0.853	4.5	0.667	39.5	0.542	156
	0.907	1.66	0.80	10.2		
			0.90	2.01		
			0.807	7.6		
			0.680	30.8		
			0.606	63.0		
			0.450	237		
			0.27	1300		
			0.128	9950		

TABLE 20

$$\frac{f.\lambda^2}{\alpha} = 1600$$

Frequency Hz →	0.02		2.0		20	
	$f\tau_c$	$\frac{f\ell_i^2}{\alpha}$	$f\tau_c$	$\frac{f\ell_i^2}{\alpha}$	$f\tau_c$	$\frac{f\ell_i^2}{\alpha}$
	0.054	4.39×10^5	0.038	6.03×10^5	0.164	4.65×10^4
	0.096	1.41×10^5	0.075	1.14×10^5	0.455	2.95×10^3
	0.121	9.69×10^4	0.161	4.L6x10^4	0.588	810
	0.192	3.37×10^4	0.26	1.34×10^4	0.35	7.26×10^3
	0.28	1.29×10^4	0.142	6.3×10^4	0.075	2.99×10^5
	0.334	8.39×10^3	0.374	5.1×10^3	0.695	307
	0.40	4.7×10^3	0.45	2.14×10^3	0.80	98.5
	0.52	1.65×10^3	0.575	803	0.94	7.6
	0.46	2.73×10^3	0.72	220		
	0.61	880	0.86	46		
	0.76	203	0.95	2.82		
	0.855	52	0.528	1.29×10^3		
	0.905	21.3	0.14	7.4×10^4		
	0.67	456	0.116	1.09×10^5		
			0.448	2.37×10^3		

TABLE 21

λ = zero

Frequency Hz	0.042		1.73		6.0		10.0	
	$f\tau_c$	$\frac{f\ell_i^2}{\alpha}$	$f\tau_c$	$\frac{f\ell_i^2}{\alpha}$	$f\tau_c$	$\frac{f\ell_i^2}{\alpha}$	$f\tau_c$	$\frac{f\ell_i^2}{\alpha}$
	0.215	0.927	0.527	0.104	0.086	4.37	0.062	3.06
	0.127	2.21	0.602	0.0545	0.154	1.97	0.154	1.55
	0.0507	6.9	0.670	0.027	0.24	0.887	0.247	0.81
	0.366	0.273	0.770	0.0080	0.365	0.361	0.346	0.41
	0.488	0.107	0.396	0.274	0.490	0.128	0.454	0.154
	0.648	0.0251	0.346	0.425	0.600	0.0745	0.654	0.043
	0.736	0.0087	0.284	0.591	0.714	0.0245	0.770	0.011
	0.827	0.0024	0.232	1.04	0.83	0.0032		
	0.874	0.0008	0.173	1.74				
			0.129	3.13				
			0.069	6.77				
			0.033	20.1				

Table 22

Tables 23-25 Effect of $(f\tau_c)$ on heat flow at various $(f\lambda^2/\alpha)$

$f = 1\text{Hz}$ $\quad \ell = 40\text{mm}$ $\quad \alpha = 5 \times 10^{-6}\ \frac{m^2}{s}$ for Tables 23-25

$\lambda = 0$

$(f\tau_c)$	(Q/Q_c)
0.1	0.837
0.2	0.937
0.3	0.974
0.4	0.987
0.5	0.996
0.6	0.989
0.7	0.999
1.0	1.0

Table 23

$\frac{f\lambda^2}{\alpha} = 1.6$ $\quad \lambda = 2.83\text{mm}$

$(f\tau_c)$	(Q/Q_c)
0.1	0.556
0.2	0.714
0.3	0.799
0.5	0.870
0.6	0.890
0.7	0.906
0.8	0.917
0.9	0.926
1.0	0.934

Table 24

$\frac{f\lambda^2}{\alpha} = 160$ $\lambda = 28.3\text{mm}$

$(f\tau_c)$	(Q/Q_c)
0.1	0.128
0.2	0.219
0.3	0.300
0.4	0.369
0.5	0.418
0.5	0.463
0.7	0.503
0.8	0.531
0.9	0.560
1.0	0.586

Table 25

Tables 26-29 Results of iterative method of solution(imperfect contact)

Input Data

Periodic time, τ, = 1.09s $(1/\sqrt{\alpha})$ = 44.70 $s^{\frac{1}{2}}m^{-1}$,

Bar length ℓ = 0.04m, μ_1 = 0, μ_2 = $35.3m^{-1}$

Contact period τ_c = variable Distance x = 0.04m

giving $(\frac{f\lambda^2}{\alpha})$ = 160.35 and $(\frac{f\ell^2}{\alpha})$ = 319.69

r = number of terms required for convergence of $\sum_{m=o}^{r} T_m(\ell,t)$

to 5 significant figures

τ_c	$(f\tau_c)$	$(\frac{f\ell_i^2}{\alpha})$	r
0.1	0.1	1.3405×10^4	5
0.2	0.2	2.6867×10^3	9
0.3	0.3	9.2690×10^2	14
0.4	0.4	3.8840×10^2	20
0.5	0.5	1.7593×10^2 *	> 20
0.6	0.6		> 20

* Slow convergence of $\sum_{m=o}^{\infty} T_m(\ell,t)$ see Table 27

Slow convergence render computation insufficiently accurate

Table 26

$T_o(\ell,t)$ taken as 100K so that $T(\ell,t) = 100 + \sum_{m=1}^{\infty} T_m(\ell,t)$

	$f\tau_c = 0.5$	$f\tau_c = 0.6$
Number of terms n	$\sum_{m=1}^{n} T_m(\ell,t)$ K	$\sum_{m=1}^{n} T_m(\ell,t)$ K
1	-70.600	-84.720
2	-20.053	-12.280
3	-55.384	-73.167
4	-30.689	-21.987
5	-47.950	-65.008
6	-35.885	-28.846
7	-44.318	-59.243
8	-38.424	-33.692
9	-42.544	-55.169
10	-39.664	-37.116
11	-41.667	-52.291
12	-40.270	-39.535
13	-41.253	-50.258
14	-40.566	-41.244
15	-41.046	-48.821
16	-40.711	-42.452
17	-40.945	-47.805
18	-40.781	-43.306
19	-40.896	-47.088
20	-40.816	-43.909

For $f\tau_c = 0.5$, $\sum_{m=1}^{\infty} T_m(\ell,t)$ taken as

$$\tfrac{1}{2}\left\{\left[\sum_{m=1}^{20} T_m(\ell,t)\right] + \left[\sum_{m=1}^{19} T_m(\ell,t)\right]\right\} = 40.856K$$

TABLE 27

$(f\tau_c) = 0.5, \qquad (1/\sqrt{\alpha}) = 447.0\ s^{\frac{1}{2}}\ m^{-1}$

Bar length $\ell = 0.04m, \qquad \mu_1 = 0$

Distance $x = 0.04m$

τ and μ_2 variable such that $(\frac{f\lambda^2}{\alpha}) \simeq 160$ constant

$r' =$ No of terms required for convergence of $\sum_{m=o}^{r} T_m(\ell,t)$ to

5 significant figures

Periodic Time s	$(\frac{f\ell_i^2}{\alpha})$	μ_2 m^{-1}	$(\frac{f\lambda^2}{\alpha})$	$(\frac{f\ell^2}{\alpha})$	$(f\tau_c)$	r'
1.000	167.56	1.1163	160.34	0.31969	0.5	4
100	167.34	3.53	160.35	3.1969	0.5	5
10	168.77	11.16	160.43	31.969	0.5	7
9.5908	168.74	11.398	160.36	33.33	0.5	8
3.1969	170.53	19.743	160.35	100	0.5002	13
1.0	175.93*	35.3	160.35	319.69		> 20
0.0959	Divergent series	113.98	160.36	3333	0.5	Divergent series

* Based on estimated sum of series $\sum_{m=o}^{\infty} T_m(\ell,t)$, see Table 27

Table 28

r = Number of terms required for convergence of

$\sum_{m=0}^{r} \left\{ T_m(\ell,t) \right\}$ to 5 significant figures

Periodic time s	$(\frac{f\ell_i^2}{\alpha})$	$\mu_m^2 - 1$	$(\frac{f\lambda^2}{\alpha})$	$(\frac{f\ell^2}{\alpha})$	$f\tau_c$	r
1000	Divergent	111.63	0.016034	0.31969	0.5	Divergent
1000	Divergent	111.63	0.016034	0.31969	0.05	Divergent
10^5	0.028281	11.163	0.016034	0.0031969	0.5	8
10^5	9.1206	11.163	0.016034	0.0031969	0.5	12
10^4	21.816	11.163	0.16034	0.031969	0.1	10
1000	2.1239×10^3	35.3	0.16035	0.31969	0.01	4
1000	167.56	1.1163	160.34	0.31969	0.5	4

Table 29

Tables 30(a) - (h)

Experimental results with test rig No.1

$\left(\frac{f\lambda^2}{\alpha}\right) \rightarrow$ 0.4 - 0.6			0.6 - 0.8		
Frequency Hz	$(f\tau_c)$	$\left(\frac{fl_i^2}{\alpha}\right)$	Frequency Hz	$(f\tau_c)$	$\left(\frac{fl_i^2}{\alpha}\right)$
0.0303	0.395	3.95	0.0467	0.395	7.2
0.0322	↓	3.16	↓	↓	4.32
0.0310	↓	3.39	0.0526	0.675	0.042
0.0312	0.573	1.10	↓	↓	0.280
0.0317	0.076	29.1	↓	↓	0.0563
↓	↓	25.6			
↓	↓	26.4			
0.0318	0.123	11.6			
		13.5			
0.0314	0.193	8.72			
0.0328	0.783	1.05			
		0.72			

Table 30(a)

$\left(\frac{f\lambda^2}{\alpha}\right) \rightarrow$ 0.8 - 1.0		
Frequency H_z	$(f\tau_c)$	$\left(\frac{fl_i^2}{\alpha}\right)$
0.063	0.395	4.66
0.0642	0.573	1.57
0.0635	↓	1.15
0.0643	0.076	48.2
↓	↓	38.8
↓	↓	42.8
↓	↓	37.2
0.0649	0.123	34.2
↓	↓	24.5
↓	↓	37.9
0.0645	0.193	9.4
↓	↓	6.1
0.0626	0.297	4.74
↓	↓	5.89
↓	↓	4.50
0.6628	0.675	0.072
↓	↓	0.109
0.0653	0.783	0.825
↓	↓	0.791

Table 30(b)

$\frac{f\lambda^2}{\alpha} \rightarrow 1.6$		
f Hz	$(f\tau_c)$	$\left(\frac{fl_i^2}{\alpha}\right)$
0.115 ↓	0.395 ↓	4.95 4.26

Table 30 (c)

$\frac{f\lambda^2}{\alpha} \rightarrow 1.8 - 2.0$		
f Hz	$(f\tau_c)$	$\left(\frac{fl_i^2}{\alpha}\right)$
0.130 ↓	0.395 ↓	4.49 5.66

Table 30 (d)

$\frac{f\lambda^2}{\alpha}$ → 3.2 - 3.4			3.4 - 3.6			3.6 - 3.8		
f Hz	$(f\tau_c)$	$\left(\frac{fl_i^2}{\alpha}\right)$	f Hz	$(f\tau_c)$	$\left(\frac{fl_i^2}{\alpha}\right)$	f Hz	$(f\tau_c)$	$\left(\frac{fl_i^2}{\alpha}\right)$
0.231 ↓	0.076 ↓	157 121 189	0.260 ↓ 0.245 ↓	0.297 ↓ 0.193 ↓	22.2 36.3 38.5 25.4 47.4	0.260 ↓	0.297 ↓	22.2 36.3

Table 30 (e)

$\frac{f\lambda^2}{\alpha}$ → 3.8 - 4.0			4.2 - 4.4		
f Hz	$(f\tau_c)$	$\left(\frac{fl_i^2}{\alpha}\right)$	f Hz	$(f\tau_c)$	$\left(\frac{fl_i^2}{\alpha}\right)$
0.278 ↓	0.395 ↓	17.3 18.6	0.299	0.844	2.33

Table 30(e) (Cont'd)

$\frac{f\lambda^2}{\alpha} \rightarrow$ 6.2 - 6.4			6.6 - 6.8			7.0 - 7.2		
f Hz	$(f\tau_c)$	$\left(\frac{fl_i^2}{\alpha}\right)$	f Hz	$(f\tau_c)$	$\left(\frac{fl_i^2}{\alpha}\right)$	f Hz	$(f\tau_c)$	$\left(\frac{fl_i^2}{\alpha}\right)$
0.448	0.395	18.0	0.470	0.573	7.78	0.497	0.297	8.83
			0.481		5.26			21.0
					4.47	0.506	0.783	0.343
					3.70			0.395

Table 30(f)

$\frac{f\lambda^2}{\alpha} \rightarrow$ 7.2 - 7.4			7.4 - 7.6		
f Hz	$(f\tau_c)$	$\left(\frac{fl_i^2}{\alpha}\right)$	f Hz	$(f\tau_c)$	$\left(\frac{fl_i^2}{\alpha}\right)$
0.519	0.395	46.6	0.528	0.076	333
		54.3			
0.576	0.197	71.2			
0.524	0.197	79.0			
0.523	0.844	1.99			

Table 30(f) (Cont'd)

$\frac{f\lambda^2}{\alpha}$ → 11.0 - 11.2			13.2 - 13.4			15.1 - 15.3			15.3 - 15.5			14.4		
f Hz	$(f\tau_c)$	$\left(\frac{fl_i^2}{\alpha}\right)$	f Hz	$(f\tau_c)$	$\left(\frac{fl_i^2}{\alpha}\right)$	f Hz	$(f\tau_c)$	$\left(\frac{fl_i^2}{\alpha}\right)$	f Hz	$(f\tau_c)$	$\left(\frac{fl_i^2}{\alpha}\right)$	f Hz	$(f\tau_c)$	$\left(\frac{fl_i^2}{\alpha}\right)$
0.782	0.395	57.3 21.6	0.445	0.573	9.94 25.4	1.08 1.075	0.573 0.395	14.6 87.0 71.2 71.4 277 401	1.10	0.076	496 556 789	1.025	0.573	17.3
						1.08	0.123							

Table 30(g)

$\frac{f\lambda^2}{\alpha}$ → 21 - 23			29.6		
f Hz	$(f\tau_c)$	$\left(\frac{fl_i^2}{\alpha}\right)$	f Hz	$(f\tau_c)$	$\left(\frac{fl_i^2}{\alpha}\right)$
1.5 1.62 1.60	0.395	91.4 169.0 112.5	2.10	0.40	260

Table 30(h)

Tables 31(a) - 38 Experimental Results with Test Rig No2

NOMENCLATURE

f = Frequency Hz

$(f\tau_c)$ = ratio contact time:periodic time

2λ = thermal contact resistance offered by contact interface, expressed as an equivalent length in inches of copper bar 1 in diameter. (1 in length of above copper bar has thermal resistance of 0.132K/W).

$2(\lambda + \ell_i)$ = thermal resistance offered by contact interface under periodic contact conditions, expressed as an equivalent length in inches of 1 in diameter copper bar as above.

$2\ell_i$ = thermal resistance due to periodic interruption of heat flow expressed as an equivalent length in inches of 1 in diameter copper bar as above.

$2\lambda_m$ = mean value of 2λ used to compute ℓ_i

$$\ell_i = (\lambda + \ell_i) - \lambda_m$$

α = diffusivity ($115 \times 10^{-6} m^2/s$)

Results with Test Rig No.2

Static Load on surfaces 7.5 lbf(33.4N)

Lapped Contact Surfaces (Flexible Adhesives Ltd Grade "W" paste)

Ref. No.	Frequency Hz	$(f\tau_c)$	2λ in	$2(\lambda+\ell_i)$ in	$2\lambda_m$ in	$(\frac{f\lambda_m^2}{\alpha})$	$(\frac{f\ell_i^2}{\alpha})$
48	0.0	1.0	4.961				
49			4.922				
50			5.630				
51			4.756				
52			4.785				
53			4.176				
54			6.428				
56	0.0444	0.5		13.26		1.616	4.147
57	0.0444	0.5		11.63	5.094	1.616	2.66
58	0.0427	0.5		11.29		1.554	2.297
59	0.0427	0.5		11.65		1.554	2.575
60	0.0	1.0	4.970				
61	0.043	0.310		17.82		1.49	9.955
62							
63	0.043	0.310		17.37		1.49	9.278
64	0.0448	0.090		49.38	4.970	1.522	123.9
65	0.0442	0.090		44.83		1.531	98.47
66	0.0450	0.090		43.36		1.559	93.02
67	0.0	1.0	3.941				
68			3.778				
69	0.0405	0.63		7.552		0.846	0.8605
70	0.0405	0.63		8.109		0.846	1.026
71	0.0405	0.63		8.173	3.860	0.846	1.057
72	0.0416	0.83		5.783		0.869	0.2159
73	0.0408	0.83		6.247		0.8253	0.3261
74	0.0	1.0	5.483				
75		1.0	4.469				
76	0.0515	0.185		19.95		1.789	16.19
77	0.0515	0.185		27.06	4.976	1.789	35.22
78	0.0458	0.43		9.628		1.591	1.30
79	0.0454	0.43		10.52		1.577	1.958
81	0.0	1.0	3.96				

TABLE 31 (a)

Re.computation of Trials 69 - 73 and 76 - 79 with revised λ_m

see section

Ref. No.	Frequency Hz	$(f\tau_c)$	$2(\lambda+\ell_i)$	$2\lambda_m$	$(\frac{f\lambda_m^2}{\alpha})$	$(\frac{f\ell_i^2}{\alpha})$
69	0.0405	0.63	7.552		1.107	0.55707
70	0.0405	0.63	8.109		1.107	0.7726
71	0.0405	0.63	8.173	4.418	1.107	0.7997
72	0.0416	0.83	5.783		1.137	0.1086
73	0.0408	0.83	6.247		1.142	0.1911
76	0.0515	0.185	19.95		1.551	16.927
77	0.0515	0.185	27.06	4.638	1.551	36.258
78	0.0458	0.43	9.628		1.379	1.547
79	0.0454	0.43	10.52		1.379	2.199

Table 31(b)

Static Load on surfaces 7.5 lbf (33.4N)

Contact surfaces coated with silver-impregnated epoxy resin

Ref. No.	Frequency Hz	$(f\tau_c)$	2λ in	$2(\lambda+\ell_i)$ in	$2\lambda_m$ in	$2\ell_i$ in	$\left(\frac{f\lambda_m^2}{\alpha}\right)$	$\left(\frac{f\ell_i^2}{\alpha}\right)$
101	0.0	1.0	1.228					
102			0.9436					
103			0.6981					
104			—					
105			0.6994					
106	0.10	0.5		2.608		1.762	0.100	0.4348
107		0.099		14.24	0.846	13.394		25.12
108		0.099		12.90		12.054		20.35
109		0.195		7.125		6.279		5.521
110		0.286		5.115		4.269		2.552
111	0.0	1.0	0.6607					
112	0.103	0.286		4.69	0.523	4.160	0.04052	2.496
113	0.098	0.382		3.402		2.872	0.0385	1.062
114	0.0	1.0	0.3851					
115	0.098	0.382		3.281		2.164	0.2595	0.6426
116	0.10	0.618		1.827	1.117	0.720	0.26481	0.0726
117	0.098	0.62		1.87		0.753	0.2595	0.07782
118	0.089	0.767		1.560		0.443	0.2357	0.02446
119	0.0918	0.767		2.538		1.42	0.2431	0.2592
120	0.0	1.0	1.486					
121			1.646					
122	0.10	0.84		1.658	1.306	0.352	0.2389	0.01735
123				2.303		0.9970	0.2389	0.1392
124	0.0	1.0	1.557					
125			0.5354					
126	1.47	0.179		10.76	0.9492	9.811	1.8548	198.2
127	1.25	0.179		10.38		9.436	1.5772	155.7
128	1.19	0.32		4.303		3.353	1.5015	18.74
129	0.0	1.0	0.7552					
130	1.67	0.394		4.473	0.9096	3.563	1.935	26.98
131	1.18	0.477		3.774	0.9096	2.864	1.367	13.56
132	0.0	1.0	1.064					
133	1.19	0.642		2.626	1.086	1.540	1.965	3.952
134	1.18	0.75		2.207		1.121	1.949	2.077
135	0.0	1.0	1.107					

TABLE 32(a)

Ref. No.	Frequency Hz	$(f\tau_c)$	2λ in	$2(\lambda+\ell_i)$ in	$2\lambda_m$ in	$2\ell_i$ in	$\left(\frac{f\lambda_m^2}{\alpha}\right)$	$\left(\frac{f\ell_i^2}{\alpha}\right)$
136	1.64	0.079		17.73		16.593	2.969	632.3
137	1.21	0.085		40.84	1.137	39.703	2.191	2671.0
138	1.27	0.559		3.471		2.334	2.299	9.688
139	0.0	1.0	1.166					
140	1.46	0.91		1.627	1.129	0.498	2.606	0.507
141	1.22	0.91		1.856		0.727	2.177	0.903
142	0.0	1.0	1.091					
143	1.27	0.328		6.659			2.121	55.22
144	1.28	0.312		6.315			2.137	48.99

TABLE 32(b)

Static Load on surfaces 7.5 lbf (33.4N)

Lapped contact surfaces

Ref. No.	Frequency Hz	$(f\tau_c)$	2λ in	$2(\lambda+\ell_i)$ in	$2\lambda_m$ in	$2\ell_i$ in	$\left(\frac{f\lambda_m}{\alpha}\right)^2$	$\left(\frac{f\ell_i}{\alpha}\right)^2$
145	0.0	1.0	5.548					
146			5.198					
147			5.799					
148			5.463					
149			5.111					
150			5.619					
151			6.471					
152	1.33	0.55		7.949		3.568	35.75	23.71
153	1.25	0.55		7.164	4.381	2.783	33.60	13.58
154	1.18	0.28		13.25		8.869	31.72	29.98
155	1.18	0.28		11.26		6.879	31.72	78.20
156	0.0	1.0	3.046					
157			3.053					
158			2.955					
159			2.934					
160	1.35	0.473		7.401		4.345	17.66	35.69
161	1.35	0.473		7.635		4.579	17.66	39.64
162	3.15	0.375		11.98		8.924	41.20	351.3
163	3.15	0.375		11.99	3.056	8.925	41.20	351.2
164	1.21	0.467		7.510		4.454	15.83	33.62
165	3.70	0.362		11.94		8.884	48.39	409.0
166	3.70	0.318		14.57		11.514	48.39	686.9
167	0.0	1.0	2.919					
168			3.362					
169			3.122					
170	3.60	0.575		6.414	3.120	3.294	44.08	54.70
171	0.0	1.0	2.912					
172			3.067					
173			3.213					
174			3.185					
175			3.000					
176			3.301					

TABLE 33

Static Load on surfaces 7.5 lbf (33.4N)

Contact gap when separated 0.006 in

Ref. No.	Frequency Hz	$(f\tau_c)$	2λ in	$2(\lambda+\ell_i)$ in	$2\lambda_m$ in	$2\ell_1$ in	$\left(\frac{f\lambda_m}{\alpha}\right)^2$	$\left(\frac{f\ell_i}{\alpha}\right)^2$
177	0.0	1.0	7.588					
178			8.018					
179			7.968					
180	1.96	0.51		24.07	8.676	15.39	206.6	650.4
181	1.98	0.525		23.37		14.69	208.7	598.7
182	0.0	1.0	9.484					
183			9.636					
184			9.359					

Table 34

Static Load on Surfaces 15 lbf (66.8N)
Lapped contact surfaces
Contact gap 0.0045 (0.114mm)

Ref. No.	Frequency Hz	$f\tau_c$	2λ in	$2(\lambda+\ell_i)$ in	$2\lambda_m$ in	$\left(\frac{f\lambda_m^2}{\alpha}\right)$	$\left(\frac{f\ell_i^2}{\alpha}\right)$
210	0.0	1.0	9.969				
211	2.7	0.5		12.38	7.376	205.7	94.68
212	0.0	1.0	6.314				
213	0.0	1.0	6.125				

Table 35

Static Load on Surfaces 15 lbf (66.8N)

Contact Gap 0.049" (1.25mm)

Ref. No.	Frequency Hz	$f\tau_c$	2λ in	$2(\lambda+\ell_i)$ in	$2\lambda_m$ in	$\left(\frac{f\lambda_m^2}{\alpha}\right)$	$\left(\frac{f\ell_i^2}{\alpha}\right)$
221	0.0	1.0	6.575				
222	2.6	0.397		15.78	6.548	156.1	310.3
223	2.74	0.375		13.29		164.5	174.4
224	0.0	1.0	6.009				
225	0.0	0.0	207.6				
226	0.0	1.0	6.351				
227	0.0	1.0	7.434				
228	0.0	1.0	6.371				
229	2.74	0.39		13.50	6.526	163.4	186.6
230	2.74	0.39		12.88		163.4	159.8
231	0.0	1.0	7.813				
232	0.0	1.0	7.386				
233	0.0	1.0	5.645				
234	1.0	1.0	5.195				

Table 36

Static Load Surfaces 15 lbf
Contact Gap 0.025 in (0.635mm)

Ref. No.	Frequency Hz	$(f\tau_c)$	2λ in	$2(\lambda+\ell_i)$ in	$2\lambda_m$ in	$2\ell_i$ in	$(\frac{f\lambda_m^2}{\alpha})$	$(\frac{f\ell_i^2}{\alpha})$
235								
235	0.0	1.0	7.191					
230			6.005					
237			6.199					
238			5.533					
239	3.33	0.387		14.89	6.585	8.305	202.2	321.6
240	3.36	0.374		14.93		8.345	204	327.7
242	0.0	1.0	6.810					
242A			7.769					
243	3.30	0.367		15.15	7.240	242.2	242.2	284.1
244	3.37	0.373		14.67			247.3	260.5
245	0.0	1.0	7.467					
246			7.098					
247			7.057					
248	1.715	0.414		13.74	6.535		102.5	124.7
249	0.0	1.0	5.654					
250			5.390					
251	1.825	0.421		13.11	7.157		130.9	90.6
252	1.78	0.428		15.32			127.7	166.1
253	1.78	0.428		16.37			127.7	211.6
254	0.0	1.0	8.295					
255			8.341					
256			7.305					
257			7.958					

Table 37

Ref. No.	Frequency Hz	$(f\tau_c)$	2λ in	$2(\lambda+\ell_i)$ in	$2\lambda_m$ in	$\left(\frac{f\lambda_m^2}{\alpha}\right)$	$\left(\frac{f\ell_i^2}{\alpha}\right)$
263	0.175	0.507		11.99		14.3	4.633
264	0.175	0.507		11.99	7.642	14.3	4.633
264A	0.0	1.0	6.337				
265	0.173	0.507		11.09		8.67	6.321
266	0.169	0.507		12.66		8.47	10.55
267	0.172	0.496		12.94	5.982	8.62	11.66
268	0.175	0.496		11.80		5177	8.295
269	0.176	0.520		11.59		8.82	7.75
270	0.0	1.0	6.005				
271			5.694				
272			5.436				
273			5.811				
274			6.614				
275	0.0858	0.495		11.62		4.14	4.097
276	0.0823	0.488		11.93	5.781	3.97	4.358
277	0.0847	0.496		11.56		4.09	3.961
278	0.0832	0.490		11.67		4.02	4.041
279	0.0838	0.491		11.46		4.05	3.784
280	0.0	1.0	5.524				
281			5.385				

Table 38

Tables 39 and 40 Effect of impact on $(\frac{f\ell_i^2}{\alpha})$

Nomenclature

G_e = $(\frac{f\ell_i^2}{\alpha})$ obtained experimentally

G_t = $(\frac{f\ell_i^2}{\alpha})$ obtained theoretically

M = momentum before impact in kg m/s

Table No.	Ref. No.	$f\tau_c$	$(\frac{f\lambda_m^2}{\alpha})$	G_t	G_e	$\frac{G_e}{G_t}$	M
31	56	0.5	1.616	2.0	4.147	2.07	0.763
	57		1.616	2.0	2.66	1.33	
	58		1.554	1.95	2.297	1.18	
	59		1.554	1.95	2.575	1.32	
33	160	0.473	17.66	23	35.69	1.55	0.763
	161	0.473	17.66	23	39.64	1.72	
	164	0.467	15.83	22	33.62	1.53	
	170	0.575	49.08	25	54.7	2.18	
34	180	0.51	206.6	170	650.4	3.85	0.187
	181	0.525	208.7	155	598.7	3.86	
35	211	0.5	205.7	185	94.68	0.51	0.264
36	222	0.397	156.1	380	310.3	0.817	0.755
	223	0.375	164.1	390	174.4	0.447	
36	229	0.39	163.4	350	186.6	0.533	0.755
	230		163.4	350	159.8	0.457	
37	239	0.387	202.2	450	321.6	0.713	0.539
	240	0.374	204	500	327.7	0.657	
	243	0.367	242.2	670	289.1	0.432	
	244	0.373	247.3	630	260.5	0.413	
	248	0.414	102.5	190	124.7	0.657	
	251	0.421	130.9	128	90.6	0.705	
	252	0.428	127.7	200	166.1	0.83	
	253	0.428	127.7	200	211.6	1.05	

Table 39

Table No.	Ref. No.	$f\tau_c$	$(\frac{f\lambda_m^2}{\alpha})$	G_t	G_e	$\frac{G_e}{G_t}$	M
38	263	0.507	14.3	13.2	4.633	0.35	0.539
	264	0.507	14.3	13.2	4.633	0.35	
	265	0.507	8.67	8.6	6.321	0.736	
	266	0.507	8.47	8.5	10.55	1.24	
	267	0.496	8.62	9.0	11.66	1.295	
	268	0.446	8.77	9.2	8.295	0.901	
	269	0.520	8.82	8.0	7.75	0.969	
	275	0.495	4.14	5.0	4.097	0.82	
	276	0.488	3.97	4.9	4.358	0.893	
	277	0.496	4.09	4.4	3.961	0.9	
	278	0.490	4.02	4.9	4.041	0.825	
	279	0.491	4.05	5.0	3.784	0.757	

Table 40

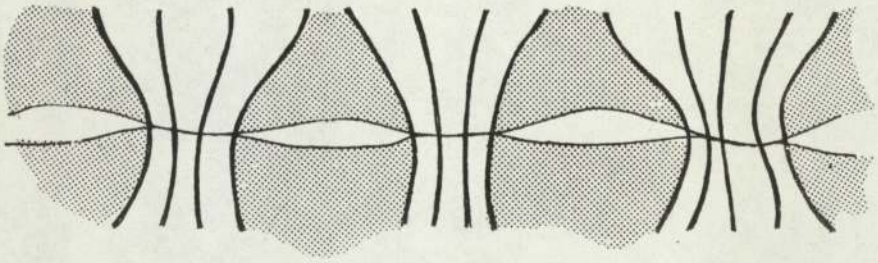

(a) Macroscopic constriction

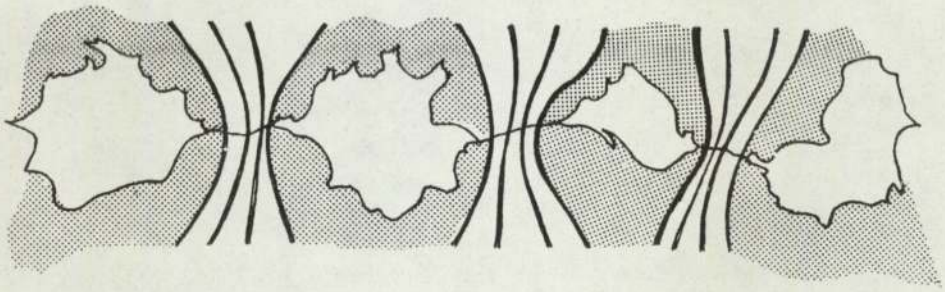

(b) Microscopic constriction

Fig. 1 Macroscopic and microscopic restrictions

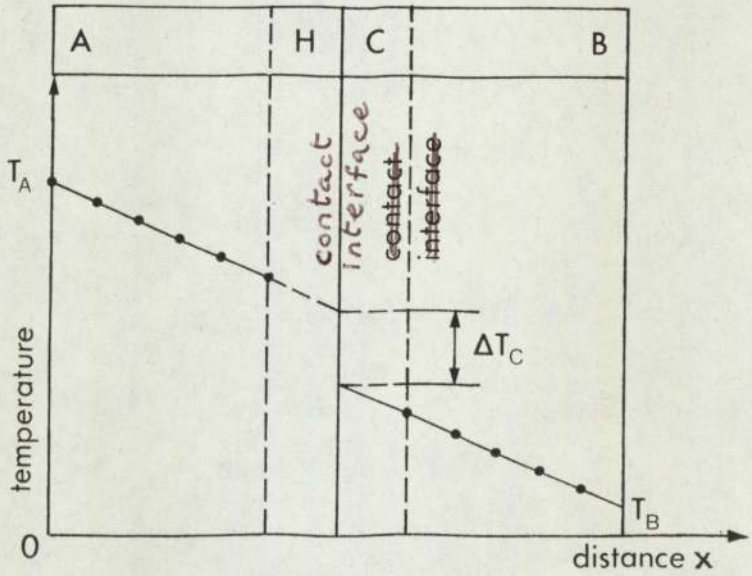

Fig. 2 Temperature distribution in two bars with adjacent ends in contact

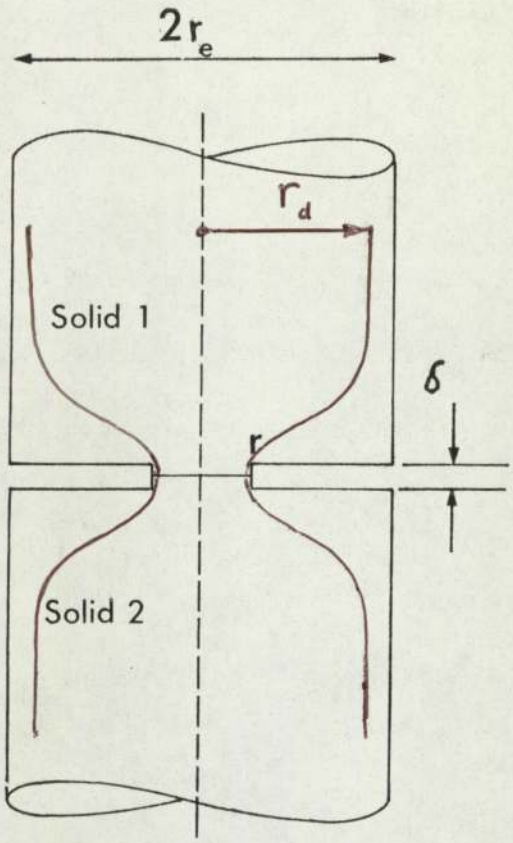

Fig.3 Centikale and Fishenden's contact element.

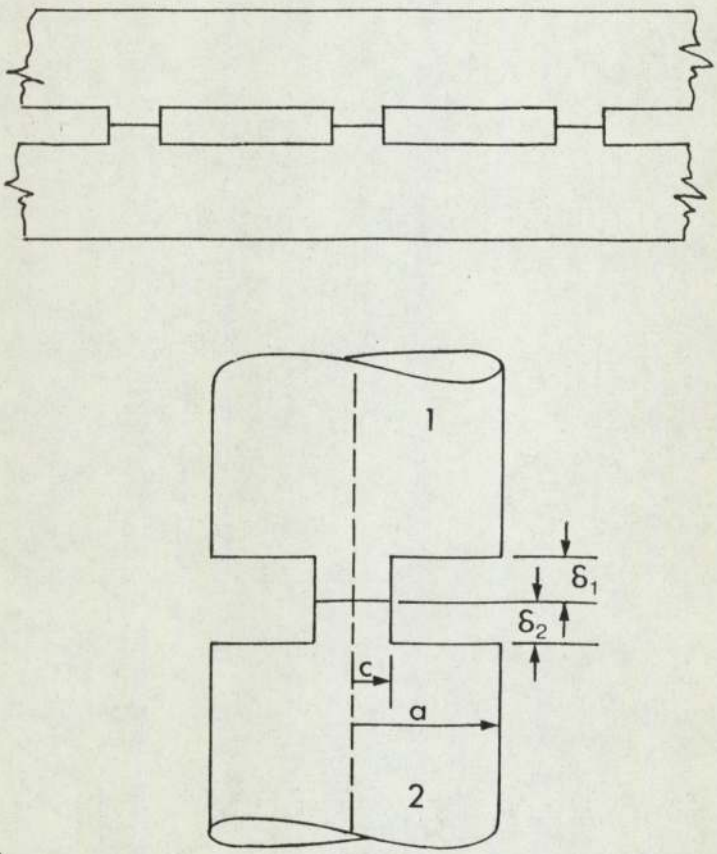

Fig.4 Fenech & Rohsenow's contact element.

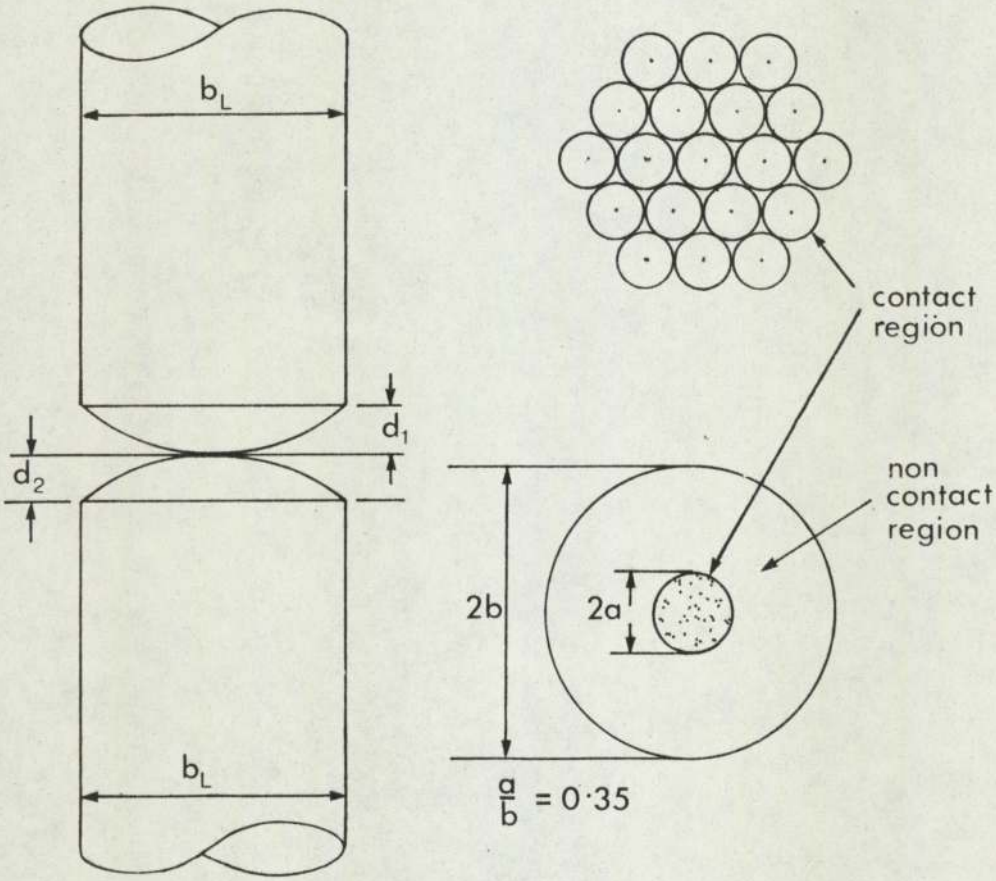

Fig.5 Clausing & Chao's model.

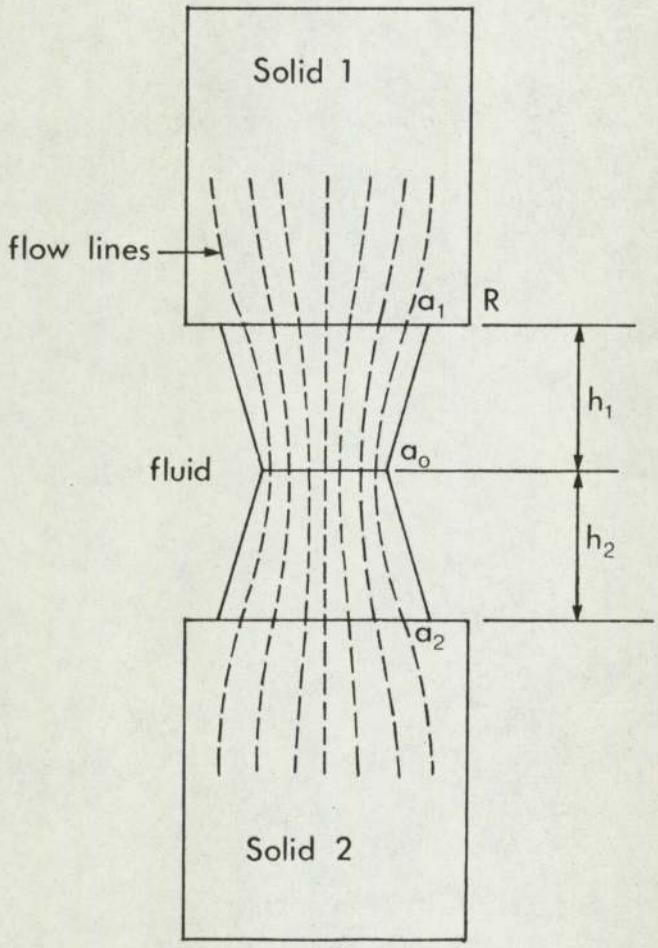

Fig.6 Wong's model contact.

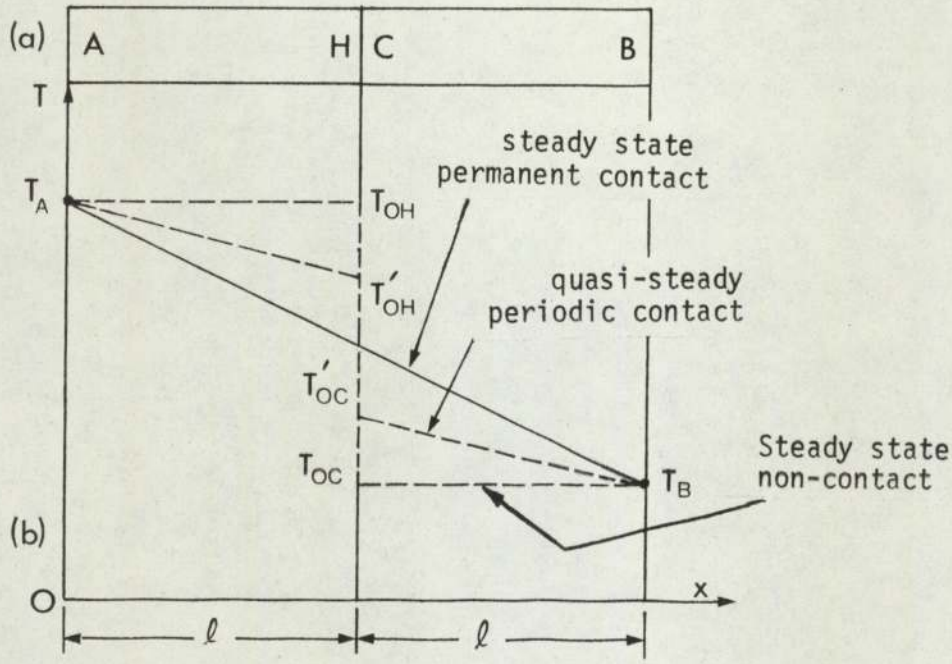

Fig.7 Temperature distributions: Ideal contact, non-contact and quasi-steady periodic contact cases.

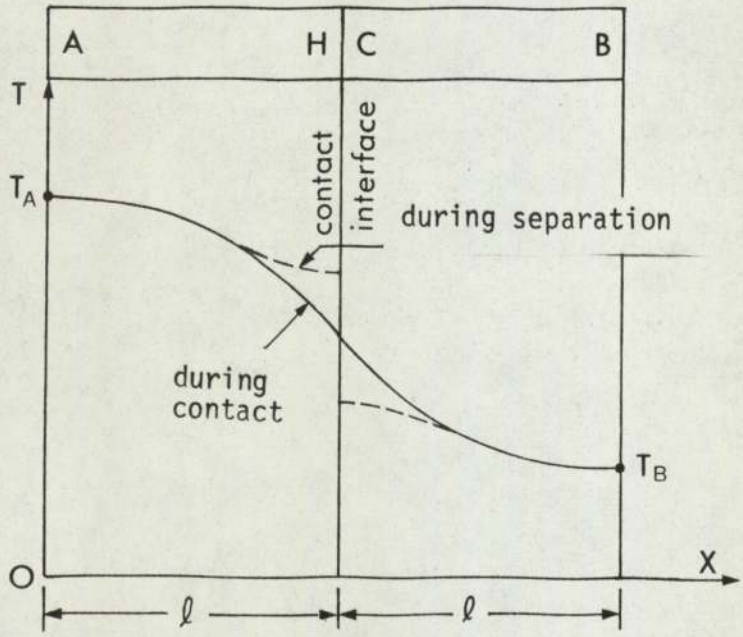

Fig.8 Instantaneous temperature distribution during contact and during separation.

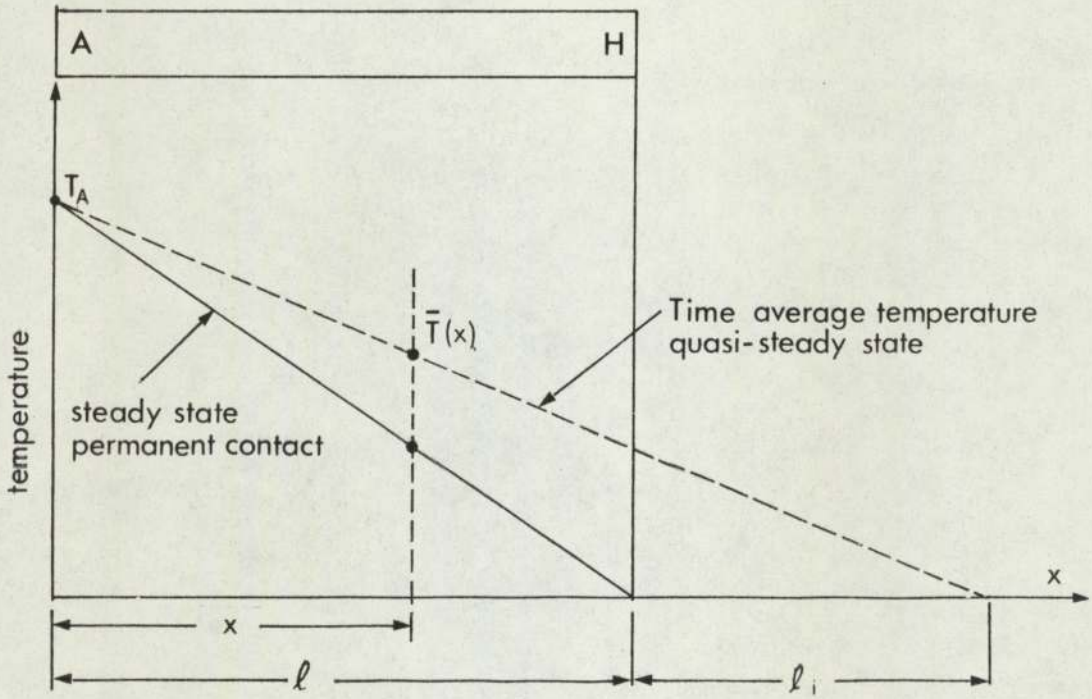

Fig. 9 Temperature distribution in heated bar : steady and quasi-steady states

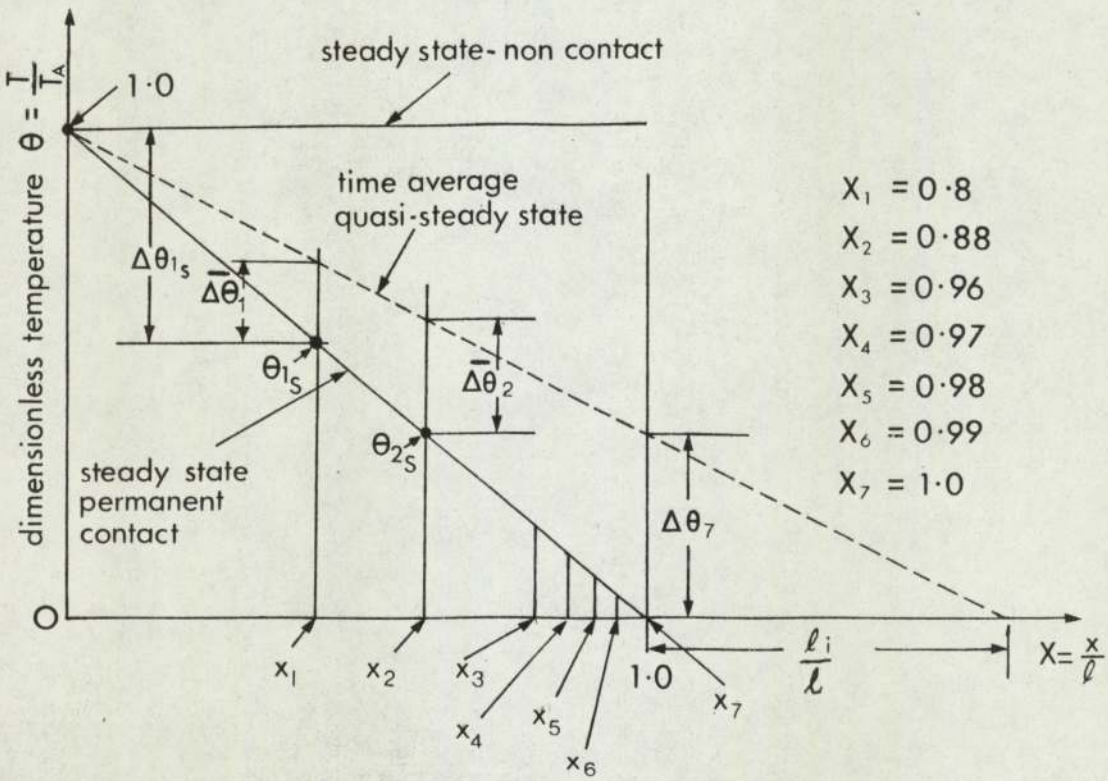

Fig. 10 Dimensionless temperature distribution in heated bar

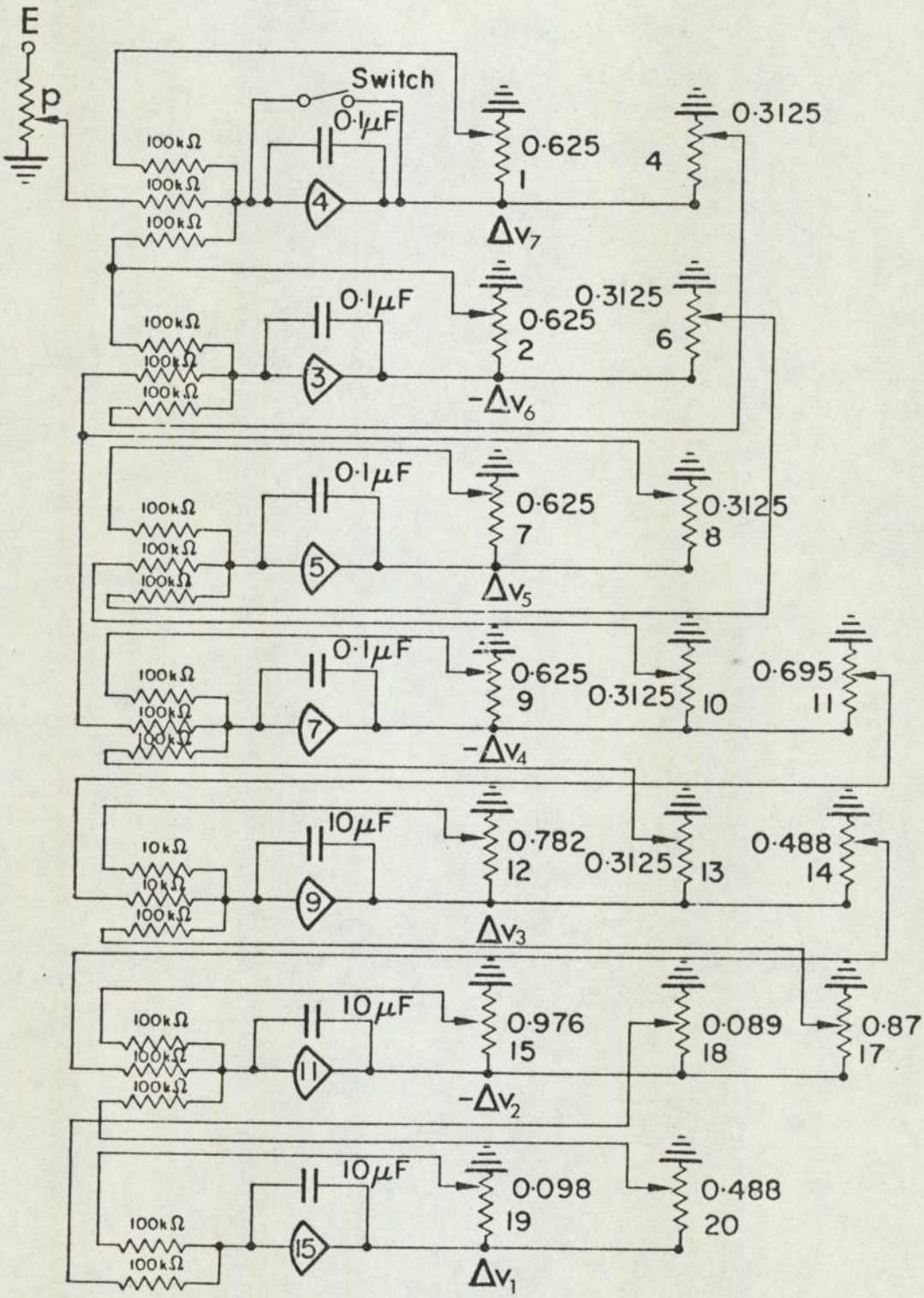

Fig. 11 Circuit diagram of analogue: perfect thermal contact

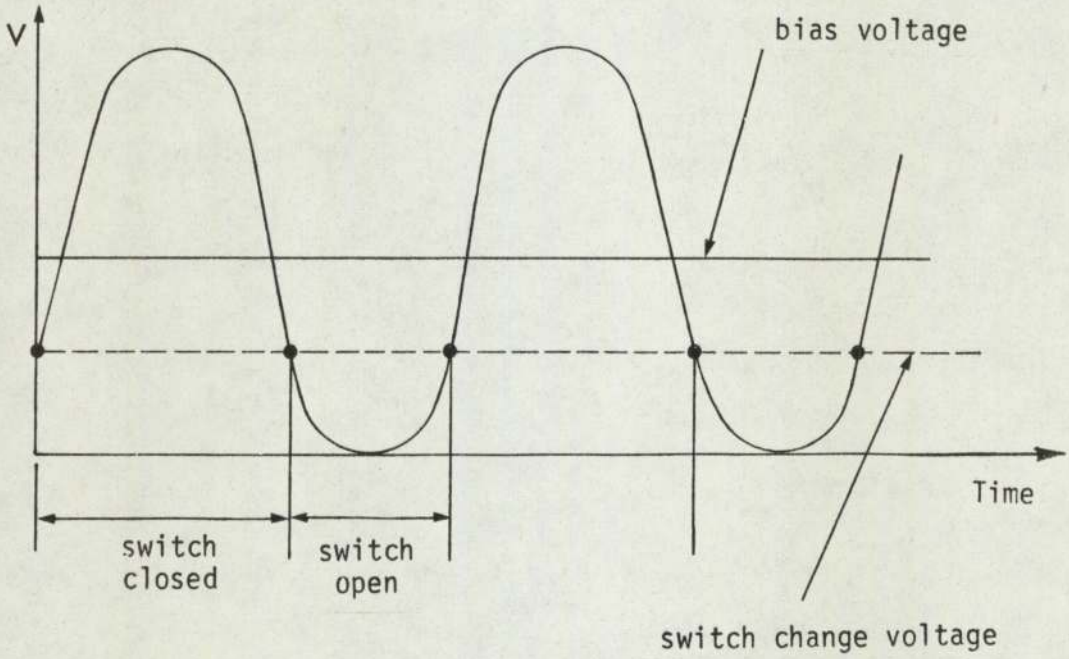

Fig.12 Effect of d.c. bias on ratio contact time: periodic time

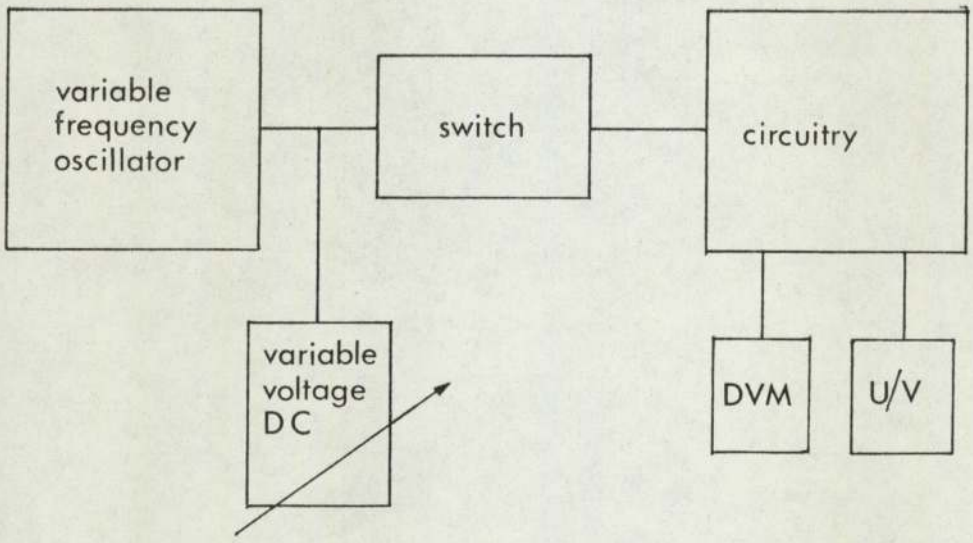

Fig.13 Block diagram of analogue computer layout.

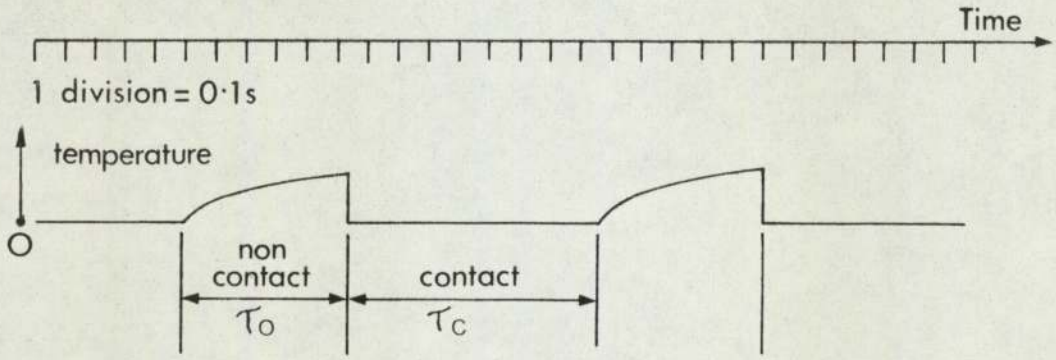

Fig.14 Trace of "temperature" variation at contact interface.

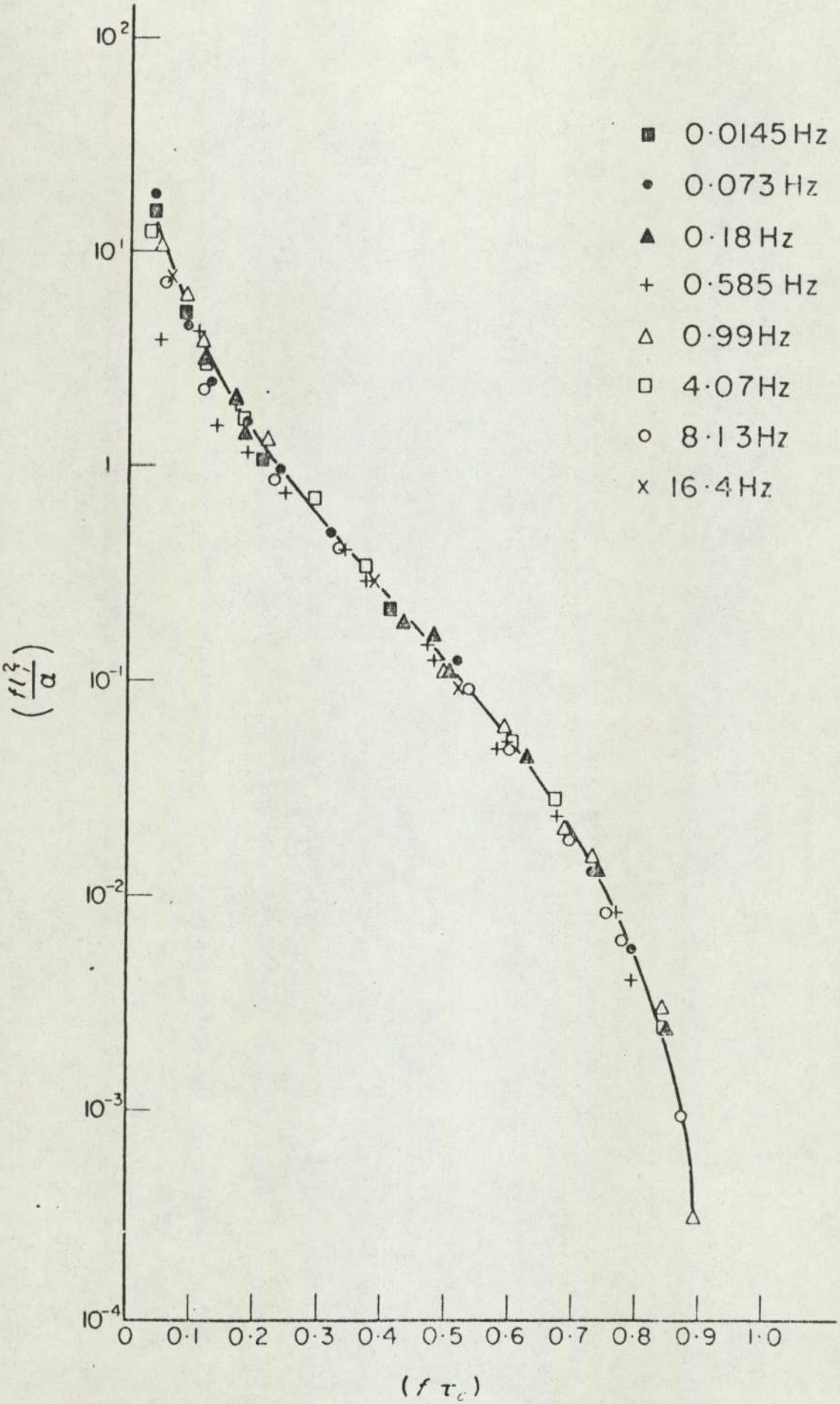

Fig. 15 Analogue computer results : $\frac{f\ell_i^2}{\alpha}$ versus $f\tau_c$

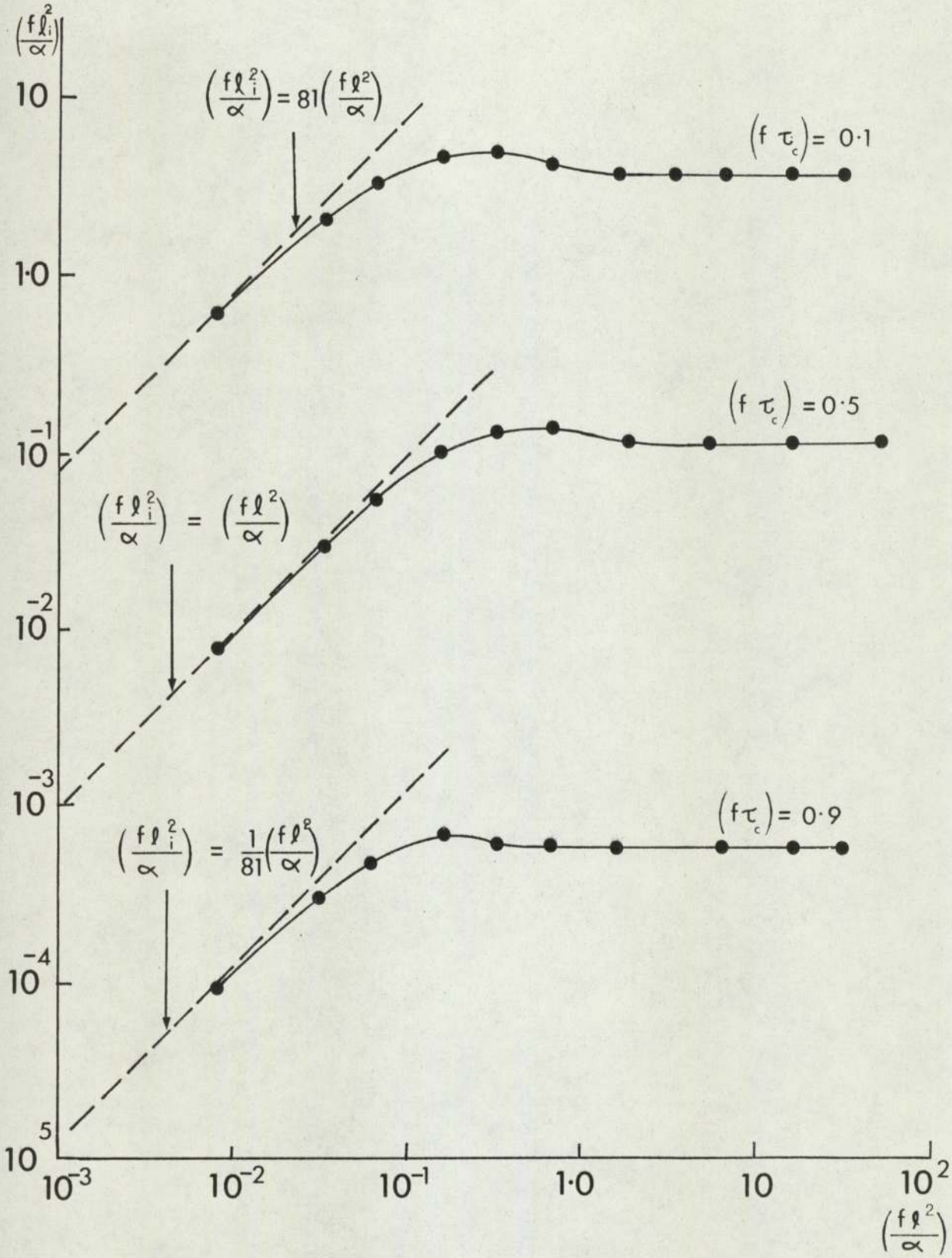

Fig. 16(a) Numerical matrix inversion method results

$$\frac{f\ell_i^2}{\alpha} \quad \text{versus} \quad \frac{f\ell^2}{\alpha}$$

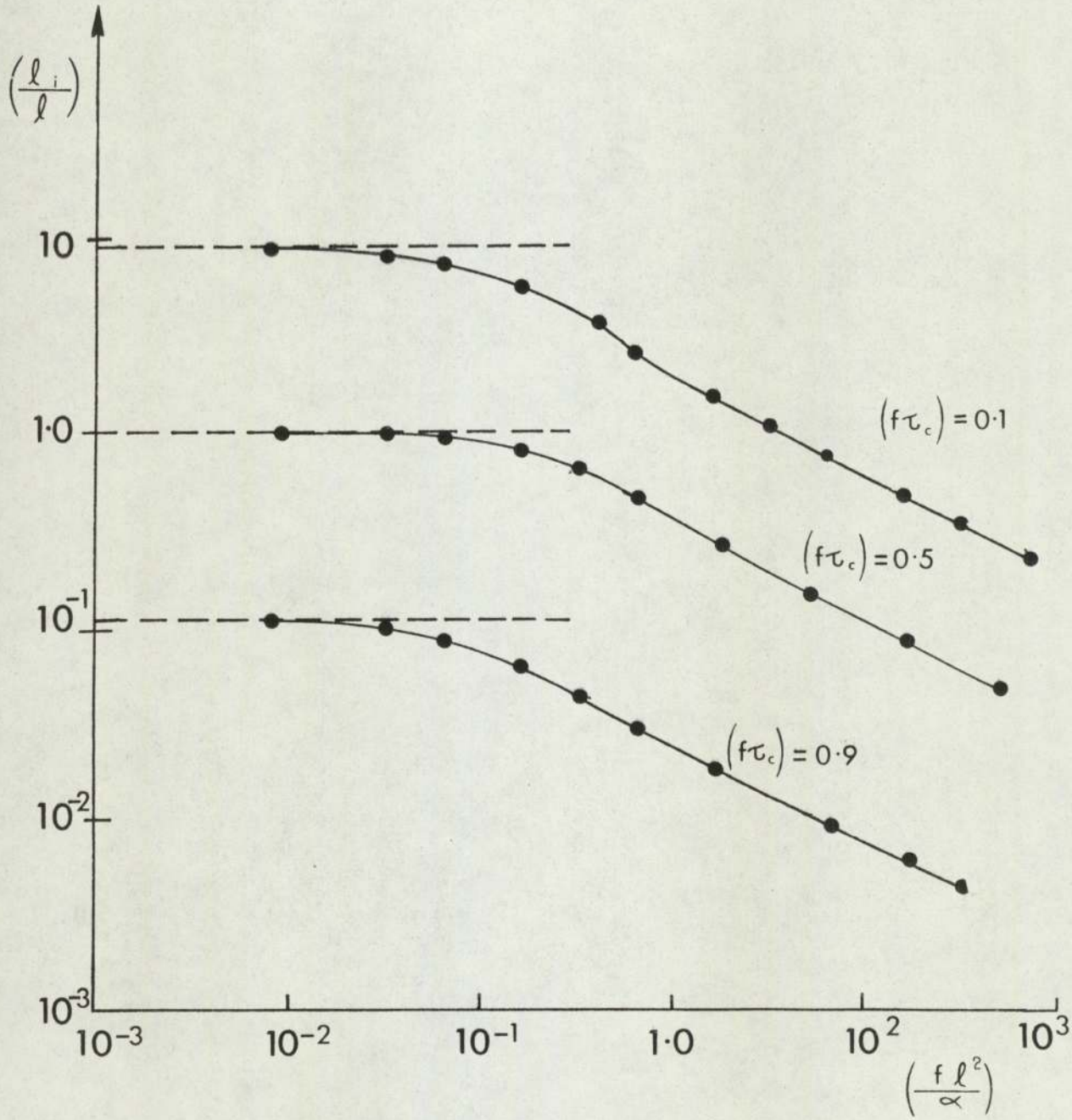

Fig. 16(b) Numerical matrix inversion results

$$\frac{\ell_i}{\ell} \quad \text{versus} \quad \frac{f\ell^2}{\alpha}$$

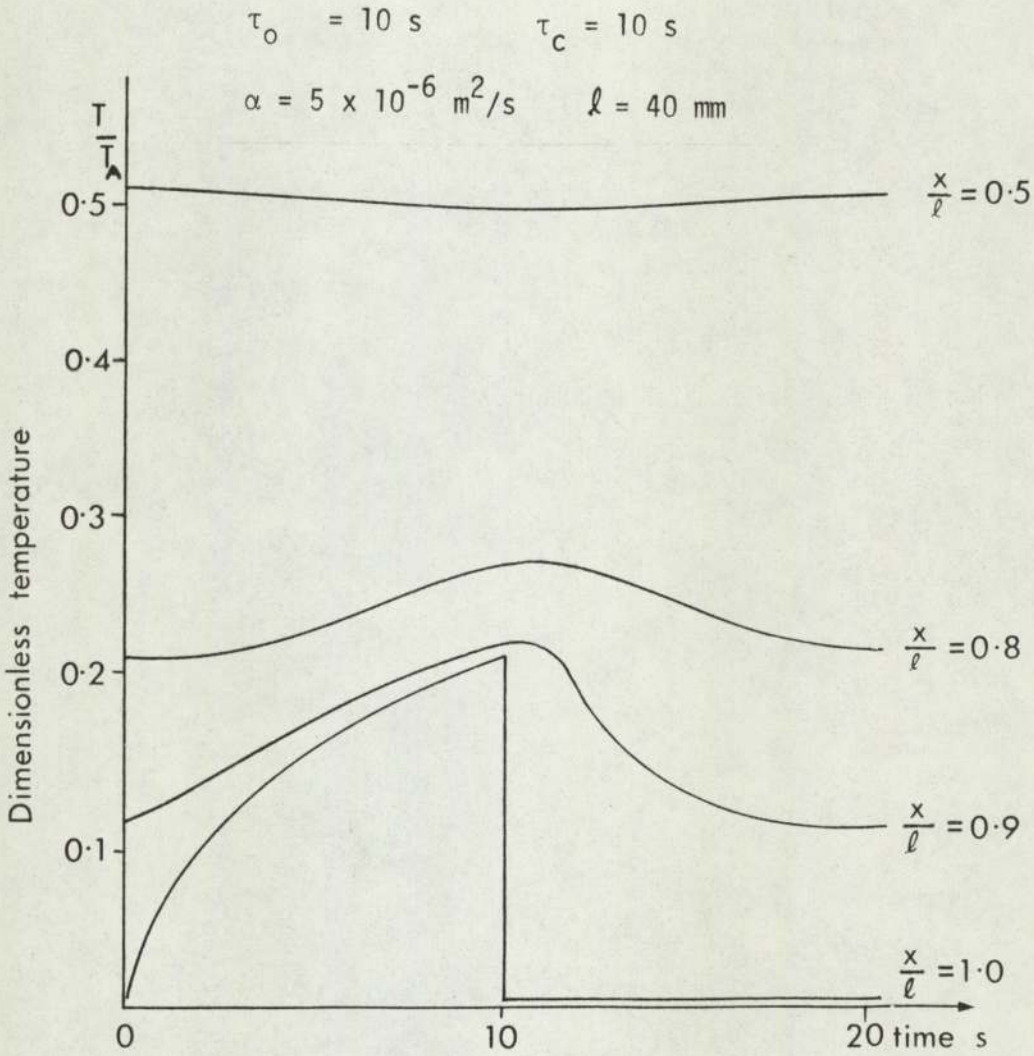

Fig. 17 Temperature-time variation at various positions $\frac{x}{\ell}$.

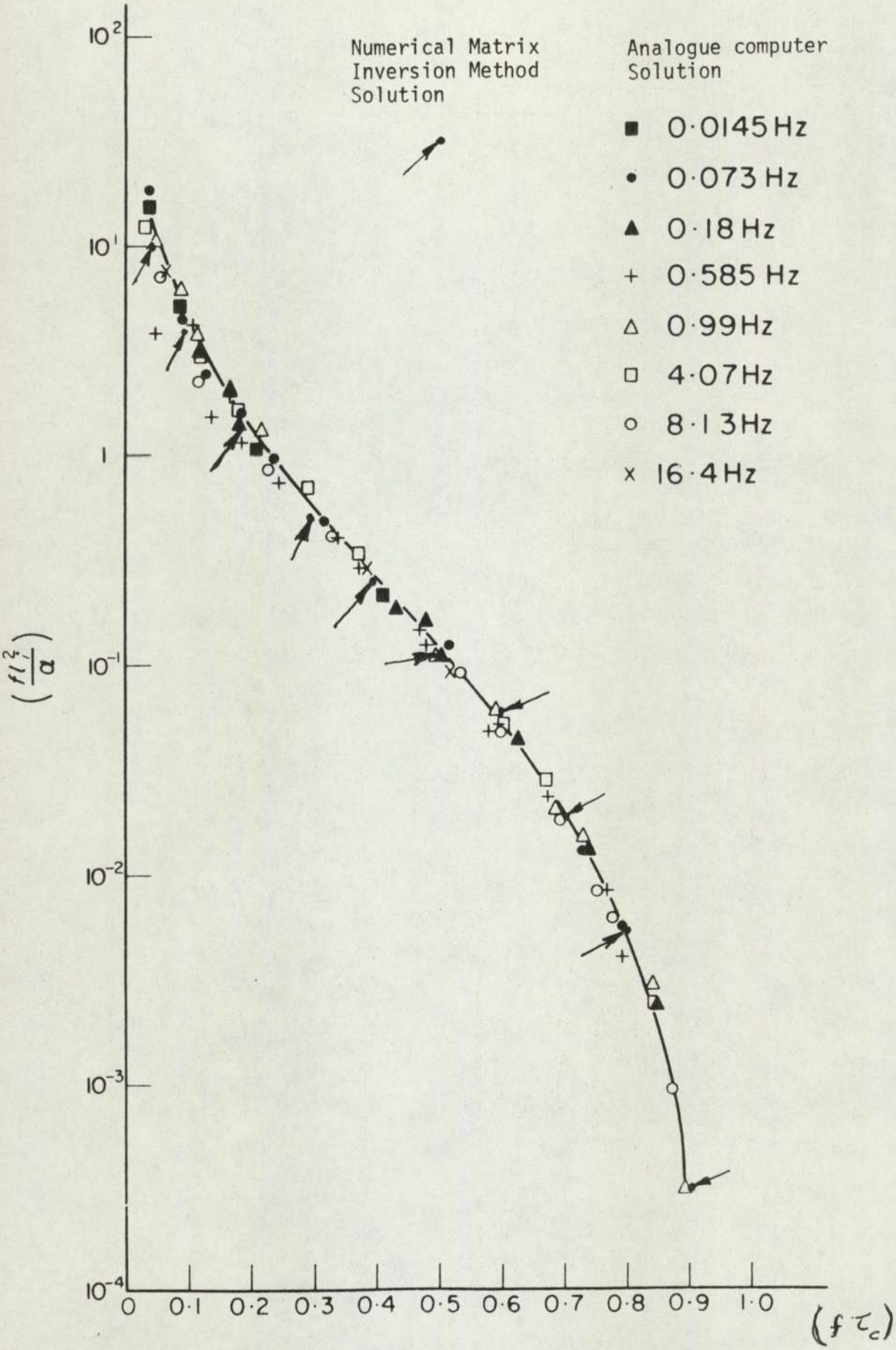

Fig. 18 Comparison of $\frac{f\ell_i^2}{\alpha}$ obtained by numerical matrix inversion method with analogue computer solution

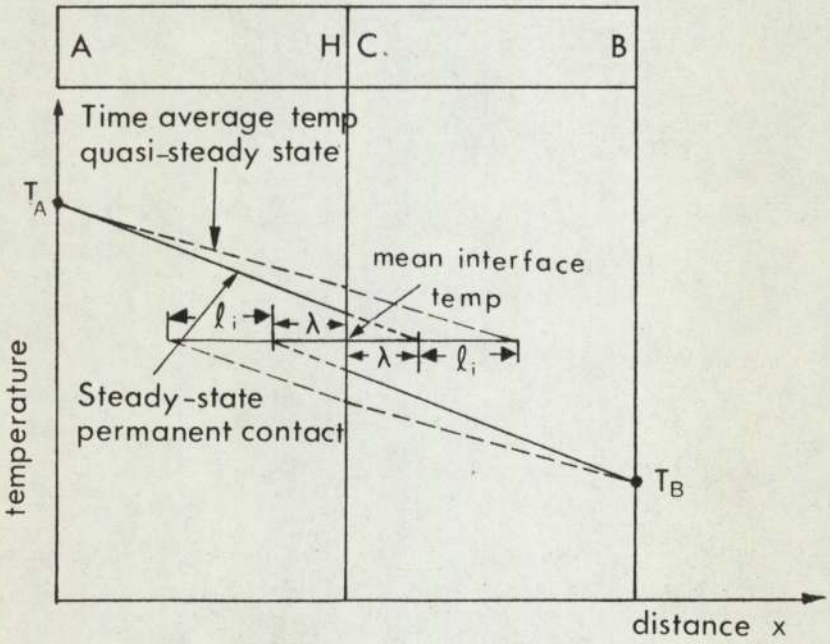

Fig. 19 Time-average temperature distributions, imperfect contact: steady and quasi-steady states

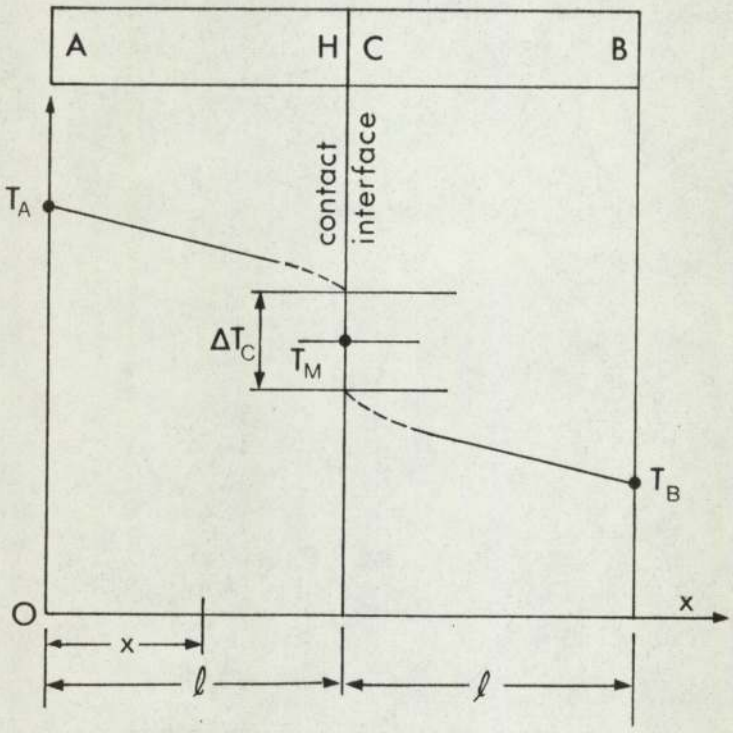

Fig. 20 Instantaneous temperature distribution during contact period

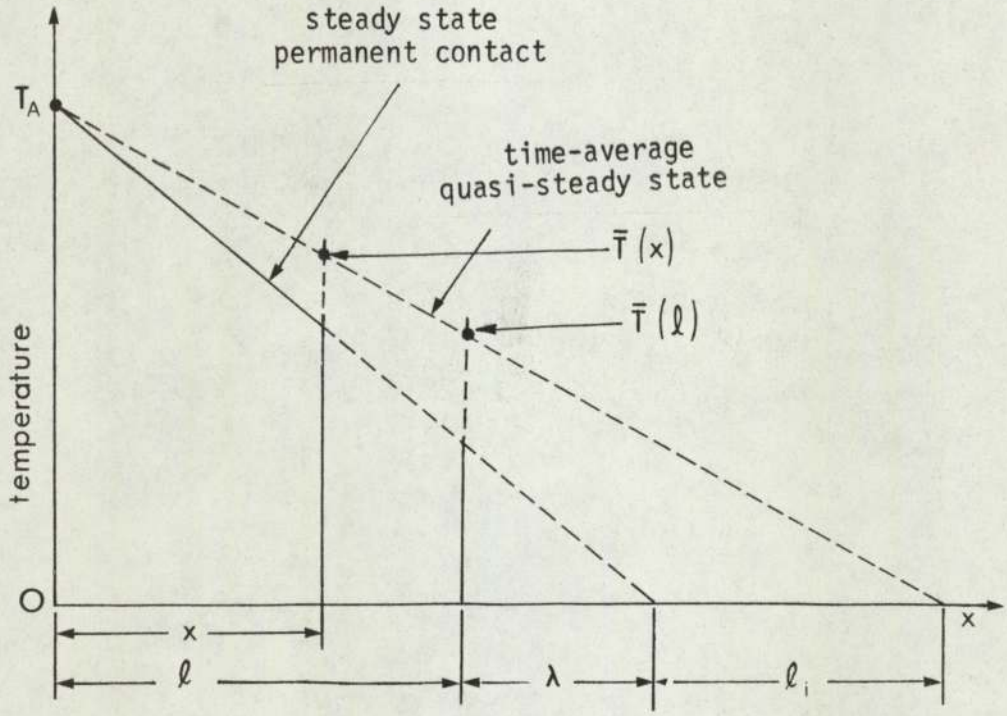

Fig. 21 Time-average temperature distributions, imperfect contact in heated bar

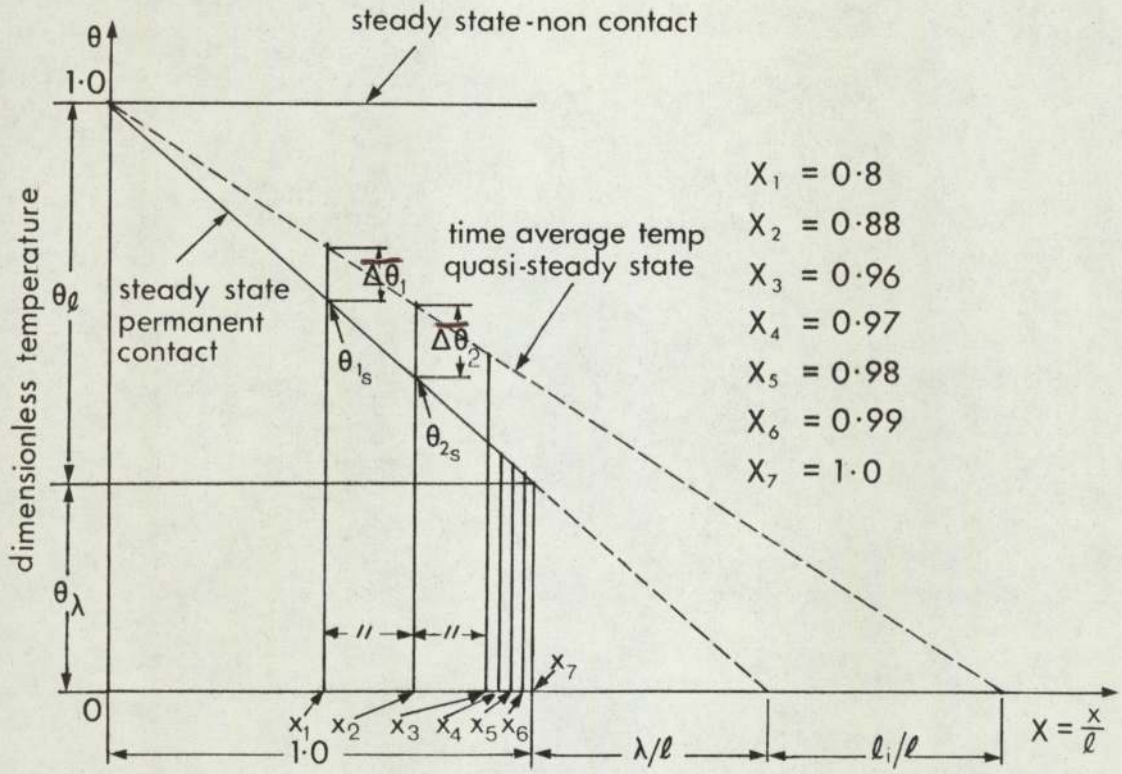

Fig. 22 Dimensionless temperature distributions in heated bar

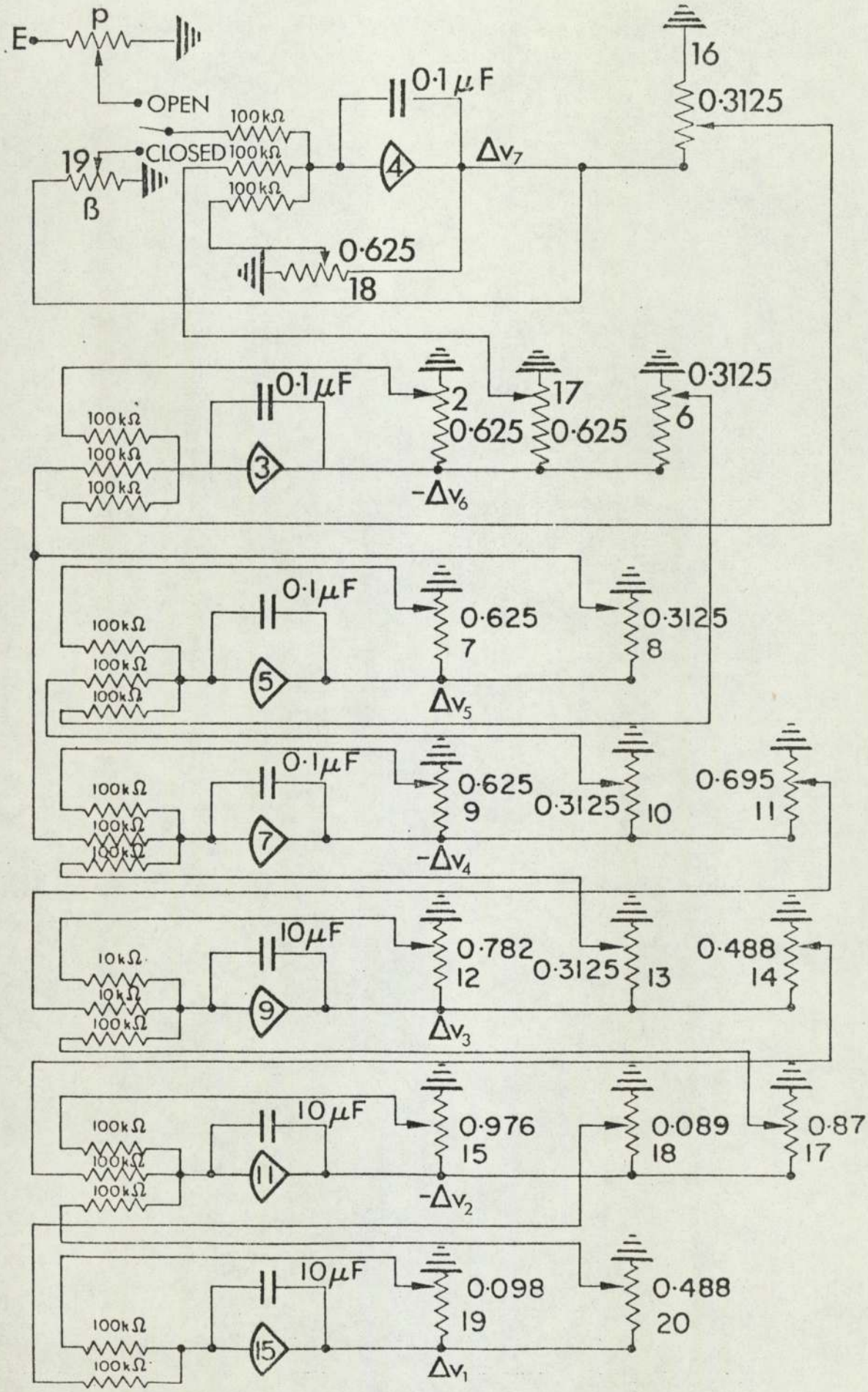

Fig. 23 Circuit diagram: imperfect contact analogue.

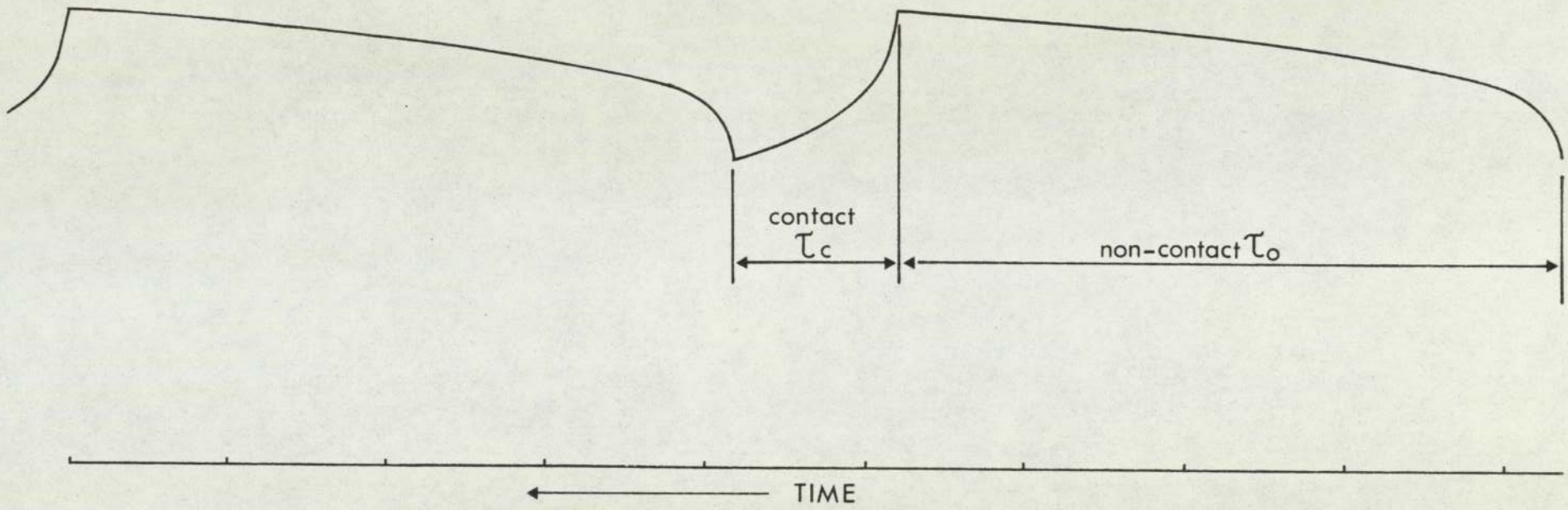

Fig. 24(a) Trace of "temperature" variation at contact interface: imperfect contact

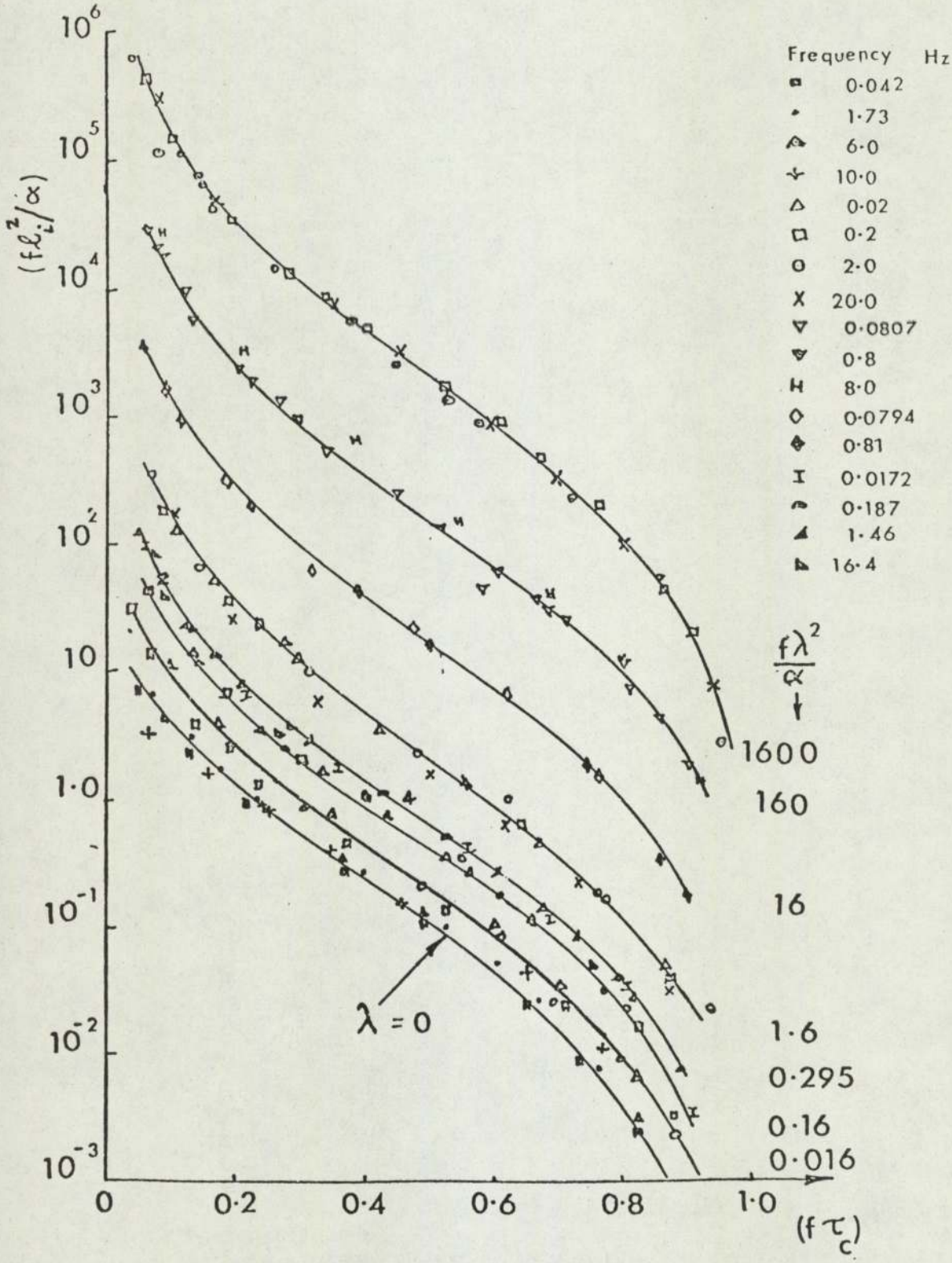

Fig. 24(b) Analogue computer results, imperfect contact: $\frac{f\ell_i^2}{\alpha}$ versus $f\tau_c$

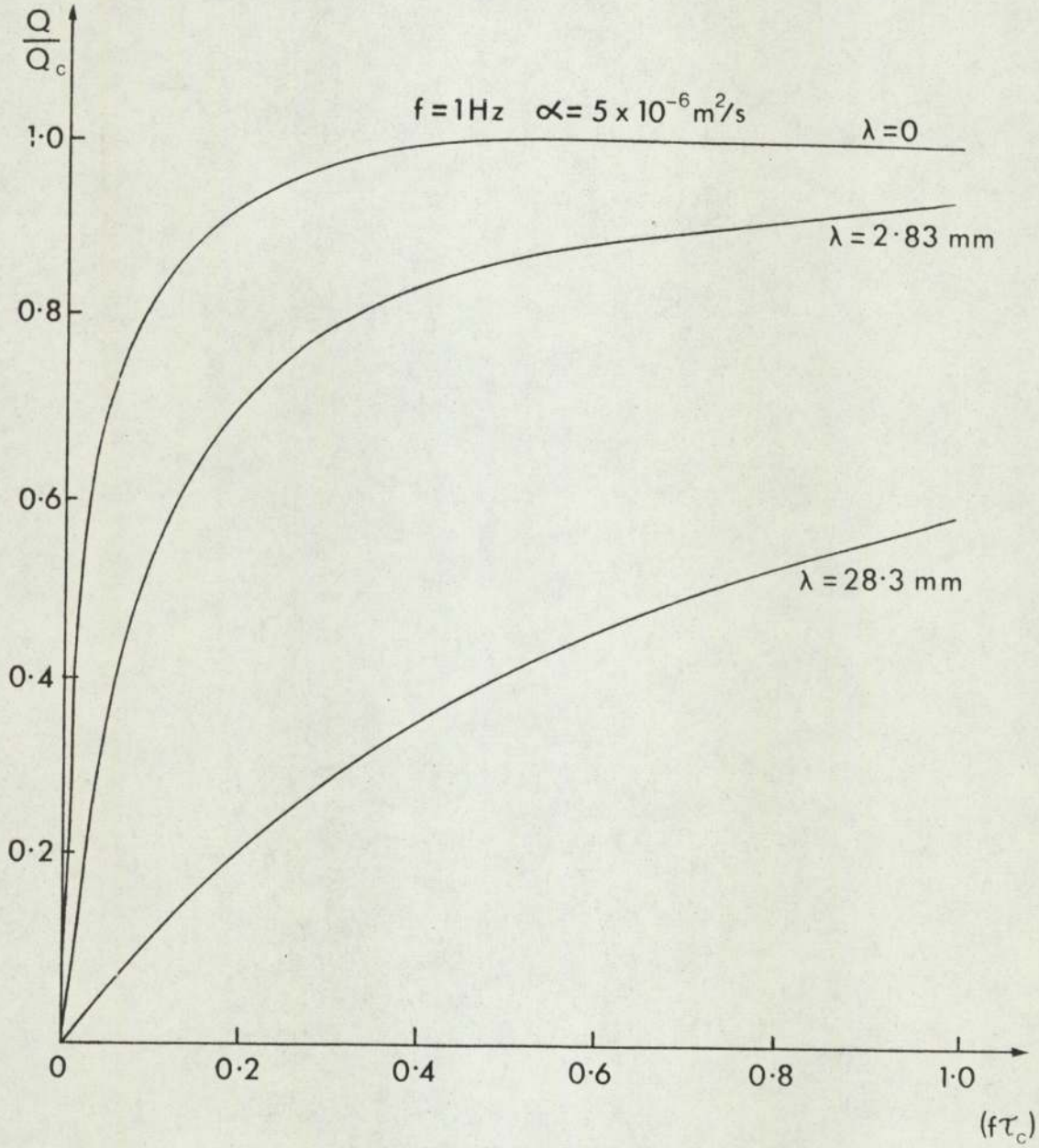

Fig. 25 Effect of $f\tau_c$ on heat flow with various thermal contact resistances

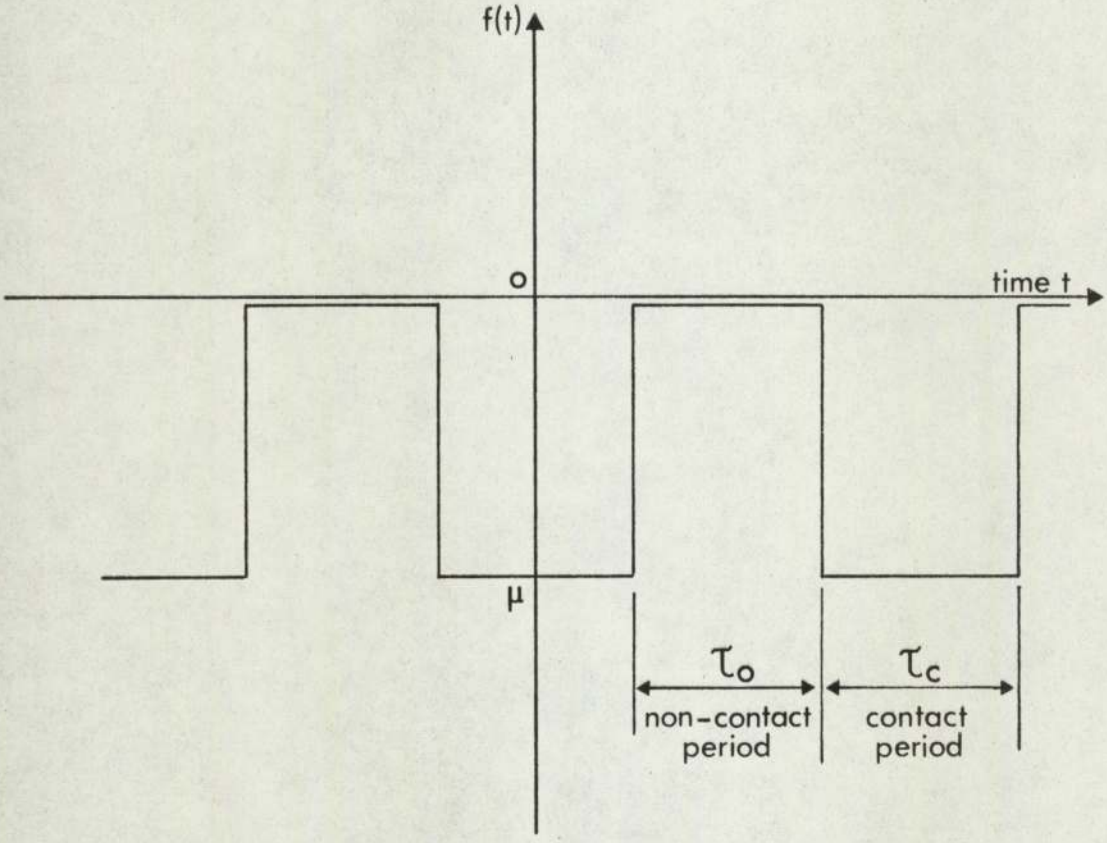

Fig. 26 Function f(t)

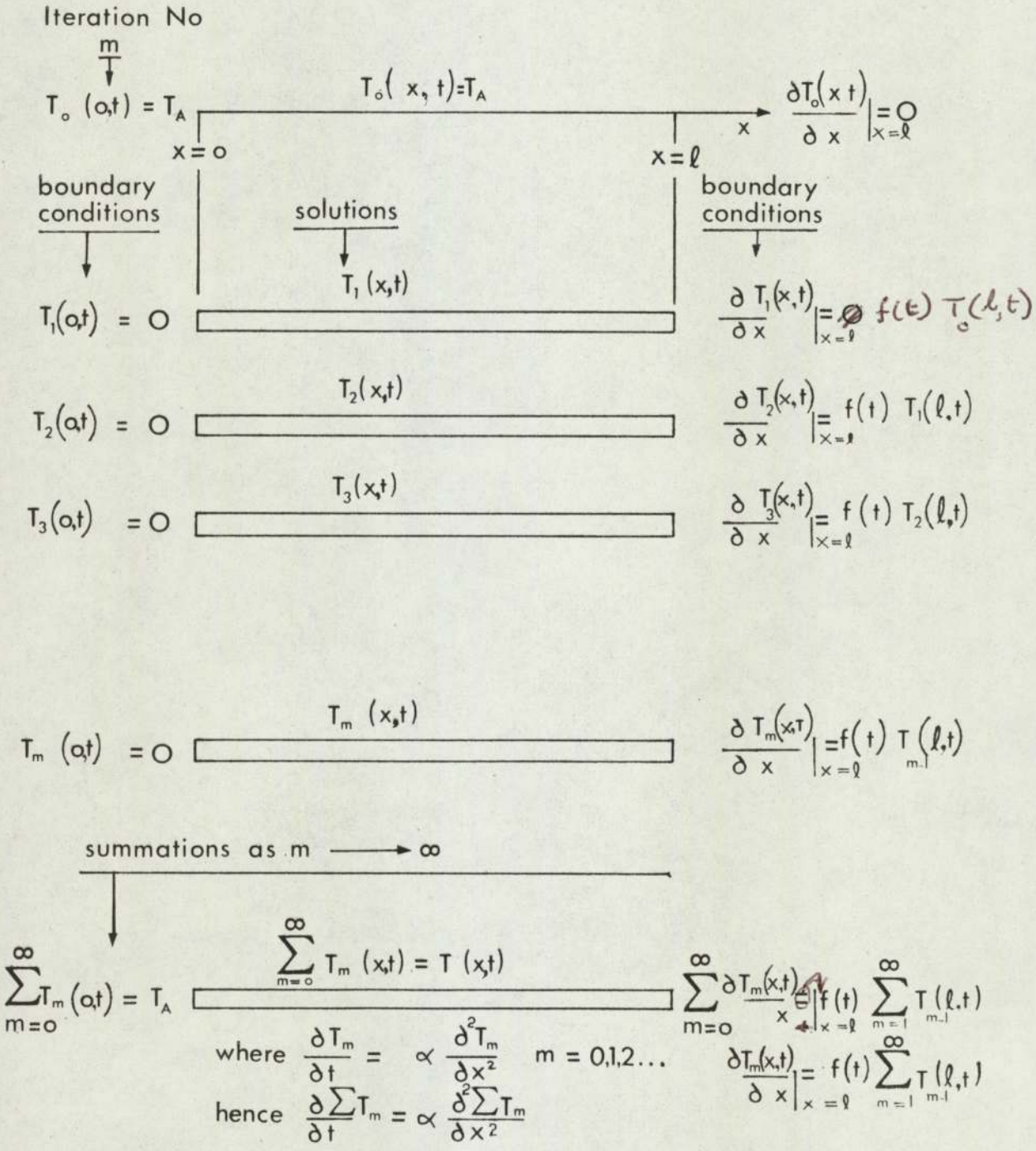
Iteration No
m
$T_o(o,t) = T_A$
$T_o(x,t) = T_A$
$\left.\frac{\partial T_o(x,t)}{\partial x}\right|_{x=\ell} = 0$
x
x = o
x = ℓ
boundary conditions
solutions
boundary conditions
$T_1(x,t)$
$T_1(o,t) = 0$
$\left.\frac{\partial T_1(x,t)}{\partial x}\right|_{x=\ell} = f(t)\, T_o(\ell,t)$
$T_2(x,t)$
$T_2(o,t) = 0$
$\left.\frac{\partial T_2(x,t)}{\partial x}\right|_{x=\ell} = f(t)\, T_1(\ell,t)$
$T_3(x,t)$
$T_3(o,t) = 0$
$\left.\frac{\partial T_3(x,t)}{\partial x}\right|_{x=\ell} = f(t)\, T_2(\ell,t)$
$T_m(x,t)$
$T_m(o,t) = 0$
$\left.\frac{\partial T_m(x,t)}{\partial x}\right|_{x=\ell} = f(t)\, T_{m-1}(\ell,t)$
summations as m → ∞
$\sum_{m=o}^{\infty} T_m(x,t) = T(x,t)$
$\sum_{m=o}^{\infty} T_m(o,t) = T_A$
$\sum_{m=o}^{\infty} \left.\frac{\partial T_m(x,t)}{\partial x}\right|_{x=\ell} = f(t) \sum_{m=1}^{\infty} T_{m-1}(\ell,t)$
where $\frac{\partial T_m}{\partial t} = \alpha \frac{\partial^2 T_m}{\partial x^2}$ m = 0,1,2...
$\left.\frac{\partial T_m(x,t)}{\partial x}\right|_{x=\ell} = f(t) \sum_{m=1}^{\infty} T_{m-1}(\ell,t)$
hence $\frac{\partial \sum T_m}{\partial t} = \alpha \frac{\partial^2 \sum T_m}{\partial x^2}$

Fig. 27

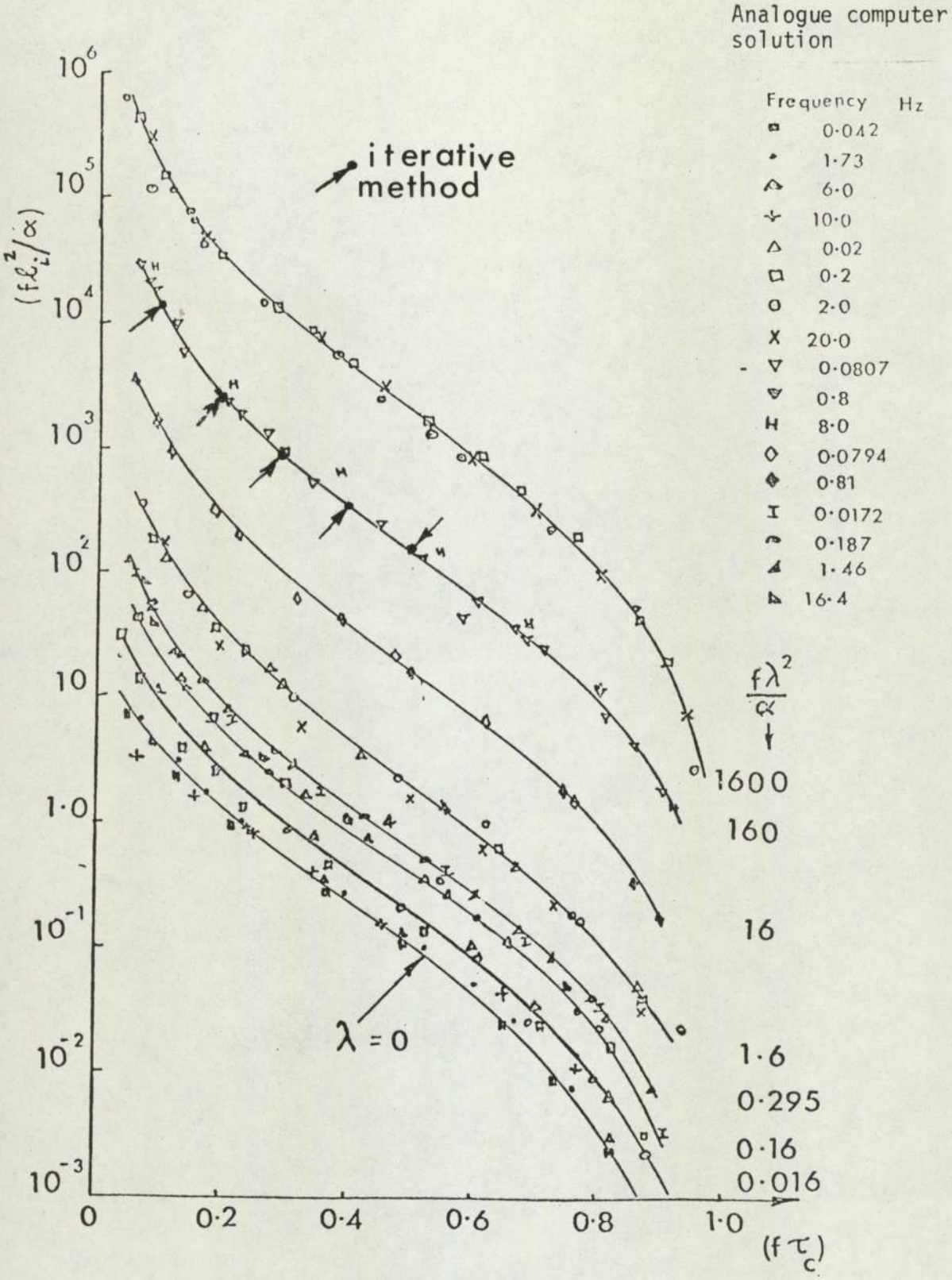

Fig. 28 Comparison of results of iterative method with analogue computer study

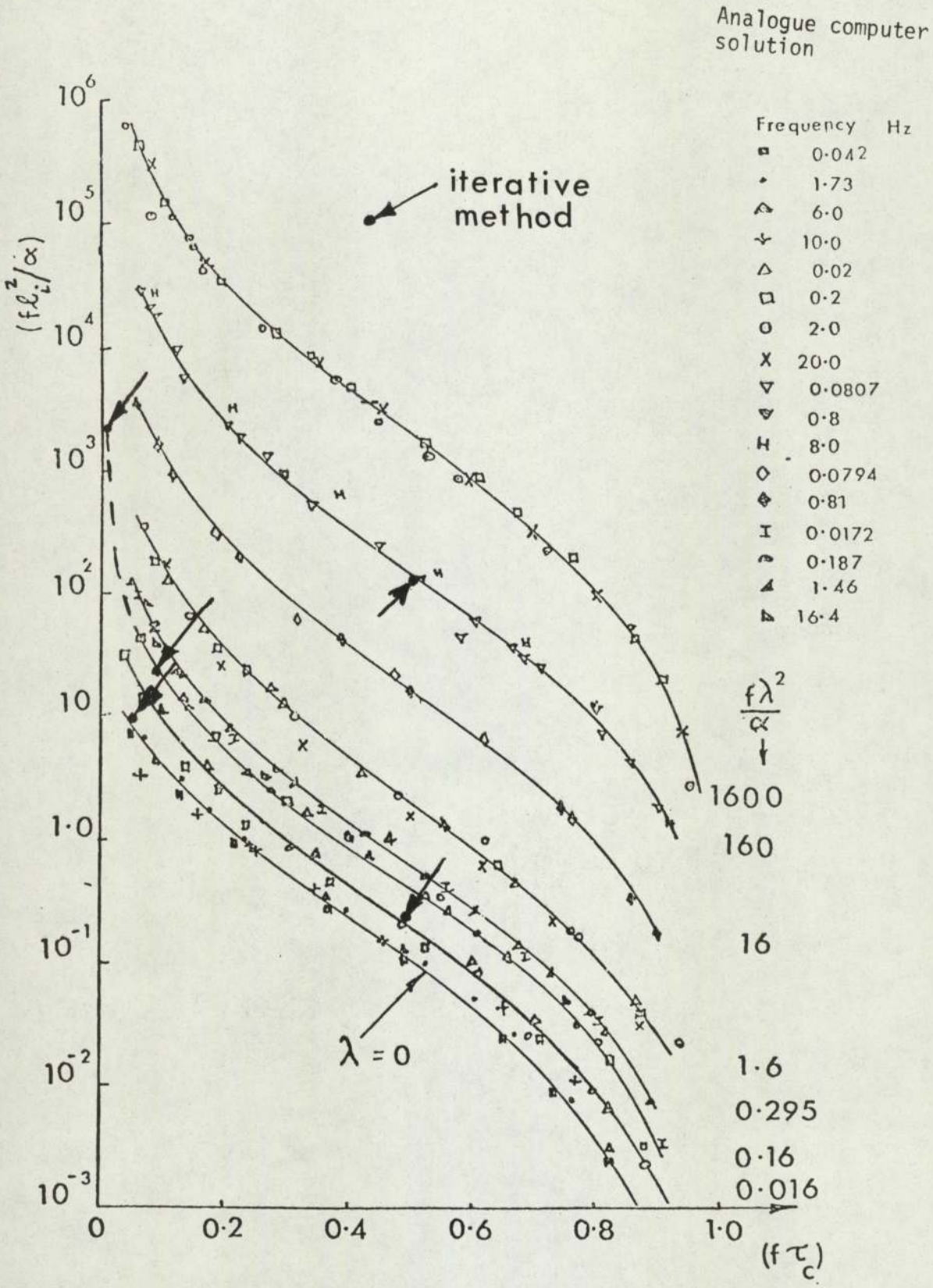

Fig. 29 Comparison of results of iterative method with analogue computer study

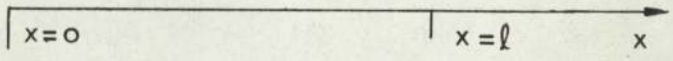

Solutions

$$T_o(o,t) = T_A \qquad T_o(x,t) = T_A \qquad \left.\frac{\partial T_o(x,t)}{\partial x}\right|_{x=\ell} = 0$$

$$T_1(o,t) = 0 \qquad T_1(x,t) \qquad \left.\frac{\partial T_1(x,t)}{\partial x}\right|_{x=\ell} = f(t)\,\beta T_o(\ell,t)$$

$$T_2(o,t) = 0 \qquad T_2(x,t) \qquad \left.\frac{\partial T_2(x,t)}{\partial x}\right|_{x=\ell} = f(t)\left\{\beta T_1(\ell,t) + \gamma T_o(\ell,t)\right\}$$

$$T_3(o,t) = 0 \qquad T_3(x,t) \qquad \left.\frac{\partial T_3(x,t)}{\partial x}\right|_{x=\ell} = f(t)\left\{\beta T_2(\ell,t) + \gamma T_1(\ell,t)\right\}$$

$$T_m(o,t) = 0 \qquad \left.\frac{\partial T_m(x,t)}{\partial x}\right|_{x=\ell} = f(t)\left\{\beta T_{m-1}(\ell,t) + \gamma T_{m-2}(\ell,t)\right\}$$

Summations to 'r' iterations

NOTE $\beta + \gamma = 1$

$$T_{r-2}(o,t) = 0 \qquad T_{r-1}(x,t) \qquad \left.\frac{\partial T_{r-2}(x,t)}{\partial x}\right|_{x=\ell} = f(t)\left\{\beta T_{r-3}(\ell,t) + \gamma T_{r-4}(\ell,t)\right\}$$

$$T_{r-1}(o,t) = 0 \qquad T_{r-1}(x,t) \qquad \left.\frac{\partial T_{r-1}(x,t)}{\partial x}\right|_{x=\ell} = f(t)\left\{\beta T_{r-2}(\ell,t) + \gamma T_{r-3}(\ell,t)\right\}$$

$$T_r(o,t) = 0 \qquad T_{r-}(x,t) \qquad \left.\frac{\partial T_r(x,t)}{\partial x}\right|_{x=\ell} = f(t)\left\{\beta T_{r-1}(\ell,t) + \gamma T_{r-2}(\ell,t)\right\}$$

NOTE Putting $\gamma = 1-\beta$

$$\sum_{m=o}^{r} T_m(o,t) = T_A \qquad T(x,t) = \sum_{m=o} T_m(x,t), \qquad \sum_{m=o}^{r} \left.\frac{\partial T(x,t)}{\partial x}\right|_{x=\ell} = f(t)\left\{\beta T_{r-1}(\ell,t) + \sum_{m=o}^{r-2} T_m(\ell,t)\right\}$$

$$\frac{\partial \sum T_m}{\partial t} = \alpha \frac{\partial^2 \sum T_m}{\partial x^2}$$

Then let $r \longrightarrow \infty$

Fig. 30

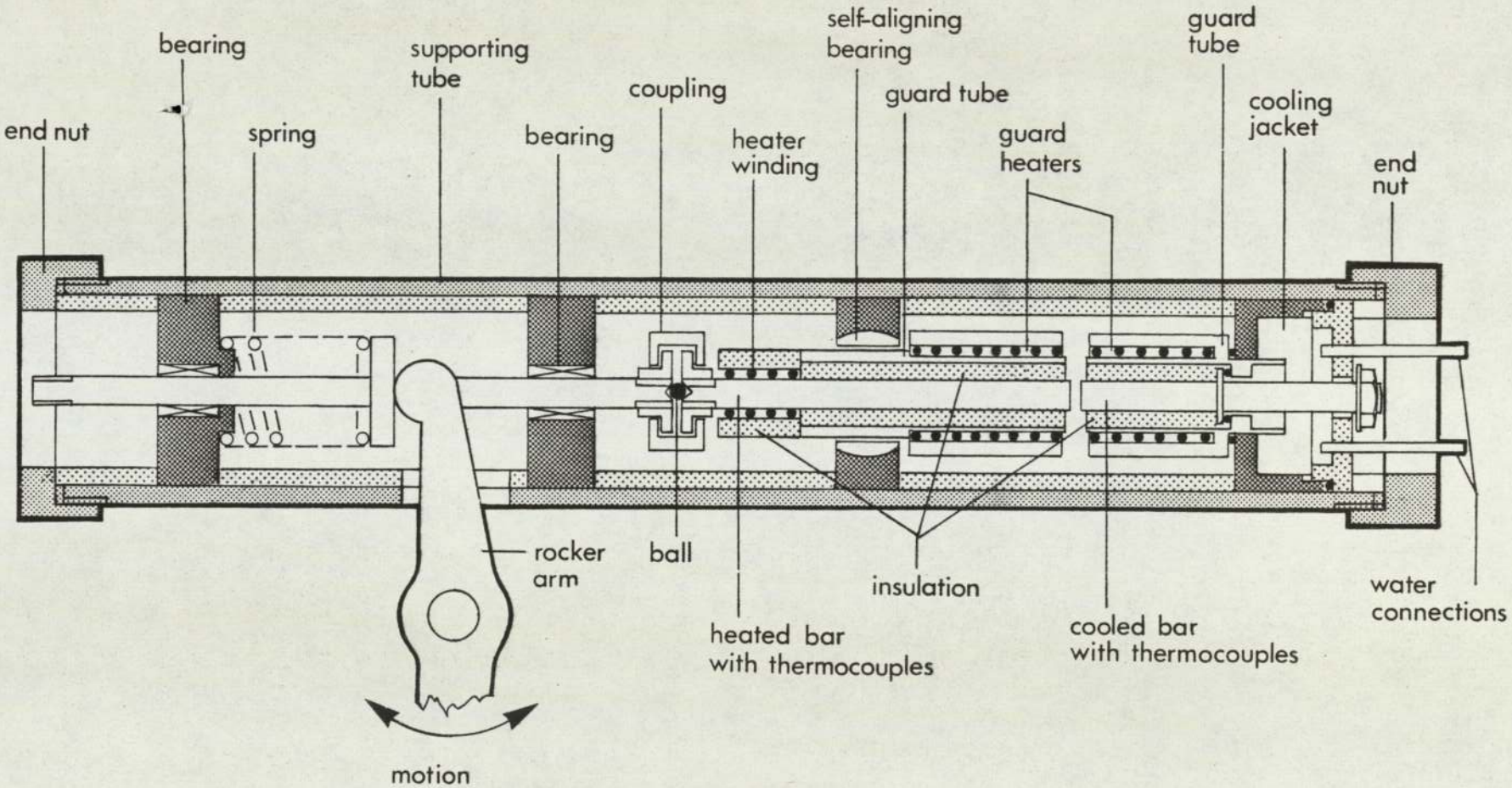

Fig. 31(a) Schematic drawing of test rig No. 1

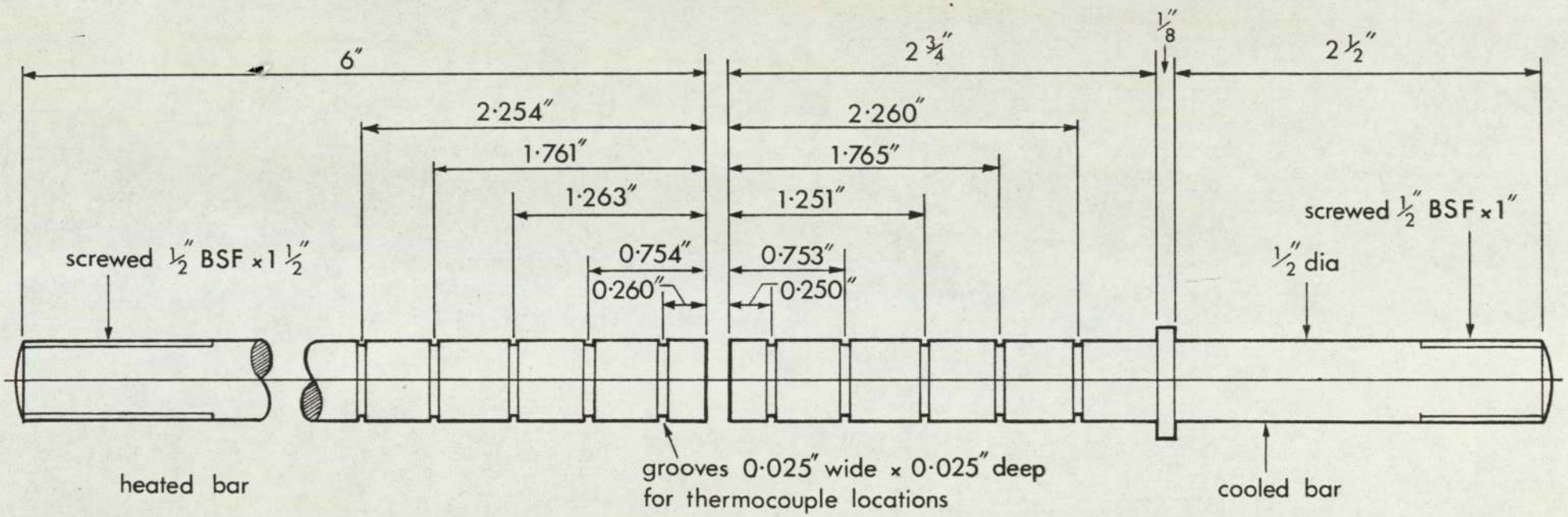

Fig. 31(b) EN52(c) specimens for test rig No. 1

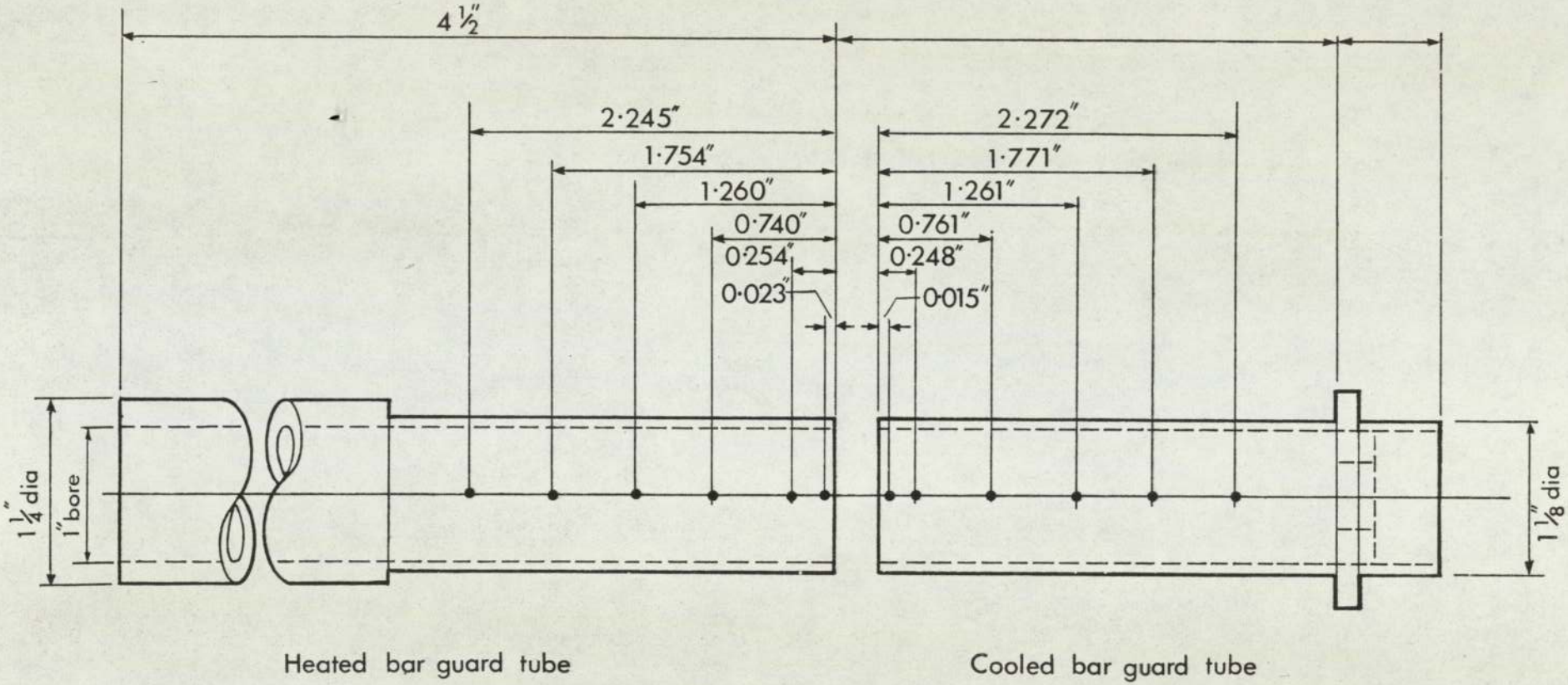

Fig. 31(c) Guard tubes for test rig No. 1

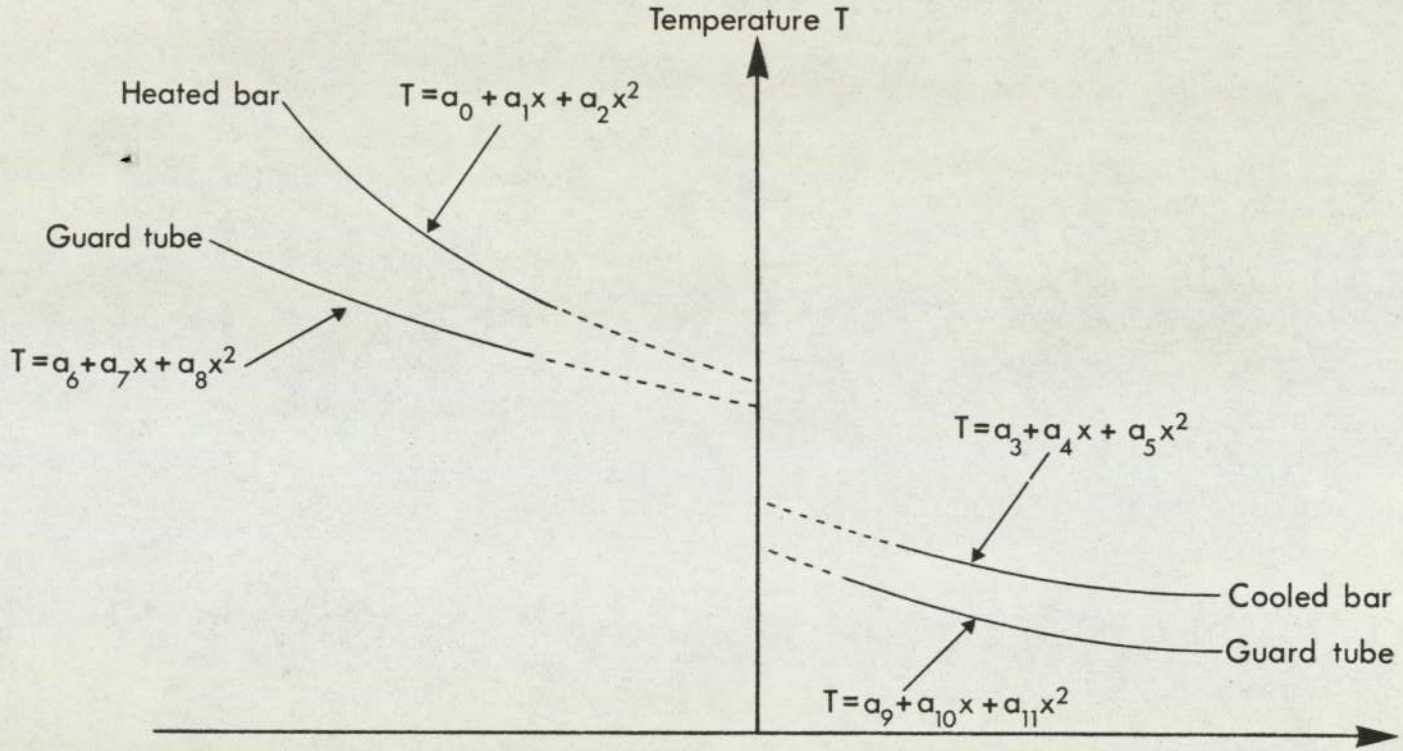

Fig. 32 Temperature distribution in bars and guard tubes

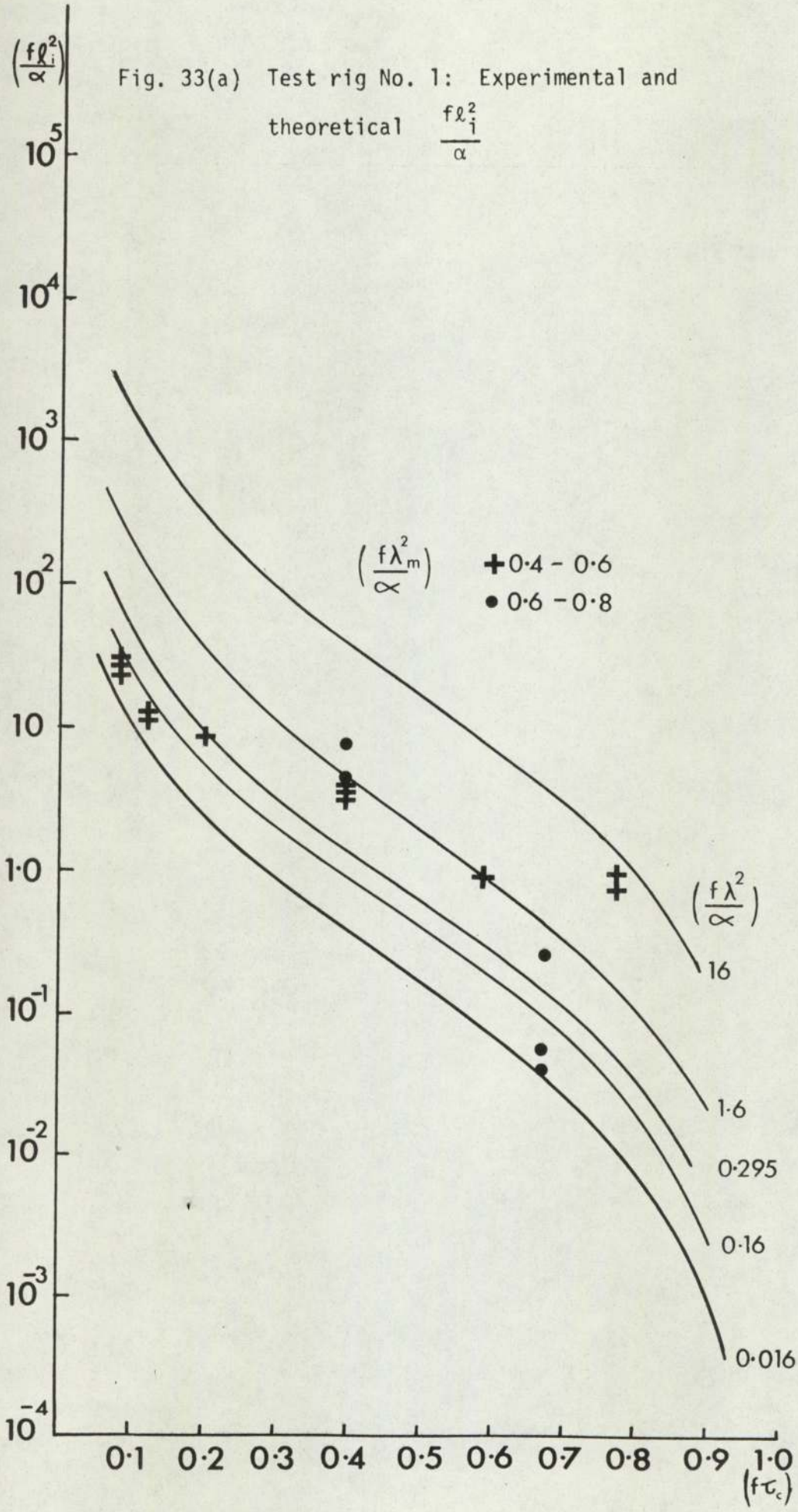

Fig. 33(a) Test rig No. 1: Experimental and theoretical $\frac{f\ell_i^2}{\alpha}$

Fig. 33(b) Test rig No. 1: Experimental and theoretical $\frac{f\ell_i^2}{\alpha}$

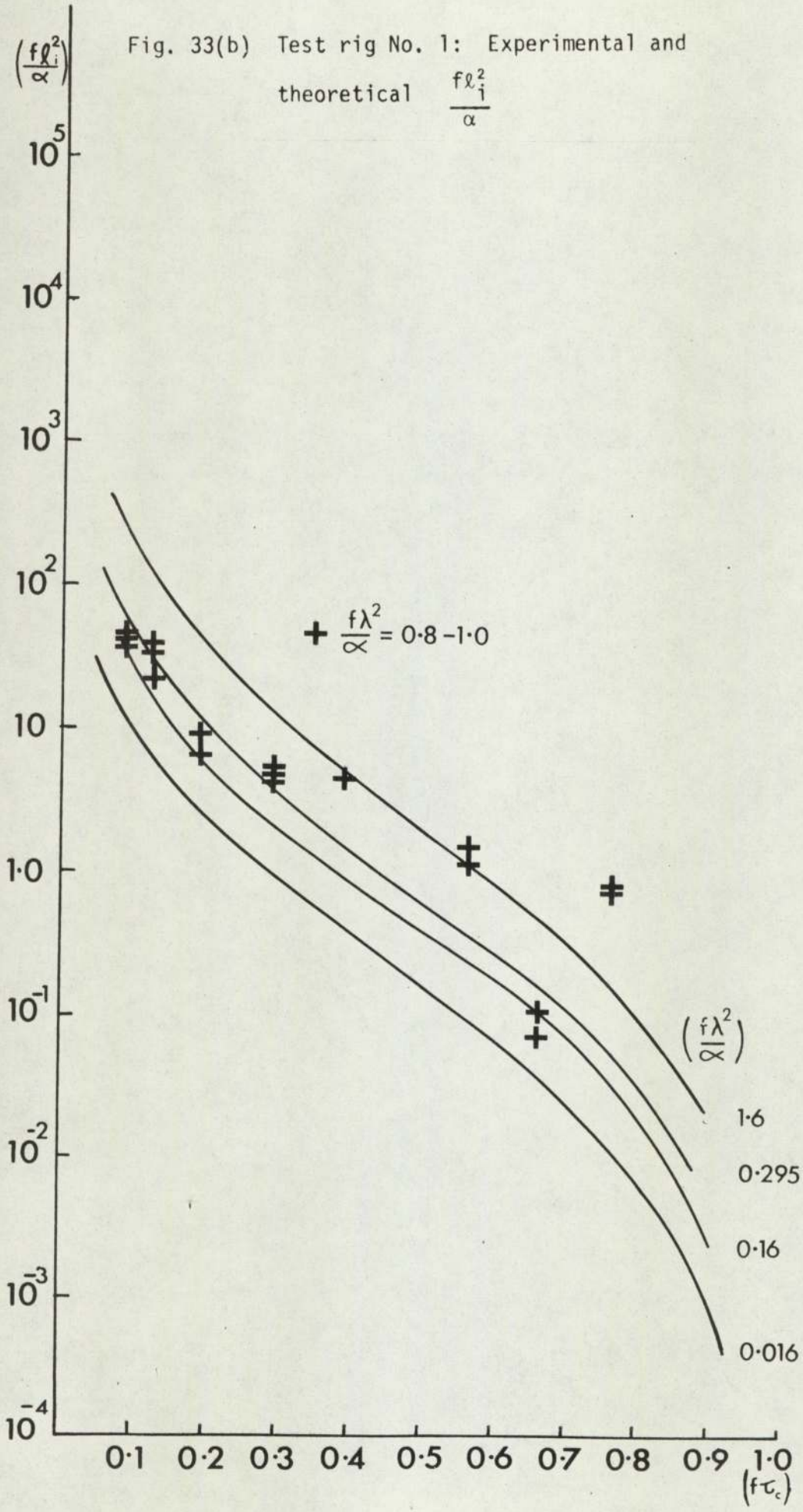

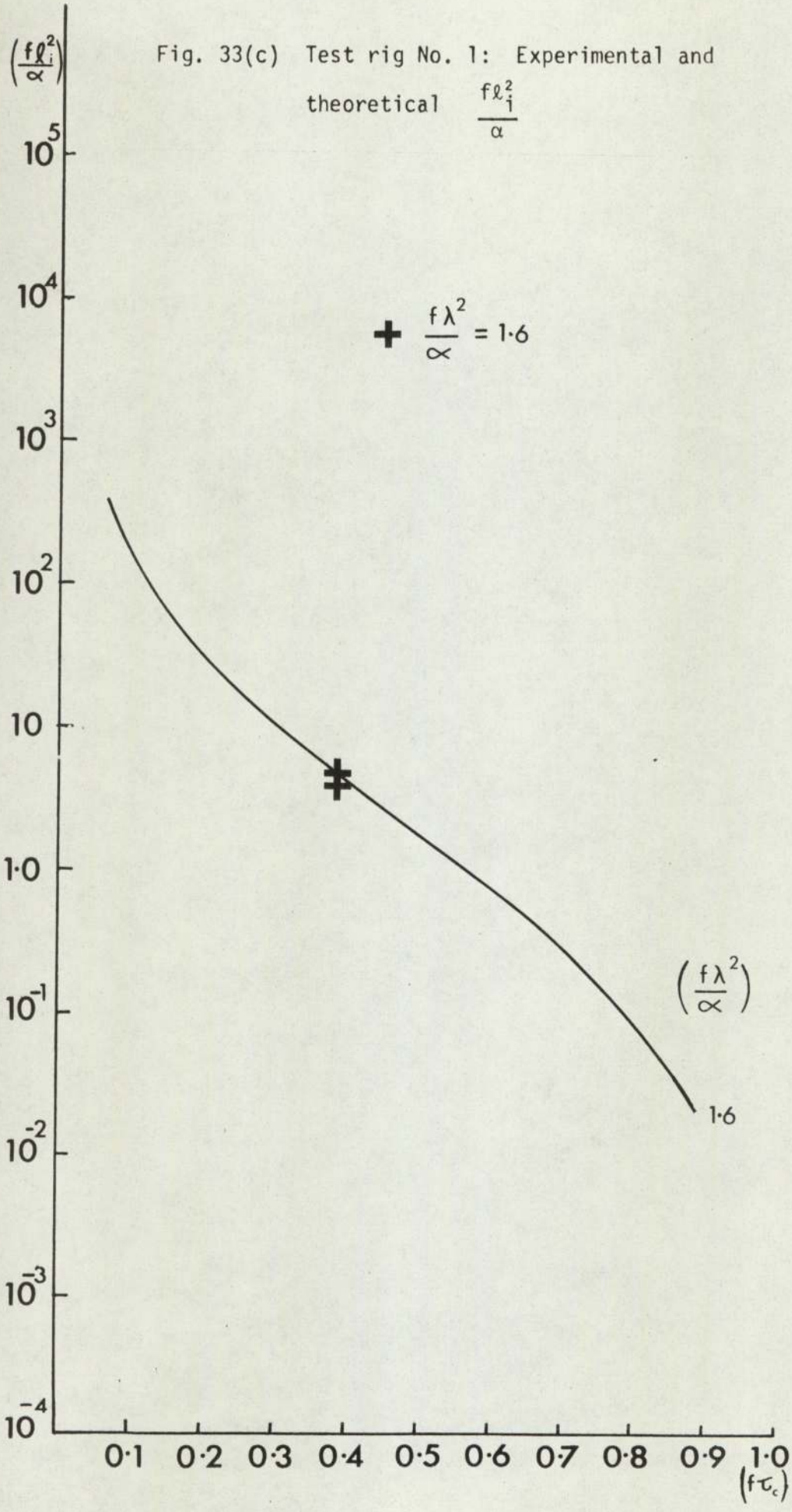

Fig. 33(c) Test rig No. 1: Experimental and theoretical $\frac{f\ell_i^2}{\alpha}$

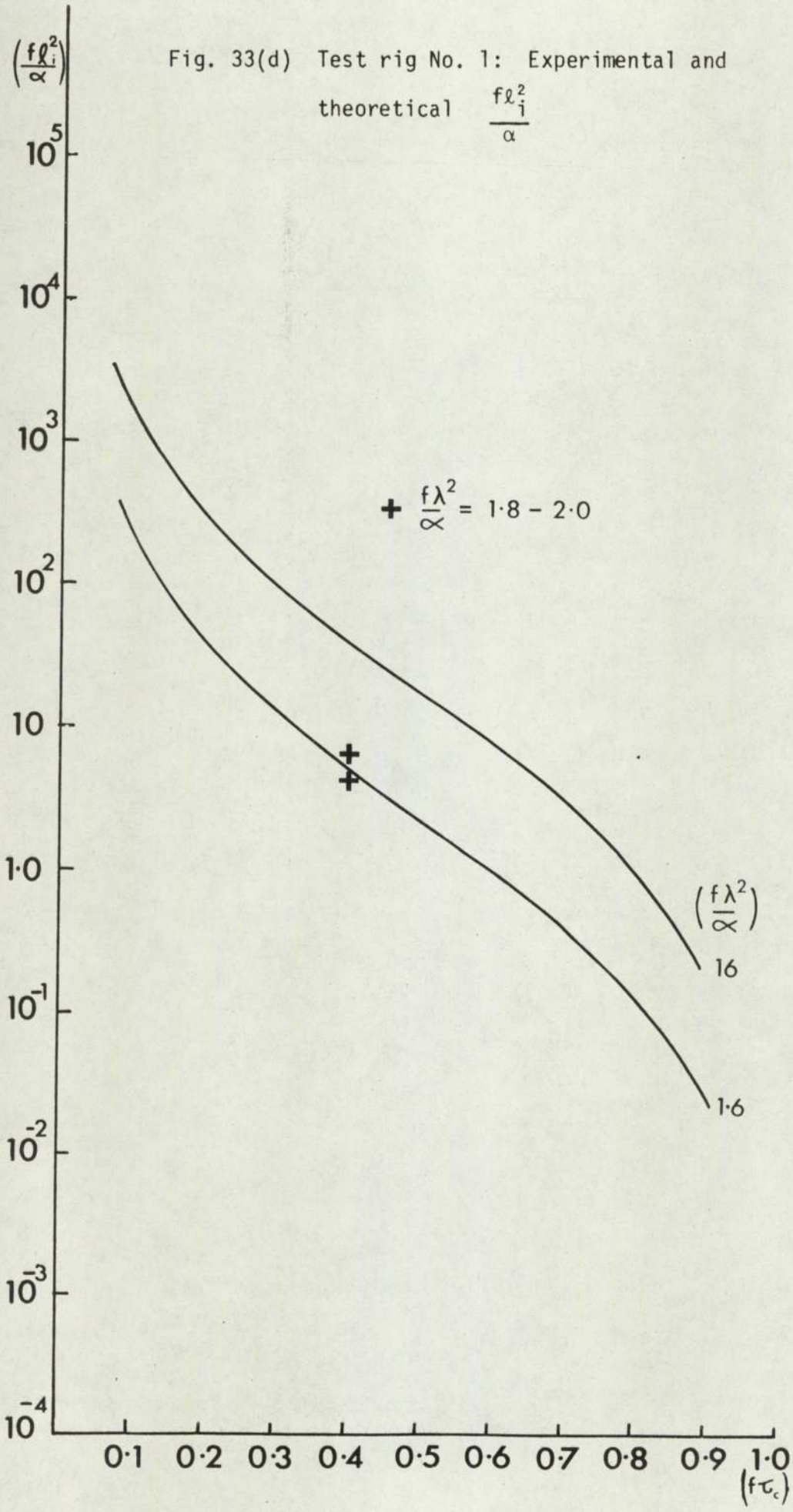

Fig. 33(d) Test rig No. 1: Experimental and theoretical $\frac{f\ell_i^2}{\alpha}$

Fig. 33(e) Test rig No. 1: Experimental and theoretical $\frac{f\ell_i^2}{\alpha}$

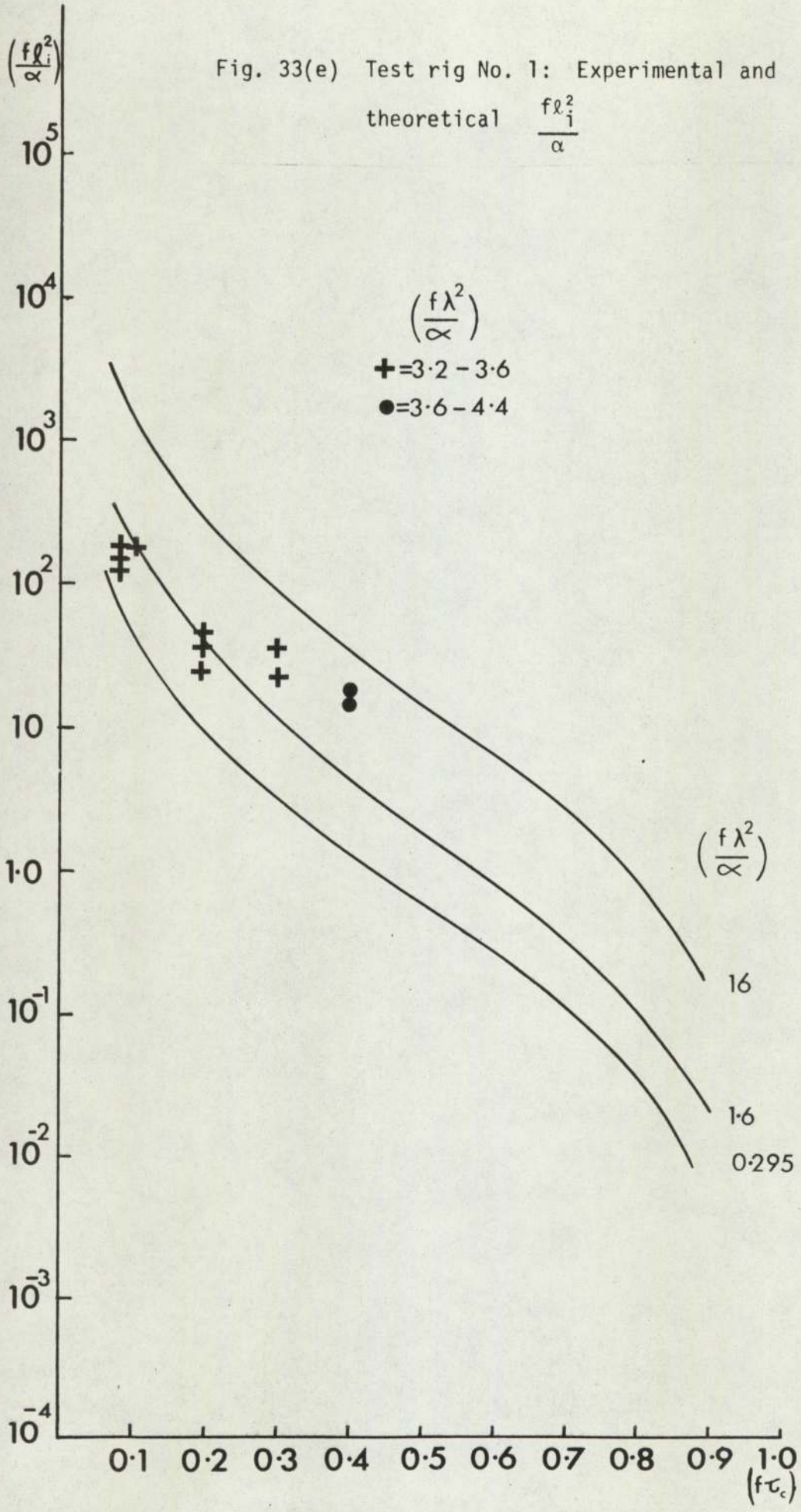

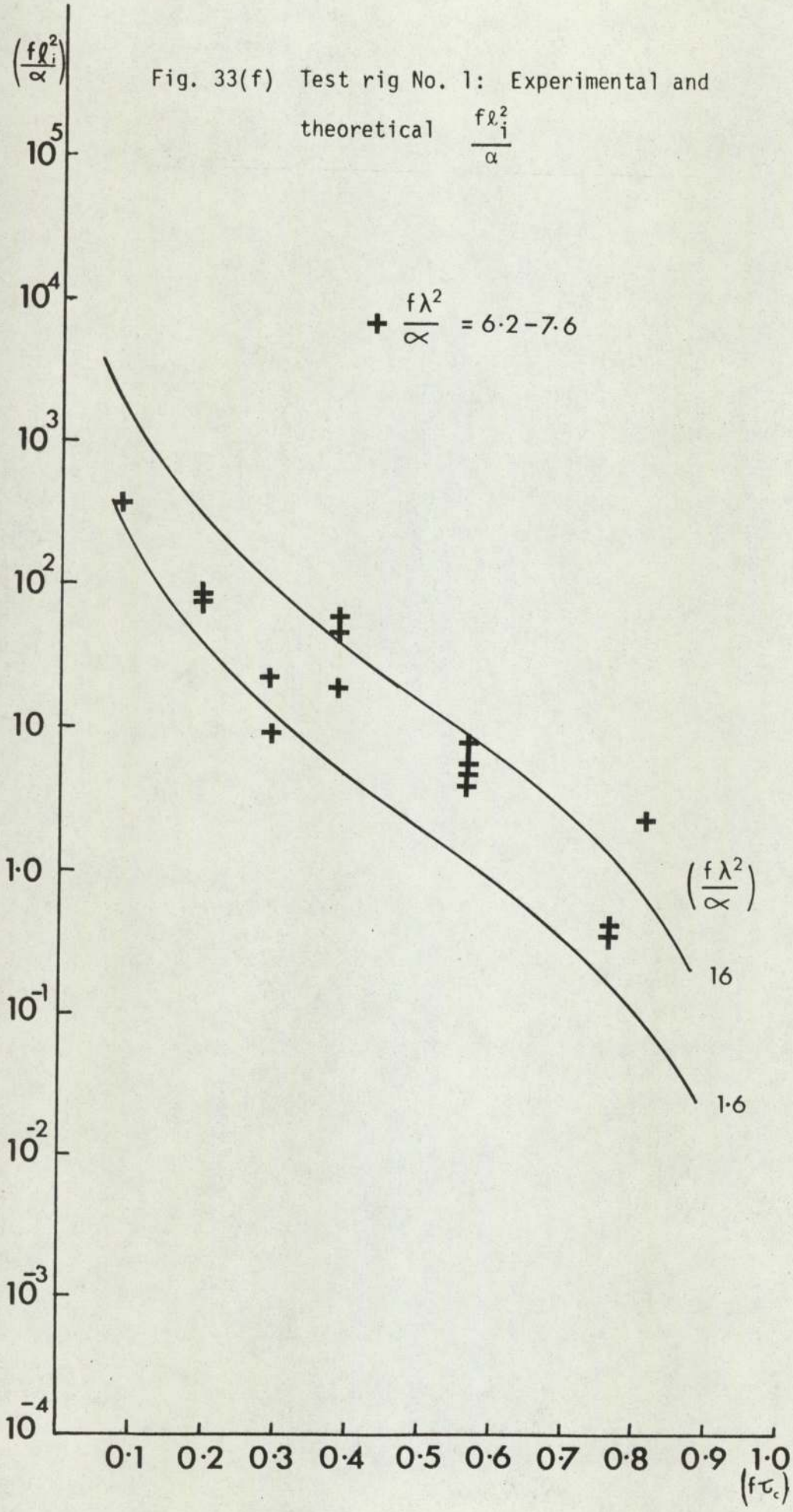

Fig. 33(f) Test rig No. 1: Experimental and theoretical $\frac{f\ell_i^2}{\alpha}$

Fig. 33(g) Test rig No. 1: Experimental and theoretical $\frac{f\ell_i^2}{\alpha}$

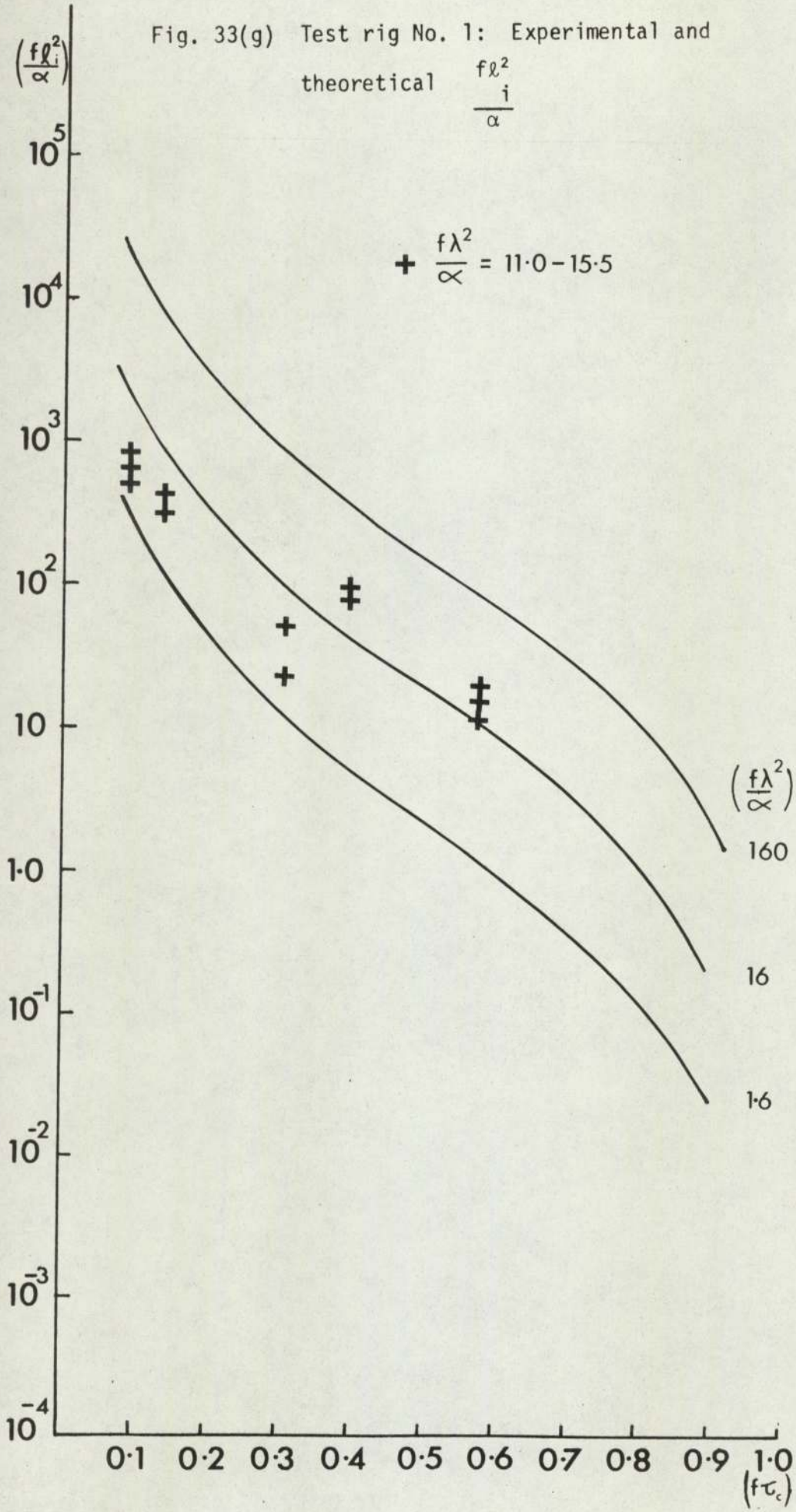

Fig. 33(h) Test rig No. 1: Experimental and theoretical $\frac{f\ell_i^2}{\alpha}$

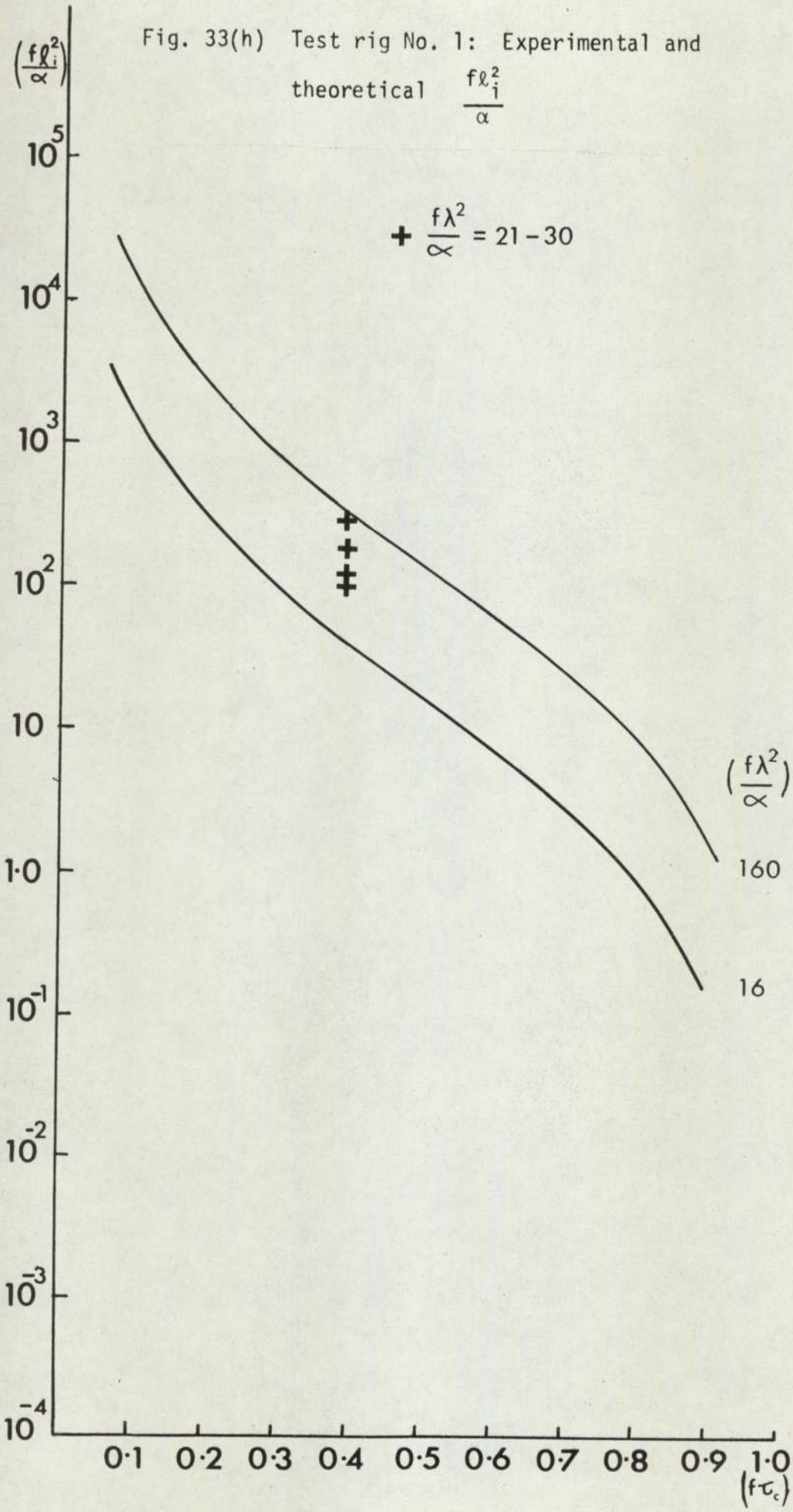

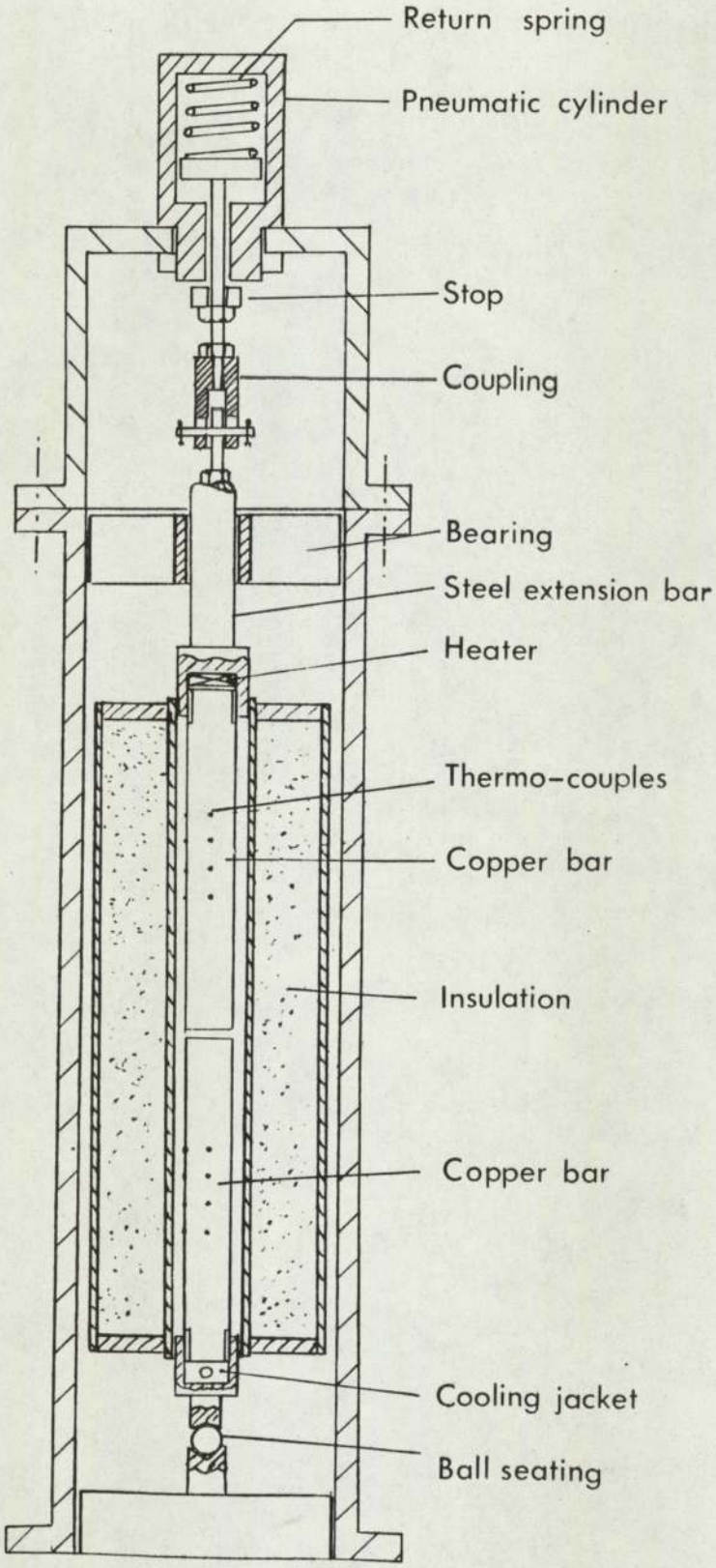

Fig. 34(a) Schematic drawing of test rig No. 2

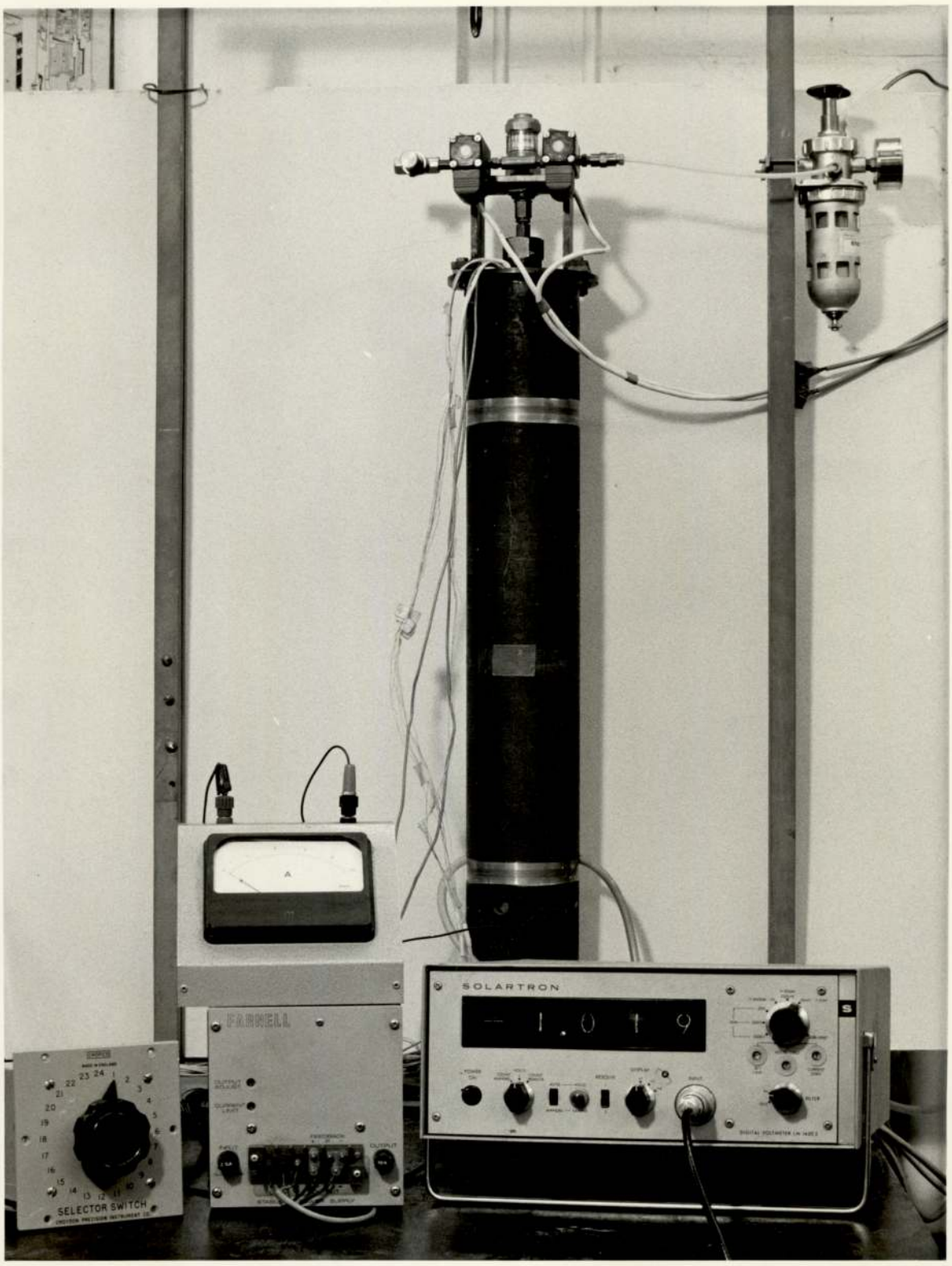

Fig. 34(b) Photograph of test rig No. 2

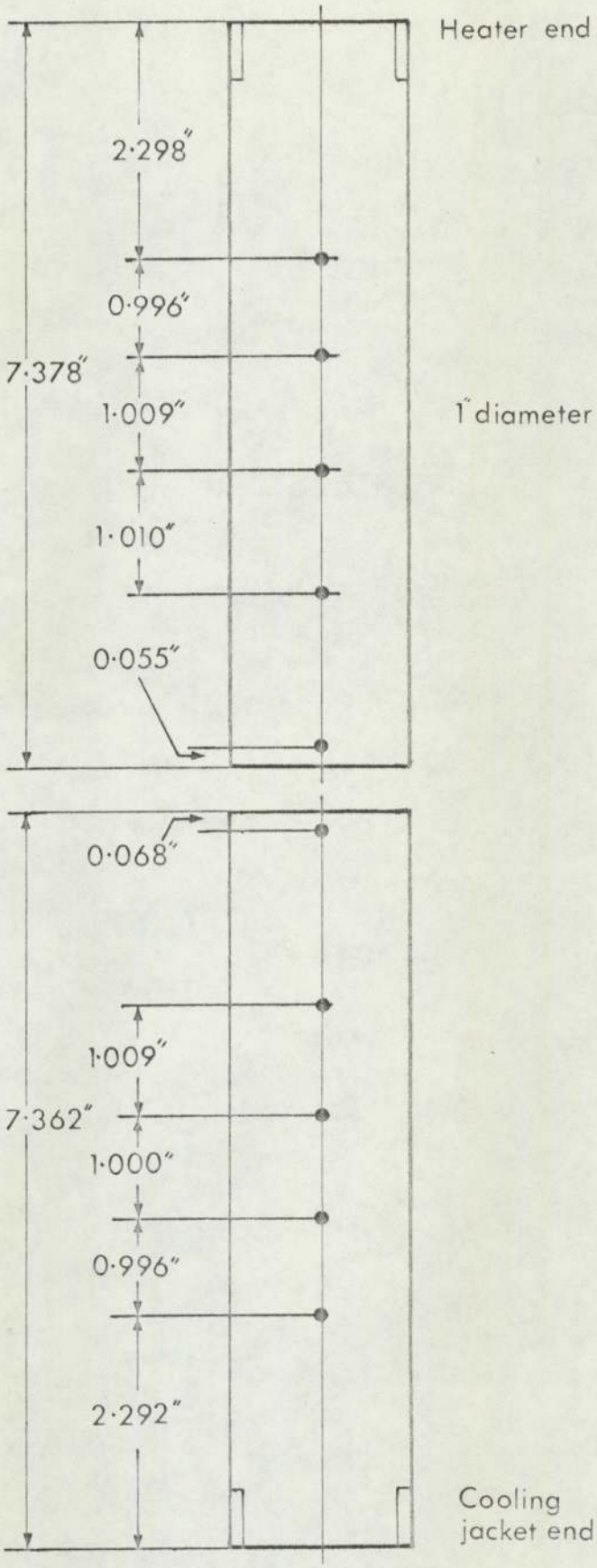

Fig. 35(a) Test rig No. 2: Thermocouple location in copper bars

Fig. 35(b) Test rig No. 2: Copper specimens and thermocouple installation

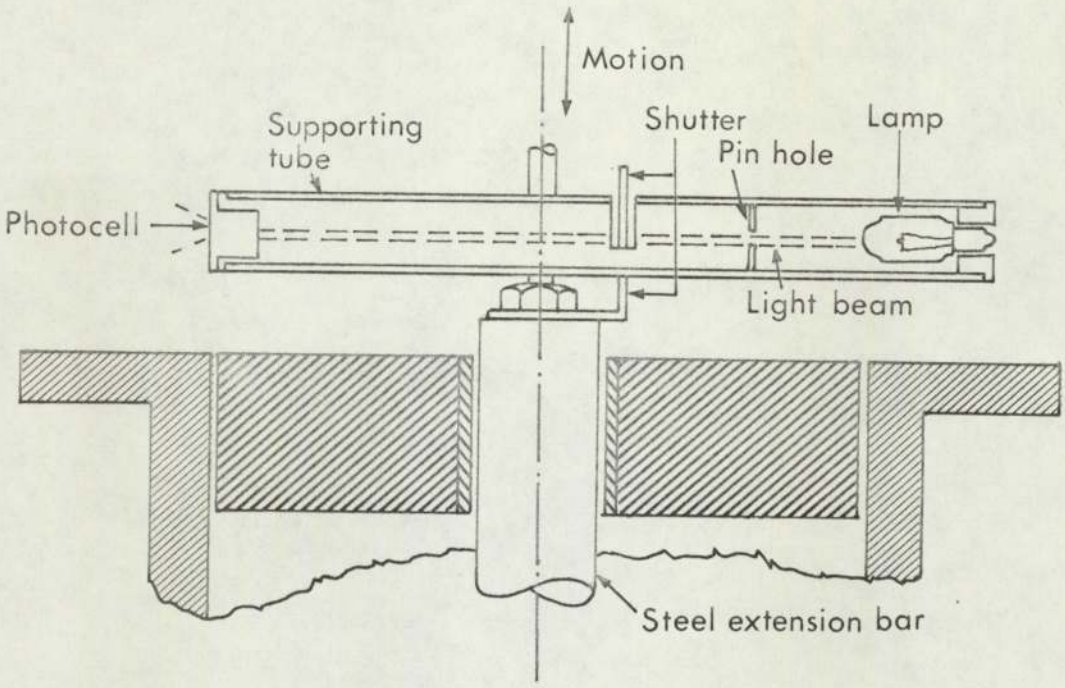

Fig. 36 Photocell arrangements for indicating contact and separation

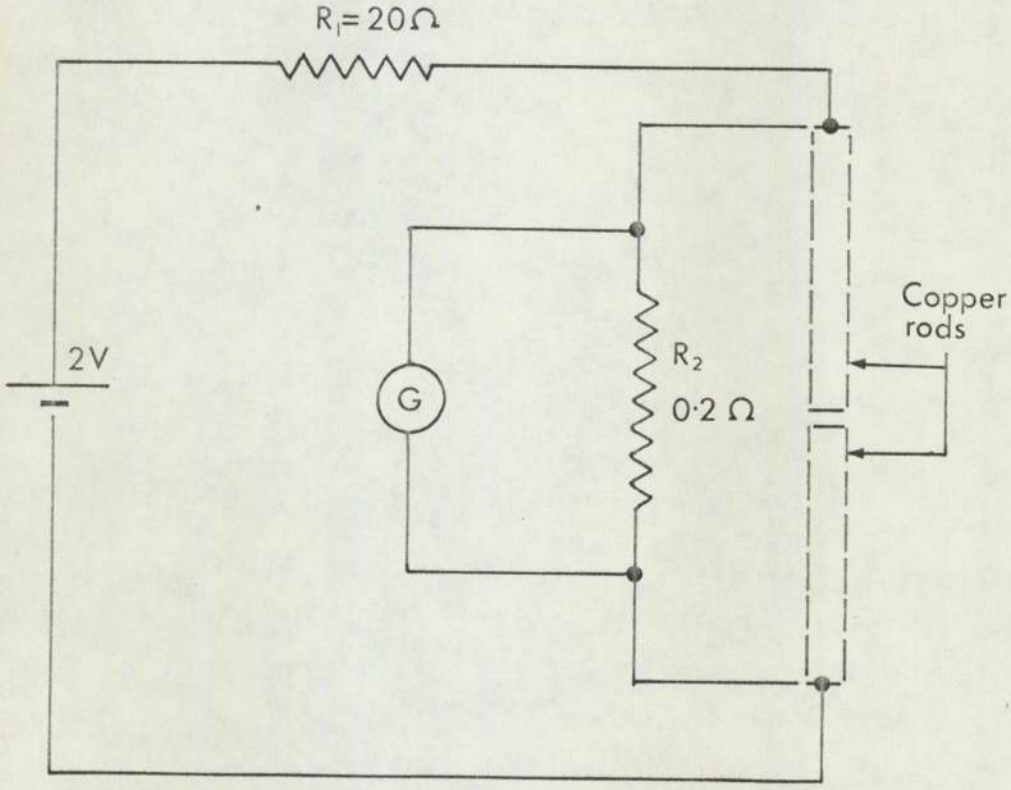

Fig. 37 Circuit for electrical resistance method of indicating contact and separation

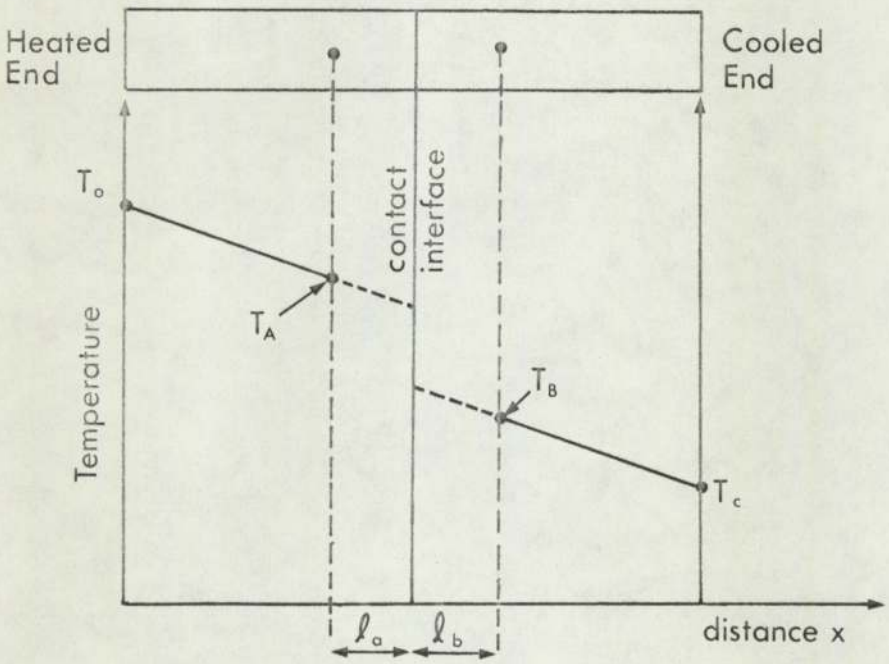

Fig. 38 Temperature distribution in bars with thermal contact resistance

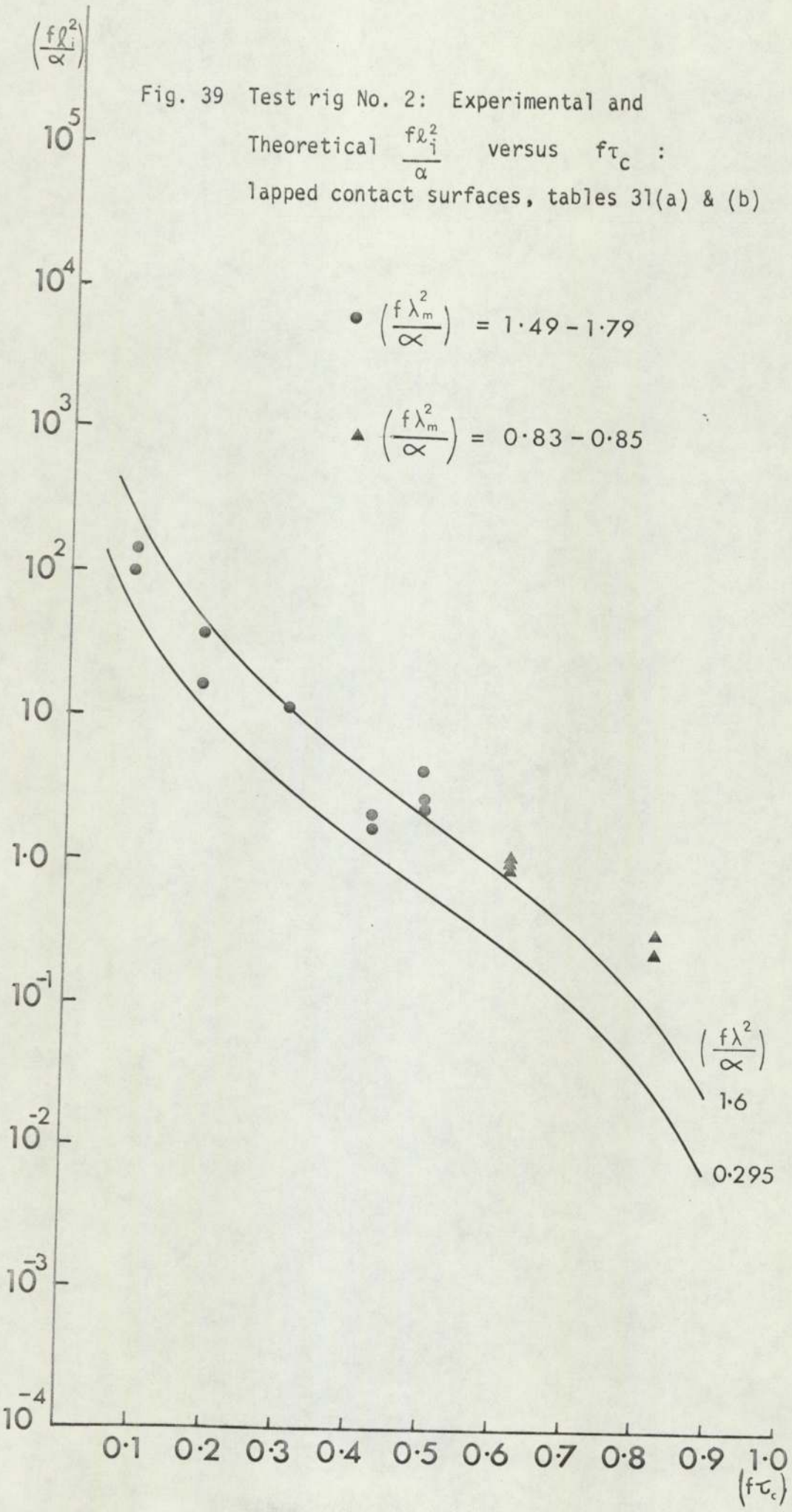

Fig. 39 Test rig No. 2: Experimental and Theoretical $\frac{f\ell_i^2}{\alpha}$ versus $f\tau_c$: lapped contact surfaces, tables 31(a) & (b)

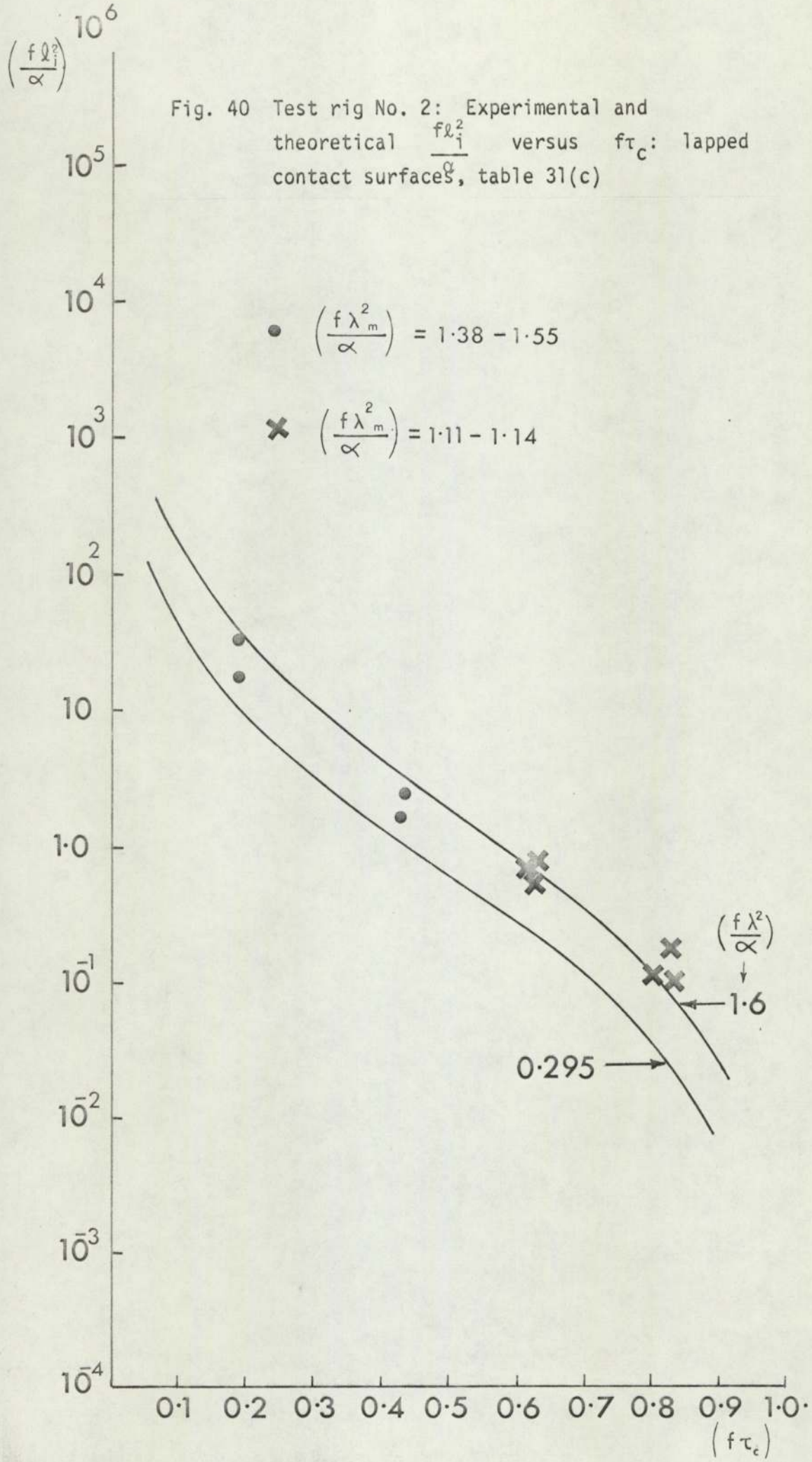

Fig. 40 Test rig No. 2: Experimental and theoretical $\frac{f\ell_i^2}{\alpha}$ versus $f\tau_c$: lapped contact surfaces, table 31(c)

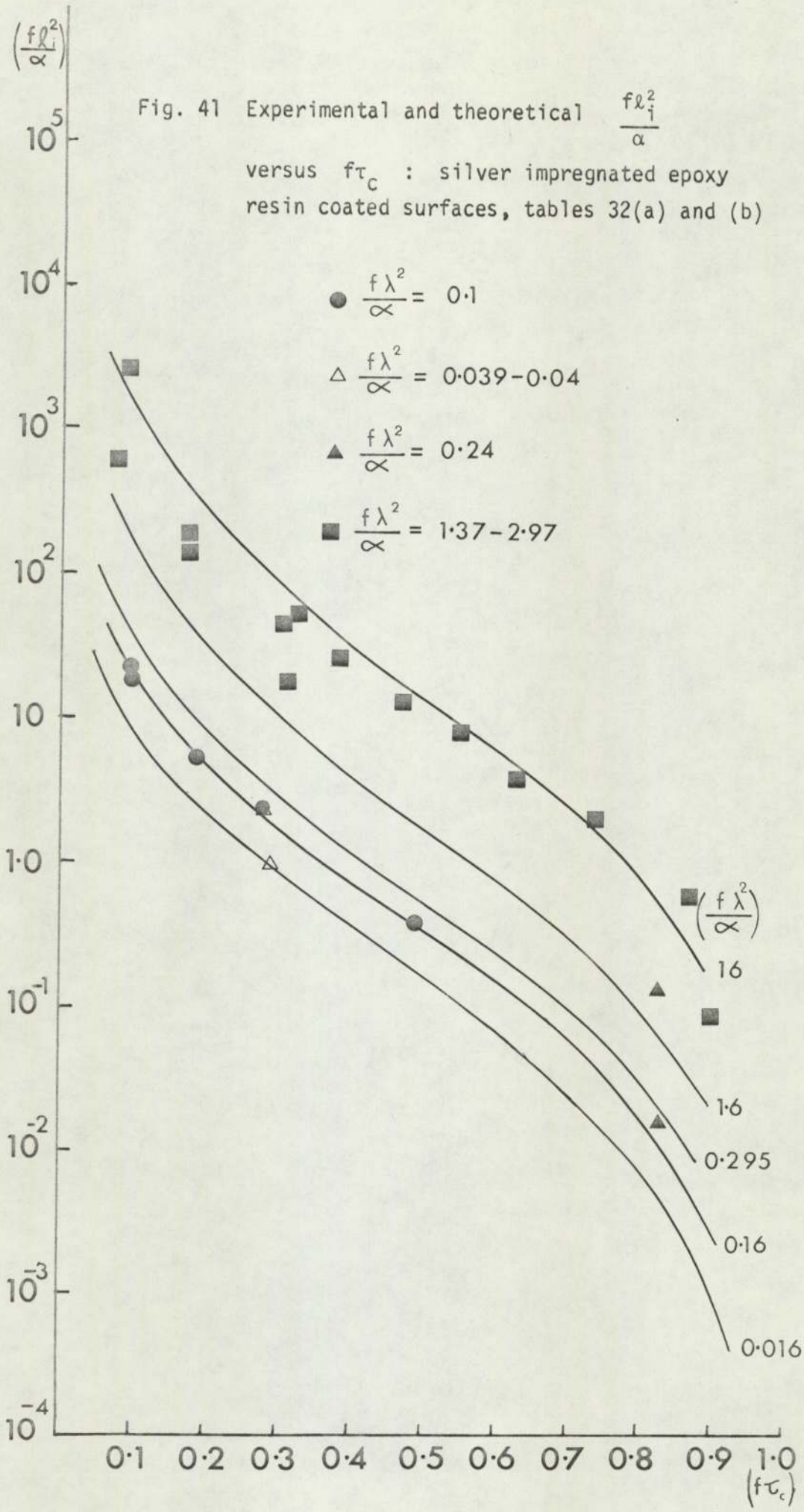

Fig. 41 Experimental and theoretical $\frac{f\ell_i^2}{\alpha}$ versus $f\tau_c$: silver impregnated epoxy resin coated surfaces, tables 32(a) and (b)

Fig. 42 Silver-impregnated epoxy resin coated contact surfaces after tests

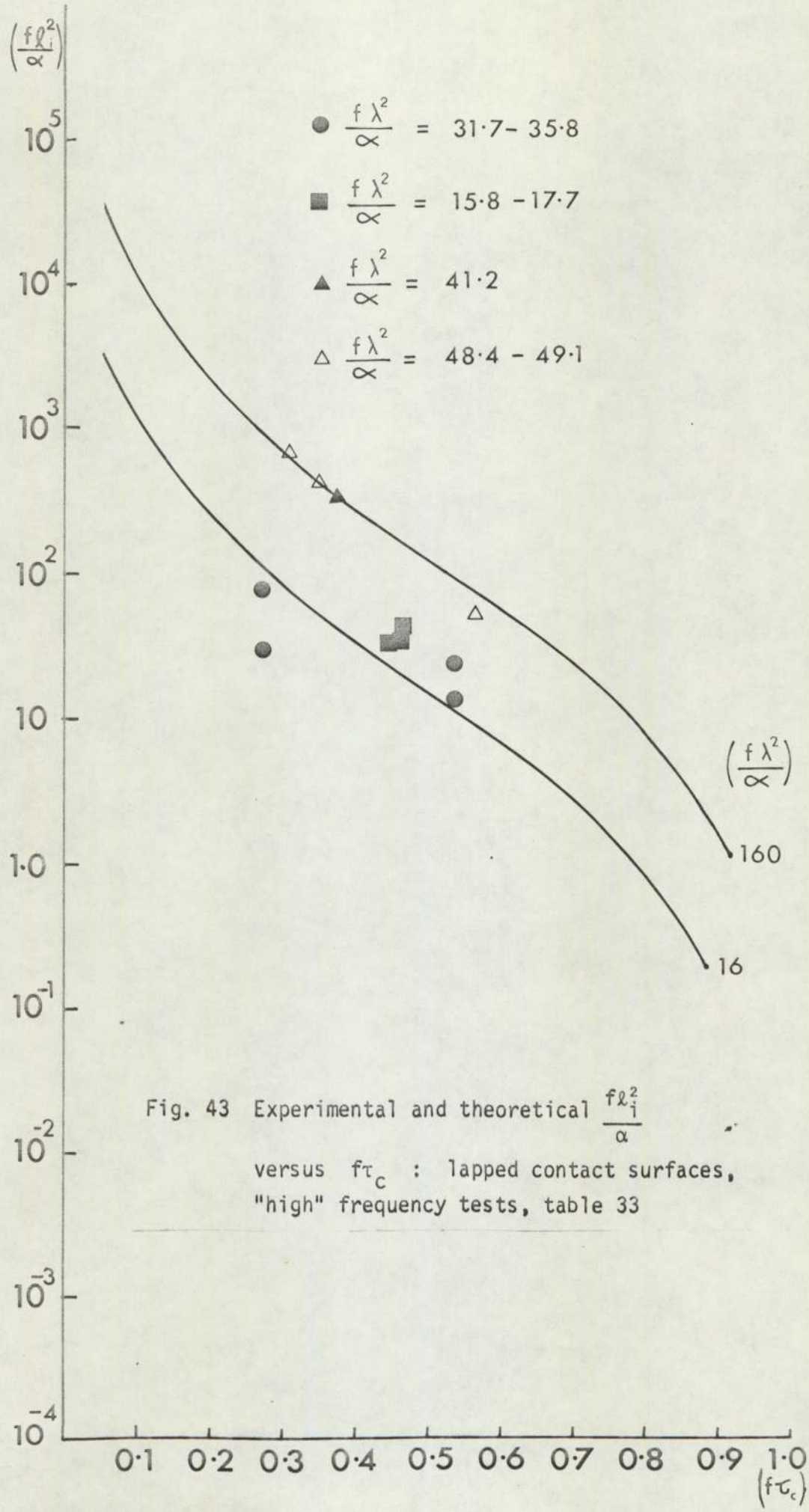

Fig. 43 Experimental and theoretical $\frac{f\ell_i^2}{\alpha}$ versus $f\tau_c$: lapped contact surfaces, "high" frequency tests, table 33

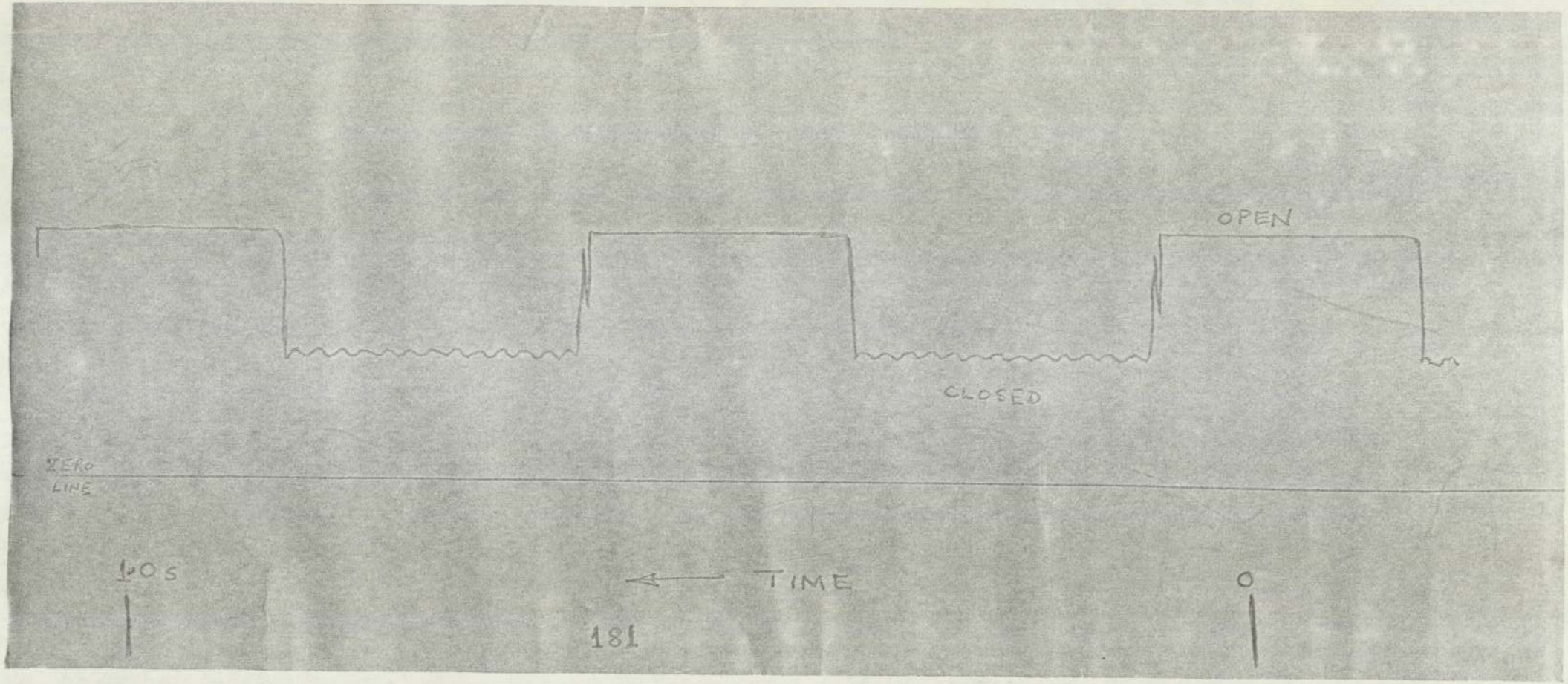

Fig. 44(a) Trace of voltage drop across resistor R_2 in Fig. 37. Static load 33.4N (7.5 lbf) before impact 0.187 kg m/s

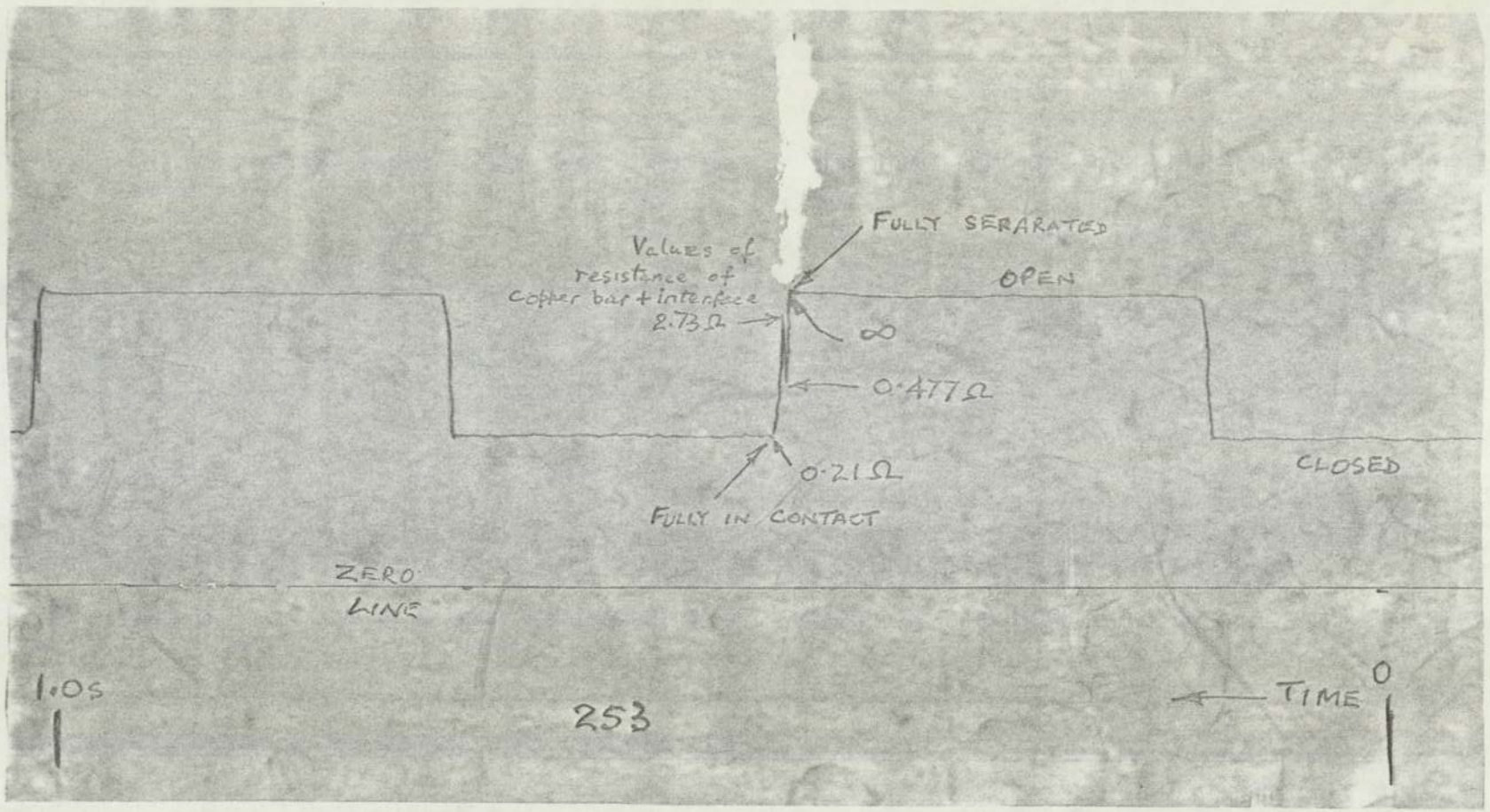

Fig. 44(b) Trace of voltage drop across resistor R_2 in Fig. 37. Static load 66.8N (15 lbf), momentum before impact 0.539 kg m/s

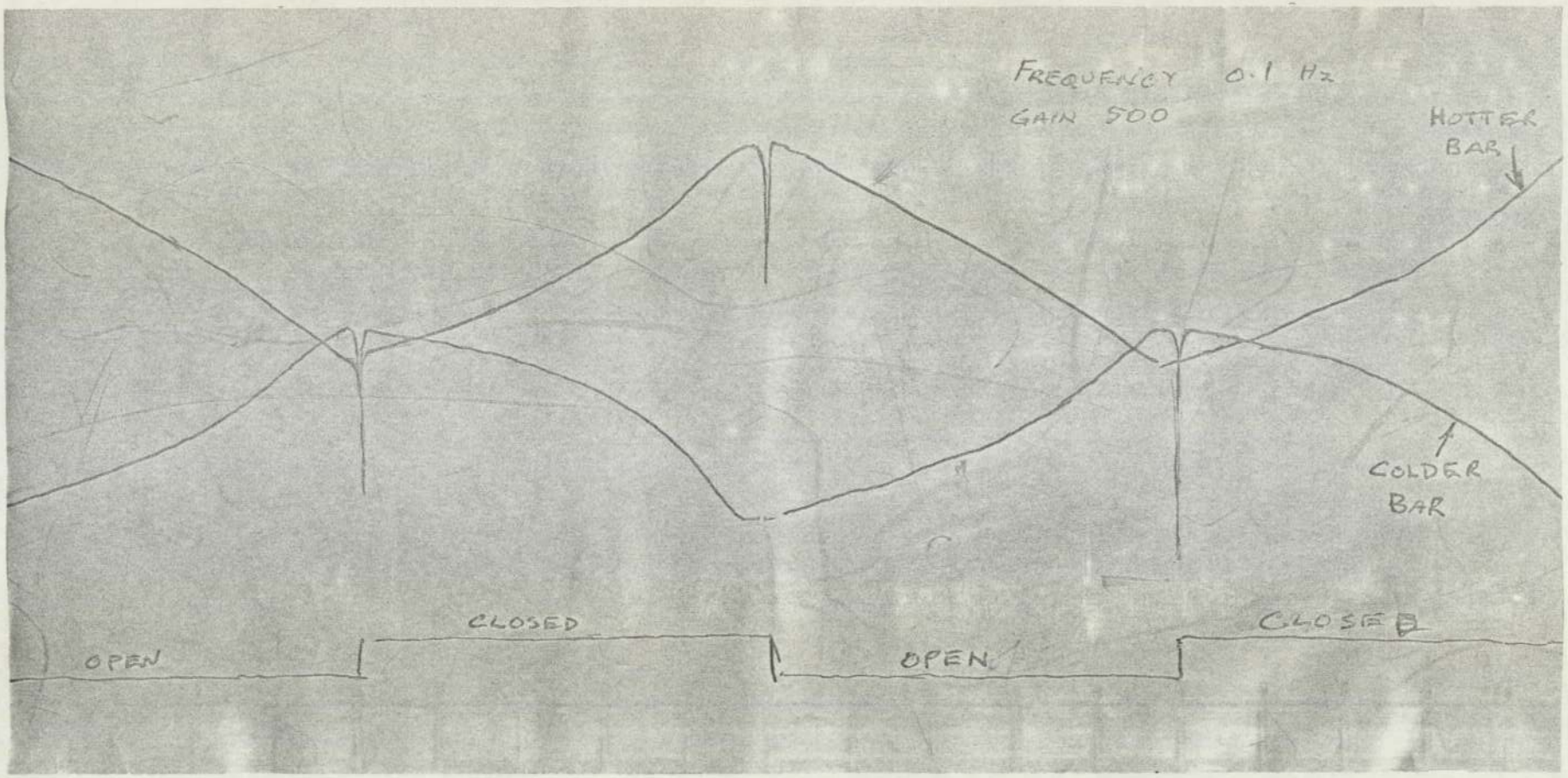

Fig. 44(c) Amplified outputs of thermocouples near contact interface

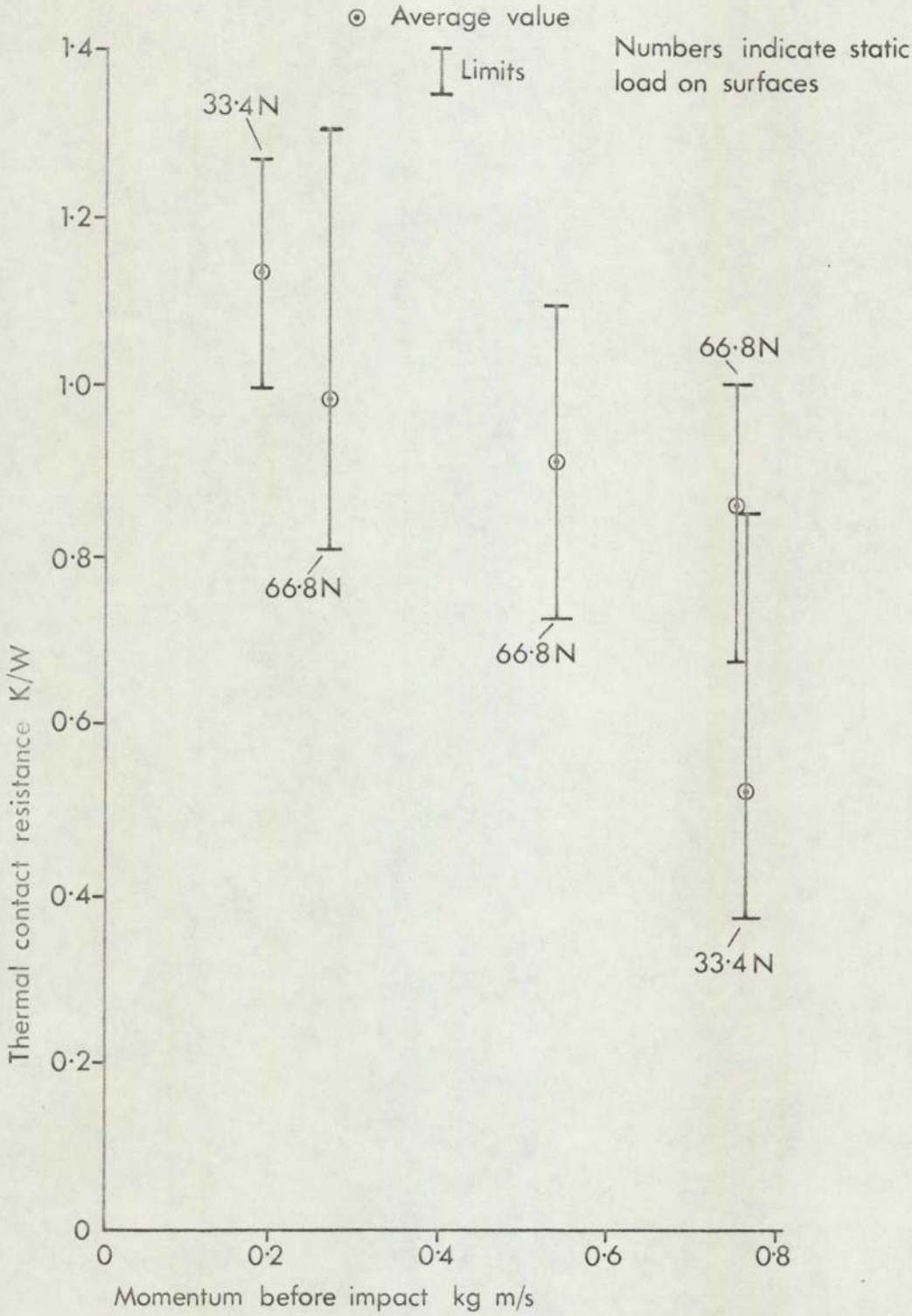

Fig. 45 Thermal contact conductance versus momentum before impact

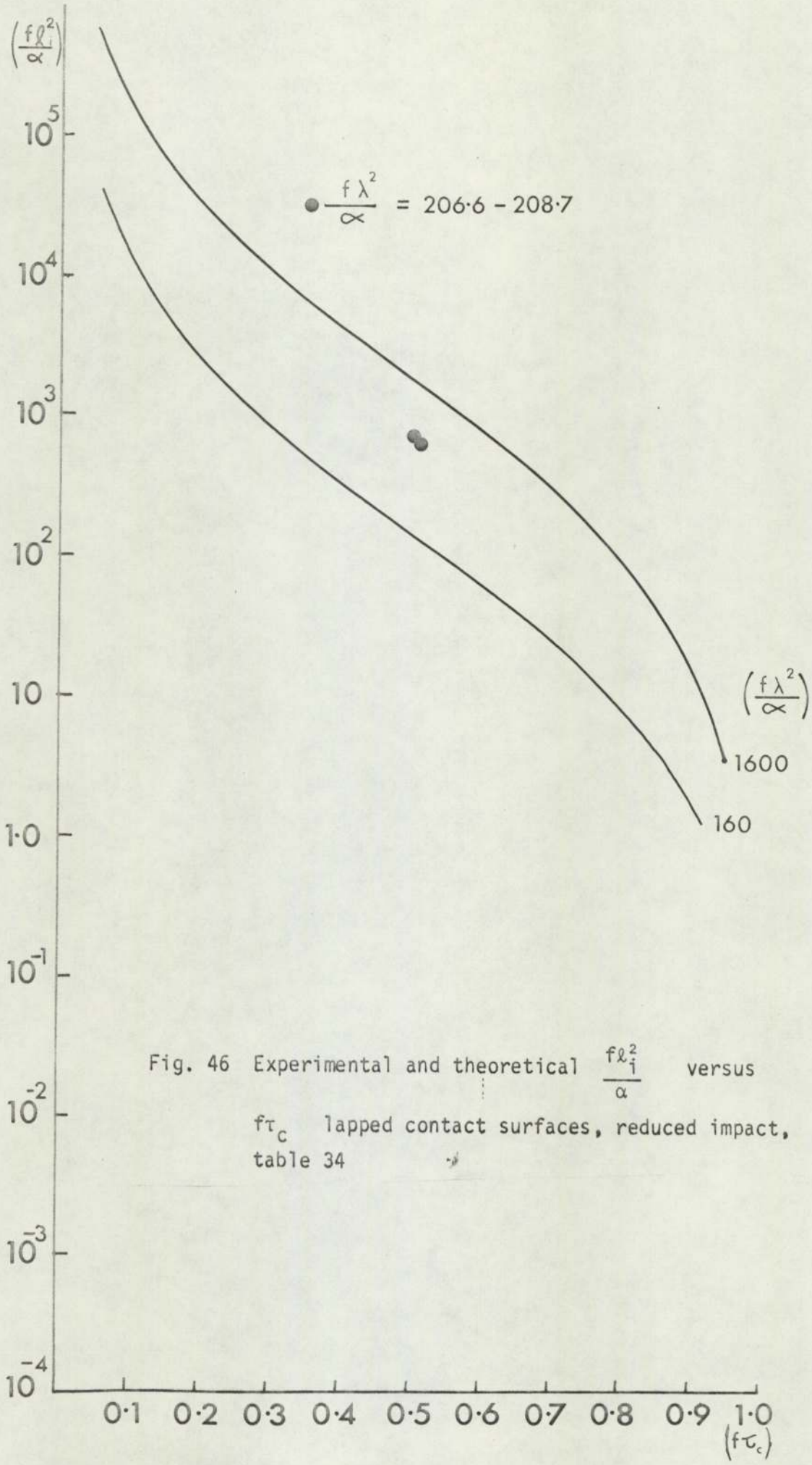

Fig. 46 Experimental and theoretical $\frac{f\ell_i^2}{\alpha}$ versus $f\tau_c$ lapped contact surfaces, reduced impact, table 34

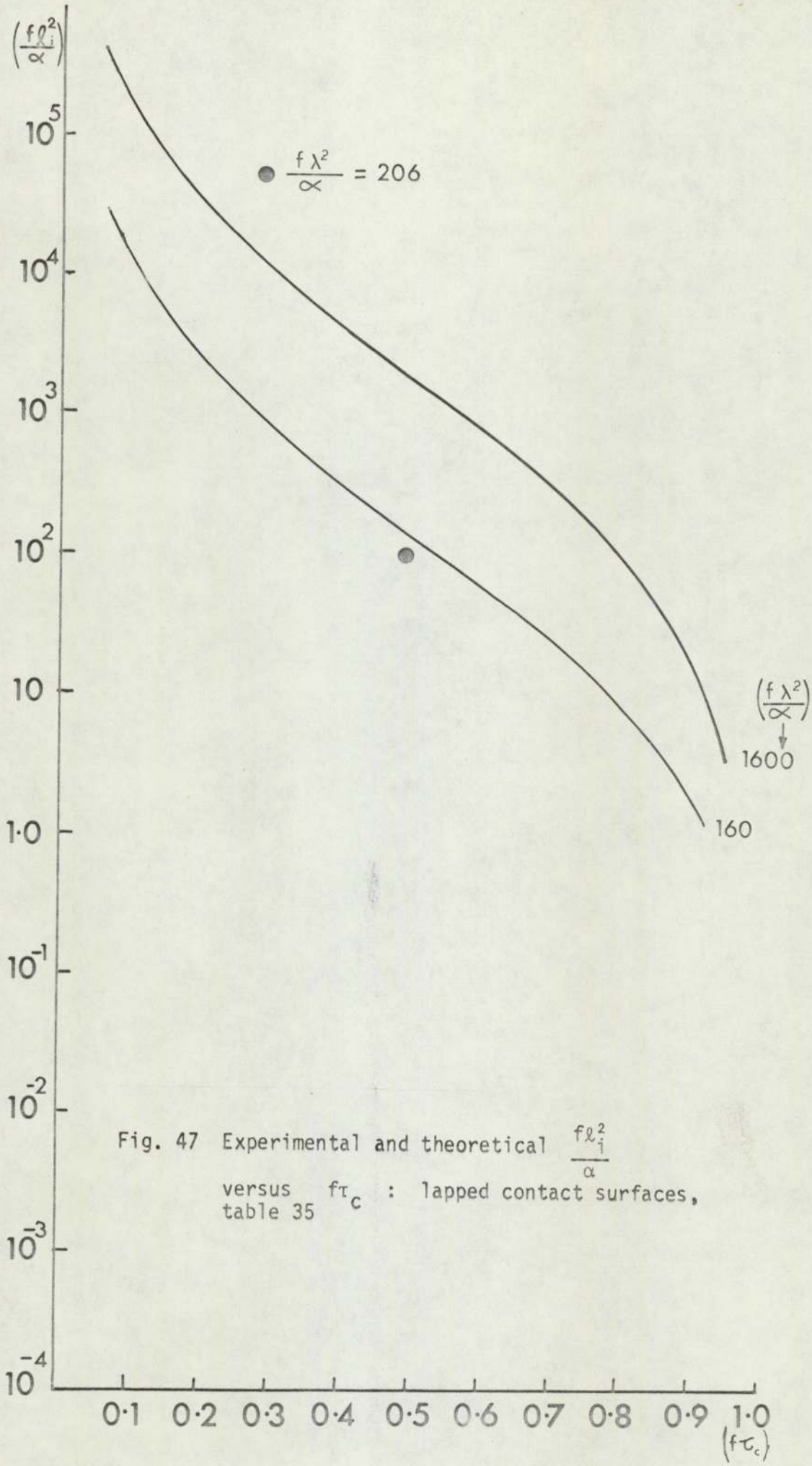

Fig. 47 Experimental and theoretical $\frac{f\ell_i^2}{\alpha}$ versus $f\tau_c$: lapped contact surfaces, table 35

Fig. 48 Contact surfaces after tests set No. 5

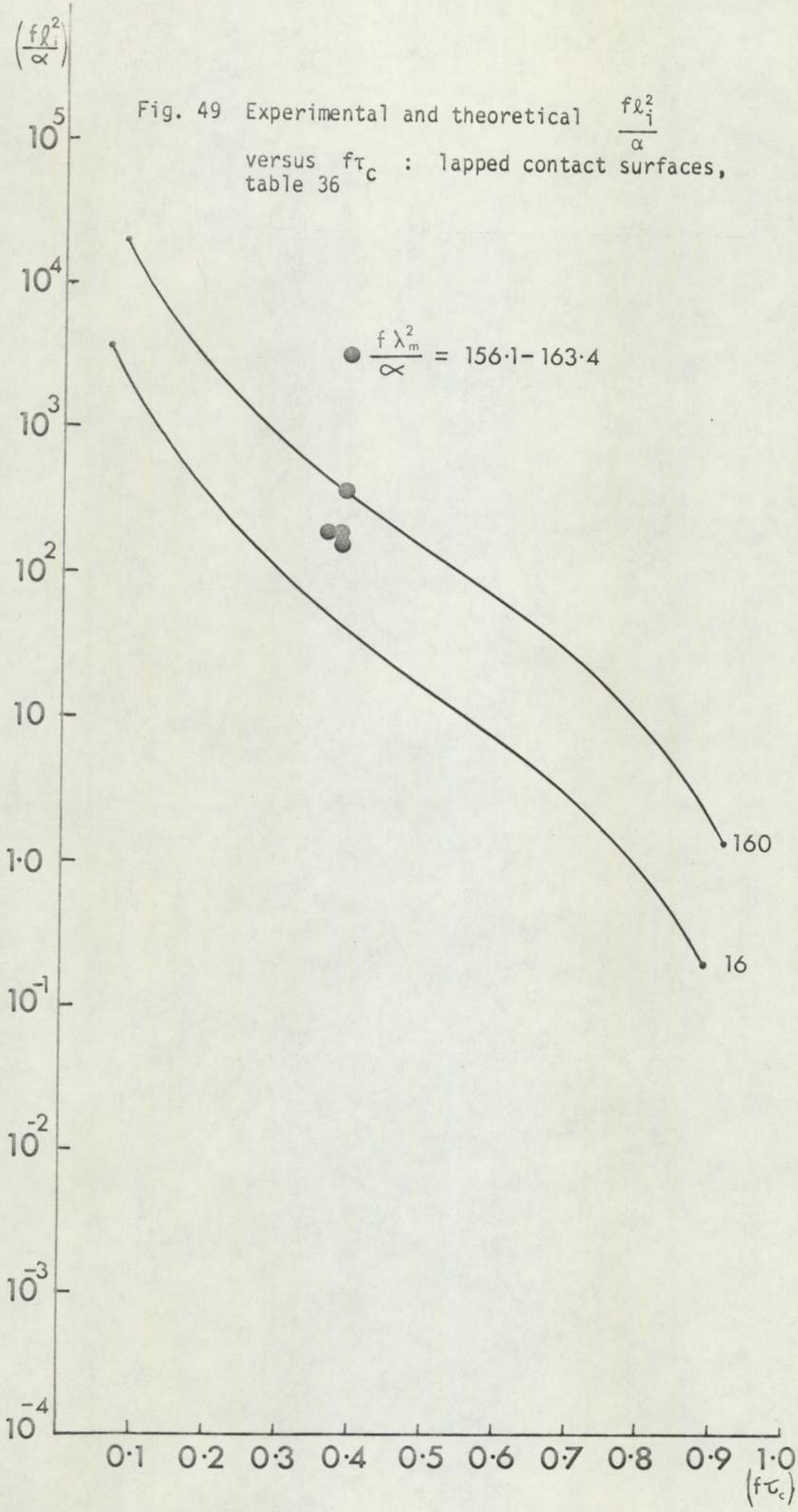

Fig. 49 Experimental and theoretical $\frac{f\ell_i^2}{\alpha}$ versus $f\tau_c$: lapped contact surfaces, table 36

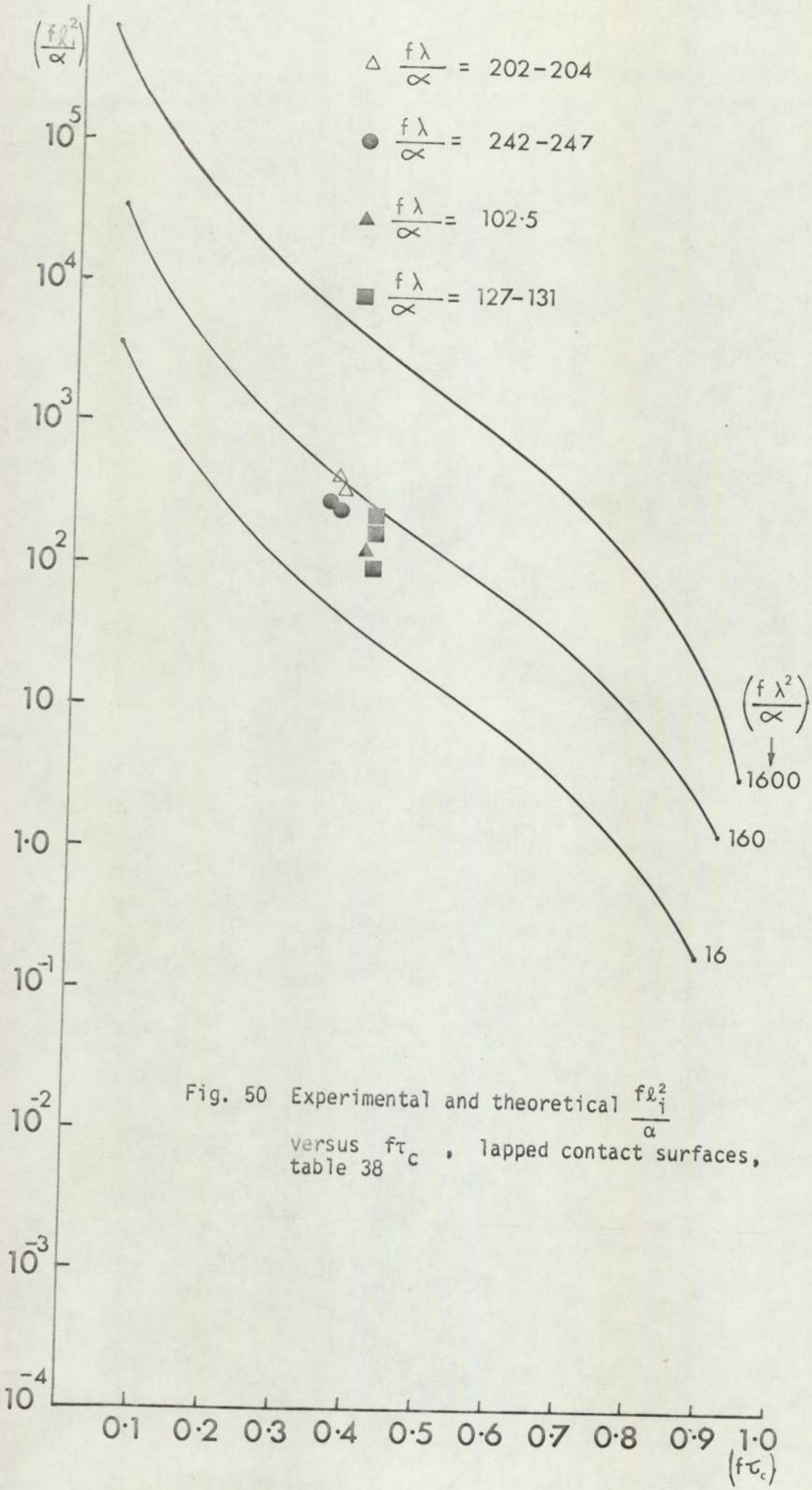

Fig. 50 Experimental and theoretical $\frac{f\ell_i^2}{\alpha}$ versus $f\tau_c$, lapped contact surfaces, table 38

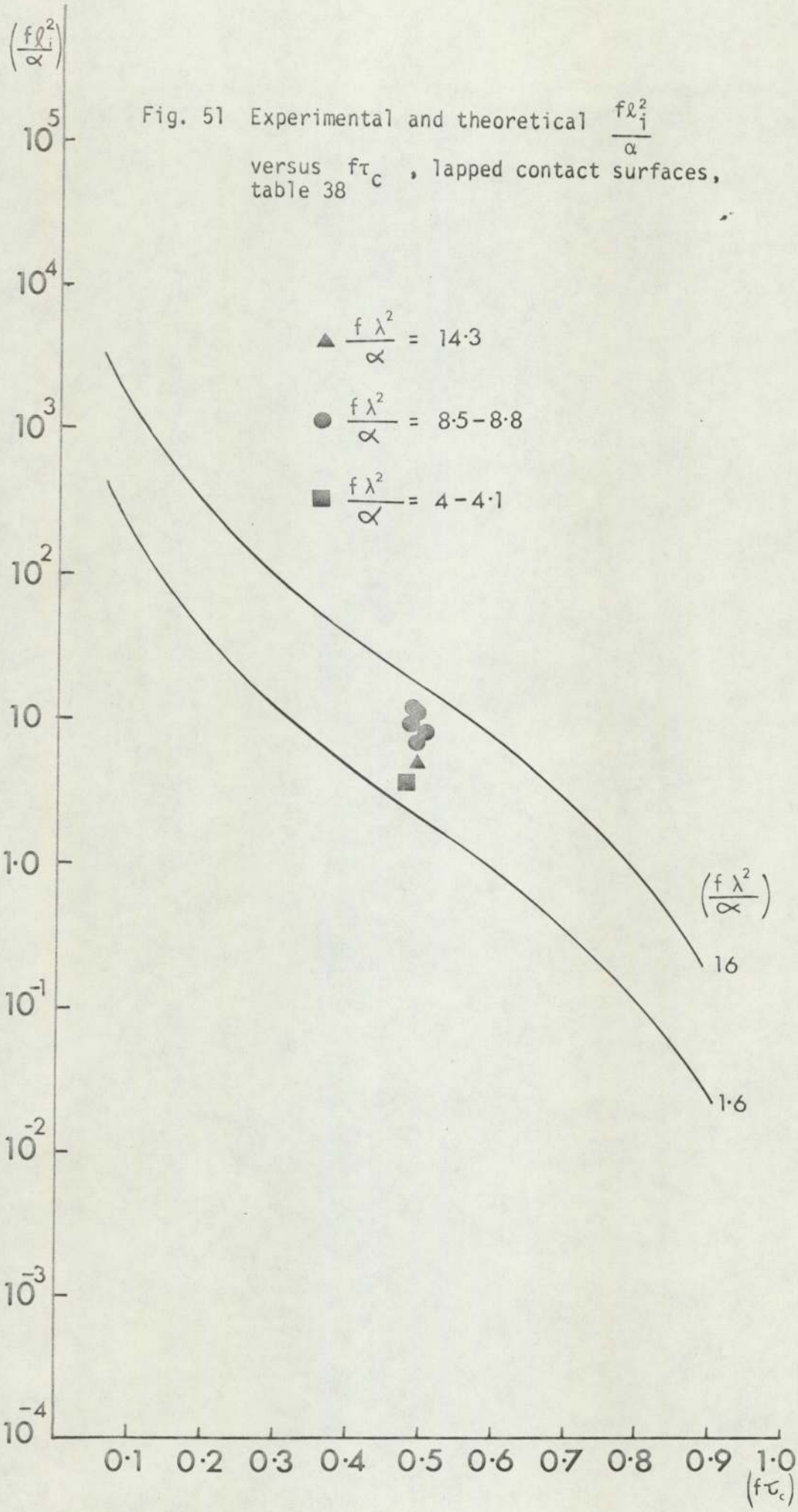

Fig. 51 Experimental and theoretical $\frac{f\ell_i^2}{\alpha}$ versus $f\tau_c$, lapped contact surfaces, table 38

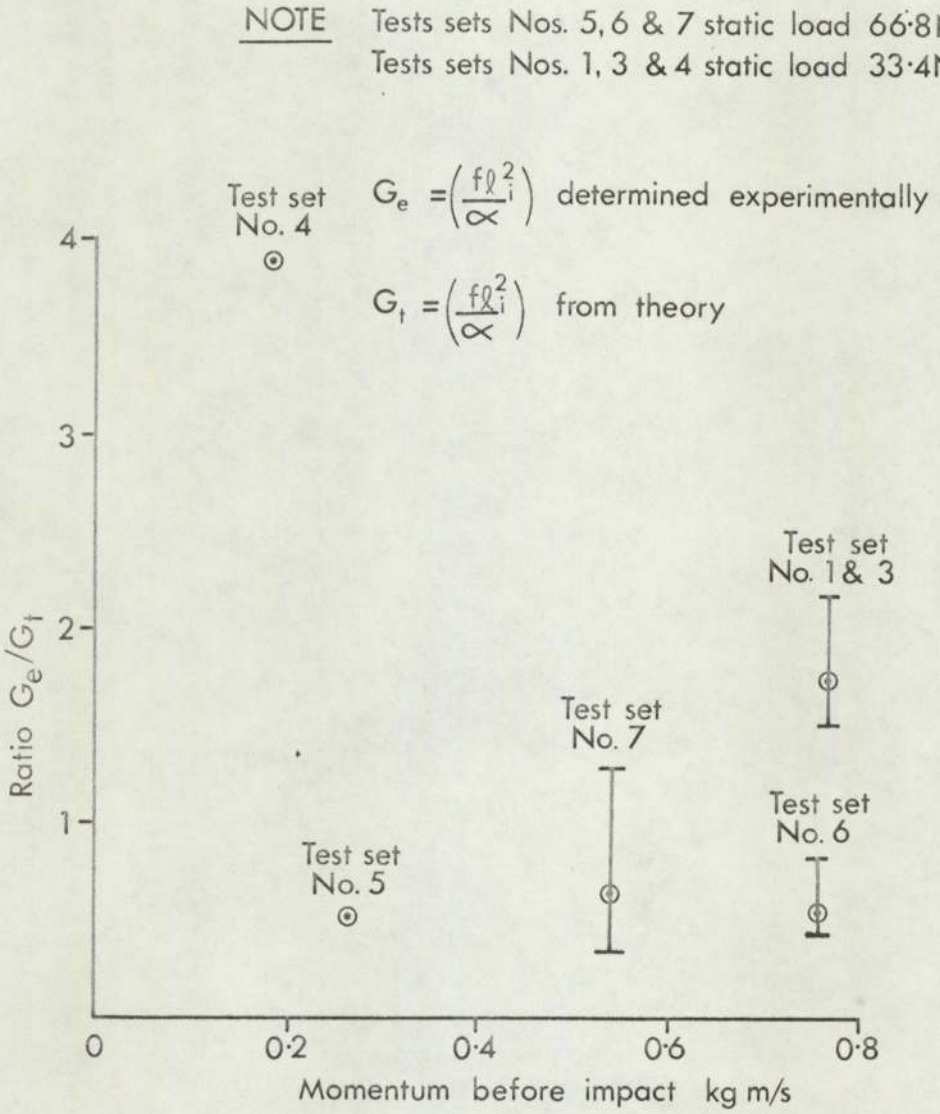

Fig. 52 Ratio G_e/G_t versus momentum before impact

(a) Hotter contact surface

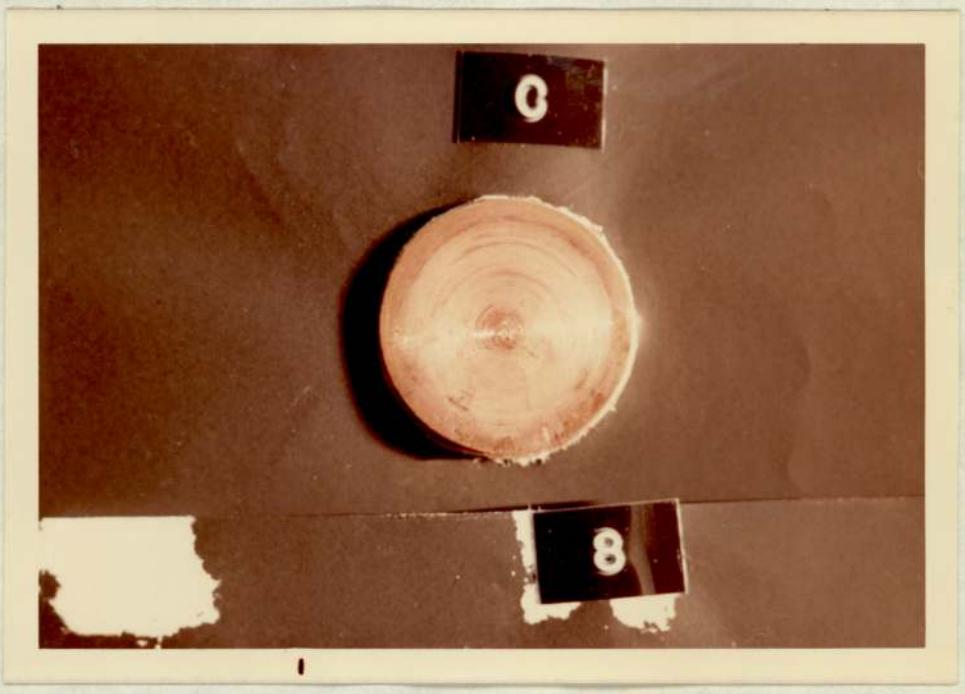

(b) Colder contact surface

Fig. 53 Condition of contact surfaces after tests set No.7

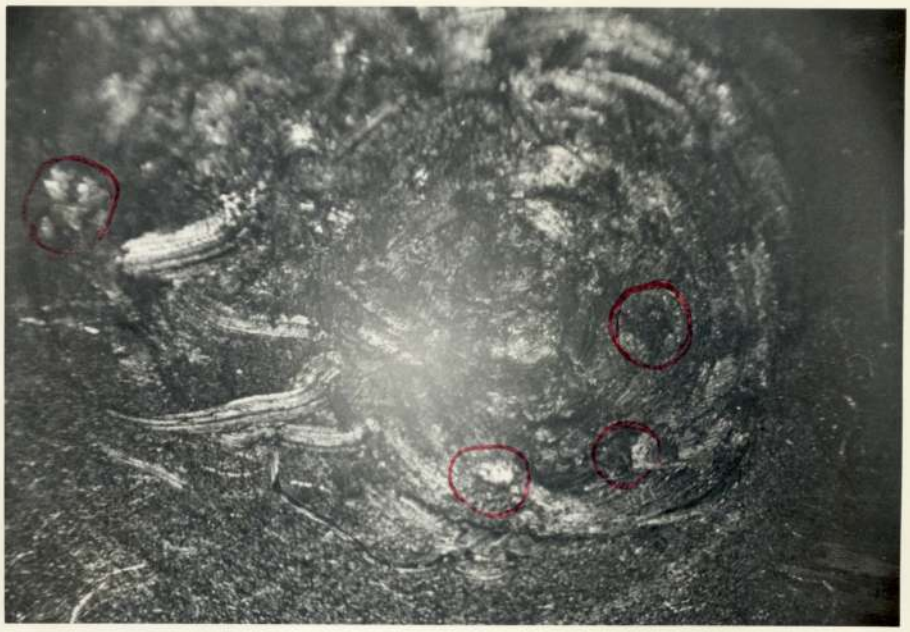

(a) Near centre

(b) 6 mm from centre

(c) Near periphery

Fig. 54 Hotter surface x27 magnification

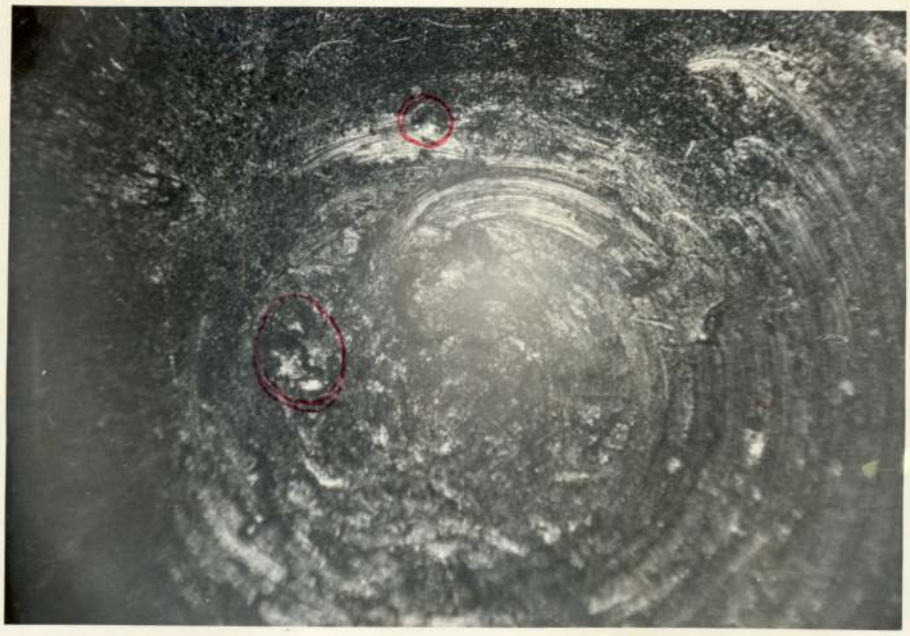

(a) Near centre

(b) 6 mm from centre

(c) Near periphery

Fig. 55 Colder surface x27 magnification

REFERENCES

1. Aaron, R.L. and Blum, H.A.,"Heat Transfer Across Surfaces in Contact: Effects of Ambient Pressure Changes" A.I.Chem.E. Paper No.63-B-9.

2. Aaron, R.L.and Blum, H.A.,"Heat Transfer Across Surface in Contact: Transient Effects of Ambient Temperatures and Pressures" N.A.S.A.Report N65 - 18445.

3. Ali, S.M.,Rooks, B.W., and Tobias, S.A. "The effect of dwell time on die wear in high speed hot forging." Proc. I.Mech. E 1970-71, 185, paper 83/71.

4. Atkins, H. "Bibliography on Thermal Metallic Contact Conductance" NASA Technical Memorandum NASA TM X - 53227 Dated 15 April 1965.

5. Baillie and Fan "Temperature transient after contact heating" Int. J. Heat and Mass Transfer 1963, vol(6) pp.926-7.

6. Baklastov, A.M.and Gorbenko, V.A."Thermal Contact Resistance of Solid Bodies with Quasi-steady State Heating" Thermal Engineering 1971, 18 (8), 123.

7. Barber, J.R. "The effect of Thermal Distortion on Constriction Resistance. Int. J. Heat and Mass Transfer, 1971, Vol. 14, pp751-766.

8. Barzelay and Holloway "Effect of an Interface on Transient Temperature Distribution in Composite Aircraft Joints" N.A.C.A TN - 3824 Apr.1957

9. Barzelay, M.E., Tong, K.N. and Holloway, G.F. "Effect of Pressure on

Thermal Conductance of Contact Joints" N.A.C.A. TN - 3295 (1955)

10. Barzelay, M.E., Tong, K.N. and Holloway, G.F. "Thermal Conductance of Contacts in Aircraft Joints" N.A.C.A. TN - 3167 (1954)

11. Barzelay, M.E., and Holloway, G.F. "Effect of an Interface on Transient Temperature Distribution in Composite Aircraft Joints" N.A.C.A. TN - 3824 Apr. 1957.

12. Barzelay, M.E. and Holloway, G.F. "Interface Conductances of Twenty-seven Rivetted Aircraft Joints" N.A.C.A. TN - 3991 July 1957.

13. Beck, J.V. "Transient Sensitivity Coefficients for Thermal Contact Conductance" Int. J. Heat Mass Transfer (1967), 10, (11), 1615-1617.

14. Beck, J.V. "Determination of Optimum Transient ~~Experiemtns~~ Experiments for Thermal Contact Conductance" Int. J. Heat and Mass Transfer 1969, 12, 621-633.

15. Beck, J.V. "Analytical Determination of Optimum Transient Experiments for Measurement of Thermal Properties". Proceedings of Third International Heat Transfer Conference, 1966 Vol. IV, pp74-80, American Inst. Chemical Engineers.

16. Bedale, P.W. and Graham, R. "Experimental Work on Exhaust Valve Life at Thornton Research Centre." Proc. I. Mech.E. Auto. Div. 1955-56, 113-123.

17. Berman, R. "Thermal Contacts at Low Temperature" Journal of Applied Physics, 1956, 27, 318.

18. Berman, R. and Mate, C.F. "Thermal Contact at Low Temperature" Nature Dec. 1958, 182, 1661-1663.

19. Bertodo, R. and Sivakumaran, S. "An Assessment of Diesel Engine Poppet Valves" Proc. I. Mech. E. 1973 Vol.187 Paper No. 2/73.

20. Bloom, M.F. "A Review of the Parameters Influencing Thermal Contact Conductance Between Metal Interfaces" Douglas Aircraft Report SM - 42082 9 August 1962.

21. Bloom, M.F. "Thermal Conductance in a Vacuum Environment" Douglas Aircraft Report No. SM 47700 Dec. 1964. N.A.S.A.

22. Blum, H.A. and Moore, C.J.Jr. "Transient Phenomena in Heat Transfer Across Surfaces in Contact" A.S.M.E. Paper No. 65 - HT - 59.

23. Bowden F.P. and Tabor, D. "Friction and Lubrication of Solids" Clarendon Press 1954.

24. Bramley, A.N. "A Discussion of Tooling Problems in High Energy Rate Forming" Int. J.Mach.Tool Des. Dec. 1967,7, 351-366.

25. Cetinkale, T.N. and Fishenden, M. "Thermal Conductance of Metallic Surfaces in Contact" General Discussion on Heat Transfer Proceedings of Inst. Mech. Eng. and A.S.M.E. 1951 pp.271-5.

26. Clausing, A.M. "Heat Transfer at the Interface of Dissimilar Metals - the Influence of Thermal Strain." Int. J. Heat Mass Transfer 1966, 9, 791-801.

27. Clausing, A.M. and Chao, B.T. "Thermal Contact Resistance in a Vacuum Environment" Trans. A.S.M.E. J. Heat Transfer 1865, 87(2), 243-251.

28. Cooper, M.G., Mikic, B.B., and Yovanovitch, M.M. "Thermal Contact Conductance" Int. J. Heat Mass Transfer. 1969, 12, 279-300.

29. Cowley, W.E., Robinson, P.J. and Flack, J. "Internal Combustion Engine Poppet Valves: A Study of Mechanical and Metallurgical Requirements" Proc. I.Mech.Eng. Auto Div. 1964-65, 179(2A),145-170.

30. Dennis, J.K. and Fuggle, J.J. "Surface Damage Resulting from a Talysurf Stylus" Trans. Inst. Metal Finishing 1969, 47, pp.177-178.

31. Dyehouse, J.R. "A Mathematical Model to Calculate the Temperature Distribution in Forging Dies" MSc Thesis Department of Metallurgy, University of Aston in Birmingham 1971.

32. Demidov, L.D. "Untersuchung der Bedingungen des Warmeübergangs vom Rohling auf das Gesenk" German translation of paper from Kuznečno-stampovočnoe proizvodsto 1966, 8(9), 14-16, National Lending Library Photocopy No. BU 40336.

33. Eckert, E.R.G., and Drake, R.M. "Heat and Mass Transfer" p.106/7 Ex.4 - 7 McGraw Hill, New York 1959.

34. Eckert, E.R.G. and Drake, R.M. Ibid p.102.

35. Fenech, H., Henry, J.J. and Rohsenow, W.M. "Thermal Contact Resistance" Chapter 13 of Developments in Heat Transfer. Edward Arnold (Publishers) Ltd. 1964.

36. Fenech, H. and Rohsenow, W.M. "Prediction of Thermal Conductance of Metallic Surfaces in Contact" Trans. A.S.M.E. Journal of Heat Transfer Vol. 85 No.1 pp 15-24, Feb. 1963.

37. Fenech, J.J. and Rohsenow, W.M. "Thermal Conductance of Metallic Surfaces in Contact" U.S.A.E.C. Report No.NYO - 2136 May 1959.

38. Fenech, H. and Henry, J.J. "An Analysis of Thermal Contact Resistance" Transactions of the American Nuclear Energy Society, Nov. 1962, 5(2), 476-477.

39. Fenech, H. and Rohsenow, W. "The Use of Analogue Computers for Determining Surface Parameters Required for Production of Thermal Contact Conductance" Trans. A.S.M.E. Journal of Heat Transfer Nov. 1964.

40. Fidelle,T.P. and Kirk, R.S. "A Study of Unidirectional versus Triderectional Heat Flux Models and the Effect of Particle Size on Heat Conduction in Composite Solids. A.I.Ch.E. Jl. 1971, 17( ), 427.

41. Fletcher, L.S. and Gyorog, D.A. "Heat Transfer Between Surfaces in Contact: An Analytical and Experimental Study of Thermal Contact Resistance of Metallic Interfaces, N.A.S.A.-CR - 114373 ME-TR-033-4, Dept. of Mechanical Engineering, Arizona State University, Tempe, Arizona 1971

42. Fried, E. and Costello, F.A. "Interface Thermal Contact Resistance Problem in Space Vehicles" ARS J 1962, 32(2), 237.

43. Graff, W. "Thermal Conductance Across Metallic Joints" Machine Design (Sept. 1960), 166.

44. Greenwood, J.A. and Tripp, J.H. "The Contact of Two Nominally Flat Rough Surfaces" Proc. I.Mech.E. (1970-71), 185, Paper 48/71, pp.625-633.

45. Greenwood, J.A. "Constriction Resistance and the Real Area of Contact" Br.J.Appl.Physics (1966), 17, 1621-1632.

46. Gröber, Erk and Grigull. "Fundamentals of Heat Transfer,Third Edition. pp133-136 and Eq. 6.14. McGraw-Hill 1961.

47. Heasley, J.H. "Transient Heat Flow between Contact Solids" Int. J. Heat and Mass Transfer 1965, (8), 147-154.

48. Henry, J.J. "Thermal Conductance of Metallic Contacts" U.S.A.E.C. Report No. NYO-9459 Reb. 1963.

49. Henry, J.J. and Fenech, H. "The Use of Analogue Computers for Determining Surface Parameters Required for Prediction of Thermal Contact Conductance" A.S.M.E. Paper 63-WA-104 see also Trans. A.S.M.E. Journal of Heat Transfer, Nov. 1964, 86, series C, No. 4, pp543-552.

50. Hertz, H. "Study of the Contact of Elastic Solid Bodies" Journal für die Reine und Angewandte Mathematik" (1882),Vol.29 pp.156-171.

51. Holm, R. Electrical Contacts Handbook 3rd Edition Publisher: Springer Verlag, Berlin 1958.

52. Holm, R. "Thermal Conduction through Nominally Flat Metallic Contacts in Vacuum Environment" Stackpole Carbon Company Report 1965.

53. Howard J.R. and Sutton, A.E. "An Analogue Study of Heat Transfer Through Periodically Contacting Surfaces" Int. J. Heat Mass Transfer 1970, 13(1), 173-183.

54. Hsieh, C.K. and Davis, F.E. "Bibliography on Thermal Contact Conductance" Purdue University Thermophysical Properties Research Centre, A.F.M.L.-TR-69-24,1969.

55. Jagannathan, P.S. and Tien, C.L. "Spacer Effects on Lateral Heat Transfer in Multilayer Insulation" J.Spacercraft and Rockets Vol.8 1971, p416.

56. Kellow, M.A., Bramley, A.N. and Bannister, F.K. "The Measurement of Temperatures in Forging Dies" Int. J.Machine Tool Design and Research 1969,9, 239-260.

57. Klafs, U. Doctoral Dissertation Tech. Univ. of Hanover 1969.

58. Laming, L.C. "Thermal Conductance of Machined Metal Contacts" Proceedings of International Heat Transfer Conference, 1961-2,pp65-76.

59. Laubitz, M.J. "Measurement of Thermal Conductivity of Solids at High Temperature by Using Steady State Linear and Quasi-Linear Heat Flow" Chapter 3,p123-4 in "Thermal Conductivity,"Vol.1 Edited by R P Tye, Published by Academic Press Inc. New York, 1969.

60. Lindholm, U.S., Baker, E.J. and Kirkpatrick, R.C.. "Transient Heat Transfer at High Thermal Flux" Trans.A.S.M.E. Journal of Heat Transfer 1965, 87c, 49-52.

61. McMillan, R. Jr. "Thermal Contact Resistance with Non-uniform Interface Pressures" Masachussets Inst. of Technology, 1970, Report No.DSR 72105-70, NASA-CR-115796.

62. McNary, R.O. "The Axial Contact of Finite Elastic Cylinders with Application to Thermal Contact Resistance" Inst. J. Heat Mass Transfer, 14, 1485 (1971)

63. Mikic, B and Carnasciali "The Effect of Thermal Conductivity of Plating Material on Thermal Contact Resistance" Trans. A.S.M.E. Journal of Heat Transfer 1970, 92 (3), 475-482.

64. Mikic, B. "Thermal Constriction Resistance Due to Non-uniform Surface Conditions; Contact Resistance at Non-uniform Interface Pressure" Int. J. Heat and Mass Transfer 1970, 13, 1497-1500.

65. Mikic, B.B. and Flangas, S. "Thermal Contact Resistance in a Vacuum Under Conditions of Non-uniform Interface Pressure" M.I.T. Heat Transfer Laboratory Memorandum 1967.

66. Minges, M.L. "Thermal Contact Resistance" U.S.A.F. Report A.F.M.L.-TR-65-375 1966

67. Molgaard, J. and Smeltzer, J.J. "Thermal Contact Resistance at Gold Foil Surfaces" Int. J. Heat and Mass Transfer 1970, 13 ( ),1153-1161.

68. Mogford, R.D. and Ball, F.A. "Exhaust Valve Life: Some Metallurgical and Mechanical Considerations" Proc. I. Mech.E. Auto Div. 1955/6, pp147-153.

69. Moore, C.J.Jr., Atkins, H. and Blum, H.A. "Subject Classification Bibliography for Thermal Contact Resistance Studies" A.S.M.E. Paper No. 68-WA/HT-18 1968.

70. Moore, C.J.Jr. (Southern Methodist University Research Thermal and Fluid Science Centre Report No.67-2) "Heat Transfer Across Surfaces in Contact: Studies of Transients in One-Dimensional Composite Systems" U S Department of Commerce/National Bureau of Standards/ Institute for Applied Technology, March 1967, Ref. No. N67 30861.

71. Novikov, V.S. "The Thermal Contact Resistance as a Function of Compression of Rough Surfaces" Heat Transfer Soviety Research 1970, 2(6), 160.

72. Novikov, V.S. "Phonon Transfer of Heat Through a Real Contact of Solids" Thermophysics and Heat Engineering No.18 Kiev (1970).

73. Nunziato, J.W. "On Heat Conduction in Materials with Memory" Q.Appl.Math. 1971 29, 187.

74. O'Callaghan, P.W. and Probert, S.D. "The Effects of Transverse Heat Losses on Longitudinal Heat Transfer Observations" Measurement and Control 1971, 4, T25-T34.

75. Popov, V.M. "Determination of Thermal Contact Resistance of Plane-Rough Surfaces with Roghnesses Deforming in Different Manners" Heat Transfer Soviet Research 1970, 2(5), 26.

76. Popov, V.M. and Yanin, L.F. "Heat Transfer During Contact of Machined Metal Surfaces with Waviness" Heat Transfer, Soviety Research 1972, 4(2), 162.

77. Roess, L.C. "Theory of Spreading Conductance" Appendix to Weills and Ryder - see ref. in Thomas & Probert Chemical & Process Engineering Nov. 1966.

78. Rogers, G.F.C. "Heat Transfer at the Interface of Dissimilar Metals" Int. J. Heat Mass Transfer 1961, 2 150-154.

79. Rominger, M.C. "Contact Resistance to Heat Transfer" Ph.D. Thesis, Ohio State University 1971

80. Sanokawa, K. "Heat Transfer Between Metallic Surfaces in Contact" (1st Report) Bull. J.S.M.E. (1968), 11 (44), 253-263.

81. Sanokawa, K. "Heat Transfer Between Metallic Surfaces in Contact (2nd Report)" Bull J.S.M.E. (1968), 11 (44), 264-275.

82. Ibid 276-286

83. Ibid 287-293

84. Schauer, D.A. and Giedt, W.H. "Contact Conductance Measurements During Transient Heating" Proc. of Third International Heat Transfer Conference 1966, Vol, IV. pp100-108 Am. Inst. Chem . Engs., New York 1966.

85. Shlykov, Yu.P, Ganin, E.A. and Demkin, N.B. "Investigation of Contact Heat Exchange" Tepleonergetika June 1960. Vol. 7 No. 6 pp.72-76 English Translation U.K. Atomic Energy Authority Translation TRG-IS-280.

86. Shlykov, Yu.P., and Gannin, E.A. "Thermal Resistance of Metallic Contacts", Int. J. Heat and Mass Transfer, 1964, 7(8),921-929.

87. Stotter, A., Wooley, K.S. and Ip, E.S. "Exhaust Valve Temperature - A Theoretical and Experimental Investigation" International Automotive Engineering Conference, Detroit, Michigan 11-15 January 1965. S.A.E. Paper No.969A 1965.

88. Taitel, Y. "On Parabolic Hyperbolic and Discrete Formulation of the Heat Conduction Equation" Int. J. Heat and Mass Transfer 1973 15, 369.

89. Tharmalingham, R. "A Transient Method of Measuring Thermal Contact Conductance Between Metal-Plastic Surfaces" M.Phil Thesis 1972, University of Aston in Birmingham.

90. Thomas, T.R. and Probert, S.D. "Correslations for Thermal Contact Conductance in Vacuo" Trans. A.S.M.E. Journal of Heat Transfer, Aug. 1972, 94(3), Series C, 276-280.

91. Thomas, T.R. and Probert, S.D. "Thermal Contact Resistance - The Directional Effect and Other Problems" Inst. J. Heat Mass Transfer 1970, 13( ), 789-807.

92. Thomas, T.R. and Probert, S.D. "Thermal Contact of Solids" Chemical and Process Engineering Vol. 47 No.11, Nov. 1966 pp 57-60.

93. Thomas, T.R. and Probert, S.D. "Establishment of Contact Parameters From Surface Profiles" J.Phys. D:Appl.Phys. (1970),3, 277-289.

94. Timoshenko, S.P. and Goodier, J.N. "Theory of Elasticity" 3rd Edition McGraw- Hill 1970 pp409-421 Also see Herz. 50

95. Tsukizoe, T and Hisakado, T. "On the Mechanism of Heat Transfer between Metal Surfaces in Contact (2nd Report Thermal Contact Resistance between Metal Surfaces in Vacuum)" Trans. Japan Soc. Mech. Engrs. 1971, 37(299), 1369.

96. Ibid. 1st Report, 1361.

97. Tsukizoe, T and Hisakado, T. Trans. A.S.M.E. (1968), 87D. 666-74. and Trans. A.S.M.E. (1968), 90F, 81-88.

98. Ulmer, G. "Thermal Problems of Dies" International Pressure Die Casting Conference, Paris. 2-6 June 1969. Printed by Copedith,Paris.

99. Vidoni, Carlotta M. "Thermal Resistance of Contacting Surfaces Heat Transfer Bibliography U.S.A.E.C. UCRL-14264 1964.

100. Velissaropoulos, P.D. "Apparatus for Measuring Contact Conductance" M.S. Thesis, Massachussets Institute of Technology, Aug. 1963.

101. Veziroglu, T.N. and Chandra, S. "Directional Effect in Thermal Conductance" Int. Conference on Heat Transfer 1970. Paper Cu3.5 Elsevier 1970.

102. Weills, N.D. and Ryder, E.A. "Thermal Resistance Measurements of Joints Formed Between Stationary Metal Surfaces" Trans. A.S.M.E. 1949, 71, pp 259-267.

103. Wheeler, R.G. "Thermal Contact Condutance" U.S.A.E.C. Report No. HW 53598 Nov. 1957.

104. Wheeler, R.G. "Thermal Contact Condutance of Fuel Element Materials" U.S.A.E.C. Report No. HW-60343 April 1959.

105. Whitehouse, D.J. and Archard, J.F. "The Properties of Random Surfaces of Significance in Their Contact" Proc. Roy. Soc. London (1970) pp.97-121.

106. Williams, A. "Heat Transfer Through Metal to Metal Joints" Proceedings of Third International Heat Transfer Conference 1966 Vol.4, p109.

107. Williams, A. "Heat Transfer at the Interface of Dissimilar Metals" Inst. J. Heat Mass Transfer 1961, 3, 159.

108. Wong, H.Y. "The Thermal Conductance of Metallic Contact - A Survey" Presented at the International Conference on Thermal Conductivity at the National Physical Laboratory, London. July 1964.

109. Wong, H.Y. Private Communication 17 October 1966.

110. Wong, H.Y. "Thermal Conductance of Metallic Contacts" University of Glasgow Ph.D Thesis No.3011, 1968.

111. Wong, H.Y. "A Survey of the Thermal Conductance of Metallic ~~Constants~~ Contacts" Ministry of Technology Aeronautical Research Council Current Papers CPNo.973 1968.

112. Yamauchi, K. "Graphical Solution of Contact Heat Conduction" Transactions of Japanese Society of Mechanical Engineers Vol. 29 No. 201 pp 1001 - 1004 1963.

ADDITIONAL REFERENCES

113. Putnaerglis, R.A. "A Review of Literature on Heat Transfer Between Metals in Contact" Report No.R34 Department of Mechanical Engineering, McGill University, 1953.

114. Moon, J.S. and Keeler, R.N. "A Theortetical Consideration of Directional Effects in Heat Transfer at the Interface of Dissimlar Metals" Int. J. Heat Mass Transfer 1962, 5, 967-971.

115. Barber, J.R. Letter Concerning the Paper "Thermal Contact Resistance - The Directional Effect and Other Problems" Int. J. Heat Mass Transfer 1971, 14, 331-332.

116. Fried, E. "Thermal Joint Conductance in a Vacuum" A.S.M.E. Paper No. 63 - AHGT-18 March 1963.

117. Barber, A.D., Weiner, J.H. and Boley, B.A. "An Analysis of the Effect of Thermal Contact Conductance in a Sheet Stringer Structure" J.Aero Sci. 1957, 24(3), 232-234.

118. Pohle, F.V., Lardner, T.J. and French, F.W. "Temperature Distribution and Thermal Stresses in Structure with Contact Resistance" Polytechnic Institute of Brooklyn Report No. PIBAL-557, May 1960.

119. Howard, J.R. and Sutton, A.E. "The Effect of Thermal Contact Resistance on Heat Transfer Between Periodically Contacting Surfaces" University of Aston in Birmingham, Department of Mechanical Engineering, Technical Note Mech/37, March 1973.

120. Carslaw, H.S. "Fourier series and integrals" Macmillan 1921. p220-224.

121. Kreider, Kuller, Ostberg and Perkins "An Introduction to Linear Analysis" Addison-Wesley, 1966, p345, ex.1.

122. Kennard, E.H. Kinetic Theory of Gases" McGraw-Hill 1938.

123. Howard, J.R. and Sutton, A.E. "The Effect of Thermal Contact Resistance on Heat Transfer Between Periodically Contacting Surfaces" Trans. A.S.M.E. Journal of Heat Transfer, Aug. 1973, 411-2.

124. Reed, J.R. and Mullineux, G. "Quasi-steady State Solution of Periodically Varying Phenomena" Int. J. Heat Mass Transfer 1973, 16(11), 2007-2012.

125. Sutton A.E.

Inversion of $\sum_{n=-\infty}^{\infty} \left[\frac{C_{m,n}(\ell)}{(s-2\pi\sqrt{\frac{n}{\zeta}})} \cdot \frac{\text{sh}\alpha x\sqrt{s}}{\alpha\sqrt{s}\ \text{ch}\ \alpha\ell\sqrt{s}} \right]$

Department of Mechanical Engineering, University of Aston in Birmingham, Technical Note ref. Mech/December 73.

126. Perkins, K.R. and McEligot, D.M. "Roughness of Heat Transfer Surfaces" Int. J. Heat Mass Transfer 1973, 16(3) 679-681.

127. Grace, A. and Hall, J.A. "A Bath for Use in Graduation and Testing of Thermometers" J.Sci. Instruments 1943, 20, 60-63,

128. Ede, A.J. "An Introduction to Heat Transfer" Pergamon Press (1967) p.266 Table 12.7

129. Lewis, D.V. and Perkins, H.C. "Heat Transfer at the Interface of Stainless Steel and Aluminium - the Influence of Surface Conditions on Directional Effect" Int. J. Heat Mass Transfer 1968, 11, 1371-1383.

130. Mayhew, Y.R. and Rogers, G.F.C. "Thermodynamic and Transfer Properties of Fluids in S.I.Units" Blackwells 2nd Editions Basil Blackwell, Oxford.

131. Ede, A.J. "An Introduction to Heat Transfer" Pergamon Press (1967) p.126

132. McAdams, W.H. Heat Transmission 3rd Edition McGraw-Hill p.181.

133. McAdams, W.H. "Heat Transmission 3rd Edition McGraw-Hill pp242,243.

134. Carslaw, H.S. and Jaeger, J.C. "Conduction of Heat in Solids, Clarendon Press, Oxford. Second Edition p.61.

135. O'Callaghan, P.W. and Probert, S.D. "Thermal resistance and directional index of pressed contacts between smooth, non-wavy surfaces" Journal Mechanical Engineering Science Feb, 1974, 16,(1), 41-55

136. O'Callaghan, P.W. and Probert S.D. "An improved thermal contact resistance rig" Measurement and Control 1972, 5,(8),311-315.

H.W. Turner and C. Thomas, 'Ten ways not to use make and break contacts', Engineering, 813 - 815, Oct. 1974

D.J. McKinzie, 'Experimental confirmation of cyclic thermal joint conductance', 5th Thermophysics Conference AIAA, June 29th 1970.

S.A. Anderson et al, 'Techniques for determining the transient heat flux at a solid interface using measured transient interfacial temperature', Trans ASME, 492 - 497, Nov. 1973

Several references by A.H. Uppal and S.D. Probert, published in Wear from 1970 to 1973.

APPENDIX 1

Effect of position of contact interface

Consider the system comprising two bars of identical material whose adjacent ends make periodic contact as shown in Fig. 1-1. The bars are of unequal length and the quasi-steady state is reached. The temperature in the immediate region of the contact interface will vary with time, but at some distance $\ell = 1.6\sqrt{\frac{\pi\alpha}{f}}$ (c.f equation (47)) from the contact interface, the temperature fluctuation due to the periodic interruption of heat flow, will be negligible.

Fig. 1-1 overleaf shows the time-average temperature distribution in such a system and the envelope formed by the cyclic maxima and minima of temperatures in the region at and near the contact interface (The envelope is the boundary of the shaded areas.) Since the bars are of identical material, the two shaded areas in Fig. 1-1 are of the same shape and size. The thermal resistance due to periodic interruption of the heat flow, may be represented by a length of bar, $2\ell_i$, as shown in Fig. 1-1. If the overall length of the system is maintained at 2ℓ, but the position of the contact interface is varied, then provided that it is not positioned so close to ends A or B that the temperature or temperature gradient at A or B fluctuates, the average heat flow through the system will not change. Thus within these limits the heat flow and thermal resistance due to periodic interruption is independent of the position of the contact interface.

If now the position of the contact interface is moved until the length of one bar, say the cooler, is zero and temperatures T_A and T_B, frequency f and ratio contact time:periodic time are

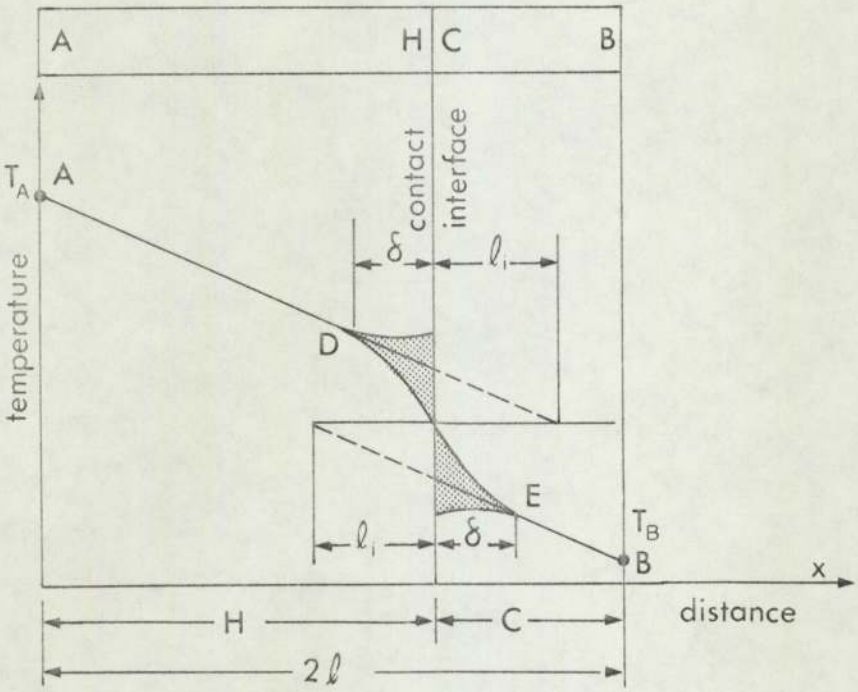

Fig. 1-1 Temperature distribution in bars making periodic contact

maintained constant, then the end of the heated bar at $x = 2\ell$ will be making periodic contact with a heat sink at temperature T_B. The total thermal resistance of the system (expressed as equivalent lengths of bar) would then be $2\ell + \ell_i$ (instead of $2(\ell + \ell_i)$ in the case when the length of each bar exceeds $1.6\sqrt{\frac{\pi\alpha}{f}}$) since boundary conditions at $x = 2\ell$ are the same as those at $x = \ell$ when $\ell > 1.6\sqrt{\frac{\pi\alpha}{f}}$.

If one bar is of length ℓ where $0 < \ell < 1.6\sqrt{\frac{\pi\alpha}{f}}$ and the length of the other greater than $1.6\sqrt{\frac{\pi\alpha}{f}}$, the thermal resistance due to periodic interruption of the heat flow will be represented by a length $\ell_i + p\ell_i$ with $0 < p < \ell$.

Derivation of Equation (53)

In the quasi-steady state the temperature-time relation at the contact interface would be of the form shown in Fig. 2-1 overleaf.

As the frequency is reduced, the highest temperature reached during the non-contact period will approach the fixed temperature T_A. Further reduction in frequency will lead to the contact interface temperature during the non-contact period tending to T_A for a large proportion of this time as shown in Fig. 2-2.

The time-average temperature distance relation is shown in Fig. 2-3.

At $x = \ell$, the mean temperature is given by:

$$T_{mean} = T_A \left(\frac{\ell_i}{\ell + \ell_i}\right) \qquad (2/1)$$

From Fig. 2-2 as $1/f \longrightarrow \infty$

$$T_{mean} = T_A \left\{ \frac{\left(\frac{1}{f} - \tau_c\right)}{\frac{1}{f}} \right\} = T_A \left[1 - (f\tau_c)\right] \qquad (2/2)$$

Eliminating ~~Elementing~~ T_{mean} and T_A

$$\frac{\ell_i}{(\ell + \ell_i)\left[1 - (f\tau_c)\right]} = 1$$

$$\text{and} \quad \ell_i = \left[\frac{1 - (f\tau_c)}{(f\tau_c)}\right] \ell \qquad (2/3)$$

and hence

$$\lim_{\left(\frac{f\ell^2}{\alpha}\right) \to 0} \left(\frac{f\ell_i^2}{\alpha}\right) = \left(\frac{f\ell^2}{\alpha}\right) \left[\frac{1 - (f\tau_c)}{(f\tau_c)}\right]^2 \qquad (2/4)$$

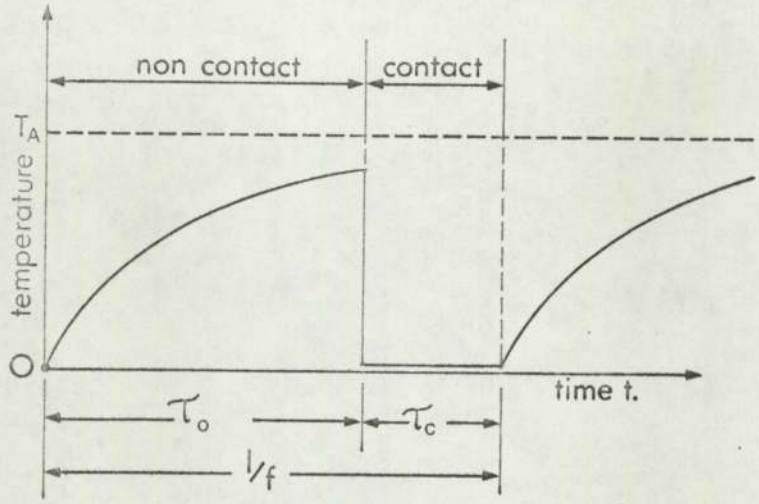

Fig. 2-1 Temperature-time variation at contact interface

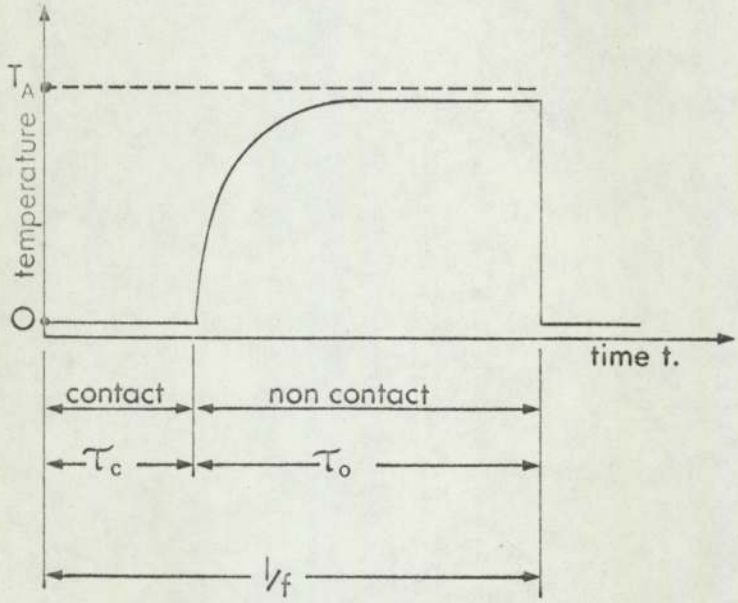

Fig. 2-2 Temperature-time variation at contact interface at low frequency

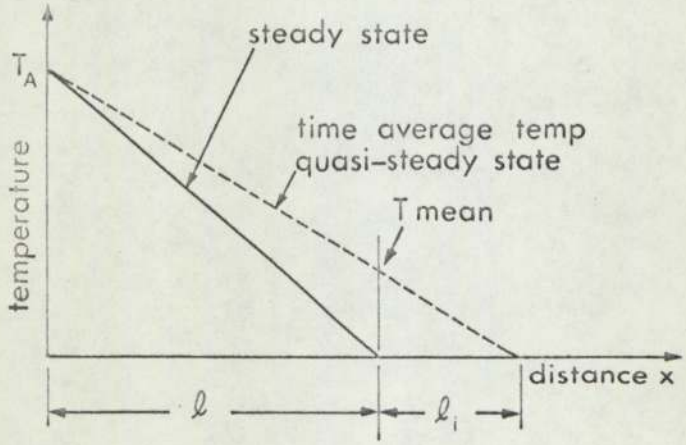

Fig. 2-3 Steady and quasi-steady state temperature distribution

APPENDIX 3

Derivation of finite-difference equations

Fig. 3-1 shows a typical instantaneous temperature distribution within a solid bar, of length ℓ . The heat flow is parallel to the longitudinal axis of the bar and the temperature T_n is known at a number of nodal points which are unevenly distributed along the bar.

If the temperature at x = 0 is fixed at some value T_A, then the temperature, T_n, at any node n, may be expressed as a dimensionless quantity, Θ_n, where

$$\Theta_n = \frac{T_n}{T_A} \qquad (3/1)$$

The distance x_n may be expressed in dimensionless form, X_n where

$$X_n = \frac{x_n}{\ell} \qquad (3/2)$$

The finite-difference from of the heat-diffusion equation in which temperature and distance are expressed as dimensionless parameters will be

$$\frac{\partial\Theta}{\partial t} = \frac{\alpha}{\ell^2}\left[\frac{\left(\frac{\Theta_{n+1} - \Theta_n}{X_{n+1} - X_n}\right) - \left(\frac{\Theta_n - \Theta_{n-1}}{X_n - X_{n-1}}\right)}{\frac{1}{2}(X_{n+1} - X_{n-1})}\right] \qquad (3/3)$$

For the analogue computerstudy described in this thesis, a value of $0.3125 \times 10^{-2}\ s^{-1}$ was chosen for (α/ℓ^2); this represents a value for a bar 40 mm long of a heat-resisting steel. The finite mesh employed in the analogue computer study is shown in Fig. 10 and Fig. 3-2. Hence at the node n = 1

$$\frac{\partial\Theta_1}{\partial t} = 0.3125 \times 10^{-2}\ s^{-1}\left[\frac{\left(\frac{\Theta_2 - \Theta_1}{0.08}\right) - \left(\frac{\Theta_1 - \Theta_0}{0.8}\right)}{\frac{1}{2}(0.88 - 0)}\right]$$

$$= 0.89 \times 10^{-2}\ (10\ \Theta_2 - 11\ \Theta_1 + \Theta_0)\quad s^{-1} \qquad (3/4)$$

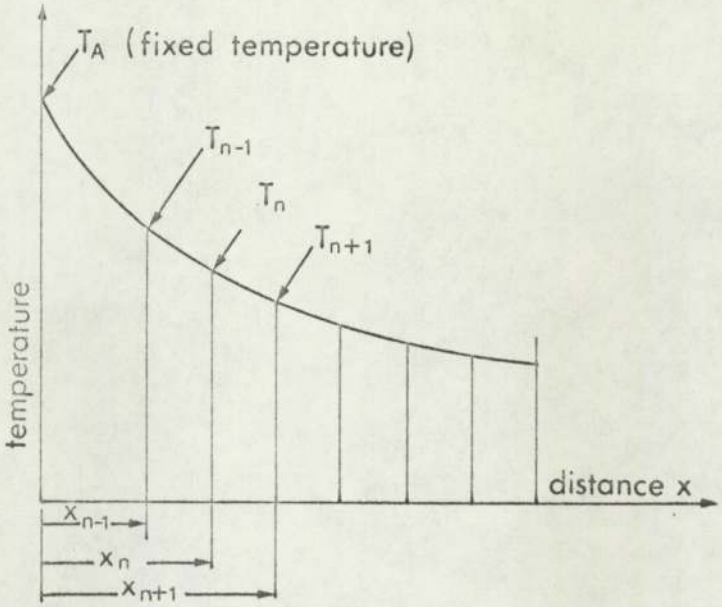

Fig. 3-1 Temperature distribution at any time t

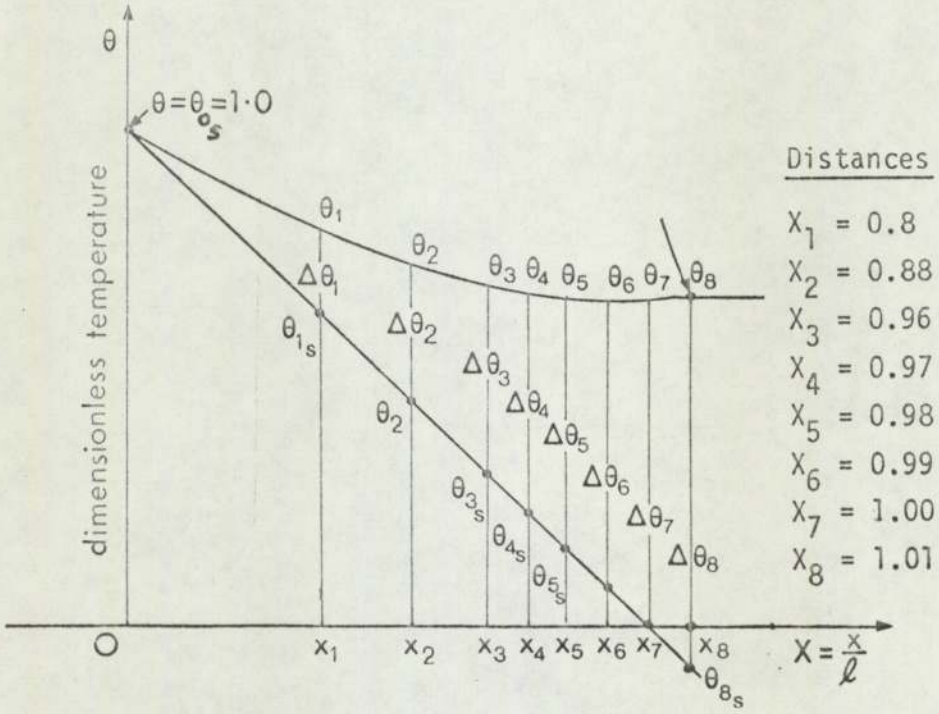

Fig. 3-2 Dimensionless temperature distribution

Consider the bar to be the hotter bar of the system described in section 4.2 and Figs. 7 and 8. To reduce the time taken for the system to reach the quasi-steady state, the initial condition had been chosen to be the steady-state, permanent contact temperature distribution.

Dimensionless temperature changes, $\Delta\Theta_n$, at each node n were measured from this datum. Thus, referring to Fig. 3-2, which shows the steady-state permanent contact dimensionless temperature distribution Θ_n, together with a typical instantaneous, dimensionless temperature distribution during the non-contact period we obtain

$$\left.\begin{aligned} \Theta_1 &= \Theta_{1_s} + \Delta\Theta_1 \\ \Theta_2 &= \Theta_{2_s} + \Delta\Theta_2 \\ &\text{etc.} \\ \Theta_8 &= \Theta_{8_s} + \Delta\Theta_8 \end{aligned}\right] \qquad (3/5)$$

Substituting equation (3/5) into equation (3/4)

$$\frac{\partial\Theta_{1_s}}{\partial t} = \frac{\partial(\Delta\Theta_1)}{\partial t} = 0.89 \times 10^{-2} \left[10(\Theta_{2_s} + \Theta_2) - 11(\Theta_{1_s} + \Theta_1) + (\Theta_{o_s} + \Theta_o) \right] \; s^{-1} \qquad (3/6)$$

$\frac{\partial\Theta_{1_s}}{\partial t}$ is zero, since the Θ_{1_s} is the dimensionless steady-state temperature and from the table of distances in Figs. 3-2 and 10 it will be seen that since $\Theta_{o_s} = 1.0$,

$$\left.\begin{aligned} \Theta_{1_s} &= 0.2 \\ \Theta_{2_s} &= 0.12 \\ &\text{etc.} \end{aligned}\right] \qquad (3/7)$$

Inserting the values from equation (3/7) into equation (3/6) and writing D for $\frac{\partial}{\partial t}$, equation (3/6) becomes:-

$$D(\Delta\Theta_1) = (0.089\Delta\Theta_2 - 0.098\Delta\Theta_1 + 0.0089\Delta\Theta_0) \quad s^{-1} \qquad (3/8)$$

The finite-difference equations at the other nodes are similarly derived and are

$$D(\Delta\Theta_2) = (0.488\Delta\Theta_3 - 0.976\Delta\Theta_2 + 0.488\Delta\Theta_1) \quad s^{-1} \qquad (3/9)$$

$$D(\Delta\Theta_3) = (6.95\ \Delta\Theta_4 - 7.82\ \Delta\Theta_3 + 0.87\ \Delta\Theta_2) \quad s^{-1} \qquad (3/10)$$

$$D(\Delta\Theta_4) = (31.25\ \Delta\Theta_5 - 62.5\ \Delta\Theta_4 + 31.25\ \Delta\Theta_3) \quad s^{-1} \qquad (3/11)$$

$$D(\Delta\Theta_5) = (31.25\ \Delta\Theta_6 - 62.5\ \Delta\Theta_5 + 31.25\ \Delta\Theta_4) \quad s^{-1} \qquad (3/12)$$

$$D(\Delta\Theta_6) = (31.25\ \Delta\Theta_7 - 62.5\ \Delta\Theta_6 + 31.25\ \Delta\Theta_5) \quad s^{-1} \qquad (3/13)$$

Boundary conditions

(c.f.) section 4.2.4)

1. Since the temperature at x = 0 (Fig.3-2 and Fig.10b) is fixed, $\Delta\Theta_0 = 0$ and equation (3/8) becomes

$$D(\Delta\Theta_1) = (0.089\ \Delta\Theta_2 - 0.098\ \Delta\Theta_1) \quad s^{-1} \qquad (3/14)$$

2. (i) When the bars are in contact

$$\Delta\Theta_7 = 0 \qquad (3/15)$$

(ii) When the bars are not in contact, the condition

$\frac{\Delta\Theta_7}{\Delta X} = 0$ has to be simulated.

Considering Fig. 3-2 again, let the instantaneous dimensionless temperature distribution extend beyond the X = 1.0 point to a fictitions point 8; let the distance $(X_8 - X_7) = (X_7 - X_6) \equiv \Delta X$. The finite-difference approximation to the heat-diffusion equation at the end of the bar, X_7, is

$$D(\Delta\Theta_7) = \frac{\alpha}{\ell^2(\Delta X)^2} \left[\Delta\Theta_8 - 2\Delta\Theta_7 + \Delta\Theta_6 \right] \quad s^{-1} \qquad (3/16)$$

For $\frac{\partial\Theta_7}{\partial X}$ to be zero

$$\Theta_8 = \Theta_6 \qquad (3/17)$$

From Fig 3-2 and the table of distances shown thereon it will be seen that for equation (3/17) to hold

$$\Delta\Theta_8 = \Delta\Theta_6 + 0.02 \qquad (3/18)$$

Substituting (3/18) into (3/16) and remembering that the chosen value for $(\alpha/\ell^2) = \cancel{31.25}\ 0.3125 \times 10^{-2}\ s^{-1}$ and that $\Delta X = 0.01$, equation (3/16) then becomes

$$D(\Delta\Theta_7) = (0.625 - 62.5\Delta\Theta_7 + 62.5\Delta\Theta_6) \quad s^{-1} \qquad (3/19)$$

Equation (3/19) is ~~than~~ an expression for boundary condition 2(ii) in finite-difference form.

APPENDIX 4

Derivation of equations for numerical matrix inversion method

Solution of the heat-diffusion equation

$$\frac{\partial T}{\partial t} = \alpha \frac{\partial^2 T}{\partial x^2} \qquad (4/1)$$

is required subject to the boundary conditions.

(i) at $x = 0$, $T(0,\ell) = T_A$ = constant

(ii) at $x = \ell$,

(a) $\frac{\partial T}{\partial x} = 0$ for $n(\tau_1 + \tau_2) < t < n(\tau_1 + \tau_2) + \tau_1$

(b) $T(\ell,t) = 0$ for $n(\tau_1 + \tau_2) + \tau_2 < t < (n+1)(\tau_1 + \tau_2)$

$n = 0,1,2 \ldots\ldots$

Condition (iia) corresponds to the case when the contact end of the bar is separated from the other bar and no heat flows. τ_1 is the time over which the contact surfaces are separated. Condition (iib) corresponds to the case when the ends of the bars are in contact. τ_2 is the time over which contact occurs. These conditions occur consecutively in a continuous cycle.

Only the quasi-steady state solution (i.e. solution as $t \to \infty$) is required thus the initial condition can be ignored.

The function

$$T_1(x,t) = T_A + \sum_{\substack{n=1 \\ n \text{ odd}}}^{\infty} a_n \sin\left(\frac{n\pi}{2} \frac{x}{\ell}\right) \qquad (4/2)$$

where $a_n = a_n(t)$ satisfies the boundary conditions (i) and (iia) while the function

$$T_2(x,t) = T_A\left(1-\frac{x}{\ell}\right) + \sum_{\substack{n=2 \\ n \text{ even}}}^{\infty} b_n \sin\left(\frac{n\pi}{2} \frac{x}{\ell}\right) \qquad (4/3)$$

where $b_n = b_n(t)$ satisfies the boundary conditions (i) and (iib).

We find a_n, b_n to satisfy the partial differential equation A(4/1). By substitution (4/2) into (4/1) we have

$$-\alpha a_n \left(\frac{n\pi}{2\ell}\right)^2 = \frac{da_n}{dt} \qquad n \text{ odd} > 0$$

Hence

$$a_n = A_n e^{-\left(\frac{n\pi}{2\ell}\right)^2 \alpha t} \qquad n = 1,3,5 \ldots \qquad (4/4)$$

where A_n is a constant.

Similarly

$$b_n = B_n e^{-\left(\frac{n\pi}{2\ell}\right)^2 \alpha t} \qquad n = 2,4,6 \ldots. \qquad (4/5)$$

where B_n is a constant.

For a complete solution the constants A_n, B_n have to be determined.

The time scale for the two periods may be shifted so that for equation (4/2) t = 0, is at the commencement of the period when the bars are separated. For equation (4/2), t = 0 is at the commencement of contact. For continuity,

$$T_1(x,\tau_1) = T_2(x,0) \qquad (4/6a)$$

and

$$T_1(x,0) = T_2(x,\tau_2) \qquad (4/6b)$$

Substituting equations (4/2),(4/3),(4/4) and (4/5) into (4/6a) leads to

$$T_A + \sum_{\substack{n=1 \\ n \text{ odd}}}^{\infty} A_n e^{-\left(\frac{n\pi}{2\ell}\right)^2 \alpha\tau_1} \sin\left(\frac{n\pi}{2}\frac{x}{\ell}\right)$$

$$= T_A\left(1 - \frac{x}{\ell}\right) + \sum_{\substack{n=2 \\ n \text{ even}}}^{\infty} B_n \sin\left(\frac{n\pi}{2}\frac{x}{\ell}\right) \qquad (4/7a)$$

and similarly substituting into (4/6b)

$$T_A + \sum_{\substack{n=1 \\ n \text{ odd}}}^{\infty} A_n \sin\left(\frac{n\pi}{2}\ \frac{x}{\ell}\right)$$

$$= T_A\left(1 - \frac{x}{\ell}\right) + \sum_{\substack{n=2 \\ n \text{ even}}}^{\infty} B_n e^{-\left(\frac{n\pi}{2\ell}\right)\alpha\tau_2} \sin\left(\frac{n\pi}{2}\ \frac{x}{\ell}\right) \qquad (4/7b)$$

For the next stage, the following standard integrals are required:

(a) for n, m integers

$$\int_0^{\ell} \sin\left(\frac{m\pi}{2}\ \frac{x}{\ell}\right)\sin\left(\frac{n\pi}{2}\ \frac{x}{\ell}\right)dx = (-1)^{\frac{m-n-1}{2}}\ \frac{\ell}{\pi}\left\{\frac{2n}{m^2 - n^2}\right\} \quad \text{If n even and m odd}$$

$$= (-1)^{\frac{m-n-1}{2}}\ \frac{\ell}{\pi}\left\{\frac{2m}{m^2 - n^2}\right\} \quad \text{If n odd and m even}$$

$$= 0 \quad \text{otherwise if } n \neq m$$

(b) $$\int_0^{\ell} \sin^2\left(\frac{n\pi}{2}\ \frac{x}{\ell}\right)dx = \frac{\ell}{2} \qquad \text{(i.e. m = n in case (a)}$$

(c) $$\int_0^{\ell} x \sin\left(\frac{n\pi}{2}\ \frac{x}{\ell}\right)dx = \frac{2\ell^2}{n\pi}\ (-1)^{\frac{n}{2}+1} \qquad \text{n even}$$

$$= \left(\frac{2\ell^2}{n\pi}\right)(-1)^{\frac{n-1}{2}} \qquad \text{n odd}$$

Multiplying equation (4/7a) by $\sin\left(\frac{m\pi}{2}\ \frac{x}{\ell}\right)$, where the m are even integers; then integrating with respect to x, between the limits o to ℓ, and using results (a), (b) and (c) of previous paragraph, leads to

$$\sum_{\substack{n=1 \\ n \text{ odd}}}^{\infty} A_n e^{-\left(\frac{n\pi}{2\ell}\right)^2 \alpha\tau_1} (-1)^{\frac{m-n-1}{2}} \frac{\ell}{\pi} \left\{ \frac{2m}{m^2 - n^2} \right\}$$

$$= -\frac{T_A}{\ell} \frac{2\ell^2}{m\pi} (-1)^{\frac{m}{2}+1} + B_m \frac{\ell}{2} \qquad (4/8a)$$

similarly, multiplying equation (4/7b) by $\sin\left(\frac{m\pi}{2} \frac{x}{\ell}\right)$, where the m are odd integers, integrating etc. as before leads to:

$$A_m \frac{\ell}{2} = -\frac{T_A}{\ell}\left(\frac{2\ell}{m\pi}\right)^2 (-1)^{\frac{m-1}{2}}$$

$$+ \sum_{\substack{n=2 \\ n \text{ even}}}^{\infty} B_n e^{-\left(\frac{n\pi}{2\ell}\right)^2 \alpha\tau_2} (-1)^{\frac{m-n-1}{2}} \frac{\ell}{\pi} \left\{ \frac{2n}{m^2-n^2} \right\} \qquad (4/8b)$$

Eliminating B's we obtain for m an odd integer > 0

$$(-1)^{\frac{m+1}{2}} A_m + \frac{16}{\pi^2} \sum_{\substack{K=1 \\ K \text{ odd}}}^{\infty} (-1)^{\frac{K-1}{2}} C_{m,K} A_K e^{-\left(\frac{K\pi}{2\ell}\right)^2 \alpha\tau_1} = \frac{8T_A}{\pi^2}\left\{ \frac{1}{m^2} - 2C_{m,o} \right\} \qquad (4/9)$$

where

$$C_{m,K} = \sum_{\substack{n=2 \\ n \text{ even}}}^{\infty} \left\{ \frac{n^2}{(n^2-m^2)(n^2-K^2)} \right\} e^{-\left(\frac{n\pi}{2\ell}\right)^2 \alpha\tau_2} \qquad (4/10)$$

Similarly eliminating the A's between (4/8a) and (4/8b) we have for m an even integer > 0.

$$- \frac{B_m}{m} (-1)^{\frac{m}{2}} + \frac{16}{\pi^2} \sum_{\substack{K=2 \\ K \text{ even}}}^{\infty} (-1)^{\frac{K}{2}} KB_K D_{m,K} e^{-(\frac{K\pi}{2\ell})^2 \tau_2}$$

$$= \frac{4T}{\pi} \quad \frac{8}{\pi^2} D_{m,o} + \frac{1}{m^2} \tag{4/11}$$

where

$$D_{m,K} = \sum_{\substack{n=1 \\ n \text{ odd}}}^{\infty} \left\{ \frac{e^{-(\frac{n\pi}{2\ell})^2 \alpha\tau_1}}{(n^2-K^2)(n^2-m^2)} \right\} \tag{4/12}$$

Note that $C_{m,K} = C_{K,m}$ and $D_{m,K} = D_{K,m}$. This result is useful in the computation of the C's and D's.

For computational purposes equations (4/9) and (4/11) were multiplied through by $\frac{\pi^2}{16}$ to give.

<u>For m odd</u>

$$\frac{\pi^2}{16} (-1)^{\frac{m+1}{2}} A_m + \sum_{\substack{k=1 \\ k \text{ odd}}}^{\infty} (-1)^{\frac{k-1}{2}} C_{m,k} e^{-(\frac{k\pi}{2\ell})^2 \alpha\tau_1} A_k$$

$$= \frac{T_A}{2m^2} - T_A C_{m,o} \tag{4/13}$$

<u>For m even</u>

$$- \frac{\pi^2}{16m} (-1)^{\frac{m}{2}} B_m + \sum_{\substack{k=2 \\ k \text{ even}}}^{\infty} (-1)^{\frac{k}{2}} D_{m,k} e^{-(\frac{k\pi}{2\ell})^2 \alpha\tau_2} B_k$$

$$= \frac{2T_A}{\pi} D_{m,o} + \frac{T_A}{4m^2} \tag{4/14}$$

The values of the variables chosen for computational purposes were

$T_A = 100K$

$\alpha = 5 \times 10^{-6} \ \frac{m^2}{s}$

$\ell = 0.04m$

APPENDIX 5 Effect of Truncation on Solution for Coefficients A_n and B_n in equations (4/13) and (4/14)

OUTPUT CAS 1

$\tau_1 = \tau_2 = 10$ s

VALUE OF DETERMINANT -0.31891E-01

SOLUTION VECTOR OF EQN. (4/13) TRUNCATED TO 5 TERMS

X(1)	-0.76872E 02	=	A_1
X(2)	0.10244E 02	=	A_3
X(3)	-0.43090E 01	=	A_5
X(4)	0.22184E 01	=	A_7
X(5)	-0.12969E 01	=	A_9

VALUE OF DETERMINANT -0.28482E-02

SOLUTION VECTOR OF EQN. (4/13) TRUNCATED TO 10 TERMS

X(1)	-0.76872E 02	=	A_1
X(2)	0.10244E 02	=	A_3
X(3)	-0.43090E 01	=	A_5
X(4)	0.22184E 01	=	A_7
X(5)	-0.12969E 01	=	A_9
X(6)	0.85196E 00	=	A_{11}
X(7)	-0.60492E 00	=	A_{13}
X(8)	0.45233E 00	=	A_{15}
X(9)	-0.35120E 00	=	A_{17}
X(10)	0.28064E 00	=	A_{19}

VALUE OF DETERMINANT 0.25437E-03

SOLUTION VECTOR OF EQN.(4/13) TRUNCATED TO 15 TERMS

X(1)	-0.76872E 02	=	A_1
X(2)	0.10244E 02	=	A_3
X(3)	-0.43090E 01	=	A_5
X(4)	0.22184E 01	=	A_7
X(5)	-0.12969E 01	=	A_9
X(6)	0.85196E 00	=	A_{11}
X(7)	-0.60492E 00	=	A_{13}
X(8)	0.45233E 00	=	A_{15}
X(9)	-0.35120E 00	=	A_{17}
X(10)	0.28064E 00	=	A_{19}
X(11)	-0.22943E 00	=	A_{21}
X(12)	0.19108E 00	=	A_{23}
X(13)	-0.16162E 00	=	A_{25}
X(14)	0.13848E 00	=	A_{27}
X(15)	-0.11999E 00	=	A_{29}

VALUE OF DETERMINANT 0.22718E-04

SOLUTION VECTOR OF EQN.(4/13) TRUNCATED TO 20 TERMS.

X(1)	-0.76872E 02	=	A_1
X(2)	0.10244E 02	=	A_3
X(3)	-0.43090E 01	=	A_5
X(4)	0.22184E 01	=	A_7
X(5)	-0.12969E 01	=	A_9
X(6)	0.85196E 00	=	A_{11}
X(7)	-0.60492E 00	=	A_{13}
X(8)	0.45233E 00	=	A_{15}
X(9)	-0.35120E 00	=	A_{17}
X(10)	0.28064E 00	=	A_{19}
X(11)	-0.22943E 00	=	A_{21}
X(12)	0.19108E 00	=	A_{23}
X(13)	-0.16162E 00	=	A_{25}
X(14)	0.13848E 00	=	A_{27}
X(15)	-0.11999E 00	=	A_{29}
X(16)	0.10497E 00	=	A_{31}
X(17)	-0.92598E-01	=	A_{33}
X(18)	0.82293E-01	=	A_{35}
X(19)	-0.73633E-01	=	A_{37}
X(20)	0.66263E-01	=	A_{39}

OUTPUT CBS 1

$\tau_1 = \tau_2 = 10$ s

VALUE OF DETERMINANT 0.83040E-05

SOLUTION VECTOR OF EQN.(4/14) TRUNCATED TO 5 TERMS

X(1)	0.59425E 01	=	B_2
X(2)	-0.43105E 01	=	B_4
X(3)	0.38369E 01	=	B_6
X(4)	-0.32666E 01	=	B_8
X(5)	0.27443E 01	=	B_{10}

VALUE OF DETERMINANT -0.76651E-12

SOLUTION VECTOR OF EQN. (4/14) TRUNCATED TO 10 TERMS

X(1)	0.59425E 01	=	B_2
X(2)	-0.43105E 01	=	B_4
X(3)	0.38369E 01	=	B_6
X(4)	-0.32666E 01	=	B_8
X(5)	0.27443E 01	=	B_{10}
X(6)	-0.23391E 01	=	B_{12}
X(7)	0.20303E 01	=	B_{14}
X(8)	-0.17904E 01	=	B_{16}
X(9)	0.15998E 01	=	B_{18}
X(10)	-0.14451E 01	=	B_{20}

VALUE OF DETERMINANT -0.59365E-20

SOLUTION VECTOR OF EQN.(4/14) TRUNCATED TO 15 TERMS

X(1)	0.59425E 01	=	B_2
X(2)	-0.43105E 01	=	B_4
X(3)	0.38369E 01	=	B_6
X(4)	-0.32666E 01	=	B_8
X(5)	0.27443E 01	=	B_{10}
X(6)	-0.23391E 01	=	B_{12}
X(7)	0.20303E 01	=	B_{14}
X(8)	-0.17904E 01	=	B_{16}
X(9)	0.15998E 01	=	B_{18}
X(10)	-0.14451E 01	=	B_{20}
X(11)	0.13173E 01	=	B_{22}
X(12)	-0.12100E 01	=	B_{24}
X(13)	0.11186E 01	=	B_{26}
X(14)	-0.10400E 01	=	B_{28}
X(15)	0.97164E 00	=	B_{30}

VALUE OF DETERMINANT 0.89058E-29

SOLUTION VECTOR OF EQN. (4/14) TRUNCATED TO 20 TERMS

X(1)	0.59425E-01	=	B_2
X(2)	-0.43105E-01	=	B_4
X(3)	0.38369E-01	=	B_6
X(4)	-0.32666E-01	=	B_8
X(5)	0.27443E-01	=	B_{10}
X(6)	-0.23391E-01	=	B_{12}
X(7)	0.20303E-01	=	B_{14}
X(8)	-0.17904E-01	=	B_{16}
X(9)	0.15998E-01	=	B_{18}
X(10)	-0.14451E-01	=	B_{20}
X(11)	0.13173E-01	=	B_{22}
X(12)	-0.12100E-01	=	B_{24}
X(13)	0.11186E-01	=	B_{26}
X(14)	-0.10400E-01	=	B_{28}
X(15)	0.97164E-00	=	B_{30}
X(16)	-0.91160E-00	=	B_{32}
X(17)	0.85860E-00	=	B_{34}
X(18)	-0.81136E-00	=	B_{36}
X(19)	0.76901E-00	=	B_{38}
X(20)	-0.73087E-00	=	B_{40}

Determination of summations in equations (71) and (72) when t = o

The error in T brought about by truncation of the various series in equations is largest when t = 0 in equations (71) and (72). These two cases were treated specially as follows. Inspection of equations (4/9) and (4/10) in Appendix 4 shows that for large m,

$$A_m \rightarrow (-1)^{\frac{m+1}{2}} \cdot \left(\frac{M_1}{m^2}\right) \qquad (6/1)$$

where M_1 is a constant

The solutions of the truncated equation (73) for the A_n agrees with this result and the value of M_1 can be found from the product $A_m \cdot m^2$ when m is large (e.g. 39 in the present case).

Now the sum to infinity of the series

$$\sum_{\substack{n \text{ odd} \\ > 0}}^{\infty} (-1)^{\frac{n+1}{2}} \left\{\frac{\sin(nz)}{n^2}\right\} = \frac{1}{4}\pi z \qquad (6/2)$$

over the range $0 < z < \frac{\pi}{2}$. See reference (120)

Equation (71) when t = 0 may be re-arranged to give

$$T_1(x,t) = T_A + \sum_{\substack{n \text{ odd} \\ > 0}}^{n=r} \left[A_n - (-1)^{\frac{n+1}{2}} \cdot \frac{M_1}{n^2}\right] \sin\left(n\frac{\pi}{2}\frac{x}{\ell}\right)$$

$$+ \sum_{\substack{n \text{ odd} \\ > 0}}^{\infty} (-1)^{\frac{n+1}{2}} \cdot \frac{M_1}{n^2} \sin\left(n\frac{\pi}{2}\frac{x}{\ell}\right) \qquad (6/3)$$

with r finite and hence

$$T_1(x,t) = T_A + \sum_{\substack{n=r \\ n \text{ odd} \\ > 0}} \left[A_n - (-1)^{\frac{n+1}{2}} \cdot \frac{M_1}{n^2} \right] \sin\left(n \frac{\pi}{2} \frac{x}{\ell}\right)$$

$$+ \frac{\pi^2}{8} \cdot M_1 \left(\frac{x}{\ell}\right) \qquad (6/4)$$

The solution of the simultaneous equations arising from equation (4/9) showed that the product $\left| A_m . m^2 \right|$ approached a steady value. Typical data is given in Appendix 5 from which it will be seen that

$A_1 . 1^2 = -76.872$

$A_3 . 3^2 = 92.196$

$A_5 . 5^2 = -107.725$

$A_7 . 7^2 = 108.702$

$A_9 . 9^2 = -105.049$

$A_{11} . 11^2 = 103.087$

$A_{13} . 13^2 = -102.231$

$A_{15} . 15^2 = 101.774$

$A_{17} . 17^2 = -101.497$

$A_{19} . 19^2 = 101.311$

$A_{21} . 21^2 = -101.179$

$A_{23} . 23^2 = 101.081$

$A_{25} . 25^2 = -101.013$

$A_{27} . 27^2 = 100.952$

$A_{29} . 29^2 = -100.912$

$A_{31} . 31^2 = 100.876$

$A_{33} . 33^2 = -100.830$

$A_{35} . 35^2 = 100.805$

$A_{37} . 37^2 = -100.799$

$A_{39} . 39^2 = 100.781$

By similar analysis the sum to infinity of the series

$$\sum_{\substack{n \text{ even} \\ 0}}^{\infty} (-1)^{1+\frac{n}{2}} \frac{\sin nz}{n} = \tfrac{1}{2}z \qquad (6/5)$$

over the range $0 < z < \frac{\pi}{2}$. Reference [121]

The t = 0 case of equation (72) yields

$$T_2(x,t) = T_A(1 - \tfrac{x}{\ell}) + \sum_{\substack{n \text{ even} \\ 0}}^{n=r} \left[B_n - (-1)^{1+\frac{n}{2}} \cdot \frac{M_2}{n}\right] \sin\left(n \tfrac{\pi}{2} \tfrac{x}{\ell}\right)$$

$$+ M_2 \tfrac{\pi}{4} (\tfrac{x}{\ell}) \qquad (6/6)$$

and the product $|B_m m|$ also approached a steady value.

Taking data from Appendix 5 again

$B_2 \cdot 2 = 11.885$

$B_4 \cdot 4 = -17.242$

$B_6 \cdot 6 = 23.021$

$B_8 \cdot 8 = -26.133$

$B_{10} \cdot 10 = 27.443$

$B_{12} \cdot 12 = -28.069$

$B_{14} \cdot 14 = 28.424$

$B_{16} \cdot 16 = -28.646$

$B_{18} \cdot 18 = 28.796$

$B_{20} \cdot 20 = -28.902$

$B_{22} \cdot 22 = 28.981$

$B_{24} \cdot 24 = -29.040$

$B_{26}.26 = 29.091$

$B_{28}.28 = -29.120$

$B_{30}.30 = 29.149$

$B_{32}.32 = -29.171$

$B_{34}.34 = 29.192$

$B_{36}.36 = -29.209$

$B_{38}.38 = 29.222$

$B_{40}.40 = -29,234$

Using the above method to determine the temperature when t = 0 it was confirmed that

$$T_1(x,0) = T_2(x,\tau_2) \quad \text{very nearly} \qquad (6/7)$$

$$T_1(x,\tau_1) = T_2(x,0) \quad \text{very nearly} \qquad (6/8)$$

(see Tables 4 to 13)

APPENDIX 7 Numerical Matrix Inversion Method

Summary of Computing Process, Flow Diagram

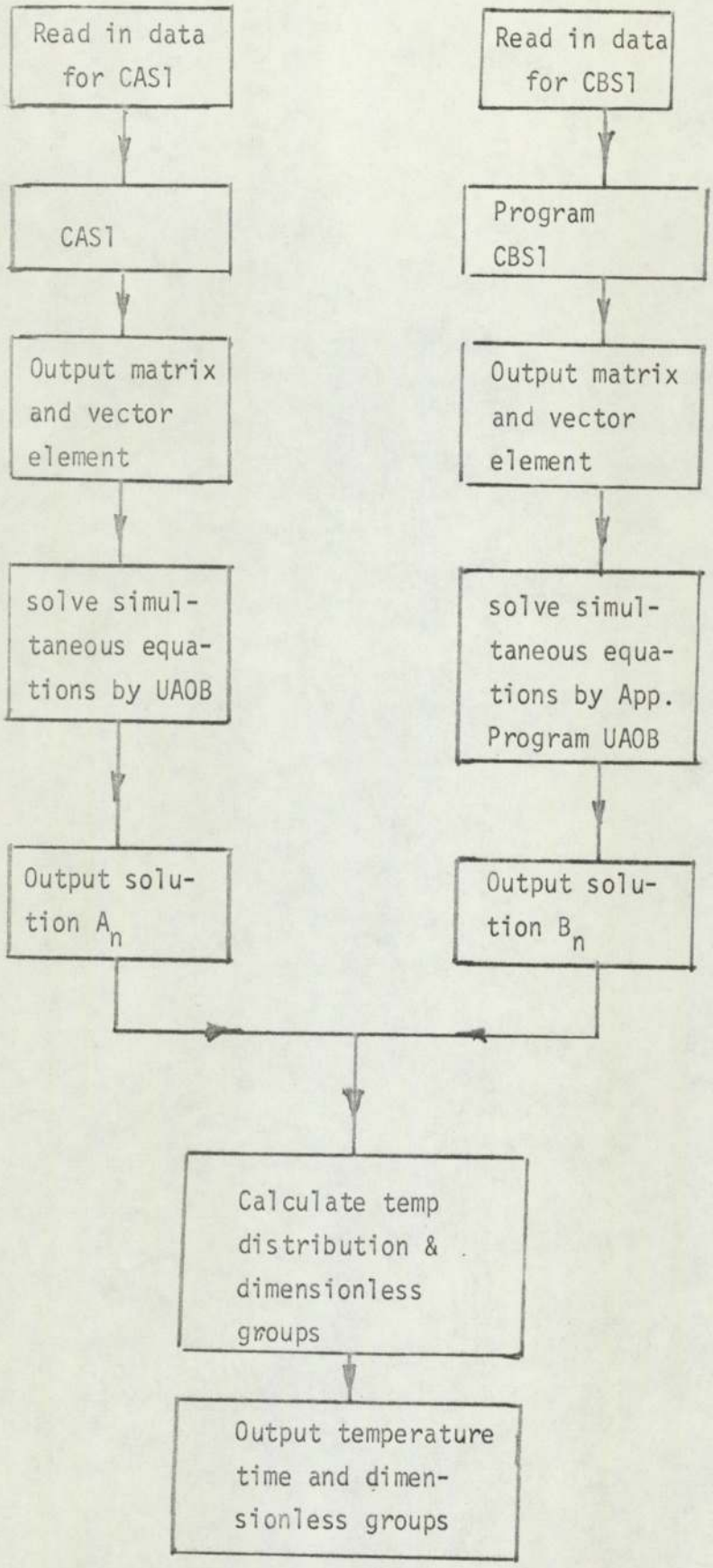

Programs CAS1, CBS1 and Groups are shown in Appendices 8,9 and 10.

APPENDIX 8 Program CAS 1 generation of matrix elements and solutions of equation (73)

```
0008          MASTER ACOEF                                          CAS  100
0009          INTEGER R, M1, M1, P1, M2, M2, A1, N3                 CAS  200
0010          REAL L                                                CAS  300
0011      100 FORMAT (4F0.0)                                        CAS  400
0012      101 FORMAT (1X,3I4)                                       CAS  500
0013      102 FORMAT (1X,1E12.6//)                                  CAS  600
0014      103 FORMAT (1X,2I4)                                       CAS  700
0015      104 FORMAT (1X,I4)                                        CAS  800
0016      105 FORMAT (1X,1E12.6)                                    CAS  900
0017      106 FORMAT(10X,SHT1 = ,FR.2,5X,SHT2 = ,FR.2,/)            CAS  910
0018      107 FORMAT (1X,1E14.5)                                    CAS  915
0019      108 FORMAT (5H ,8E14.5,/,8E14.5,/,4E14.5)                 CAS  920
0020      201 DIMENSION V(41), W(41), AM(41), ZR(41), RS(41),       CAS 1000
0021         1CA(41,41), AK(41,41)                                  CAS 1100
0022      301 READ (1,104) A1                                       CAS 1400
0023          WRITE (3, 104) A1                                     CAS 1500
0024          N3 = 1                                                CAS 1600
0025      300 READ (1,101) M1, M1, P1                               CAS 1700
0026      302 READ (1,100) T1, T2, D, L                             CAS 1710
0027          WRITE(2,106) T1, T2                                   CAS 1210
0028          M2 =(M1 + 1)/2                                        CAS 1800
0029          WRITE (3, 104) M2                                     CAS 1900
0030      401 P1 = -(T1*((3.1416/(2*L+D))**2))                      CAS 2000
0031      402 P2 = -(T2*((3.1416/(2*L+D))**2))                      CAS 2100
0032      403 Q1 = EXP (P1)                                         CAS 2200
0033      404 Q2 = EXP (P2)                                         CAS 2300
0034      405 M = 1                                                 CAS 2400
0035      406 R = 0                                                 CAS 2500
0036      407 N = 2                                                 CAS 2600

0037      408 SUM = 0                                               CAS 2700
0038      409 IF (N .GT. M1) GO TO 502                              CAS 2800
0039              N2 = (N**2)                                       CAS 2900
0040              M2 = (M**2)                                       CAS 3000
0041              R2 = (R**2)                                       CAS 3100
0042          V(N) = (Q2**M2)                                       CAS 3200
0043          W(N) = (V(N)*M2)/((N2 - R2)*(N2 - M2))                CAS 3300
0044          SUM = SUM + W(N)                                      CAS 3400
0045          WRITE (2,104) N                                       CAS 3500
0046          WRITE (2,107) SUM                                     CAS 3600
0047          N = N + 2                                             CAS 3700
0048          GO TO 409                                             CAS 3800
0049      502 IF (R.EQ.0) GO TO 501                                 CAS 3900
0050          GO TO 503                                             CAS 4000
0051      501 AM(M) = ((-1)**((M+1)/2))*((3.1416**2)/16)            CAS 4100
0052          RS(M) = 50.0/(M**2) - 100.0*SUM                       CAS 4200
0053      503 IF (R .GE. 1) GO TO 520                               CAS 4300
0054          GO TO 622                                             CAS 4400
0055      520 ZR(R) = Q1**(R**2)                                    CAS 4500
0056          AK(R,M) = ((-1)**((R-1)/2))*ZR(R)*SUM                 CAS 4600
0057          IF (M .EQ. R) GO TO 607                               CAS 4700
0058          CA(R,M) = AK(R,M)                                     CAS 4800
0059          GO TO 621                                             CAS 4900
0060      607 CA(R,M) = AK(R,M) + AM(M)                             CAS 5000
0061          GO TO 621                                             CAS 5100
0062      621 IF (M .GE. M1) GO TO 630                              CAS 5400
0063          M=M+2                                                 CAS 5500
0064          GO TO 407                                             CAS 5600
0065      630 IF (R .GE. R1.AND.M.GE.M1) GO TO 609                  CAS 5700
0066          GO TO 623                                             CAS 5800
0067      622 IF (M .GE. M1) GO TO 623                              CAS 5900
0068          M = M +2                                              CAS 6000
0069          GO TO 407                                             CAS 6100
0070      623 IF (R.EQ.0) GO TO 624                                 CAS 6200
0071          R = R +2                                              CAS 6202
0072          M = 1                                                 CAS 6203
0073          GO TO 407                                             CAS 6204
0074      624 R = 1                                                 CAS 6205
0075          M =1                                                  CAS 6300
0076          GO TO 407                                             CAS 6400
0077      609 M = 1                                                 CAS 6500
0078      610 WRITE (2, 104) M                                      CAS 6600
0079      611 R = 1                                                 CAS 6700
0080      612 WRITE (3,107) CA(R,M)                                 CAS 6900
0081          IF (R .GE. P1) GO TO 613                              CAS 7000
0082          R = R + 2                                             CAS 7100
0083          GO TO 612                                             CAS 7200
0084      613 IF (M .GE. M1) GO TO 614                              CAS 7300
0085          M = M + 2                                             CAS 7400
0086          GO TO 610                                             CAS 7500
0087      614 M = 1                                                 CAS 7600
0088      615 WRITE (3,107) RS(M)                                   CAS 7700
0089          IF (M .GE. M1) GO TO 617                              CAS 7800
0090          M = M + 2                                             CAS 7900
0091          GO TO 615                                             CAS 8000
0092      617 WRITE (2,108)((CA(I,J),I=1,39,2),J=1,39,2)            CAS 8350
0093          WRITE(2,104)(RS(M),M=1,39,2)                          CAS 8360
0094          IF (N3.GE.A1) GO TO 616                               SUM 8100
0095          N3 = N3 + 1                                           CAS 8200
0096          GO TO 302                                             CAS 8300
0097      616 STOP                                                  CAS 8400

0098          END                                                   CAS 8500

END OF SEGMENT, LENGTH  655, NAME  ACOEF

0099          FINISH                                                CAS 8600
```

Input and Output of Program CAS1

* Numbers above program statements in the tables below, and overleaf refer to the line number in program CAS1

Program Statement	Input Data
0022 301 READ (1,104) A1	A1 = No. of cases to be solved
0025 300 Read (1,101)N1,M1,R1	N1 = Highest value of n used in equation (4/10) for summation to obtain C_m,k namely n = 20 M1 = Highest subscript of A_m=39 (m odd) R1 = Highest subscript of A_k=39 (k odd)
0026 302 READ (1,100) T1,T2,D,L	T1 = Time bars are separated = 10_s (Typical value) T2 = Time bars are separated = 10s (Typical value) $D = \frac{1}{\sqrt{\text{Diffusivity}}} = \sqrt{\frac{10^6}{5m^2}\ \frac{s}{}} = 447.0\ \frac{s^{\frac{1}{2}}}{m}$ L = Length of bar = 0.04m

The above data is followed by a card punched with the following statement

UAFORTRAN LOAD : LIBF.UA0B, PAGE, DATA RUNCAS1, TIME 500, LINES 15000

This card commands the computer to use applications program UA08 to solve the simultaneous equations whose matrix and vector have been generated from the input data above.

Program Statement	Output Data
0023 WRITE(3,104) A1	<u>To file store</u> A1 as in input above
0029 WRITE (3,104) M2	M2 = Number of simultaneous equations in system to be solved. 20
0080 612 WRITE (3,107) CA (R,M)	CA(R,M) = typical element in coefficient matrix (equ.(73)
0088 615 WRITE (3,107) RS(M)	RS(M) = typical element of vector R in equation (73)
0026 WRITE (2,106) T1, T2	<u>To line printer</u> T1 and T2 as in input
0045 WRITE (2,104) N	N = even integer, Eq (4/10)
0046 WRITE (2,107) SUM	SUM = sum to n terms, eq. (4/10)
0078 610 WRITE (2,104) M	M = 2 x row number of coefficient matrix eq (73)
0092 617 WRITE (2,108) CA(I,J) I = 1,39,2. J = 1,39,2	CA (I,J) = typical element in coeffcient matrix eq. (73)
0093 WRITE (2,108) (RS/M), M = 1,39,2	RS(M) = typical element of vector R in eq. (73)

..
19
21
23
25
27
29
31
33
35
37
39

k

m

OUTPUT CAS 1

$\tau_1 = \tau_2 = 10s$

-0.29375E 00	0.74295E-01	-0.10906E-01	0.81062E-03	-0.37225E-04	0.10750E-05	-0.18437E-07	0.18102E-09	
-0.99910E-12	0.30676E-14	-0.52037E-17	0.40543E-20	-0.24816E-23	0.69347E-27	-0.10571E-30	0.87769E-35	
-0.39440E-39	0.97207E-44	-0.12964E-48	0.93720E-54					
-0.13794E 00	0.59915E 00	-0.55591E-02	0.29364E-03	-0.94503E-05	0.21579E-06	-0.37346E-08	0.29206E-10	
-0.15235E-12	0.44945E-15	-0.74037E-18	0.67548E-21	-0.33943E-24	0.93571E-28	-0.14109E-31	0.11610E-35	
-0.52053E-40	0.12697E-44	-0.16831E-49	0.12114E-54					
-0.49520E-01	0.19044E-01	-0.60481E 00	-0.89561E-04	0.88540E-05	-0.30732E-06	0.55780E-08	-0.56104E-10	
0.31369E-12	-0.97073E-15	0.16553E-17	-0.15498E-20	0.79442E-24	-0.22244E-27	0.33961E-31	-0.28232E-35	
0.12763E-39	-0.31350E-44	0.41863E-49	-0.30233E-54					
-0.33941E-01	0.64597E-02	0.57092E-03	0.61637E 00	0.98116E-05	-0.29451E-06	0.49920E-08	-0.48356E-10	
0.24623E-12	-0.80539E-15	0.13589E-17	-0.12626E-20	0.64346E-24	-0.17937E-27	0.27289E-31	-0.22621E-35	
0.10203E-39	-0.25014E-44	0.33301E-49	-0.24056E-54					
-0.17872E-01	0.24480E-02	0.66712E-03	-0.11597E-03	-0.61684E 00	-0.17197E-06	0.28010E-08	-0.26609E-10	
0.14386E-12	-0.43568E-15	0.73201E-18	-0.67810E-21	0.34484E-24	-0.95969E-28	0.14582E-31	-0.12076E-35	
0.54425E-40	-0.13334E-44	0.17742E-49	-0.12810E-54					
-0.11316E-01	0.12253E-02	0.50743E-03	-0.76291E-04	0.37690E-05	0.61685E 00	0.16085E-08	-0.15240E-10	
0.83388E-13	-0.24962E-15	0.41960E-18	-0.38885E-21	0.19782E-24	-0.55069E-28	0.83697E-32	-0.69326E-36	
0.31250E-40	-0.76572E-45	0.10190E-49	-0.73582E-55					
-0.28863E-02	0.74621E-03	0.37430E-03	-0.52547E-04	0.24945E-05	-0.65363E-07	-0.61685E 00	-0.10005E-10	
0.54722E-13	-0.19455E-15	0.27491E-18	-0.25683E-21	0.13073E-24	-0.36410E-28	0.55358E-32	-0.45866E-36	
0.20479E-40	-0.50606E-45	0.67452E-50	-0.48715E-55					
-0.58341E-02	0.50769E-03	0.28366E-03	-0.38353E-04	0.17855E-05	-0.46642E-07	0.75383E-09	0.61685E 00	
0.39063E-13	-0.11847E-15	0.19948E-18	-0.18569E-21	0.94239E-25	-0.26252E-28	0.39921E-32	-0.33080E-36	
0.14916E-40	-0.36559E-45	0.48862E-50	-0.35147E-55					
-0.44986E-02	0.36997E-03	0.22157E-03	-0.29273E-04	0.13486E-05	-0.35242E-07	0.57076E-09	-0.54490E-11	
-0.61685E 00	-0.89935E-16	0.15148E-18	-0.14057E-21	0.71586E-25	-0.19944E-28	0.30331E-32	-0.25135E-36	
0.11334E-40	-0.27782E-45	0.36979E-50	-0.26710E-55					
-0.35779E-02	0.28273E-03	0.17762E-03	-0.23117E-04	0.10580E-05	-0.27659E-07	0.44869E-09	-0.42873E-11	
0.23297E-13	0.61685E 00	0.11929E-18	-0.11071E-21	0.56385E-25	-0.15710E-28	0.23893E-32	-0.19801E-36	
0.80992E-41	-0.21887E-45	0.29134E-50	-0.21044E-55					
-0.29153E-02	0.22370E-03	0.14548E-03	-0.18235E-04	0.85380E-06	-0.22331E-07	0.36267E-09	-0.34674E-11	
0.18867E-13	-0.57294E-16	-0.61685E 00	-0.89557E-22	0.45633E-25	-0.12715E-28	0.19338E-32	-0.16027E-36	
0.79275E-41	-0.17716E-45	0.23582E-50	-0.17034E-55					
-0.24219E-02	0.18176E-03	0.12130E-03	-0.15502E-04	0.70437E-06	-0.18431E-07	0.29954E-09	-0.28652E-11	
0.15576E-13	-0.47358E-16	0.79793E-19	0.61685E 00	0.37726E-25	-0.10512E-28	0.15988E-32	-0.13251E-36	
0.54757E-41	-0.14648E-45	0.19498E-50	-0.14084E-55					
-0.20445E-02	0.15082E-03	0.10267E-03	-0.13046E-04	0.59149E-06	-0.15482E-07	0.25179E-09	-0.24090E-11	
0.13098E-13	-0.39827E-16	0.67108E-19	-0.62297E-22	-0.61685E 00	-0.88417E-29	0.13448E-32	-0.11146E-36	
0.50264E-41	-0.12321E-45	0.16401E-50	-0.11847E-55					
-0.17493E-02	0.12730E-03	0.88021E-04	-0.11134E-04	0.50401E-06	-0.13197E-07	0.21471E-09	-0.20547E-11	
0.11173E-13	-0.33975E-16	0.57251E-19	-0.53148E-22	0.27072E-25	0.61685E 00	0.11474E-32	-0.95093E-37	
0.42886E-41	-0.10512E-45	0.13994E-50	-0.10108E-55					
-0.15138E-02	0.10697E-03	0.76294E-04	-0.96170E-05	0.43478E-06	-0.11387E-07	0.18533E-09	-0.17733E-11	
0.96465E-14	-0.29335E-16	0.49433E-19	-0.45891E-22	0.23376E-25	-0.65138E-29	-0.61685E 00	-0.82114E-37	
0.37032E-41	-0.90777E-46	0.12084E-50	-0.87287E-56					
-0.13731E-02	0.94392E-04	0.66761E-04	-0.83917E-05	0.37901E-06	-0.99279E-08	0.16164E-09	-0.15472E-11	
0.84148E-14	-0.25596E-16	0.43124E-19	-0.40035E-22	0.20393E-25	-0.56828E-29	0.86437E-33	0.61685E 00	
0.32308E-41	-0.79193E-46	0.10543E-50	-0.76153E-56					
-0.11665E-02	0.82597E-04	0.58909E-04	-0.73877E-05	0.33339E-06	-0.87345E-08	0.14224E-09	-0.13617E-11	
0.74042E-14	-0.22524E-16	0.37958E-19	-0.35239E-22	0.17950E-25	-0.50021E-29	0.76084E-33	-0.63059E-37	
-0.61685E 00	-0.69713E-46	0.92800E-51	-0.67033E-56					
-0.10359E-02	0.72911E-04	0.52365E-04	-0.65544E-05	0.29559E-06	-0.77454E-08	0.12615E-09	-0.12078E-11	
0.65496E-14	-0.19980E-16	0.33672E-19	-0.31261E-22	0.15924E-25	-0.44374E-29	0.67495E-33	-0.55941E-37	
0.25229E-41	0.61685E 00	0.82426E-51	-0.59467E-56					
-0.92622E-03	0.64353E-04	0.46853E-04	-0.58552E-05	0.26392E-06	-0.69162E-08	0.11267E-09	-0.10788E-11	
0.58679E-14	-0.17846E-16	0.30076E-19	-0.27923E-22	0.14224E-25	-0.39637E-29	0.60290E-33	-0.49969E-37	
0.22536E-41	-0.55242E-46	-0.61685E 00	-0.53119E-56					
-0.83313E-03	0.58009E-04	0.42163E-04	-0.52626E-05	0.23710E-06	-0.62140E-08	0.10124E-09	-0.96942E-12	
0.52733E-14	-0.16038E-16	0.27029E-19	-0.25095E-22	0.12783E-25	-0.35622E-29	0.54184E-33	-0.44908E-37	
0.20253E-41	-0.49648E-46	0.66091E-51	0.61685E 00					
0.23392E 02	0.15044E 02	0.81451E 01	0.39631E 01	0.21963E 01	0.14056E 01	0.98329E 00	0.73139E 00	
0.54522E 00	0.45023E 00	0.36725E 00	0.30535E 00	0.25793E 00	0.22079E 00	0.19115E 00	0.16712E 00	
0.14735E 00	0.13090E 00	0.11707E 00	0.10532E 00					

COEFFICIENT MATRIX

VECTOR

OUTPUT CAS 1

$\tau_1 = \tau_2 = 10s$

VALUE OF DETERMINANT 0.22718E-04

SOLUTION VECTOR OF EQN. (73)

X(1)	-0.76872E 02	=	A_1
X(2)	0.10244E 02	=	A_3
X(3)	-0.43090E 01	=	A_5
X(4)	0.22184E 01	=	A_7
X(5)	-0.12969E 01	=	A_9
X(6)	0.85196E 00	=	A_{11}
X(7)	-0.60492E 00	=	A_{13}
X(8)	0.45233E 00	=	A_{15}
X(9)	-0.35120E 00	=	A_{17}
X(10)	0.28064E 00	=	A_{19}
X(11)	-0.22943E 00	=	A_{21}
X(12)	0.19108E 00	=	A_{23}
X(13)	-0.16162E 00	=	A_{25}
X(14)	0.13848E 00	=	A_{27}
X(15)	-0.11999E 00	=	A_{29}
X(16)	0.10497E 00	=	A_{31}
X(17)	-0.92598E-01	=	A_{33}
X(18)	0.82293E-01	=	A_{35}
X(19)	-0.73633E-01	=	A_{37}
X(20)	0.66263E-01	=	A_{39}

APPENDIX 9 Program CBS 1 for generation of matrix elements and solutions of equation (77).

```
0008          MASTER BCOEF                                          CBS  200
0009          INTEGER N, M1, K1, A1, N2, M2                         CBS  200
0010          REAL L                                                CBS  400
0011      100 FORMAT (4F6.0)                                        CBS  500
0012      101 FORMAT (1X,3I4)                                       CBS  600
0013      102 FORMAT (1X,1F12.4///)                                 CBS  700
0014      103 FORMAT (1X,2I4)                                       CBS  800
0015      104 FORMAT (1X,1I4)                                       CBS  900
0016      105 FORMAT (1X,1F12.4)                                    CBS 1000
0017      106 FORMAT(1X,5HT1 = ,F8.2,5X,5HT2 = ,F8.2,/)             CBS 1010
0018      107 FORMAT (1X,E14.5)                                     CBS 1020
0019      108 FORMAT (1H ,8E14.5,/,6E14.5,/,4E14.5)                 CBS 1030
0020      201 DIMENSION Z(41), Y(41), ZK(41), BM(41), RHS(41),      CBS 1100
0021         1CB(41,41), BK(41,41)                                  CBS 1200
0022      300 READ (1, 104) A1                                      CBS 1500
0023          WRITE (3, 104) A1                                     CBS 1600
0024          N2 = 1                                                CBS 1601
0025      301 READ (1,101) N1, M1, K1                               CBS 1700
0026      302 READ (1,100) T1, T2, D, L                             CBS 1710
0027          WRITE(2,106) T1, T2                                   CBS 1310
0028          M2 = M1/2                                             CBS 1701
0029          WRITE (3, 104) M2                                     CBS 1702
0030      401 P1 = -(T1*((3.1416/(2*L+D))**2))                      CBS 1800
0031      402 P2 = -(T2*((3.1416/(2*L+D))**2))                      CBS 1900
0032      403 Q1 = EXP (P1)                                         CBS 2000
0033      404 Q2 = EXP (P2)                                         CBS 2100
0034      405 M = 2                                                 CBS 2200
0035      406 K = 0                                                 CBS 2300
0036      407 N = 1                                                 CBS 2400
```

```
0037      408 SUMC = 0                                              CBS 2500
0038      409 IF (N .GT. M1) GO TO 502                              CBS 2600
0039          Z(N) = (Q1**(N**2))                                   CBS 2700
0040          Y(N) = (Z(N))/(((N**2) - (K**2))*((N**2) - (M**2)))   CBS 2800
0041          SUMC = SUMC + Y(N)                                    CBS 2900
0042          WRITE (2,104) N                                       CBS 3000
0043          WRITE (2,107) SUMC                                    CBS 3100
0044          N = N + 2                                             CBS 3200
0045          GO TO 409                                             CBS 3300
0046      502 IF (K.EQ.0) GO TO 501                                 CBS 3301
0047          GO TO 503                                             CBS 3302
0048      501 BM(M) = ((-1)**(M/2))*((3.1416**2)/(16*M))            CBS 3400
0049          RHS(M) = 200.0*SUMC/3.1416 + 78.54/(M**2)             CBS 3500
0050      503 IF (K .GE. 2) GO TO 520                               CBS 3501
0051          GO TO 622                                             CBS 3502
0052      520 ZK(K) = Q2**(K**2)                                    CBS 3600
0053          BK(K,M) = ((-1)**(K/2))*K*ZK(K)*SUMC                  CBS 3700
0054          IF (M .EQ. K) GO TO 607                               CBS 3800
0055          CB(K,M) = BK(K,M)                                     CBS 3900
0056          GO TO 621                                             CBS 4000
0057      607 CB(K,M) = BK(K,M) - BM(M)                             CBS 4100
0058          GO TO 621                                             CBS 4200
0059      621 IF (M .GE. M1) GO TO 630                              CBS 4500
0060          M=M+2                                                 CBS 4600
0061          GO TO 407                                             CBS 4700
0062      630 IF (K.GL.K1.AND.M.GE.M1) GO TO 609                    CBS 4701
0063          GO TO 623                                             CBS 4702
0064      622 IF (M .GE. M1) GO TO 623                              CBS 4800
0065          M = M + 2                                             CBS 4900
0066          GO TO 407                                             CBS 5000
0067      623 K = K + 2                                             CBS 5001
0068          M = 2                                                 CBS 5002
0069          GO TO 407                                             CBS 5003
0070      609 M = 2                                                 CBS 5300
0071      610 WRITE (2, 104) M                                      CBS 5400
0072      611 K = 2                                                 CBS 5500
0073      612 WRITE (3,107) CB(K,M)                                 CBS 5700
0074          IF (K .GE. K1) GO TO 613                              CBS 5800
0075          K = K + 2                                             CBS 5900
0076          GO TO 612                                             CBS 6000
0077      613 IF (M .GE. M1) GO TO 614                              CBS 6100
0078          M = M + 2                                             CBS 6200
0079          GO TO 610                                             CBS 6300
0080      614 M = 2                                                 CBS 6400
0081      615 WRITE (3,107) RHS(M)                                  CBS 6500
0082          IF (M .GE. M1) GO TO 617                              CBS 6600
0083          M = M + 2                                             CBS 6700
0084          GO TO 615                                             CBS 6800
0085      617 WRITE (2,108) ((CB(I,J),I=2,40,2),J=2,40,2)           CBS 7110
0086          WRITE (2,108)(RHS(M),M=2,40,2)                        CBS 7120
0087          IF (N2 .EQ. A1) GO TO 616                             CBS 6900
0088          N2 = N2 + 1                                           CBS 7000
0089          GO TO 302                                             CBS 7100
0090      616 STOP                                                  CBS 7200
0091          END                                                   CBS 7300
```

```
END OF SEGMENT, LENGTH  628, NAME  BCOEF
```

```
0092          FINISH                                                CBS 7400
```

Input and Output of Program CBS1

* Numbers above program statements in the tables below and overleaf refer to the line number in program CBS1

Program Statement		Input Data
0022 300 READ	(1,104)A1	A1 = No. of cases to be solved
0025 301 READ	(1,101)N1,M1,K1.	N1 = Highest value of n in equation(A.12) for summation to obtain D_{mk} n odd = 19 M1 = Highest subscript of B_m = 40 m even K1 = Highest subscript of B_k = 40 m even
0026 302 READ	(1,100) T1,T2,D,L.	T1 = Time bars are = 10s(typical value) separated T2 = Time bars are = 10s (typical value) in contact $D = \frac{1}{\sqrt{\text{Diffusivity}}} = \sqrt{\frac{10^6}{5m^2}\ \frac{s}{}} = 447.0\frac{s^{\frac{1}{2}}}{m}$ L = Length of bar = 0.04m

The above data is followed by a card punched with the following statement UAFORTRAN LOAD LIBF. UAOB, PAGE, DATA RUNCBS1, TIME 500, LINES 15000

This card commands the computer to use applications program UAOB to solve the simultaneous equations whose matric and vector have been generated from the input data above.

Program Statement	Output Data
0023 WRITE (3,104) A1	A1 as in input above
0029 WRITE (3,104) M2	M2 = Number of simultaneous equations in system to be solved 20.
0073 WRITE 93,107) CB(k,m)	CB(k,m) = typical element in coefficient matrix (eq.(77))
0081 615 WRITE (3,107) RHS(M)	RHS(M) = typical element of vector S, eq. (77)
0036 WRITE (2,106) T1,T2	<u>To line printer</u>:- T1 and T2 as in input
0042 WRITE (2,104) N	N = odd integer (eq (4/12))
0043 WRITE (2,107) SUMC	SUMC = sum to n terms, eq. (4/12)
0071 610 WRITE (2,104) M	M = 2 x row number of coefficient matrix eq. (77)
0085 617 WRITE (2,108) (CA (I,J) , I = 2,40,2, J = 2,40,2.)	CA(I,J) = typical element in coefficient matrix eq.(77)
0086 WRITE (2,108) (RHS(M) M = 2,30,2)	RHS(M) = typical element in vector S eq. (77)

OUTPUT CBS 1

$\tau_1 = \tau_2 = 10s$

COEFFICIENT MATRIX

0.12752E 00	0.82503E-02	-0.16884E-02	0.16451E-03	-0.85221E-05	0.24220E-06	-0.37869E-08	0.32479E-10
-0.15232E-12	0.30966E-15	-0.54263E-18	0.41075E-21	-0.16880E-24	0.37628E-28	-0.45460E-32	0.29750E-36
-0.10540E-40	0.20208E-45	-0.20959E-50	0.11756E-55				
-0.10415E-01	-0.13546E 00	-0.11153E-02	0.10413E-03	-0.52343E-05	0.14602E-06	-0.22569E-08	0.19212E-10
-0.89438E-13	0.22846E-15	-0.31728E-18	0.23967E-21	-0.98338E-25	0.21893E-28	-0.26423E-32	0.17277E-36
-0.61149E-41	0.11721E-45	-0.12150E-50	0.68121E-56				
-0.66521E-02	0.54309E-02	0.10177E 00	0.56132E-04	-0.27121E-05	0.73983E-07	-0.11290E-08	0.95349E-11
-0.44258E-13	0.11240E-15	-0.15569E-18	0.11738E-21	-0.48039E-25	0.10693E-28	-0.12894E-32	0.84265E-37
-0.29808E-41	0.57066E-46	-0.59152E-51	0.33151E-56				
-0.42197E-02	0.21156E-02	-0.36543E-03	-0.77072E-01	-0.14308E-05	0.38522E-07	-0.58442E-09	0.49213E-11
-0.22804E-13	0.57850E-16	-0.80074E-19	0.60339E-22	-0.24711E-25	0.54932E-29	-0.66222E-33	0.43259E-37
-0.15304E-41	0.29305E-46	-0.30363E-51	0.17015E-56				
-0.28145E-02	0.13094E-02	-0.22734E-03	0.18422E-04	0.61684E-01	0.22968E-07	-0.34869E-09	0.29388E-11
-0.13427E-13	0.34537E-16	-0.47893E-19	0.36100E-22	-0.14788E-25	0.32879E-29	-0.39442E-33	0.25899E-37
-0.91634E-42	0.17549E-46	-0.18183E-51	0.10190E-56				
-0.10892E-02	0.95001E-03	-0.15422E-03	0.12335E-04	-0.57118E-06	-0.51404E-01	-0.23399E-09	0.19741E-11
-0.91403E-14	0.23260E-16	-0.32920E-19	0.24292E-22	-0.99524E-26	0.22132E-29	-0.26887E-33	0.17437E-37
-0.61498E-42	0.11816E-46	-0.12244E-51	0.68623E-57				
-0.16752E-02	0.69042E-03	-0.11162E-03	0.88755E-05	-0.41128E-06	0.11098E-07	0.44061E-01	0.14262E-11
-0.66199E-14	0.16813E-16	-0.23293E-19	0.17563E-22	-0.71964E-26	0.16004E-29	-0.19299E-33	0.12610E-37
-0.44421E-42	0.85400E-47	-0.86557E-52	0.49633E-57				
-0.13353E-02	0.53219E-03	-0.84631E-04	0.67096E-05	-0.31118E-06	0.84056E-08	-0.12803E-09	-0.38553E-01
-0.58191E-14	0.12749E-16	-0.17664E-19	0.13320E-22	-0.54578E-26	0.12138E-29	-0.14638E-33	0.95646E-38
-0.33844E-42	0.64821E-47	-0.67171E-52	0.37647E-57				
-0.90075E-03	0.41983E-03	-0.66427E-04	0.52574E-05	-0.24400E-06	0.65953E-08	-0.10049E-09	0.84873E-12
0.34270E-01	0.10010E-16	-0.13870E-19	0.10459E-22	-0.42858E-26	0.95316E-30	-0.11495E-33	0.75110E-38
-0.26578E-42	0.50904E-47	-0.52750E-52	0.29565E-57				
-0.73149E-03	0.33973E-03	-0.53554E-04	0.42339E-05	-0.19660E-06	0.53166E-08	-0.81027E-10	0.68440E-12
-0.31778E 14	-0.30843E-01	-0.11166E-19	0.84354E-23	-0.34566E-26	0.76876E-30	-0.92709E-34	0.60580E-38
-0.21437E-42	0.41058E-47	-0.42547E-52	0.23846E-57				
-0.60566E-03	0.28053E-03	-0.44106E-04	0.34845E-05	-0.16186E-06	0.43787E-08	-0.66742E-10	0.56379E-12
-0.26179E-14	0.66508E-17	0.28039E-01	0.69496E-23	-0.28478E-26	0.63337E-30	-0.76182E-34	0.49912E-38
-0.17442E-42	0.33828E-47	-0.33055E-52	0.19647E-57				
-0.50964E-03	0.23556E-03	-0.36465E-04	0.29188E-05	-0.13562E-06	0.36697E-08	-0.55943E-10	0.47259E-12
-0.21945E-14	0.55753E-17	-0.77254E-20	-0.25702E-01	-0.23874E-26	0.53097E-30	-0.64034E-34	0.41843E-38
-0.14807E-42	0.26359E-47	-0.29388E-52	0.16471E-57				
-0.43471E-03	0.20061E-03	-0.31433E-04	0.24810E-05	-0.11531E-06	0.31207E-08	-0.47576E-10	0.40193E-12
-0.18665E-14	0.47419E-17	-0.65707E-20	0.49552E-23	0.23725E-01	0.45162E-30	-0.54464E-34	0.35590E-38
-0.12594E-42	0.24121E-47	-0.24996E-52	0.14010E-57				
-0.37514E-03	0.17290E-03	-0.27059E-04	0.21352E-05	-0.99256E-07	0.26866E-08	-0.40961E-10	0.34605E-12
-0.16070E-14	0.40828E-17	-0.56575E-20	0.42665E-23	-0.17484E-26	-0.22030E-01	-0.46895E-34	0.30644E-38
-0.10844E-42	0.20709E-47	-0.21523E-52	0.12063E-57				
-0.32701E-03	0.15059E-03	-0.23541E-04	0.18572E-05	-0.86345E-07	0.23374E-08	-0.35639E-10	0.30110E-12
-0.13983E-14	0.35525E-17	-0.49227E-20	0.37124E-23	-0.15213E-26	0.33835E-30	0.20562E-01	0.26664E-38
-0.94355E-43	0.18072E-47	-0.18728E-52	0.10497E-57				
-0.28757E-03	0.13229E-03	-0.20669E-04	0.16303E-05	-0.75805E-07	0.20522E-08	-0.31292E-10	0.26438E-12
-0.12278E-14	0.31194E-17	-0.43225E-20	0.32598E-23	-0.13359E-26	0.29711E-30	-0.35831E-34	-0.19277E-01
-0.82854E-43	0.15869E-47	-0.16445E-52	0.92171E-58				
-0.25485E-03	0.11716E-03	-0.18293E-04	0.14427E-05	-0.67088E-07	0.18164E-08	-0.27697E-10	0.23401E-12
-0.10867E-14	0.27611E-17	-0.38260E-20	0.28854E-23	-0.11824E-26	0.26298E-30	-0.31716E-34	0.20725E-38
0.18143E-01	0.14047E-47	-0.14555E-52	0.81585E-58				
-0.22741E-03	0.10448E-03	-0.16305E-04	0.12857E-05	-0.59795E-07	0.16190E-08	-0.24688E-10	0.20859E-12
-0.96871E-15	0.24612E-17	-0.34105E-20	0.25721E-23	-0.10540E-26	0.23443E-30	-0.28272E-34	0.18474E-38
-0.65374E-43	-0.17135E-01	-0.12976E-52	0.72726E-58				
-0.20416E-03	0.93756E-04	-0.14625E-04	0.11531E-05	-0.53632E-07	0.14522E-08	-0.22145E-10	0.18711E-12
-0.86895E-15	0.22077E-17	-0.30593E-20	0.23072E-23	-0.94548E-27	0.21029E-30	-0.25360E-34	0.16572E-38
-0.58443E-43	0.11232E-47	0.10253E-01	0.65237E-58				
-0.18431E-03	0.84602E-04	-0.13192E-04	0.10401E-05	-0.48376E-07	0.13100E-08	-0.19976E-10	0.16878E-12
-0.78386E-15	0.19916E-17	-0.27598E-20	0.20813E-23	-0.85291E-27	0.18970E-30	-0.22877E-34	0.14950E-38
-0.52901E-43	0.10132E-47	-0.10500E-52	-0.15421E-01				

VECTOR

0.71519E 00	0.51737E 00	0.33526E 00	0.21616E 00	0.14572E 00	0.10369E 00	0.77230E-01	0.59636E-01
0.47389E-01	0.38540E-01	0.31945E-01	0.26903E-01	0.22962E-01	0.19826E-01	0.17290E-01	0.15209E-01
0.13483E-01	0.12034E-01	0.10806E-01	0.97566E-02				

OUTPUT CBS 1

$\tau_1 = \tau_2 = 10s$

VALUE OF DETERMINANT 0.89058E-29

SOLUTION VECTOR OF EQN. (77)

X(1)	0.59425E-01	=	B_2
X(2)	-0.43105E-01	=	B_4
X(3)	0.38369E-01	=	B_6
X(4)	-0.32666E-01	=	B_8
X(5)	0.27443E-01	=	B_{10}
X(6)	-0.23391E-01	=	B_{12}
X(7)	0.20303E-01	=	B_{14}
X(8)	-0.17904E-01	=	B_{16}
X(9)	0.15998E-01	=	B_{18}
X(10)	-0.14451E-01	=	B_{20}
X(11)	0.13173E-01	=	B_{22}
X(12)	-0.12100E-01	=	B_{24}
X(13)	0.11186E-01	=	B_{26}
X(14)	-0.10400E-01	=	B_{28}
X(15)	0.97164E-00	=	B_{30}
X(16)	-0.91160E-00	=	B_{32}
X(17)	0.85860E-00	=	B_{34}
X(18)	-0.81136E-00	=	B_{36}
X(19)	0.76901E-00	=	B_{38}
X(20)	-0.73087E-00	=	B_{40}

APPENDIX 10 Program GROUPS - Computation of temperature-time data and dimensionless groups

```
0012          TRACE 1
0013          READ FROM (CR)                                                  SUM  200
0001          MASTER SUMS                                                     SUM  300
0002          INTEGER I1, I2, R                                               SUM 1000
0003          DIMENSION C(40), A(40), TERM(40),  X(11), Y(40), DA(40), DB(40) SUM 1100
0004          REAL L, LI, LI2                                                 SUM  400
0005      101 FORMAT (4F0.0)                                                  SUM  500
0006      102 FORMAT (1F0.0)                                                  SUM  600
0007      103 FORMAT (1X,2I4)                                                 SUM  700
0008      105 FORMAT (5E12.5)


0009      106 FORMAT (1X,1E12.6)                                              SUM  800
0010      107 FORMAT (I12)                                                    SUM  900
0011      109 FORMAT (/30X,1HR,11X,4HY(R)/)                                   SUM  910
0012      110 FORMAT (//54X,3HFTC,10X,1HF,11X,2HLI,8X,5HGROUP,10X,4HX(J)/)    SUM  911
0013      111 FORMAT (30X,5E14.7)                                             SUM  912
0014      112 FORMAT (25X,I3,F12.6)                                           SUM  913
0015      113 FORMAT(2X,2F12.6)                                               SUM  914
0016      114  FORMAT (1X,5F12.6)
0017          READ (1,103) I1,I2                                              SUM 1200
0018          DO 200 J=1,1                                                    SUM 1210
0019      200 READ (1,102) X(J)                                               SUM 1220
0020          DO 600 K=1,1                                                    SUM 1230
0021          READ (1,101) T1, T2, D, L                                       SUM 1240
0022          READ (1,105) (C(I), I=1,40)                                     SUM 1250
0023          CA = C(20)*1521                                                 SUM 1300
0024          CB = -C(40)*40                                                  SUM 1400
0025          DO 500 J=1,1                                                    SUM 1410
0026          PIB2 = ASIN(1.0)                                                SUM 1430
0027          TH = PIB2*X(J)                                                  SUM 1500
0028          P = -(PIB2/(1*D))**2                                            SUM 1900
0029          Q = EXP(P)                                                      SUM 1800
0030          DO 413 R=1,11                                                   SUM 2210
0031          T=(R-1)*T1/10.0                                                 SUM 2220
0032      302 SUM = 0                                                         SUM 2200
0033      304 DO 402 I=1,I1                                                   SUM 2300
0034          N = 2*I - 1                                                     SUM 2400
0035          CALL SERIES (A,C,Q,N,T,TH,SUM,TERM,I,I1,CA,CB)                  SUM 2500
0036      402 CONTINUE                                                        SUM 2600
0037          WRITE (2,106) T                                                 SUM 2700
0038          WRITE (2,106) SUM                                               SUM 2800
0039          IF (T.EQ.0) GO TO 411                                           SUM 2810
0040          V = SUM + 100.0                                                 SUM 2830
0041          GO TO 412                                                       SUM2835
0042      411 V = SUM + 100.0 - (CA/2)*(PIB2**2)*X(J)                         SUM 2850
0043      412 Y(R) = V                                                        SUM 2860
0044          WRITE (2,109)                                                   SUM 2861
0045          WRITE (2,112) R, Y(R)                                           SUM 2870
0046      413 CONTINUE                                                        SUM 4201
0047          DO 424 R=12,22                                                  SUM3240
0048          T=(R-12)*T2/10.0                                                SUM 3250
0049      404 SUM = 0                                                         SUM 3230
0050          DO 403 I = I1 + 1, I1 + I2                                      SUM 3300
0051          N = 2*I - 40                                                    SUM 3400
0052          CALL SERIES (A,C,Q,N,T,TH,SUM,TERM,I,I1,CA,CB)                  SUM 3500
0053      403 CONTINUE                                                        SUM 3600
0054          WRITE (2,106) T                                                 SUM 3700
0055          WRITE (2,106) SUM                                               SUM 3800
0056          IF (T.EQ.0) GO TO 421                                           SUM 3810

0057          V = SUM + 100*(1 - X(J))                                        SUM 3830
0058          GO TO 422                                                       SUM 3840
0059      421 IF (X(J).EQ.1.0) GO TO 423                                      SUM 3855
0060          V = SUM + 100*(1 - X(J)) + (CB/2)*PIB2*X(J)                     SUM 3860
0061          GO TO 422                                                       SUM 3865
0062      423 V=0                                                             SUM 3867
0063          GO TO 422                                                       SUM 3869
0064      422 Y(R) = V                                                        SUM 3870
0065          WRITE (2,109)                                                   SUM 3871
0066          WRITE (2,112) R, Y(R)                                           SUM 3880
0067      424 CONTINUE                                                        SUM 4202
0068      431 AA = 4*(Y(2)+Y(4)+Y(6)+Y(8)+Y(10))
0069          AA = AA+2*(Y(3)+Y(5)+Y(7)+Y(9))
0070          AA = AA+Y(22)+Y(11)
0071          AA = AA*1/3
0072          IF (X(J).EQ.1.0) GO TO 432
0073          AB = 4*(Y(13)+Y(15)+Y(17)+Y(19)+Y(21))
0074          AB = AB+2*(Y(14)+Y(16)+Y(18)+Y(20))
0075          AB = (1.0/3.0)*(AB+Y(11)+Y(22))
0076          GO TO 433
0077      432 AB = 0.0
0078      433 WRITE (2,113) AA,AB                                             SUM4205
0079          AVT = (AA*(T1/T2) + AB )/(10*(T1/T2) + 10)                      SUM 4206
0080          WRITE (2,106) AVT                                               SUM 4207
0081          LI = L*((AVT*X(J))/(100 - AVT) - 1 + X(J))                      SUM 4208
0082          LI2 = LI**2                                                     SUM 4209
0083          FTC = T2/(T1 + T2)                                              SUM 4210
0084          F = 1/(T1 + T2)                                                 SUM 4211
0085          ALPHA = 1/D**2                                                  SUM 4212
0086          GROUP = F*LI2/ALPHA                                             SUM 4213
0087          WRITE (2, 110)                                                  SUM 4214
0088          WRITE (2, 111) FTC, F, LI, GROUP , X(J)                         SUM 4215
0089      500 CONTINUE                                                        SUM 4222
0090      600 CONTINUE                                                        SUM 4223
0091          STOP                                                            SUM 4300
0092          END                                                             SUM 4400

END OF SEGMENT, LENGTH   527, NAME  SUMS

0093          SUBROUTINE SERIES (A,C,Q,N,T,TH,SUM,TERM,I,I1,CA,CB)            SUM 4500
0094          DIMENSION C(40), A(40), TERM(40)                                SUM 4600
0095      108 FORMAT (1X,I4,2X,1F12.6)                                        SUM 4605
0096          IF (T.EQ.0.AND.I.LE.I1) GO TO 601                               SUM 4610
0097          IF (T.EQ.0.AND.I.GT.I1) GO TO 602                               SUM4620


0098          GO TO 603
0099      601 A(N) = C(I) - CA/((-1)**((N+1)/2)*(N**2))                       SUM 4630
0100          WRITE (2,108) N, A(N)                                           SUM 4631
0101          GO TO 604
0102      602 A(N) = C(I) - CB*((-1)**(1+N/2))/N                              SUM 4640
0103          WRITE (2,108) N, A(N)                                           SUM 4650
0104          GO TO 604
0105      603 A(N) = C(I)*(Q**((N**2)*T))                                     SUM 4700
0106      604 TERM(N) = A(N)*SIN(N*TH)                                        SUM 4800
0107          SUM = SUM + TERM(N)                                             SUM 4900
0108          RETURN                                                          SUM 5000
0109          END                                                             SUM 5100

END OF SEGMENT, LENGTH   215, NAME  SERIES

0110          FINISH                                                          SUM 5200
```

Input and Output of Program Groups

* Numbers above program statements in the tables below and overleaf refer to the line number in program GROUPS

Program Statement	Input Data
0017 READ (1,103)I1,I2	I1 = Number of terms in truncated series equation (73) = 20 I2 = Number of terms in truncated series equation (77) = 20
0019 200 READ (1,102) x(J)	X(J) = value of $(\frac{x}{\ell})$ at which temperature is to be calculated
0021 READ (1,101)T1,T2,D,L.	T1 = Time bars are = 10 s (typical value) separated T2 = Time bars are = 10 s (typical value) in contact $D = \frac{1}{\text{Diffusivity}} = \frac{10^6 s}{5m^2} = 477.0 \frac{s^{\frac{1}{2}}}{m}$ l = Length of bar = 0.04m
0022 READ (1,105)(C(I), I = 1,40)	C(I) = A_1 to A_{39} (equation 73, typical values on Appendix 8) where I = 1 to 20 C(I) = B_2 to B_{40} (equation 77, typical values in Appendix 9) where I = 1 to 20

Program Statement	Output Data
0037 00 WRITE (2,106)T	T = Time in seconds from when bars are first separated.
0038 01 WRITE (2,106) SUM	See equation (3) $SUM = \sum_{n=1}^{39} A_n \exp\left\{-\left(\frac{n\pi}{2\ell}\right)^2 \alpha t\right\} \sin\frac{n\pi}{2}\frac{x}{\ell}$
0045 03 WRITE (2,112)R, Y(R)	R = Time step number in period when bars are separated Y(R) = Temperature at time step R
0054 04 WRITE (2,106)T	T = Time in seconds from when bars are first in contact
0055 05 WRITE (2,106) SUM	See equation (4) $SUM = \sum_{n=2}^{40} B_n \exp\left\{-\left(\frac{n\pi}{2\ell}\right)^2 \alpha t\right\} \sin\frac{n\pi}{2}\frac{x}{\ell}$
0066 07 WRITE (2,112)R,Y(R)	R = Time step number from when bars are separated Y(R) = Temperature at time step R (Note temperature at x = 0 is taken as 100K)
0079 08 WRITE (2,106)AVT	AVT = Time-average temperature
0088 10 WRITE (2,111) FTC,F,LI, GROUP X(J)	$FTC = \frac{\tau_1}{\tau_1 + \tau_2}$ F = Frequency of contact $LI = \ell_i$ m. GROUP $= \left(\frac{f\ell_i^2}{\alpha}\right)$ $X(J) = \frac{x}{\ell}$

APPENDIX 11 Spot Verification that temperature-time data output from numerical matrix inversion method satisfied the heat-diffusion equation

The finite- difference form of the heat-diffusion equation (45) at the jth position at the ith instant in time is given by

$$\frac{T_{i+1,j} - T_{i-1,j}}{2\Delta t} = \alpha \left\{ \frac{T_{i,j+1} - 2T_{i,j} + T_{i,j-1}}{(\Delta x)^2} \right\} \quad (11/1)$$

where Δt = time increment

and Δx = distance increment.

Applying this to the data in Tables 7 - 9 at time t = 5s after instant of separation of bars, at distance $(\frac{x}{\ell}) = 0.9$.

where $\Delta x = 0.01 \times 0.04\text{m} = 4 \times 10^{-4}\text{m}$

and $\Delta t = 1\text{s}$

From table 8,

$$T_{i+1,j} = 20.427983 \text{ K}$$

$$T_{i-1,j} = 17.827601 \text{ K}$$

From table 7,

$$T_{i,j+1} = 18.729811 \text{ K}$$

From table 8,

$$T_{i,j} = 19.178909 \text{ K}$$

From table 9,

$$T_{i,j-1} = 19.669464 \text{ K}$$

Then , the left hand side of equation (11/1) becomes

$$\frac{(20.427983 - 17.827601)\text{K}}{2 \times 1\text{s}} = 1.300191 \frac{\text{K}}{\text{s}}$$

and the right hand side of equation (11/1) becomes

$$5 \times 10^{-6} \frac{m^2}{s} \frac{(18.729811 - 2 \times 19.178909 + 19.669464)}{(4 \times 10^{-4})^2 \, m^2} K$$

$$= \frac{5}{16} \times 10^2 \times 0.041457 \frac{K}{s}$$

$$= 1.2955 \frac{K}{s}$$

Agreement between the two sides of equation 11/1 to within ½%.

APPENDIX 12 Effect of small changes in coefficients on solutions to finite-difference equations

Solutions of finite difference equations (3/14),(3/9) to (3/13) and (3/19) when $D(\Delta\Theta_n) = 0$ and also of above equations when various coefficients of $\Delta\Theta_n$ are altered a small amount. Altered element shown ringed thus O Solutions are in the extreme righthand column.

Coefficient Matrix and Vectors — Solution Vector $\Delta\Theta_{n_s}$

$$\begin{bmatrix} -0.098 & 0.89 & 0 & 0 & 0 & 0 & 0 \\ 0.488 & -0.976 & 0.488 & 0 & 0 & 0 & 0 \\ 0 & 0.87 & -7.82 & 6.95 & 0 & 0 & 0 \\ 0 & 0 & 31.25 & -62.5 & 31.25 & 0 & 0 \\ 0 & 0 & 0 & 31.25 & -62.5 & 31.25 & 0 \\ 0 & 0 & 0 & 0 & 31.25 & -62.5 & 31.25 \\ 0 & 0 & 0 & 0 & 0 & 62.5 & -62.5 \end{bmatrix} \cdot \begin{bmatrix} \Delta\Theta_{1_s} \\ \Delta\Theta_{2_s} \\ \Delta\Theta_{3_s} \\ \Delta\Theta_{4_s} \\ \Delta\Theta_{5_s} \\ \Delta\Theta_{6_s} \\ \Delta\Theta_{7_s} \end{bmatrix} = \begin{bmatrix} 0 \\ 0 \\ 0 \\ 0 \\ 0 \\ 0 \\ 0.625 \end{bmatrix} \qquad \begin{bmatrix} 0.78997 \\ 0.86986 \\ 0.94974 \\ 0.95974 \\ 0.96974 \\ 0.97974 \\ 0.98974 \end{bmatrix}$$

Coefficient Matrix and Vectors — Solutio- Vector $\Delta\Theta_{n_s}$

$$\begin{bmatrix} -0.100 & 0.089 & 0 & 0 & 0 & 0 & 0 \\ 0.488 & -0.976 & 0.488 & 0 & 0 & 0 & 0 \\ 0 & 0.87 & -7.82 & 6.95 & 0 & 0 & 0 \\ 0 & 0 & 31.25 & -62.5 & 31.25 & 0 & 0 \\ 0 & 0 & 0 & 31.25 & -62.5 & 31.25 & 0 \\ 0 & 0 & 0 & 0 & 31.25 & -62.5 & 31.25 \\ 0 & 0 & 0 & 0 & 0 & 62.5 & -62.5 \end{bmatrix} \cdot \begin{bmatrix} \Delta\Theta_{1_s} \\ \Delta\Theta_{2_s} \\ \Delta\Theta_{3_s} \\ \Delta\Theta_{4_s} \\ \Delta\Theta_{5_s} \\ \Delta\Theta_{6_s} \\ \Delta\Theta_{7_s} \end{bmatrix} = \begin{bmatrix} 0 \\ 0 \\ 0 \\ 0 \\ 0 \\ 0 \\ -0.625 \end{bmatrix} \qquad \begin{bmatrix} 0.64634 \\ 0.72623 \\ 0.80611 \\ 0.81611 \\ 0.82611 \\ 0.83611 \\ 0.84611 \end{bmatrix}$$

Coefficient Matrix and Vectors	Solution Vector $\Delta\Theta_{n_s}$

$$\begin{bmatrix} -0.098 & 0.089 & 0 & 0 & 0 & 0 & 0 \\ 0.488 & -0.976 & 0.488 & 0 & 0 & 0 & 0 \\ 0 & 0.87 & -7.9 & 6.95 & 0 & 0 & 0 \\ 0 & 0 & 31.25 & -62.5 & 31.25 & 0 & 0 \\ 0 & 0 & 0 & 31.25 & -62.5 & 31.25 & 0 \\ 0 & 0 & 0 & 0 & 31.25 & -62.5 & 31.25 \\ 0 & 0 & 0 & 0 & 0 & 62.5 & -62.5 \end{bmatrix} \begin{bmatrix} \Delta\Theta_{1_s} \\ \Delta\Theta_{2_s} \\ \Delta\Theta_{3_s} \\ \Delta\Theta_{4_s} \\ \Delta\Theta_{5_s} \\ \Delta\Theta_{6_s} \\ \Delta\Theta_{7_s} \end{bmatrix} = \begin{bmatrix} 0 \\ 0 \\ 0 \\ 0 \\ 0 \\ 0 \\ -0.625 \end{bmatrix} \quad \begin{bmatrix} 0.37739 \\ 0.41556 \\ 0.45372 \\ 0.46372 \\ 0.47372 \\ 0.48372 \\ 0.49372 \end{bmatrix}$$

Coefficient Matrix and Vectors	Solution Vector $\Delta\Theta_{n_s}$

$$\begin{bmatrix} -0.098 & 0.089 & 0 & 0 & 0 & 0 & 0 \\ 0.488 & -0.976 & 0.488 & 0 & 0 & 0 & 0 \\ 0 & 0.87 & -7.82 & 6.95 & 0 & 0 & 0 \\ 0 & 0 & 31.25 & -62.5 & 31.25 & 0 & 0 \\ 0 & 0 & 0 & 31.25 & -62.5 & 31.25 & 0 \\ 0 & 0 & 0 & 0 & 31.25 & -63.0 & 31.25 \\ 0 & 0 & 0 & 0 & 0 & 62.5 & -62.5 \end{bmatrix} \begin{bmatrix} \Delta\Theta_{1_s} \\ \Delta\Theta_{2_s} \\ \Delta\Theta_{3_s} \\ \Delta\Theta_{4_s} \\ \Delta\Theta_{5_s} \\ \Delta\Theta_{6_s} \\ \Delta\Theta_{7_s} \end{bmatrix} = \begin{bmatrix} 0 \\ 0 \\ 0 \\ 0 \\ 0 \\ 0 \\ -0.625 \end{bmatrix} \quad \begin{bmatrix} 0.30767 \\ 0.33878 \\ 0.36990 \\ 0.37379 \\ 0.37769 \\ 0.38158 \\ 0.39158 \end{bmatrix}$$

APPENDIX 13 Derivation of boundary condition during contact period; (imperfect contact), finite difference method

For finite-difference equations the same mesh as in Appendix 3 was used. Fig 13-1 shows the instantaneous dimensionless temperature distribution in the hotter bar during the contact period.

Since the identical mesh to that used in Appendix 3 is employed, the finite-difference form of the heat diffusion equation at the contact end (X_7) of the bar is

$$D(\Theta_7) = \frac{\partial \Theta_7}{\partial t} = \frac{\alpha}{\ell^2} \left\{ \frac{\Theta_8 - 2\Theta_7 + \Theta_6}{(\Delta X)^2} \right\} \qquad (13/1)$$

where Θ_8 is a fictitious temperature.

To satisfy boundary condition 2(ii) in section 4.3.2.3, Θ_8 is given a value such that the slope of the tangent to the instantaneous temperature distribution at the contact end of the bar (at X_7) is given by

$$\frac{\partial \Theta_7}{\partial X} = - \Theta_7 \frac{\ell}{\lambda} \qquad (13/2)$$

The finite-difference form of boundary condition 2(ii) is then

$$\frac{\Theta_8 - \Theta_6}{2\Delta X} = - \Theta_7 \frac{\ell}{\lambda} \qquad (13/3)$$

so that

$$\Theta_8 = \Theta_6 - \frac{2\ell\Delta X}{\lambda} \Theta_7 \qquad (13/4)$$

Substituting for Θ_8 in equation (13/1) gives

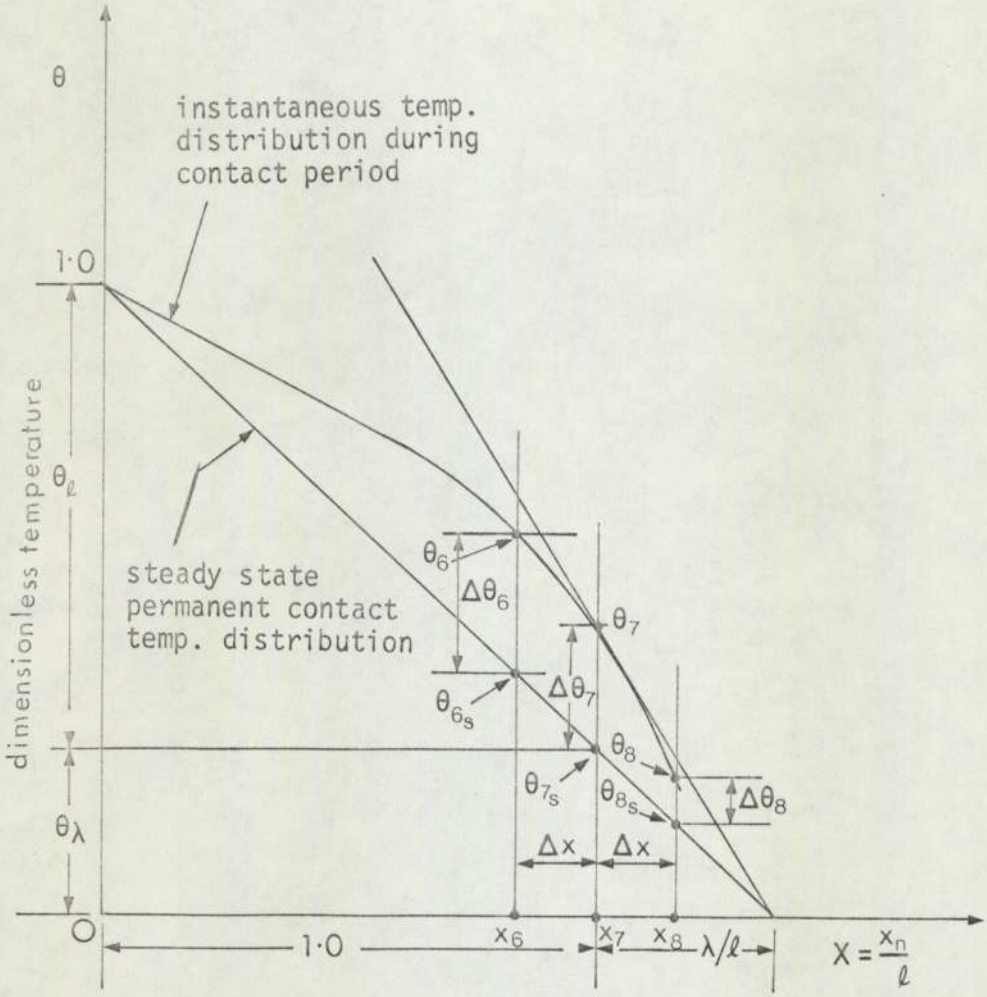

Fig. 13-1 Steady state and instantaneous temperature distribution

$$D(\Theta_7) = \frac{\partial\Theta 7}{\partial t} = \frac{2\alpha}{\ell^2(\Delta X)^2}\left\{\Theta_6 - \Theta_7(1 + \frac{\ell\Delta X}{\lambda})\right\} \qquad (13/5)$$

As in Appendix 3, the values chosen for (α/ℓ^2) and ΔX were respectively $0.3125 \times 10^{-2}\ s^{-1}$ and 0.01 respectively. Likewise, the datum from which temperature is to be measured was the steady state permanent contact temperature distribution,

Referring to Fig 13-1

$$\Theta_6 = \Theta_{6_s} + \Delta\Theta_6 \qquad (13/6)$$

$$\Theta_7 = \Theta_{7_s} + \Delta\Theta_7 \qquad (13/7)$$

and if we write Θ_ℓ for the temperature drop due to the solid resistance of the bar (of length ℓ) and Θ_λ for the temperature drop due to $\frac{1}{2}$ x thermal contact resistance (equivalent to length λ of bar) then substitution into equation (13/5) gives

$$D(\Delta\Theta_7) = 62.5\left\{\Delta\Theta_6 - \Delta\Theta_7(1 + \frac{\ell}{100\lambda}) + \frac{1}{100}(\Theta_\ell - \frac{\ell}{\lambda}\Theta_\lambda)\right\}\ s^{-1}$$

(13/8)

and by similar triangles (Fig.13-1)

$$\Theta_\ell = \frac{\ell}{\lambda}\Theta_\lambda \qquad (13/9)$$

and hence the required boundary condition in finite-difference form is

$$D(\Delta\Theta_7) = 62.5\,\Delta\Theta_6 - 62.5\,\Delta\Theta_7(1 + \frac{\Theta_\ell}{100\Theta_\lambda})\ s^{-1} \qquad (13/9)$$

Finally if $\Theta_\lambda = 0$, equation (13/9) reduces to $\Delta\Theta_7 = 0$, which is the boundary condition during the contact period when there is perfect thermal contact at the contact interface, (equation (13/15) in Appendix 3.)

APPENDIX 14

ITERATIVE PROCESS FOR SOLUTION OF HEAT DIFFUSION EQUATION - (IMPERFECT CONTACT)

Boundary condition at $x = \ell$

Referring to Fig 27(m), at the mth iteration at $x = \ell$

$$\left.\frac{\partial T_m(x,t)}{\partial x}\right|_{x=\ell} = f(t).\ T_{m-1}(\ell,t) \qquad (14/1)$$

where f(t) is a periodic function of time.

The right side of equation (14/1) can also be written as the periodic function

$$\left.\frac{\partial T_m(x,t)}{\partial x}\right|_{x=\ell} = \sum_{n=-\infty}^{\infty} C_{m,n}(\ell)\ \exp\left(2\pi jn\ \frac{t}{\tau}\right) \qquad (14/2)$$

where $$C_{m,n}(\ell) = a_{m,n}(\ell) + j\ b_{m,n}(\ell) \qquad (14/3)$$

$a_{m,n}(\ell)$ and $b_{m,n}(\ell)$ both being real.

At the $(m-1)^{th}$ iteration at $x = \ell$, let the temperature $T_{m-1}(\ell,t)$ be given by

$$T_{m-1}(\ell\ t) = \sum_{L=-\infty}^{\infty} r_{m-1,L}(\ell)\ .\ \exp\left(2\pi jL\ \frac{t}{\tau}\right) \qquad (14/4)$$

where $r_{m-1,L}(x)$ is a function of x given by

$$r_{m-1,L}(x) = p_{m-1,L}(x) + jq'_{m-1,L}(x) \qquad (14/5)$$

$p_{m-1,L}(x)$ and $q_{m-1,L}(x)$ both being real.

Since $T_{m-1}(\ell,t)$ is real, then using equations (14/4) and (14/5) the imaginary part of

$$\sum_{L=-\infty}^{\infty} \left[\left\{p_{m-1,L}(x) + jq_{m-1,L}(x)\right\}\left\{\cos(2\pi L\frac{t}{\tau}) + j\sin(2\pi L\frac{t}{\tau})\right\}\right]$$

is zero, from which it follows that for $L \neq 0$ $p_{m-1,L}(x)$ is an even function of L and $q_{m-1,L}(x)$ is an odd function of L. For L = 0, $q_{m-1,o}(x) = 0$.

Let the periodic function of time, in equation (14/1), f(t), be written in the form

$$f(t) = \sum_{n=-\infty}^{\infty} \omega_n . \exp(2\pi jn\frac{t}{\tau}) \qquad (14/6)$$

where $\omega_b = u_n + jv_n$ (14/6a)

(u_n and v_n being real)

Equating equation (14/1) to (14/2) and substituting for f(t) and T_{m-1} from equations (14/4) and (14/6) gives

$$\left[\sum_{n=-\infty}^{\infty} \omega_n . \exp(2\pi jn\frac{t}{\tau})\right] . \left[\sum_{L=-\infty}^{\infty} r_{m-1,L}(e) . \exp(2\pi j L\frac{t}{\ell})\right]$$

$$= \sum_{m=-\infty}^{\infty} C_{m,n}(\ell) \exp(2\pi jn\frac{t}{\tau}) \qquad (14/7)$$

The left hand side of equation (14/7) may be written as

$$\sum_{n=-\infty}^{\infty} \sum_{L=-\infty}^{\infty} \omega_n \, r_{m-1,L}(\ell) \exp(2\pi j(n+L)\frac{t}{\tau}) \qquad (14/8)$$

Putting n+ L = k this then becomes

$$\sum_{K-L=-\infty}^{\infty} \left\{ \left(\sum_{L=-\infty}^{\infty} \omega_{K-L}\, r_{m-1,L}(\ell) \right) \exp\left(2\pi jk \frac{t}{\tau}\right) \right\} \qquad (14/8)$$

Equating coefficients of the exponential on both sides of equation (14/7) and then putting k = n

$$C_{m,n}(\ell) = \sum_{L=-\infty}^{\infty} r_{m-1,L}(\ell)\, \omega_{n-L} \qquad (14/9)$$

Substituting for $r_{m-1,L}(\ell)$ and ω_{n-L} from equations (14/3) and (14/4) gives the relationship

$$a_{m,n}(\ell) + jb_{m,n}(\ell) = \sum_{L=-\infty}^{\infty} \left(p_{m-1,L}(\ell) + jq_{m-1,L}(\ell)\right)\left(u_{n-L} + jv_{n-L}\right) \qquad (14/20)$$

Hence at $x=\ell$

$$a_{m,n}(\ell) = \sum_{L=-\infty}^{\infty} (p_{m-1,L}(\ell)\, u_{n-L} - q_{m-1,L}(\ell)\, v_{n-L}) \qquad (14/21)$$

$$b_{m,n}(\ell) = \sum_{L=-\infty}^{\infty} (p_{m-1,L}(\ell)\, v_{n-L} + q_{m-1,L}(\ell) \cdot u_{n-L}) \qquad (14/22)$$

Solution, $T_m(x,t)$ for $0 < x < \ell$

Let the solution of the heat diffusion equation within the bar, Fig 29(m) at the mth iteration be written in the form

$$T_m(x,t) = \sum_{n=-\infty}^{\infty} C_{m,n}(\ell) \cdot f_n(x) \cdot \exp\left(2\pi jn \frac{t}{\tau}\right) \qquad (14/23)$$

where $\quad f_n(x) = g_n(x) + h_n(x) \qquad (14/24)$

$g_n(x)$ and $h_n(x)$ being real functions of x (The appropriate expression for $f_n(x)$ is derived in Appendix 16).

Substitution for $C_{m,n}(\ell)$ and $f_n(x)$ in equation (14/23), using equations (14/3) and (14/24) yields

$$T_m(x,t) = \sum_{n=-\infty}^{\infty} \left[(a_{m,n}(\ell) + jb_{m,n}(\ell)).(g_n(x) + jh_n(x)).\exp(2\pi n \frac{t}{\tau}) \right] \tag{14/25}$$

$a_{m,n}(x)$ and $b_{m,n}(x)$ being defined by equations (14/21) and (14/22).

Sequence of computation

(a) Starting values

Fig.27(i) shows the conditions at the commencement of iteration. The solution $T_o(x,t)$ is arbitrary, but it is convenient to choose

$$T_o(x,t) = T_A \quad \text{(constant)} \tag{14/26}$$

Using equations (14/4) and (14/5) with m = 1;

$$T_o(x,t) = \sum_{L=-\infty}^{\infty} \left[\left\{ p_{o,L}(x) + jq_{o,L}(x) \right\} . \exp\left(2\pi jL \frac{t}{\tau}\right) \right] = T_A \tag{14/27}$$

The real part of equation (14/27) is given by

$$\sum_{L=-\infty}^{\infty} \left[p_{o,L}(x) \cos\left(2\pi L \frac{t}{\tau}\right) - q_{o,L}(x) \sin\left(2\pi L \frac{t}{\tau}\right) \right] \equiv T_A \tag{14/28}$$

To find the $p_{o,L}(x)$ multiply both sides by $\cos(2\pi k\frac{t}{\tau})$ and integrating with respect to time between t = 0 and t = τ gives

$$\int_0^{\tau} T_A \cos\left(2\pi k \frac{t}{\tau}\right) dt = \sum_{L=-\infty}^{\infty} \int_0^{\tau} \left(p_{o,L}(x) \cos\left(2\pi L \frac{t}{\tau}\right) \cos\left(2\pi k \frac{t}{\tau}\right) - q_{o,L}(x) \sin\left(2\pi L \frac{t}{\tau}\right) \cos\left(2\pi k \frac{t}{\tau}\right) \right) dt \tag{14/29}$$

Terms in the right hand side are all zero except for the case when $K = L$ so that

$$\int_0^\tau T_A \cos\left(2\pi L \frac{t}{\tau}\right) dt = p_{o,L}(x) \int_0^\tau \tfrac{1}{2}\left[\cos\left(4\pi L \frac{t}{\tau}\right) + 1\right] dt$$

$$+ q_{o,L}(x) \int_0^\tau \tfrac{1}{2} \sin\left(4\pi L \frac{t}{\tau}\right) dt = \frac{\tau}{2} p_{o,L}(x).$$

For $L \neq 0$,

$$p_{0,L}(x) = 0 \qquad (14/30)$$

For $L = 0$

$$\int_0^\tau T_A \, dt = p_{o,o}(x) \int_0^\tau dt$$

$$\therefore \quad p_{o,o}(x) = T_A \qquad (14/31)$$

To find the $q_{o,L}(x)$ multiply both sides of (14/28) by $\sin\left(2\pi k \frac{t}{\tau}\right)$ and integrate between $t = 0$ and $t = \tau$. Terms in the right hand side of (14/28) are then zero except for $k = L$ term. Hence

$$\int_0^\tau T_A \sin\left(2\pi L \frac{t}{\tau}\right) dt = p_{o,L}(x) \int_0^\tau \tfrac{1}{2}\sin\left(4\pi L \frac{t}{\tau}\right) dt$$

$$+ q_{o,L}(x) \int_0^\tau \tfrac{1}{2}\left(\cos 4\pi L \frac{t}{\tau} + 1\right) dt$$

giving $\quad q_{o,L}(x) = 0 \qquad (14/32)$

for all L

Equations (14/30) to (14/32) can be used as starting values to generate the $a_{m,n}(x)$ and $b_{m,n}(x)$ defined by equations (14/21) and (14/22) when $m = 1$. (Note that $a_{o,n}(x)$ and $b_{o,n}(x)$ are both zero since $p_{-1,L}(x)$ and $q_{-1,L}(x)$ do not exist.

The $p_{m-1,L}(x)$ and $q_{m-1.L}(x)$ for $m > 1$ are obtained from equations (14/36) and (14/37). In (x) and $h_n(x)$ are defined by equations (14/40) and (14/41)

(b) <u>Expressions for $p_{m,L}(x)$, $q_{m,L}(x)$ $g_n(x)$ and $h_n(x)$</u>

Using equations (14/4) and (14/5) substituting m for (m-1) gives

$$T_m(x,t) = \sum_{L=-\infty}^{\infty} \left[\left\{ p_{m,L}(x) + jq_{m,L}(x) \right\} . \exp\left(2\pi jL \frac{t}{\tau}\right) \right] \qquad (14/34)$$

Equating (14/34) to (14/25) gives

$$\sum_{L=-\infty}^{\infty} \left\{ p_{m,L}(x) + jq_{m,L}(x) . \exp\left(2\pi jL \frac{t}{\tau}\right) \right\} = \sum_{n=-\infty}^{\infty} \left[\left\{ a_{m,n}(x) + j_{m,n}b(x) \right\} \times \left\{ g_n(x) + jh_n(x) \right\} . \exp\left(2\pi jn \frac{t}{\tau}\right) \right] \qquad (14/35)$$

Equating real and imaginary parts of (14/35) gives:-

Real terms

$$P_{m,n}(x) = a_{m,n}(x) . g_n(x) - b_{m,n}(x) . h_n(x) \qquad (14/36)$$

Imaginary Terms

$$q_{m,n}(x) = a_{m,n}(x) . h_n(x) + b_{m,n}(x) . g_n(x) \qquad (14/37)$$

The functions $g_n(x)$ and $h_n(x)$ required above are obtained as follows

It is shown in Appendix 16 that $f_n(x)$, (equation (14/23) be given by

$$f_n(x) = \frac{\mathrm{sh}\left(\alpha x \sqrt{\frac{2\pi n j}{\tau}}\right)}{\left(\alpha\sqrt{\frac{2\pi n j}{\tau}} \cdot \mathrm{ch}\left(\alpha\ell\sqrt{\frac{2\pi n j}{\tau}}\right)\right)} \qquad (14/38)$$

(Note that sh and ch are hyperbolic sine and cosine)

Since $f_n(x) = g_n(x) + jh_n(x)$, see equation (14/24) and writing

$$A_n = \alpha\sqrt{\frac{\pi n}{\tau}} \qquad (14/39)$$

it can be shown that for n = 0

$$g_n(x) = \frac{\left[\begin{array}{l}(\mathrm{sh}A_n x) \cdot (\cos A_n x) \cdot (\mathrm{ch}A_n \ell) \cdot (\cos A_n \ell) + \\ (\mathrm{ch}A_n x) \cdot (\sin A_n x) \cdot (\mathrm{sh}A_n \ell) \cdot (\sin A_n \ell) + \\ (\mathrm{ch}A_n x) \cdot (\sin A_n x) \cdot (\mathrm{ch}A_n \ell) \cdot (\cos A_n \ell) - \\ (\mathrm{sh}A_n x) \cdot (\cos A_n x) \cdot (\mathrm{sh}A_n \ell) \cdot (\sin A_n \ell)\end{array}\right]}{2A_n\left[(\mathrm{ch}^2 A_n \ell)(\cos^2 A_n \ell) + (\mathrm{sh}^2 A_n \ell) \cdot (\sin^2 A_n \ell)\right]}$$

(14/40)

and

$$h_n(x) = \frac{\left[\begin{array}{l}(\mathrm{ch}A_n x)(\sin A_n x)(\mathrm{ch}A_n \ell)(\cos A_n \ell) - \\ (\mathrm{sh}A_n x)(\cos A_n x)(\mathrm{sh}A_m \ell)(\sin A_n \ell) - \\ (\mathrm{sh}A_n x)(\cos A_n x)(\mathrm{ch}A_n \ell)(\cos A_n \ell) - \\ (\mathrm{ch}A_n x)(\sin A_n x)(\mathrm{sh}A_n \ell)(\sin A_n \ell)\end{array}\right]}{2A_n\left[(\mathrm{ch}^2 A_n \ell)(\cos^2 A_n \ell) + (\mathrm{sh}^2 A_n \ell)(\sin^2 A_n \ell)\right]}$$

(14/41)

When n = 0

$$g_o(x) = x \tag{14/42}$$

$$h_o(x) = 0 \tag{14/43}$$

Note that

$$g_n(\ell) = \frac{(\mathrm{sh}2A_n\ell)(\cos 2A_n\ell) + (\mathrm{ch}2A_n\ell)(\sin 2A_n\ell)}{4A_n\left[(\mathrm{ch}^2A_n\ell) - (\sin^2A_n\ell)\right]} \tag{14/44}$$

$$h_n(\ell) = \frac{(\mathrm{ch}2A_n\ell)(\sin 2A_n\ell) - (\mathrm{sh}2A_n\ell)(\cos 2A_n\ell)}{4A_n\left[(\mathrm{ch}^2A_n\ell) - (\sin^2A_n\ell)\right]} \tag{14/45}$$

$$g_o(\ell) = \ell \tag{14/46}$$

and

$$h_o(\ell) = 0 \tag{14/47}$$

(c) Equations of iteration

Equation (14/34) is used to calculate temperature $T_m(x,t)$ at the mth iteration. $T_m(x,t)$ is real so that

$$T_m(x,t) = \sum_{L=-\infty}^{\infty}\left\{p_{m,L}(x).\cos(2\pi L\frac{t}{\tau}) - q_{m,L}(x).\sin(2\pi L\frac{t}{\tau})\right\}$$

$$= p_{m,o}(x) + 2\sum_{L=1}^{\infty}\left\{p_{m,L}(x)\cos(2\pi L\frac{t}{\tau}) - q_{m,L}(x)\sin(2\pi L\frac{t}{\tau})\right\} \tag{14/48}$$

since from equations (14/4) and (14/5) $p_{m,L}(x)$ is an even function of L and $q_{m,L}(x)$ is an odd function of L.

Finally, the temperature at a given point, x, at a given time, t, is given by

$$T(x,t) = \sum_{m=0}^{\infty} T_m(x,t) \qquad (14/49)$$

Since only the time-average temperature is required for computation of the length, ℓ_i, of bar equivalent to the thermal resistance due to periodic interruption of the heat flow, the periodic part of equation (14/48) need not be computed. So that the time-average temperature, $\overline{T}(x)$ is given by:

$$\overline{T}(x) = \sum_{m=0}^{\infty} p_{m,o}(x) \qquad (14/50)$$

with $$\overline{T}_m(x) = p_{m,o}(x) \qquad (14/51)$$

which using equation (14/36) gives

$$\overline{T}(x) = \sum_{m=o}^{\infty} \left\{ a_{m,o}(x) \cdot g_o(x) - b_{m,o}(x) h_o(x) \right\} \qquad (14/52)$$

But from equations 14/42 and 14/43 $g_o(x) = x$ and $h_o(x) = o$. Hence

$$\overline{T}(x) = \sum_{m=o}^{\infty} \left\{ a_{m,o}(x) \cdot x \right\} \qquad (14/53)$$

From equation (14/21)

$$a_{m,o}(x) = \sum_{L=-\infty}^{\infty} \left\{ p_{m-1,L}(x)\, u_{-L} - q_{m-1,L}(x)\, v_{-L} \right\} \qquad (14/54)$$

If the function f(t) in equation (14/6) is such that an origin can be chosen so that f(t) is made into an even function of time, t, then the v_n in equation (14/6a) is zero for all n and the $u_n = u_{-n}$. (Fig. 15 - 1 in Appendix 15 shows wave form of the function f(t) used to express the boundary condition 2 at $x = \ell$, section 4.3.2.3) $p_{m-1,L}(x)$ is an even function (see argument after equation (14/5)).

Equation (14/54) can then be written

$$a_{m,o}(x) = 2\left\{\sum_{L=-}^{\infty} p_{m-1,L}(x) \cdot u'_L\right\} + p_{m-1,o}(x)\, u'_o \qquad (14/55)$$

where u'_L and u'_o are the values of the u_n in equation (14/6a) when f(t) is an even function. Similarly equation (14/21) can be written:-

$$a_{m,n}(x) = \sum_{L=-\infty}^{\infty} \left\{p_{m-1,L}(x) \cdot u'_{n-L}\right\}$$

$$= \sum_{L=1}^{\infty} \left\{p_{m-1,L}(x) \cdot u'_{n-L}\right\} + \sum_{L=-1}^{-\infty} \left\{p_{m-1,L}(x) \cdot u'_{n-L}\right\}$$

$$+ p_{m-1,o}(x) \cdot u'_n \qquad (14/56)$$

For programming purposes it is desirable that subscripts are positive numbers. Since the function f(t) is an even function of time $u'_{n-L} = u'_{n-L}$ and $p_{m-1,L}(x)$ is an even function of x (equation (14/5)), eq. (14/56) may be written:-

$$a_{m,n}(x) = \sum_{L=1}^{n-1} \left\{p_{m-1,L}(x) \cdot u'_{n-L}\right\} + \sum_{L=n+1}^{\infty} \left\{p_{m-1,L}(x) \cdot u'_{L-n}\right\}$$

$$+ p_{m-1,n}(x) \cdot u_o + \sum_{L=1}^{\infty} \left\{p_{m-1,L}(x) \cdot u'_{n+1}\right\} + p_{m-1,o}(x) \cdot u'_n$$

$$(14/57)$$

<u>NOTE</u> <u>Restrictions</u>

When using equation (14/57) it should be noted that there are restrictions on the value of n in two expressions. This arises as follows:- Equating the right hand side of equation (14/56) to the right hand side of equation (14/57) leads to:-

$$\sum_{L=1}^{\infty} p_{m-1,L}(x).u_{n-L} = \sum_{L=1}^{n-1}\left\{p_{m-1,L}(x).u'_{n-L}\right\} + \sum_{L=n+1}^{\infty}\left\{p_{m-1,L}(x).u'_{L-n}\right\}$$

$$+ p_{n-1,n}(x).u'_o \qquad (14/57a)$$

When n = o, the terms

$$\sum_{L=1}^{n-1}\left\{p_{m-1,L}(x).u'_{n-L}\right\} + p_{m-1,n}(x)\ u'_o$$

should not be included in the right hand side, otherwise the two sides of (14/57a) will not be equal.

Similarly the term

$$\sum_{L=1}^{n-1}\left\{p_{m-1,L}(x).u'_{n-L}\right\}$$

should be included only when $n \geqslant 2$.

Thus equation (14/57) is re-written as

$$a_{m,n}(x) = \boxed{\sum_{L=1}^{n-1}\left\{p_{m-1,L}(x).u'_{n-L}\right\}} \quad \text{for } n \geqslant 2$$

$$+ \sum_{L=n+1}^{\infty}\left\{p_{m-1,L}(x).u'_{n-L}\right\} + \boxed{p_{m-1,n}(x).u'_o} \quad \text{for } n \neq 0$$

$$+ \sum_{L=1}^{\infty}\left\{p_{m-1,L}(x)\ u'_{n-L}\right\} + p_{m-1,o}(x)\ u'_n \qquad (14/57b)$$

Likewise, equation (14/22) is reduced to

$$b_{m,n}(x) = \sum_{L=-\infty}^{\infty} \left\{ q_{m-1,L}(x) . u'_{n-L} \right\}$$

$$= \sum_{L=1}^{\infty} \left\{ q_{m-1,L}(x) . u'_{n-L} \right\} + \sum_{L=-1}^{-\infty} \left\{ q_{m-1,L}(x) . u'_{n-L} \right\}$$

$$+ \; q_{n-1,o}(x) \; u'_n \qquad (14/58)$$

But sin $q_{m-1,L}(x) = - q_{m-1,L}(x)$, and $u'_{n-L} = u'_{L-n}$

$$b_{m,n}(x) = \sum_{L=1}^{\infty} \left\{ q_{m-1,L}(x) . u'_{n-L} \right\} - \sum_{L=1}^{\infty} \left\{ q_{m-1,L}(x) . u'_{n+L} \right\} + q_{m-1,o}(x) . u'_n$$

$$= \sum_{L=1}^{n-1} \left\{ q_{m-1,L}(x) . u'_{n-L} \right\} + \sum_{L=n+1}^{\infty} \left\{ q_{m-1,L}(x) . u'_{L-n} \right\}$$

$$+ q_{m-1,n}(x) . u'_o - \sum_{L=1}^{\infty} \left\{ q_{m-1,L}(x) . u'_{n+L} \right\} + q_{m-1,o}(x) . u'_A$$

(14/59)

<u>NOTE</u> <u>Restrictions</u>

When using equation (14/59), there are restrictions on the value of n as follows:

Equating right hand sides of equations (14/58) and (14/59) leads to:

$$\sum_{L=1}^{\infty}\left\{q_{m-1,L}(x).u'_{n-L}\right\} = \sum_{L=1}^{n=1}\left\{q_{m-1,L}(x).u'_{n-L}\right\} + \sum_{L=n+1}^{\infty}\left\{q_{m-1,L}(x).u'_{L-n}\right\}$$

$$+ \; q_{m-1,n}(x).u'_{o} \qquad (14/59a)$$

When n = 0

$$\sum_{L=1}^{n-1}\left\{q_{m-1,L}(x).u'_{n}\right\} \quad + q_{m-1,n}(x).u'_{o}$$

should be excluded from (14/59a) otherwise the two sides will be unequal.

Similarly

$$\sum_{L=1}^{n-1}\left\{q_{m-1,L}(x).u'_{n-L}\right\} \qquad \text{should be included}$$

only when $n \geqslant 2$.

Thus equation (14/59) must be written

$$b_{m,n}(x) = \boxed{\sum_{L=1}^{n=1}\left\{q_{m-1,L}(x)\; u'_{n-L}\right\}} \quad + \sum_{L=1}^{\infty}\left\{q_{m-1,L}(x).u'_{n+L}\right\}$$

when $n \geqslant 2$

$$+ \boxed{q_{m-1,n}(x).u'_{o}} \quad - \sum_{L=1}^{\infty}\left\{q_{m-1,L}(x)u'_{n+L}\right\} + q_{m-1,o}(x).u'_{n}$$

when n = o

(14/59b)

Equations of iteration

The equations of iteration are therefore equations (14/57c),(14/59), (14/36) and (14/37) with equations (14/30), (14/31) and (14/32) as starting values. Gathering all these equations together:

$$p_{o,L}(x) = 0 \text{ for } L \neq 0 \qquad (14/30)$$

$$p_{o,o}(x) = T_A \qquad (14/31)$$

$$q_{o,L}(x) = 0 \text{ for all } L \qquad (14/32)$$

For $m > 1$

$$a_{m,n}(x) = \underbrace{\boxed{\sum_{L=1}^{n-1} \left\{ p_{m-1,L}(x).u_{n-L} \right\}'}}_{\text{only when } n>2} + \sum_{L=n+1}^{\infty} \left\{ p_{m-1,L}(x).u'_{L-n} \right\}$$

$$+ \underbrace{\boxed{p_{m-1,L}(x).u'_o}}_{\text{only when } n \neq 0} + \sum_{L=1}^{\infty} \left\{ p_{m-1,L}(x).u'_{n+1} \right\}$$

$$+ \; p_{m-1,o}(x).u'_n \qquad (14/57b)$$

$$b_{m,n}(x) = \underbrace{\sum_{L=1}^{n-1} \left\{ q_{m-1,L}(x).u'_{n-L} \right\}}_{\text{only when } n>2} + \sum_{L=n+1}^{\infty} \left\{ q_{m-1,L}(x).u'_{L-n} \right\}$$

$$+ \underbrace{\boxed{q_{m-1,n}(x).u'_o}}_{\text{only when } n \neq o} - \sum_{L=1}^{\infty} \left\{ q_{m-1,L}(x).u'_{L+n} \right\} + q_{m-1,o}(x).u'_n \qquad (14/59b)$$

$$p_{m,n}(x) = a_{m,n}(x).g_n(x) - b_{m,n}(x).h_n(x) \qquad (14/36)$$

$$q_{m,n}(x) = a_{m,n}(x).h_n(x) + b_{m,n}(x)g_n(x) \qquad (14/37)$$

with $g_o(x) = x$ and $h_o(x) = o$

$$\overline{T}_m(x,t) = p_{m,o}(x)$$

<u>m = o</u>

<u>n = o</u>

$p_{-1,L}(x)$ does not exist hence

$a_{o,o}(x) = 0$

$q_{-1,L}(x)$ does not exist

$b_{o,o}(x) = 0$

$p_{o,o}(x) = T_A$

$q_{o,o} = 0$

$T_o(x,t) = T_A$

<u>n ≥1</u>

$p_{-1,L}(x)$ & $q_{-1,L}(x)$ do not exist

$$\left.\begin{array}{l} a_{o,n}(x) \\ b_{o,n}(x) \\ p_{o,n}(x) \\ q_{o,n}(x) \end{array}\right] \text{— all = zero}$$

<u>m = 1</u>

<u>n = 0</u>

$$a_{1,o}(x) = 2\sum_{L=1}^{\infty}\left\{p_{o,L}(x).u_L'\right\} + p_{o,o}(x)u_o' = p_{o,o}(x)u_o'$$

$$= \underline{T_A u_o'}$$

$b_{1,o}(x) = 0$ from (14/32) above

$p_{1,o}(x) = a_{1,o}(x)\, g_o(x) = a_{1,o}(x)x = T_A u_o' x$

$$q_{1,o}(x) = 0 \text{ from } (14/37)$$

$$T_1(x,t) = T_A u_o' x$$

<u>n=1</u>

$$a_{1,1}(x) = p_{o,o}(x).u_1' = T_A u_1'$$

$$b_{1,1}(x) = 0$$

$$p_{1,1}(x) = a_{1,1}(x).g_1(x)$$

$$q_{1,1}(x) = a_{1,1}(x).h_1(x)$$

<u>n≥2</u>

$$a_{1,n}(x) = p_{o,o}(x).u_n' = T_A.u_n'$$

$$b_{1,n} = 0$$

$$p_{1,n}(x) = a_{1,n}(x)\, g_n(x)$$

$$q_{1,n}(x) = a_{1,n}(x).h_n(x)$$

<u>m ≥ 2</u>

<u>n=0</u>

$$a_{m,o}(x) = 2\sum_{L=1}^{\infty}\left\{p_{m-1,L}(x).u_L'\right\} + p_{m-1,o}(x).u_o'$$

$$b_{m,o}(x) = q_{1,o}(x)\, u_n' = 0$$

$$p_{m,o}(x) = a_{m,o}(x)\, g_o(x) = a_{m,o}(x).x$$

$$q_{m,o}(x) = 0$$

$$T_m(x,t) = p_{m,o}(x) = \left[2\sum_{L=1}^{\infty}\left\{p_{m-1,L}(x)\, u_L'\right\} + p_{m-1,o}(x)u_o'\right]x$$

<u>n=1</u>

$$a_{m,1}(x) = \sum_{L=2}^{\infty}\left\{p_{m-1,L}(x).u_{L-1}'\right\} + p_{m-1,1}(x)u_o' + \sum_{L=1}^{\infty}\left\{p_{m-1,1}(x).u_{1+L}'\right\}$$

$$+ p_{m-1,o}(x)\, u_1'$$

$$b_{m,1}(x) = \sum_{L=2}^{\infty}\left\{q_{m-1,L}(x).u'_{L-1}\right\} + q_{m-1,1}(x)u_o - \sum_{L=1}^{\infty}\left\{q_{m-1,L}(x)u'_{L+1}\right\}$$

$$+ q_{m-1,o}(x).u'_1$$

$$p_{m,1}(x) = a_{m,1}(x).g_1(x) - b_{m-1,1}(x)h_1(x)$$

$$q_{m,1}(x) = a_{m,1}(x)h_1(x) + b_{m,1}(x)g_1(x)$$

<u>$n \geqslant 2$</u>

As per equations (14/57) and (14/59)

$$a_{m,n}(x) = \sum_{L=1}^{n-1} p_{m-1,L}(x).u_{n-L} + \sum_{L=n+1}^{\infty}\left\{p_{m-1,L}(x).u'_{L-n}\right\}$$

$$+ p_{m-1,n}(x).u'_o + \sum_{L=1}^{\infty}\left\{p_{m-1,L}(x).u'_{n+L}\right\} + p_{m-1,o}(x).u'_n$$

$$b_{m,n}(x) = \sum_{L}^{n-1}\left\{q_{m-1,L}(x).u'_{n-L}\right\} + \sum_{L=n+1}^{\infty}\left\{q_{m-1,L}(x).u'_{L-n}\right\}$$

$$+ q_{m-1,n}(x)u'_o - \sum_{L=1}^{\infty}\left\{q_{m-1,L}(x)u'_{n+1}\right\} + q_{m-1,o}(x).u'_n$$

$$p_{m,n}(x) = a_{m,n}(x).g_n(x) - b_{m,n}(x)h_n(x)$$

$$q_{m,n} = a_{m,n}(x).h_n(x) + b_{m,n}(x)g_n(x)$$

APPENDIX 15

Series for f(t)

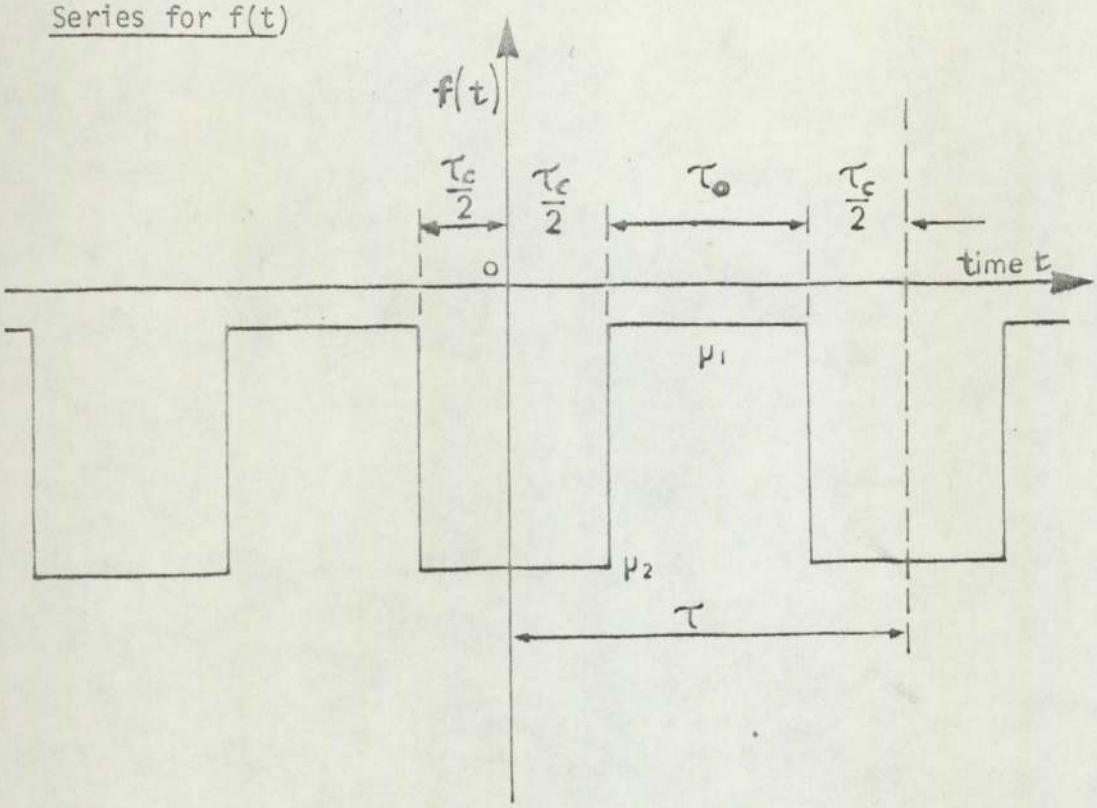

Fig. 15-1 Function f(t)

Fig. 15-1 shows that wave form of the function f(t) appropriate to boundary condition 2 at $x = \ell$, section 4.3.2.3. The origin has been arranged to make f(t) an even function of time. The series for f(t) will therefore be of the form

$$f(t) = u_o'' + \sum_{n=1}^{\infty} u_n'' \cos\left(2\pi n \frac{t}{\tau}\right) \qquad (15/1)$$

Coefficients u_n'' are obtained as follows:

Multiplying both sides of (15/1) by $\cos 2\pi n \frac{t}{\tau}$ and integrating from $t = o$ to $t = \tau/2$

$$\int_o^{\tau} f(t).\cos\left(2\pi m \frac{t}{\tau}\right)dt = \sum_{n=1}^{\infty} \int_o^{\tau} u_n'' \cos\left(2\pi n \frac{t}{\tau}\right) \cos\left(2\pi m \frac{t}{\tau}\right) dt \qquad (15/2)$$

Terms on the right hand side of equation (15/2) are all zero except when m = n hence

$$2\int_0^{\tau/2} f(t)\cos 2\pi n\frac{t}{\tau}\,dr = 2u_n''\int_0^{\tau/2}\cos^2 2\pi n\frac{t}{\tau}\,dr \qquad (15/3)$$

so

$$\int_0^{\tau_c/2}\mu_2\cos 2\pi n\frac{t}{\tau}\,dr + \int_{\tau_c/2}^{\tau/2}\mu_1\cos 2\pi n\frac{t}{\tau} = u_n''\int_0^{\tau/2}\tfrac{1}{2}(\cos 4\pi n\frac{t}{\tau}+1)\,dr$$

$$\frac{\tau}{2\pi n}\left\{\mu_2\left[\sin 2\pi n\frac{t}{\tau}\right]_0^{\tau_c/2} + \mu_1\left[\sin 2\pi n\frac{t}{\tau}\right]_{\tau_c/2}^{\tau/2}\right\} = \frac{u_n''}{2}\left\{\frac{\tau}{4\pi n}\left[\sin 4\pi n\frac{t}{\tau}\right]_0^{\tau/2} + \frac{\tau}{2}\right\}$$

$$\frac{\tau}{2\pi n}\left\{\mu_2\sin(\pi n\frac{\tau_c}{\tau}) - \mu_1\sin(\pi n\frac{\tau_c}{\tau})\right\} = \frac{u_o''\tau}{4}$$

$$u_n'' = \frac{2(\mu_2-\mu_i)}{\pi n}\sin(\pi n\frac{\tau_c}{\tau}) \qquad (15/4)$$

and

$$u_o'' = \frac{\mu_2\tau_c + \mu_1\tau_o}{\tau} \qquad (15/5)$$

Equation (14/6) in Appendix 14 defines the function f(t) as a complex series from $-\infty$ to ∞ .

Equation (15/8) can be written as

$$f(t) = u_o'' + \sum_{n=1}^{\infty}\left\{u_n''\left(\frac{\exp(2\pi jn\frac{t}{\tau}) + \exp(-2\pi jn\frac{t}{\tau})}{2}\right)\right\} \qquad (15/6)$$

Equating the right hand sides of equation (15/6) and (14/6) gives

$$\sum_{n=-\infty}^{\infty}\left\{\omega_n.\exp(2\pi jn\frac{t}{\tau})\right\} = u_o'' + \sum_{n=1}^{\infty}\left\{u_n''\left(\frac{\exp(2\pi jn\frac{t}{\tau}) + \exp(-2\pi jn\frac{t}{\tau})}{2}\right)\right\}$$

(15/7)

Since f(t) is an even function and is real, ω_n is real, and $\omega_n = -\omega_{-n}$ so that in equation (14/6a), $\omega_n = u_n$. Writing, for this special case u_n' for u_n, equation (15/7) becomes

$$u_o' + 2\sum_{n=1}^{\infty}\left\{u_n'.\exp(2\pi jn\frac{t}{\tau})\right\} = u_o'' + \sum_{n=1}^{\infty}\left\{u_n''.\cos(2\pi n\frac{t}{\tau})\right\} \tag{15/8}$$

Hence

$$u_n' = \tfrac{1}{2}u_n'' = \frac{(\mu_2 - \mu_i)}{\pi n}\sin(\pi n\frac{\tau_c}{\tau}) \tag{15/9}$$

and

$$u_o' = u_o'' = \left(\frac{\mu_2\tau_c + \mu_1\tau_o}{\tau}\right) \tag{15/10}$$

APPENDIX 16

Derivation of $f_n(x)$ for iterative process - (imperfect contact)

A solution of the heat diffusion equation is required when the boundary conditions are as stated in section 4.3.2.

For convenience, the heat diffusion equation will now be written in the form

$$\frac{\partial^2 T}{\partial x^2} = \alpha^2 \frac{\partial T}{\partial t} \qquad (16/1)$$

where α^2 = (Thermal diffusivity)$^{-1}$ (16/2)

Solution of equation (16/1) is required when the temperature distribution in the system is quasi-steady, subject to the boundary conditions

(i) At $x = o$, $T = T_A$ = constant

(ii) As formulated in section 4.3.4.1, i.e.

At $x = \ell$, $\frac{\partial T}{\partial x} = T.f(t)$ (16/3)

$$\text{where } f(t) = \sum_{n=-\infty}^{\infty} \left\{ \omega_n \exp\left(2\pi j n \frac{t}{\tau}\right) \right\} \qquad (16/4)$$

where $\omega_n = u_n + jv_n$ (16/5)

u_n and v_n both being real.

Consider Fig. 27 and the situation described in section 4.3.4.2. To solve equation (16/1) above, it will be re-written putting $\phi = T$. Taking its Laplace Transform assuming the initial condition to be zero, yields

$$\frac{d^2\bar{\phi}}{dx^2} - \alpha^2 s \bar{\phi} = 0 \qquad (16/6)$$

which after the mth iteration, see Fig 27, becomes

$$\frac{d^2\bar{\phi}}{dx^2} - \alpha^2 s \bar{\phi} = 0 \qquad (16/7)$$

Since the boundary condition at $x = 0$, at the mth iteration is $\phi = T_m(o,t) = 0$, the solution to equation (16/7) is

$$\bar{\phi} = A \, sh(\alpha x \sqrt{S}) \qquad (16/8)$$

where A is a constant of integration. At $x = \ell$, the boundary condition described by equation (16/3) and (14/2) in Appendix 14 may be written

$$\left.\frac{\partial T_m}{\partial x}\right|_{x=\ell} = \sum_{n=-\infty}^{\infty} \left\{ C_{m,n}(\ell) \exp(2\pi jn \frac{t}{\tau}) \right\} \qquad (16/9)$$

Again, writing $\phi_m = T_m$ and taking its Laplace Transform, equation (16/9) becomes

$$\left.\frac{\partial \bar{\phi}_m}{\partial x}\right|_{x=\ell} = \sum_{n=-\infty}^{\infty} \left\{ \frac{C_{m,n}(\ell)}{S - 2\pi jn/\tau} \right\} \qquad (16/10)$$

Differentiating (16/8) and equating to (16/10) (with $x = \ell$), yields

$$(A\alpha \sqrt{s}) ch(\alpha\ell\sqrt{s}) = \sum_{n=-\infty}^{\infty} \frac{C_{m,n}(\ell)}{S - 2\pi jn/\tau} \qquad (16/11)$$

$$A = \frac{\sum_{n=-\infty}^{\infty} \left\{ \frac{C_{m,n}(\ell)}{S - 2\pi jn/\tau} \right\}}{(\alpha\sqrt{s}) \, ch(\alpha\ell\sqrt{s})} \qquad (16/12)$$

and hence from equation (16/8)

$$\bar{\phi}_m = \frac{\sum_{n=-\infty}^{\infty} \left\{ \frac{C_{m,n}(\ell)}{s - 2\pi jn/\tau} \right\}}{(\alpha\sqrt{s})\ \mathrm{ch}(\alpha\ell\sqrt{s})}\ \mathrm{sh}(\alpha x\sqrt{s}) \qquad (16/13)$$

Equation (16/13) may be inverted and manipulated to yield

$$\phi_m = C_{m,o}(\ell).x + \sum_{n=1}^{\infty} 2\,\mathcal{R}\left\{ \frac{C_{m,n}(\ell).\mathrm{sh}(\alpha x\ \frac{2\pi jn}{\tau}).\ \exp(2\pi jn\ \frac{t}{\tau}\ )}{\alpha\sqrt{\frac{2\pi jn}{\tau}}\ \mathrm{ch}(\alpha\ell\ \frac{2\pi jn}{\tau}\ )} \right\}$$

$$+ \quad \text{Terms} \to 0 \text{ at } t \to \infty. \qquad \left[\mathcal{R} = \{\text{real part}\}\right] \qquad (16/14)$$

The procedure for doing this is to be found in reference[125]

Since only the quasi-steady state solution is required the Terms $\to 0$ as $t \to \infty$ part may be neglected.

Comparing equation (16/14) (in which ϕ_m can be replaced by T_m) with equation (14/23) in Appendix 14, it will be seen that

$$f_n(x) = 2\sum_{n=1}^{\infty} \left\{ \frac{\mathrm{sh}(\alpha x\sqrt{\frac{2\pi jn}{\tau}}\ )}{(\alpha\sqrt{\frac{2\pi jn}{\tau}})(\mathrm{ch}\alpha\ell\sqrt{\frac{2\pi jn}{\tau}})} \right\} \qquad (16/15)$$

Using the well known identities below

$$\begin{aligned} \mathrm{sh}(A+B) &= \mathrm{sh}A\mathrm{ch}B + \mathrm{ch}A\mathrm{sh}B \\ \mathrm{ch}(A+B) &= \mathrm{ch}A\mathrm{ch}B + \mathrm{sh}A\mathrm{sh}B \\ \mathrm{sh}jZ &= j\ \sin Z \\ \mathrm{ch}jZ &= \cos Z \end{aligned} \qquad (16/16)$$

$$\sin jZ = j\,\mathrm{sh}Z$$

$$\cos jZ = \mathrm{ch}Z \qquad (16/16)$$

$$\sqrt{2j} = 1 + j$$

and writing A_n for $\alpha\sqrt{\frac{\pi jn}{\tau}}$, and $g_n(x)$ and $h_n(x)$ for the real and imaginary parts respectively equation (16/15) becomes

$$f_n(x) = g_n(x) + jh_n(x) \qquad (16/17)$$

where $g_n(x)$ and $h_n(x)$ are defined by equations (14/44) and (14/45) in Appendix 14.

When n = 0, from equation (16/14)

$$f_o(x) = x \qquad (16/18)$$

$$g_o(x) = x \qquad (16/19)$$

$$h_o(x) = 0 \qquad (16/20)$$

APPENDIX 17

Computer program "Fred" for determination of dimensionless groups

(Imperfect contact)

```
      TRACE 1
      READ FROM (CR)
      MASTER UXT
101   FORMAT (1F0.0)
102   FORMAT (1F0.0)
103   FORMAT (1F0.0)
104   FORMAT (2F0.0)
105   FORMAT (//10X,3HTAU,10X,5HALPHA,5X,2HL1,5X,3HMU1,5X,3HMU2,5X,
     1              4HTAUC/)
106   FORMAT (//10X,1HK,5X,5HAN(K)/)
107   FORMAT (3X,1I2,3X,1E12.5)
108   FORMAT (//10X,1HM,5X,1HN,5X,2HU0,15X,3HpX0,15X,3HpL0/)
109   FORMAT (3X,1I2,3X,1I2,3X,1E12.5,3X,1E12.5,3X,1E12.5)
110   FORMAT (//10X,1HM,5X,1HN,5X,4HU(M),15X,2HA0/)
111   FORMAT (3X,1I2,3X,1I2,3X,1E12.5,3X,1E12.5)
112   FORMAT(//5X,1HM,5X,1HN,5X,4HA(N),12X,4HB(N),12X,5HPX(N),12X,
     15HPL(N),12X,5HQX(N),12X,5HQL(N)/)
113   FORMAT (2(I2.2X),6(E12.5,3X))
114   FORMAT (//10X,1HL,5X,3HSUM/)


115   FORMAT (//10X,1HN,5X,2HA0/)
116   FORMAT (//5X,1HM,5X,1HN,5X,1HL,5X,3HSA1,15X,3HSB1/)
117   FORMAT(2X,3(I2,3X),2(E12.5,3X))
118   FORMAT (//5X,1HM,5X,1HN,5X,1HL,5X,3HSA2/)
119   FORMAT (2X,3(I2,3X),1E12.5)
120   FORMAT (//5X,1HM,5X,1HN,5X,1HL,5X,3HSB2/)
121   FORMAT (//5X,1HM,5X,1HN,5X,2HA3,12X,2HB3/)
122   FORMAT (2X,2(I2,3X),2(E12.5,3X))
123   FORMAT (//5X,1HM,5X,1HN,5X,1HL,5X,3HSA4,12X,3HSB4/)
124   FORMAT (//10X,1HM,5X,1HN,5X,2HA5/)
125   FORMAT (//5X,1HK, 5X,5HGL(K),10X,5HHL(K)/)
126   FORMAT (2X,I2,2(E12.5,3X))
127   FORMAT (//5X,1HK,5X,5HGX(K),10X,5HHX(K)/)
128   FORMAT (//5X,1HM,5X,1HN,5X,4HA(N),12X,4HB(N)/)
129   FORMAT (//5X,1HM,5X,1HN,5X,5HPL(N),12X,5HQL(N)/)
131   FORMAT (//5X,1HM,5X,5HSUMUM/)
132   FORMAT (3X,F6.4,3X,E12.5,3X,F5.3,3X,3(E12.5,3X))
133   FORMAT (3X,2(I2,3X),3X,E12.5)
134   FORMAT (//10X,1HN,10X,5HUB(N)/)
135   FORMAT (9X,I2,6X,E12.5)
136   FORMAT (//10X,1HK,10X,5HUB(K)/)
137   FORMAT (//10X,6HGROUPS/)
138   FORMAT (8E12.5)
139   FORMAT (//6X,1HF,12X,2HLA,11X,2HLT,11X,2HLI,12X,2HG1,12X,2HG2
     112X,2HG3,12X,2HG4/)
140   FORMAT(//2X,3HSA1,14X,3HSA2,14X,2HA3,14X,3HSA4,14X,2HA5/)
141   FORMAT(5E14.5)
142   FORMAT (//2X,3HSB1,14X,3HSB2,14X,2HB3,14X,3HSB4,14X,2HB5/)
```

```
      REAL L1,LA,LT,LT
      REAL MU1,MU2
      INTEGER  M1,R
      DIMENSION GL(81),HL(81),GX(81),HX(81),UB(81),PL(81),QL(81),
     1      PX(81),QX(81),A(81),B(81),U(201),ANL(81),AN(81),ANX(81)
      DO 600 I=1,17
      READ (1,101) TAU
      READ (1,102) ALPHA
      READ (1,103) L1
      READ (1,104) MU1, MU2
      T = 100.0
      READ (1,101) TAUC
      TAU0 = TAU - TAUC
C     CALCULATION OF THE FUNCTIONS G(L) AND H(L) FOR N = 1 TO 20
      WRITE (2,105)
      WRITE (2,132) TAU, ALPHA,L1,MU1,MU2,TAUC
      PI=4*ATAN(1.0)
      PI2 = 8*ATAN(1.0)
      READ (1,103) X
      DO 180 K=1,40
      AN(K) = ALPHA*SQRT(ABS(PI*K/TAU))
      ANX(K) = AN(K)*X
      ANL(K) = AN(K)*L1
      IF (ABS(ANL(K)).GT.(8.4E+1)) GO TO 171
      SHL=SINH(ANL(K))
      CHL = COSH(ANL(K))
      SNL=SIN(ANL(K))
      CSL=COS(ANL(K))
      CHL2 = CHL**2
      SHL2 = SHL**2
      SNL2 = SNL**2
      CSL2 = CSL**2
      SH2 = SINH(2*ANL(K))
      CN2 = COSH(2*ANL(K))
      GL(K) = (SH2 + SN2)/(4*AN(K)*(CHL2*CSL2 + SHL2*SNL2))


      HL(K) = (-SH2 + SN2)/(4*AN(K)*(CHL2*CSL2 + SHL2*SNL2))
      GO TO 180
171   GL(K)=1/(2*AN(K))
      HL(K)=-GL(K)
      WRITE (2,125)
180   WRITE (2,126) K,GL(K),HL(K)
C     N.EQ.0 CASE
      GX0 = X
      HX0 = 0
      GL0 = L1
      HL0 = 0
C     WRITE FOR DATA
```

```
C       SERIES FOR F(T)
C       F(T) = -(MU2*TAUC + MU1*TAU0) + SIGMA FROM N=1 TO IMFINITY
C               UB(N)*COS(2PI*N*T/TAU)
C       UB(N) =  (MU2 - MU1)*SIN(PI*N*TAUC/TAU)/PI*N)
C       N = 0  CASE TREATED  SEPARATELY
        UB0 = -(MU2*TAUC + MU1*TAU0)/TAU
        Z3 = (MU2 - MU1)/PI
        WRITE (2,134)
        DO 150 N = 1,81
        Z1 = SIN(PI*N*TAUC/TAU)
        Z2 = N
        UB(N) = -Z3*Z1/Z2
  150   WRITE (2,135) N,UB(N)
        M=0
        N=0
        U0 = T
        PL0= T
        PX0= T
        QL0= 0
        QX0=0
        WRITE (2,108)
        WRITE (2,109) M,N,U0,PX0,PL0
C       N.GE.1 CASE
        DO 155 N =1,40
        PL(N)=0
        PX(N)=0
        QL(N)=0
        QX(N)=0
        A(N) =0
  155   B(N) =0
        M=1
C       N=0 CASE
        N=0
        A0 = UB0*T
        B0 = 0
        PX0= A0*X
        PL0 = A0*L1
        QX0=0
        QL0=0
        U(M) = PL0
        WRITE (2,110)
        WRITE (2,111) M,N,U(M),A0
C       N.GE.1 CASE
        WRITE (2,112)
        DO 160 N = 1,40
        A(N) = UB(N)*T
        B(N) = 0
        PX(N) = A(N)*GX(N)
        PL(N) = A(N)*GL(N)
        QX(N) = A(N)*HX(N)
  160   QL(N) = A(N)*HL(N)
        DO 400 M = 2,20


C       N=0 CASE
```

```
      N=0
      SUM = 0
      B0 = 0
      QL0= 0
      QX0= 0
      DO 200 L = 1,40
      TERM = UB(L)*PL(L)
      SUM = SUM + TERM
  200 CONTINUE
      A0 = 2*SUM + UB0*PL0
      PL0 = A0*L1
      PX0 = A0*X
      U(M)= PL0
      WRITE (2,110)
      WRITE (2,111) M,N,U(M),A0
C     N.GE.1 CASE
      SA1=0
      SB1=0
      DO 400 N = 1,40
      IF (N.EQ.1) GO TO 205
      J=N-1
      DO 210 L = 1,J
      K=N-L
      IF (K.LT.1) GO TO 215
      A1 = UB(K)*PI(L)
      B1 = UB(K)*QI(L)
      SA1= SA1 + A1
  210 SB1=SB1+B1
      GO TO 215
  205 A1=0
      B1=0
  215 SA2=0
      SB2 = 0
      J=N+1
      DO 220 L = J,40
      K=L-N
      A2= UB(K)*PL(L)
      B2 = UB(K)*QI(L)
      SB2 = SB2 + B2
  220 SA2 = SA2 + A2
      A3 = UB0*PL(N)
      B3 = UB0*QL(N)
      SA4=0
      SB4=0
      DO 230 L = 1,40
      K=N+L
      A4 = UB(K)*PI(L)
      B4 = UB(K)*QI(L)
      SA4= SA4 + A4
  230 SB4= SB4 + B4
      A5 = UB(N)*PI0
      B5 = UB(N)*QI0
      A(N) = SA1 + SA2 +  A3 + SA4 + A5
      B(N) = SB1 + SB2 +  B3 - SB4 + B5
      PL(N) = A(N)*GL(N) - B(N)*HL(N)
```

```
      QL(N) = A(N)*HL(N) + B(N)*GL(N)
  400 CONTINUE
      WRITE (2,131)
      SUMUM=0
      DO 500 M = 1,20
      TERM = U(M)
      SUMUM = SUMUM + TERM


  500 WRITE (2,107) M,SUMUM
      F=1.0/TAU
      LA=1.0/MU2
      LT=-0.04*(100.0 + SUMUM)/SUMUM
      LI=LT - LA
      G1 = F*(LI**2)*(ALPHA**2)
      G2 = F*(LA**2)*(ALPHA**2)
      G3=F*319.69
      G4=TAUC/TAU
      WRITE (2,137)
      WRITE (2,139)
600   WRITE (2,138) F,LA,LT,LI,G1,G2,G3,G4
      STOP
      END
```

APPENDIX 18

Computer program 'Avtenps' for determination of dimensionless groups (Perfect thermal contact)

```
      TRACE 1
      READ FROM (CR)
      MASTER SUMMATION
      DIMENSION A(40),B(40),X(10),P(40),      R(40),S(40),P1(40),
     1          Q1(40),P2(40),Q2(40),C(40),TERMA(40),TERMB(40)
      REAL  L, LI, LI2,L2
  101 FORMAT (4F0.0)
  102 FORMAT (1F0.0)
  103 FORMAT (4E12.5)
  104 FORMAT (1E12.5)
  105 FORMAT (5E12.5)
  106 FORMAT (//10X,2HT1,14X,2HT2,14X,1HD,14X,1HL/)
  107 FORMAT (//10X,1HN,4X,4HA(N)/)
  108 FORMAT (5X,I3,E12.5)
  109 FORMAT (//5X,1HN,4X,5HP1(N),14X,5HQ1(N),14X,4HR(N),14X,4HS(N)
     114X,8HTERMA(N),14X,4HSUMA/)
  110 FORMAT (3X,I3,6E14.5)


  111 FORMAT (//5X,1HN,4X,5HP1(N),14X,5HQ1(N),14X,4HR(N),14X,4HS(N)
     1     14X,8HTERMB(N),14X,4HSUMB/)
  112 FORMAT (//10X,1HN,4X,4HB(N)/)
  113 FORMAT (//5X,1HF,14X,3HTAU,14X,3HFTC,14X,4HX(J),14X,3HAVT/)
  114 FORMAT (//5X,3HFTC,14X,2HFL,14X,3HFLI,14X,4HX(J)/)
  115 FORMAT (//5X,4HX(J)/)
      READ (1,102)  (X(J), J=1,1)
      DO 600 K = 1,20
      READ (1,101) T1,T2,D,L
      READ (1,105) (C(I), I=1,40)
      ALPHA=1/D**2
      TAU = T1 + T2
      WRITE (2,106)
      WRITE (2,103) T1,T2,D,L
      WRITE (2,104) (C(I),I=1,40)
      WRITE (2,107)
      DO 202 I= 1,20
      N = 2*I - 1
      A(N) = C(I)
  202 WRITE (2,108) N, A(N)
      PIB2 = ASIN(1.0)
      DO 600 J=1,1
      WRITE (2,115)
      WRITE (2,104) X(J)
      WRITE (2,109)
```

```
      SUMA = 0
      DO 203 N = 1,39,2
      P(N) =((N*PIB2/L)**2)*ALPHA
      P1(N) =-T1*P(N)
      Q1(N) = EXP(P1(N))
      R(N) = N*PIB2*X(J)
      S(N) = SIN(R(N))
      TERMA(N) = (A(N)*(1 - Q1(N))*S(N))/P(N)
      SUMA = SUMA + TERMA(N)
  203 WRITE (2,110) N,P1(N),Q1(N),R(N),S(N),TERMA(N),SUMA
      IF (X(J).EQ.1.0) GO TO 206
      WRITE (2,112)
      DO 204 I =  21,40
      N = 2*I - 40
      B(N) = C(I)
  204 WRITE (2,108) N,B(N)
      WRITE (2,111)
      SUMB = 0
      DO 205 N = 2,40,2
      P(N) = ((N*PIB2/L)**2)*ALPHA
      P2(N)= -T2*P(N)
      Q2(N)= EXP(P2(N))
      R(N) = N*PIB2*X(J)
      S(N) = SIN(R(N))
      TERMB(N) = (B(N)*(1 - Q2(N))*S(N))/P(N)
      SUMB = SUMB + TERMB(N)
  205 WRITE (2,110) N,P2(N),Q2(N),R(N),S(N),TERMB(N),SUMB
      GOTO 211
  206 SUMB=0
  211 WRITE  (2,113)
      AVT = (100*(T1 + T2*(1- X(J))) + SUMA + SUMB )/(T1 + T2)
      FTC = T2/(T1 + T2)
      F=1/(T1 + T2)
      WRITE (2,105) F,TAU,FTC,X(J),AVT
      L2 = L**2
      LI = L*(AVT - 100*(1 - X(J)))/(100 - AVT)
      LI2 = LI**2
      FLI = F*LI2/ALPHA


      FL  = F*L2/ALPHA
      WRITE (2,114)
  600 WRITE (2,103) FTC,FL,FLI,X(J)
      STOP
      END
```

APPENDIX 19 Analysis of Thermal Resistance Network approximate To Test Rig No.2

Referring to Fig 19-1 the method of calculating the thermal resistance offered by the contact interface in test rig No.2 Fig 34(a) amounted to observing the temperature T_{x_1} and T_{x_2} at two points, x_1 and x_2 one on either side of the interface, finding the temperature gradient, a_2, from the line of best fit among the observed temperature distribution "downstream" of the contact interface, and calculating length of bar, , equivalent to thermal resistance from

$$\ell' = \frac{T_{x_1} - T_{x_2}}{-a_2} - (\ell_a + \ell_b) \qquad (19/1)$$

where ℓ_a and ℓ_b are the distance of x_1 and x_2 respectively from the interface see Fig. 19-1 overleaf.

Thermal resistance network

A thermal resistance network approximate to the copper bars contact interface and surrounding tube and insulation of test rig No. 2, Fig 34(a), is shown in Fig 19-2. Resistor R_g represents the thermal resistance offered by the contact interface while other resistors represent elemental lengths of the copper bar, surrounding copper tube, or annular air gap surrounding the copper bars. The thermal resistance of the annular air gap surrounding the copper bars is due to conduction only since the Grashof number Gr is less than 2000[133]. This is shown below:

$$Gr = \frac{x^3 \rho^2 \beta \Delta T g}{\mu^2} \qquad (19/2)$$

where x = radial thickness of annular air gap = 4.77m

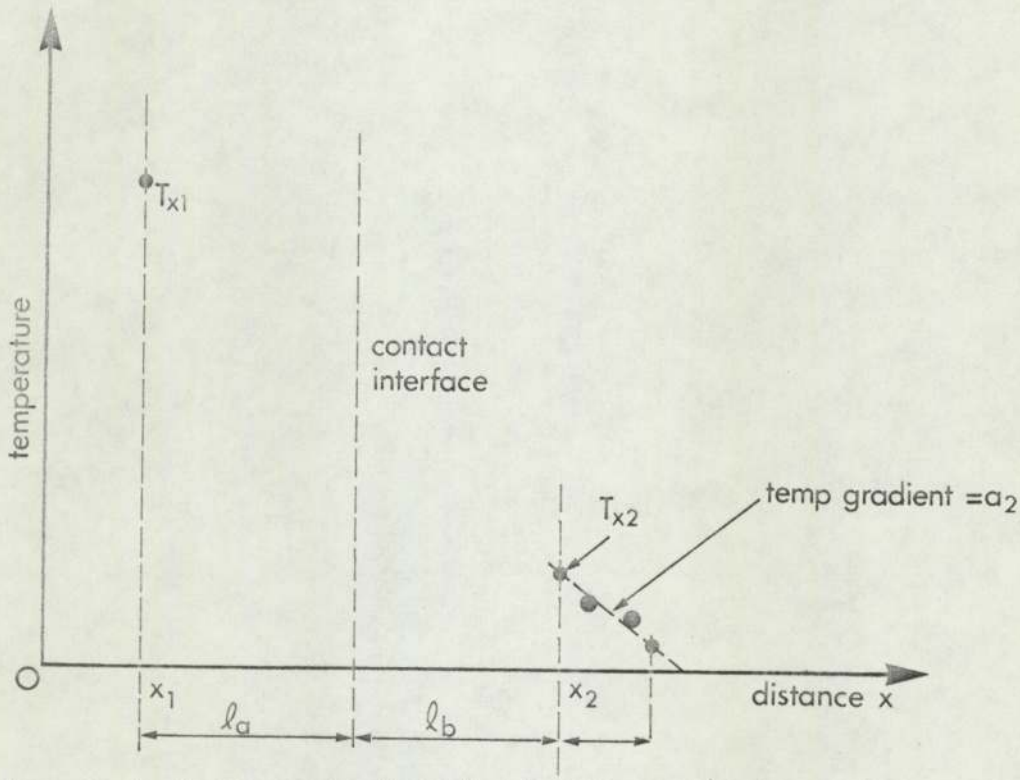

Fig. 19-1 Temperature distribution for calculation of thermal resistance of contact interface

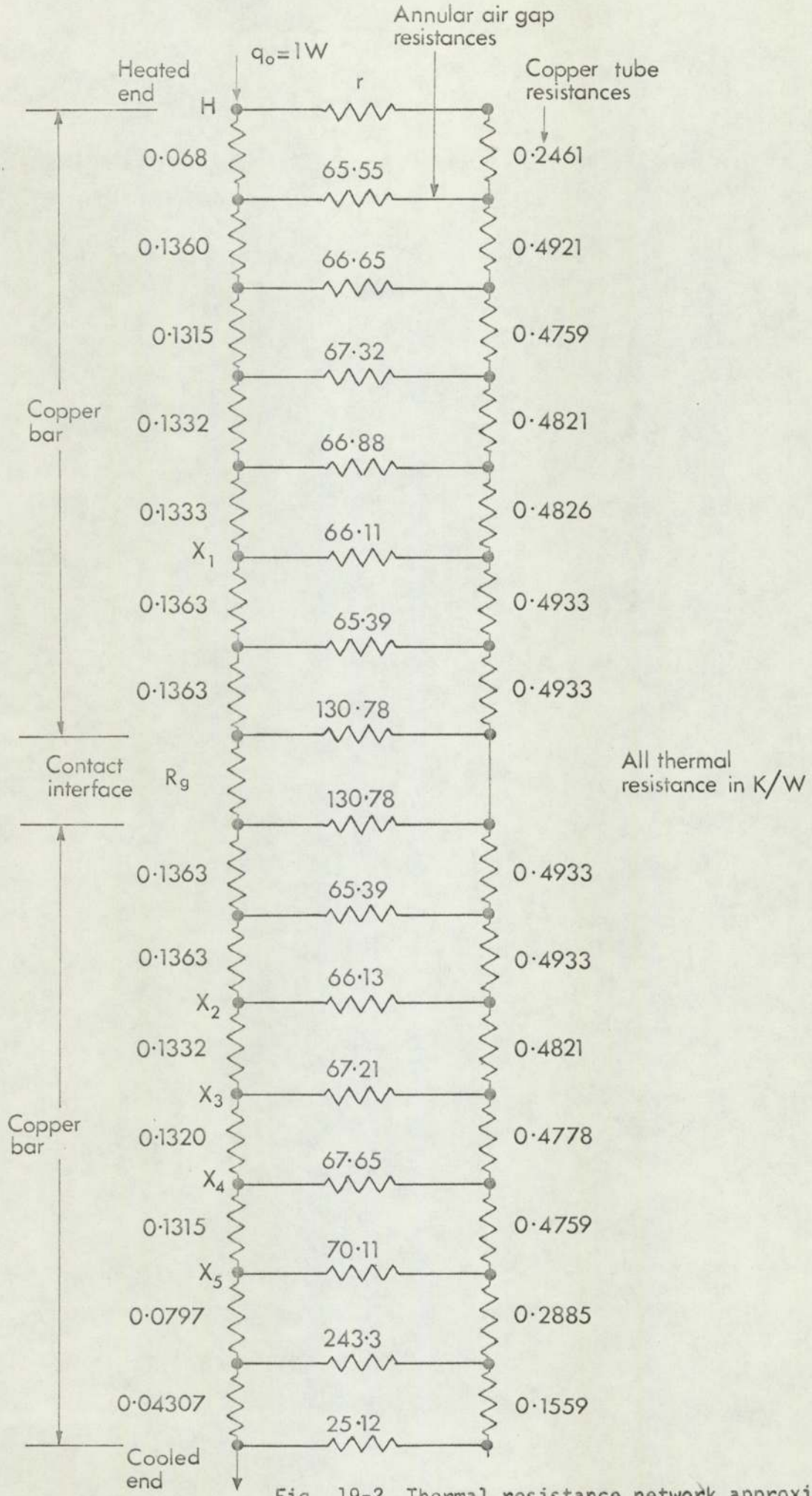

Fig. 19-2 Thermal resistance network approximate to test rig No. 2

ρ = air density = $1.77 kg/m^3$

β = coefficient of expension of air $1/273K^{-1}$

μ = viscosity of air = $1.846 \times 10^{-5} Ns/m^2$

ΔT = temperature drop across annular air gap = 30K maximum

g = gravitational acceleration = $9.81 m/s^2$

When the above values are inserted in equation (19/2), Gr = 475.

Air interchange between annular air space and the gap between contact faces when separated

The temperature of the air flowing into the gap between the contact surfaces when separated will be at the mean temperature at the contact interface. Since this air gap is small and the hotter surface is at the top, heat will be conducted from the hotter contact surface to the air and from the air to the colder contact surface at about the same rate. The mean temperature of the air will be unchanged and there will be no net heat transfer from the air gap to the annular air space.

Apparent thermal resistance

A test to determine the thermal resistance of a known air gap between the contact surfaces of the two copper bars when separated was conducted on test rig No. 2. The true value of this thermal resistance was 68.8 K/W. The value calculated from the test observations was 19.4K/w.

Branch currents in the resistance network Fig. 19-2 were calculated for resistor R_g = 68.8K/W with various values of the unknown resistor r. This resistor r represented the thermal contact resistance of the fixing of the copper tube to the upper copper bar Fig. 34(a). The

branch currents were used to calculate the temperatures at the modes X_1, X_2, X_3, X_4 and X_5 which correspond to thermocouple sites in test rig No.2. The equation of the straight line of best fit among the temperatures at X_2 to X_5 was found by least squares method and the apparent resistance R_g' offered by the contact interface (Fig. 19-2) was calculated from

$$R_g = \frac{T_{x_1} - T_{x_2}}{-a_2} - 0.5452 \qquad (19/2)$$

where, referring to Fig.-912, T_{x_1} and T_{x_2}' are the calculated temperatures at x_1 and x_2 respectively,

a_2 = gradient of line of best fit through temperatures at X_2 to X_5

0.5452 K/W = thermal resistance between X_1 and X_2

The value of resistor r which made R_g = 19.4 K/W was found from this data.

Using this value of r, the apparent thermal resistance R_g' offered by the contact interface was determined for various values of the time thermal resistance R_g. The values are set out in the table below

R_g K/W	R_g' K/W	$\frac{R_g'}{R_g}$	ℓ' in
0.1	0.082	0.82	0.758
0.2	0.174	0.87	1.516
0.5	0.454	0.908	3.788
1.0	0.908	0.908	7.58
2.0	1.771	0.886	15.16
5.0	4.057	0.811	37.88

Note ℓ' = length of copper bar in diameter equivalent to R_g in in.

This covers the range of thermal resistance of the contact interface met during experiments with test rig. No.2. It will be seen that the apparent thermal resistance offerred by the contact interface are from 9 - 19 per cent below the true value.

Effect on values of $(\frac{f\ell_i^2}{\alpha})$

From equation (123) section 5.5.7.5

$$\ell_i = (\ell_i' + \lambda) - \lambda_m \qquad (123)$$

Most values of $(\ell_i + \lambda)$ and λ_m had an apparent value between 0.2K/W and 2K/W and from the above table the indicated values of $(\ell_i + \lambda)$ and λ_m are both about 11 per cent low. The values of $(\frac{f\ell_i^2}{\alpha})$ quoted for the experimental results with test rig No.2 are likely to be low, the true values being about 20 per cent higher.

Int. J. Heat Mass Transfer. Vol. 13, pp. 173–183. Pergamon Press 1970. Printed in Great Britain

AN ANALOGUE STUDY OF HEAT TRANSFER THROUGH PERIODICALLY CONTACTING SURFACES

J. R. HOWARD and A. E. SUTTON

Dept. of Mechanical Engineering and Dept. of Mathematics, University of Aston, Birmingham

(*Received* 16 *October* 1968 *and in revised form* 25 *April* 1969)

Abstract—An analogue computer was used to determine the effect of frequency and duration of contact per cycle on heat transfer through surfaces which are meeting and separating according to a regular cycle. The surfaces were of identical materials and perfect thermal contact and separation are assumed.

The results show that at high frequencies, the loss of heat transfer rate arising from the interruption of heat flow due to separation of the surfaces, is small and less dependent on duration of contact per cycle than at low frequencies. The relationship between loss of heat transfer rate, frequency and duration of contact is shown by a single curve.

NOMENCLATURE

C, distance from contact plane to point B (Fig. 1);
h, thermal conductance at contact plane;
H, distance from point A to contact plane (Fig. 1);
K_c, thermal conductivity of hotter member;
K_H, thermal conductivity of colder member;
$l\ l_i$, length;
L, dimensionless loss of heat transfer (equation 12);
t, time;
T, temperature;
T_c, temperature at any point in colder member;
T_H, temperature at any point in hotter member;
T_0, temperature at contact plane with perfect thermal contact;
T_{0_C}, temperature at contact plane on colder member;
T_{0_H}, temperature at contact plane on hotter member;
$\Delta T, \overline{\Delta T}$, respectively, instantaneous and mean temperature difference from steady-state permanent contact condition;
$\Delta T_{1s}, \Delta T_{2s}$, $(T_A - T_{1s})$ and $(T_A - T_{2s})$ see Fig. 4(b);
x, distance;
ϕ, heat flux – transfer rate per unit area;
α, thermal diffusivity;
τ_c, time surfaces are in contact;
τ_0, time surfaces are separated;
f, frequency;
δ, depth below surface at which temperature fluctuation is negligible;
$F(y), g(y)$, function of y.

1. INTRODUCTION

THIS work is concerned with heat transfer through two surfaces which are undergoing a continuous, regular cycle of contact and separation. Practical examples of this, include that part of the heat transfer from the exhaust valve of an internal combustion engine which travels via the seating. While the valve is closed, the valve head is in contact with the valve seat

in the cylinder head and heat flows from the valve through the contacting surfaces. When the valve opens and the contact surfaces are separated, heat transfer is severely curtailed. Other examples are the heat transfer between workpiece and die in repetitive hot metal deformation processes and between soldering iron and workpieces.

In such cases, the heat transfer will depend upon the frequency and duration of contact, the overall temperature difference, thermal contact resistance at the contact surfaces, and the thermal properties of the materials in contact. A great deal of work has been done on thermal contact resistances of surfaces which are permanently in contact. References [1–3] contain valuable sources of information on both steady state and transient heat transfer.

However, in this present report, one-dimensional heat flow only is considered, with the simplifying assumptions of perfect thermal contact at the surfaces (i.e. no thermal contact resistance) and perfect thermal separation when the surfaces were not in contact.

The report describes an investigation using an analogue computer and forms part of a wider study by one of the authors (JRH). Current experimental work and further computer investigation now in progress will be reported later.

2. STATEMENT OF PROBLEM

2.1 *General*

Consider two bars of material AH and CB with their axes in line as shown in Fig. 1(a), and with one end H of one bar touching one end C of the other. If there were a steady, one-dimensional flow of heat along the axes of the bars i.e. no radial heat loss, then the temperature distribution would be as shown by line A, T_0, B in Fig. 1(b).

If then the ends of the bars were separated by a small distance and the temperature at A and B were to remain unchanged, the steady heat flow through the system would be very

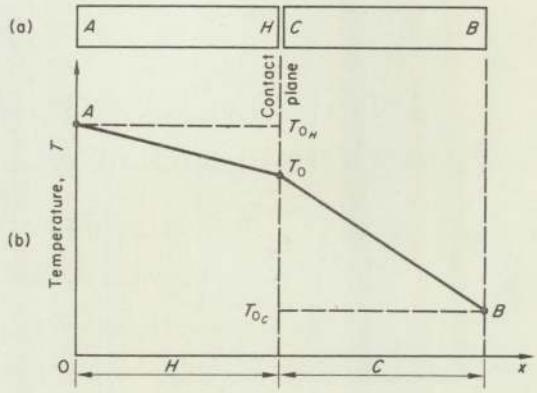

FIG. 1.

greatly reduced. Thus the temperature distribution would be given by A, T_0 , T_{0_C} and B. Clearly, under intermittent contact conditions, the temperature distribution will be between these two extremes, with the temperature near the contacting surfaces varying with time. Intermittent contact conditions will now be considered.

2.2 *Assumptions*

(i) The two bars are of equal cross-sectional area and have identical thermal properties.

(ii) When the two faces are brought together, perfect thermal contact is made. Under these circumstances, the temperature at the contact plane will change instantaneously [4] to the mean value of the two surface temperatures which existed just before contact was made.

(iii) When the surfaces are separated by a very small distance, the heat transfer rate is very small compared with that when the surfaces are in perfect thermal contact. For simplicity it is therefore assumed that when the surfaces are separated no heat transfer occurs.

(iv) Temperatures T_A and T_B are known. In our case we stipulate that they are at a fixed value for all time. This enables the temperature gradient at A and B to be determined. Instantaneous temperature distributions are shown in Fig. 2 for two cases; one with the surfaces in contact (line AbT_0dB) the other when the sur-

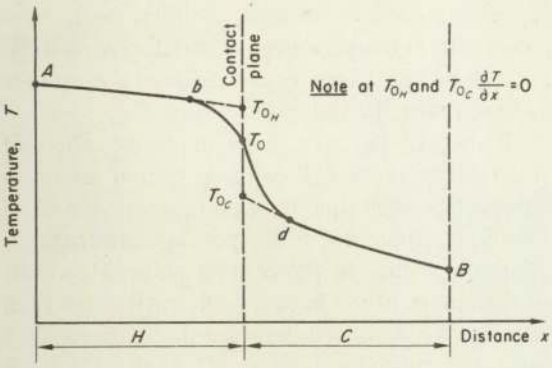

FIG. 2.

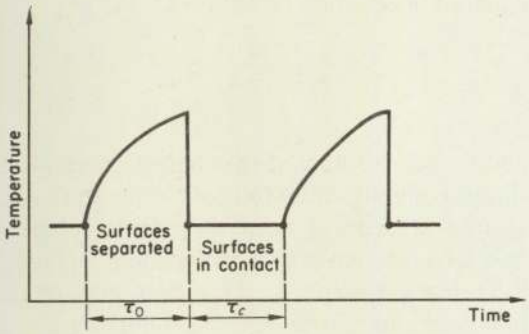

FIG. 3. Temperature/time relation at contact plane.

faces are separated (line $AbT_{0_H}T_{0_C}dB$). Figure 3 shows the temperature–time relation at the contact plane of the hotter member.

2.3 *Basic equation*

Referring to Fig. 2 the heat diffusion equation

$$\frac{\partial T}{\partial t} = \alpha\left(\frac{\partial^2 T}{\partial x^2}\right) \tag{1}$$

applies on either side of the contact plane, at all times.

Since the contact plane represents a discontinuity, equation (1) must be solved in four parts, because (a) the two members may be different materials, (although in our case identical materials are assumed) and (b) because of the two separate time periods; viz. surfaces in contact and when they are separated. Using the nomenclature given in the List of Symbols and referring to Fig. 2 the following boundary conditions arise.

2.4 *Boundary conditions*

1. T_A and T_B fixed at all times.
2. At $x = H$ and $0 < t < \tau_c$ (i.e. during contact period)

$$T_{0_H} = T_{0_C}$$

[Note that this is only true when assumption (1) Section 2.2 is made].

3. At $x = H$ and $\tau_c < t < (\tau_c + \tau_0)$

$$k_H\left(\frac{\partial T_H}{\partial x}\right) = k_c\left(\frac{\partial T_c}{\partial x}\right) = 0.$$

2.5 *Initial condition*

$$T(x)_{t=0} = T_A - \left(\frac{T_A - T_B}{H + C}\right)x,$$

i.e. "steady state, surfaces permanently in contact" temperature distribution, chosen in order to reach the quasi-steady state rapidly.

2.6 *Heat flow*

The time–average heat flux is given by

$$\phi = -k_H\left(\frac{\partial T_H}{\partial x}\right)_A = -k_c\left(\frac{\partial T_c}{\partial x}\right)_B. \tag{2}$$

3. ANALOGUE

3.1 *The model*

For convenience it was assumed that the two members were of identical material so that the temperature distribution would be symmetrical about the contact plane. The heat flux will be unaffected by the location of the plane of contact, so long as the zone in its immediate region, where the temperature is fluctuating, does not encroach on to the ends where the temperature is fixed (see Appendix A). Only the hotter member was therefore considered and it was divided into finite elements shown by the table of distances in Fig. 4(a). The steady state temperature distribution, with the end permanently in contact with the colder

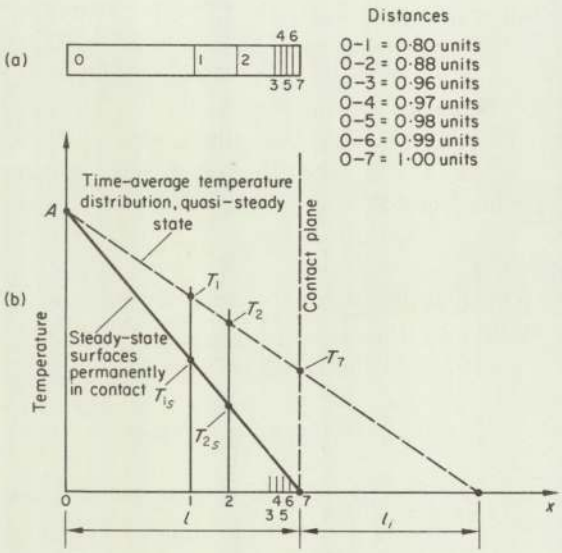

FIG. 4.

member is also shown in Fig. 4(b) by the line $A7$. The following material properties were assumed.

Specific heat C $= 460 \dfrac{\text{J}}{\text{kg degC}}$

Density ρ $= 7550 \dfrac{\text{kg}}{\text{m}^3}$

Diffusivity α $= \dfrac{k}{\rho C} = 5 \times 10^{-6} \dfrac{\text{m}^2}{\text{s}}$

Thermal conductivity $k = 17{\cdot}4 \dfrac{\text{W}}{\text{m degC}}$

Specimen length 0–7 $= 0{\cdot}04$ m.

3.2 *Dimensional analysis*

Referring to the model Fig. 4 the heat transfer rate per unit cross-sectional area ϕ, depends on the temperature difference $(T_A - T_7)$ between the ends, the overall length l, thermal conductivity K, thermal diffusivity α, frequency of contact f and duration of contact per cycle $(f\tau_c)$.

Boundary condition 1, Section 2.4, implies that ends A and B of the two bars, Figs. 1 and 2, are in perfect thermal contact with heat reservoirs at temperatures T_A and T_B respectively, of infinite heat capacity and made of a substance whose thermal conductivity is infinite.

If instead the bars were in perfect thermal contact at A and B with a system of finite properties then the temperature at A and B would fluctuate due to the periodic interruption of the heat flow at the contact plane. However, if the length of the bars is sufficiently large then the amplitude of temperature fluctuations at A and B would be very small once a "quasi-steady" state had been reached. If length l equals δ in equation (3) below, [5, 6],

$$\delta = 1{\cdot}6\sqrt{\frac{\pi\alpha}{f}} \tag{3}$$

and the temperature at the contact plane varies sinusoidally, the amplitude of temperature fluctuation at depth δ from the contact plane is only 0·66 per cent of that at the contact plane.

To test the accuracy of the analogue simulation, the amplitude of the temperature at stations 2 and 7 in the rod, Fig. 4(a), were compared. The ratio of these two amplitudes agreed closely with that computed from the exact solution of the heat diffusion equation (1) for a semi-infinite solid whose surface temperature varies periodically with time [6].

Furthermore, once l exceeds δ and providing that the time–average heat flux is unchanged, an increase in l will only introduce an additional series thermal resistance into the system. Thus the thermal resistances of the system consists of two *independent* thermal resistances in series, R_s and R_i, R_s being the resistance under continuous contact conditions due to the length l of the conducting material (of unit cross-sectional area) and R_i being due to the periodic interruption of the heat flow.

R_i may also be represented by a length, l_i, of the same conducting material of unit cross-sectional area.

It is desirable therefore to choose dimensionless groups which reflect the independence of

R_s and R_b, isolating l in one of them. Note: $R_i = F[f, (f\tau_c)]$.

Notice that if the contact plane is situated at a distance less than δ from the extreme ends A and B of the two bars (a case we have not considered), then the loss of heat flow is reduced, until when the contact plane is at the end, the loss of heat flow is half that when the contact plane is located at a distance greater than δ from the ends.

Referring again to Fig. 4(b) which shows the quasi-steady state time-average temperature distribution when the surfaces are meeting and parting regularly, together with the distribution under steady state surfaces permanently in contact condition, it will be seen that the *loss* of heat flux due to periodic interruption of the heat flow is given by

$$\phi_s - \phi = \frac{k(T_1 - T_{1s})}{(x_1 - x_0)} = \frac{k(T_2 - T_{2s})}{x_2 - x_0} = \frac{k(T_7 - T_{7s})}{(x_7 - x_0)}. \quad (4)$$

This may be expressed non-dimensionally as

$$L = \frac{\phi_s - \phi}{\phi_s} = \frac{T_1 - T_{1s}}{T_A - T_{1s}} = \frac{T_7 - T_{7s}}{T_A - T_{7s}} = \frac{l_i}{l + l_i}, \quad (5)$$

whence

$$l_i = \frac{lL}{1 - L}. \quad (6)$$

The relationship between the dimensionless parameters can be expressed in the form

$$\left(\frac{fl_i^2}{\alpha}\right) = g\left[\left(\frac{fl^2}{\alpha}\right), (f\tau_c)\right]. \quad (7)$$

But using equation (3), when $(fl^2/\alpha) > 2{\cdot}56\pi$, l_i is independent of l and hence (fl_i^2/α) is independent of (fl^2/α)

Hence

$$\left(\frac{fl_i^2}{\alpha}\right) = g(f\tau_c) \text{ only}. \quad (8)$$

Thus, the number of significant dimensionless groups involved is two instead of three, with the advantage of saving a complete dimension of computation without loss of generality.

In our experiment the values of $(f/l^2/\alpha)$ ranged from 4·64 to 3210.

3.3 *Finite-difference equations*

Equation (1) was written in finite-difference form.

At any position on the model the temperature difference T between the "steady-state surfaces permanently in contact" condition and the temperature when the surfaces are meeting and parting regularly (and quasi-steady state is reached) is described by the equations below. Thus, referring to Fig. 4(b), $\Delta T_1 = T_1 - T_{1s}$, etc. i.e. ΔT_1 is the difference between the actual temperature in the quasi-steady state and the temperature when the steady state surfaces permanently in contact is attained. Putting $D \equiv (\mathrm{d}/\mathrm{d}t)$

$$D(\Delta T_1) = 0{\cdot}089\,\Delta T_2 - 0{\cdot}098\,\Delta T_1 + 0{\cdot}0089\,\Delta T_0 \quad (9)$$

in which ΔT_0 is zero since our boundary condition at position 0 is that the temperature remains fixed for all cases.

$$D(\Delta T_2) = 0{\cdot}488\,\Delta T_3 - 0{\cdot}976\,\Delta T_2 + 0{\cdot}488\,\Delta T_1 \quad (10)$$

$$D(\Delta T_3) = 6{\cdot}95\,\Delta T_4 - 7{\cdot}82\,\Delta T_3 + 0{\cdot}87\,\Delta T_2 \quad (11)$$

$$D(\Delta T_4) = 31{\cdot}25\,\Delta T_5 - 62{\cdot}5\,\Delta T_4 + 31{\cdot}25\,\Delta T_3 \quad (12)$$

$$D(\Delta T_5) = 31{\cdot}25\,\Delta T_6 - 62{\cdot}5\,\Delta T_5 + 31{\cdot}25\,\Delta T_4 \quad (13)$$

$$D(\Delta T_6) = 31{\cdot}25\,\Delta T_7 - 62{\cdot}5\,\Delta T_6 + 31{\cdot}25\,\Delta T_5. \quad (14)$$

When surfaces are in contact

$$\Delta T_7 = 0. \quad (15)$$

When surfaces are separated

$$D(\Delta T_7) = 62{\cdot}5\,\Delta T_6 - 62{\cdot}5\,\Delta T_7 + 62{\cdot}5. \quad (16)$$

3.4 *Circuitry*

Figure 5 shows the circuit diagram employed on a PACE analogue computer.

Meeting and parting of the surfaces was simulated by the closing and opening of a switch whose frequency of operation and duration of closure could be varied. The switch was connected across amplifier 4 as shown in Fig. 5.

Outputs ΔT_1 and ΔT_2 were measured with a digital voltmeter. At low frequencies of contact however, these outputs fluctuated cyclically and they were then measured with an U.V. recorder and time mean values determined. Output ΔT_7 was measured with an U.V. recorder at all times so that frequency and duration of contact could be determined (A typical trace of ΔT_7 is shown in Fig. 6.)

4. PROCEDURE

4.1 *Temperature distribution*

The computer was switched on with the variable-frequency switch permanently open. When steady conditions were reached, outputs ΔT_1, ΔT_2, . . . ΔT_7 were measured with the digital voltmeter. Thus the temperature distribution under "steady-state surfaces permanently in contact" condition was obtained. At this condition, see Fig. 4(b),

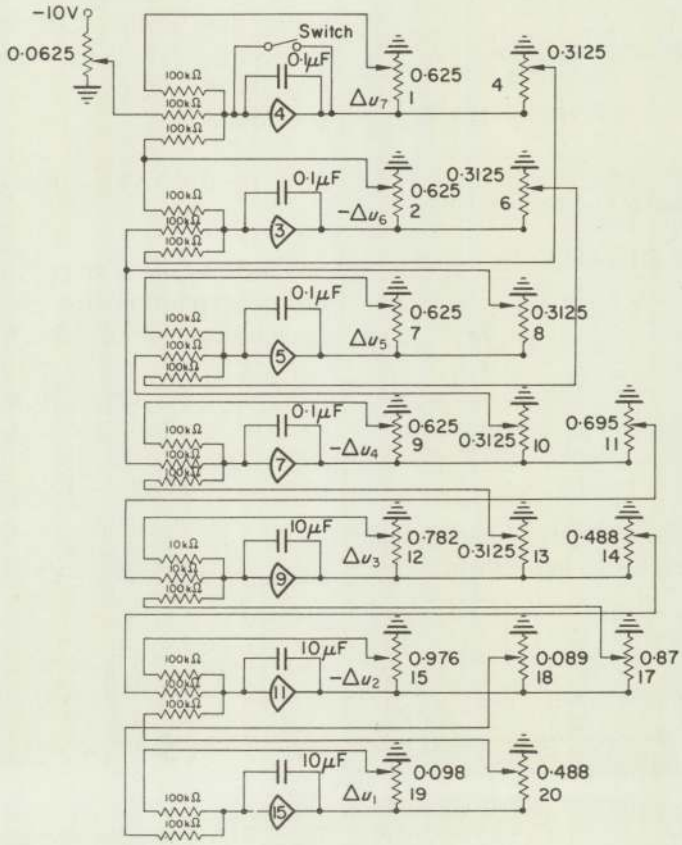

FIG. 5.

$$\Delta T_1 = T_A - T_{1s} = \Delta T_{1s} \tag{17}$$

$$\Delta T_2 = T_A - T_{2s} = \Delta T_{2s}. \tag{18}$$

Outputs ΔT_1, ΔT_2 and ΔT_7 were then observed at various switching frequencies and durations of contact, once the quasi-steady state was reached. After each series of tests the "steady-state surfaces permanently in contact" temperature distribution was checked.

5. RESULTS

Referring to Fig. 4(b) the loss L was evaluated from equation (5) using mean values of ΔT. (viz. $\overline{\Delta T_1}$, $\overline{\Delta T_2}$), ΔT_{1s} and ΔT_{2s}—see equations (17) and (18). Thus,

$$L = \frac{\overline{\Delta T_1}}{\Delta T_{1s}} = \frac{\overline{\Delta T_2}}{\Delta T_{2s}}. \tag{19}$$

The values obtained for L were in very close agreement. l_i was calculated from equation (6) and used to evaluate the dimensionless group $(f l_i^2/\alpha)$.

These results are tabulated in Table 1 while Fig. 7 shows a plot of $(f l_i^2/\alpha)$ against $(f\tau_c)$.

6. DISCUSSION

It will be seen from the plot of $(f l_i^2/\alpha)$ against $(f\tau_c)$, Fig. 7, that all the points lie very close indeed to a single curve drawn among them, thus verifying the relationship given by equation (8). For small values of loss L, it will be seen from equation (6) that

$$\frac{1}{L} \simeq \frac{l}{l_i}, \tag{20}$$

Table 1.

Frequency, $H_z \rightarrow$ 0·0145			0·073			0·18			0·585		
$(f\tau_c^2)$	L	$(f l_c^2/\alpha)$	$(f\tau_c^2)$	L	$(f l_i^2/\alpha)$	$(f\tau_c^2)$	L	$(f l_i^2/\alpha)$	$(f\tau_c)$	L	$(f l_i^2/\alpha)$
0·0828	0·51	5·05	0·0327	0·472	18·7	0·0372	0·343	15·7	0·0612	0·170	7·86
0·0204	0·325	1·08	0·0871	0·303	4·44	0·061	0·272	8·05	0·105	0·127	4·06
0·403	0·176	0·212	0·126	0·244	2·43	0·115	0·191	3·22	0·167	0·0937	2·00
0·515	0·125	0·0945	0·182	0·205	1·56	0·18	0·138	1·48	0·378	0·038	0·292
0·667	0·072	0·0279	0·234	0·168	0·945	0·304	0·085	0·498	0·467	0·0275	0·149
0·786	0·034	0·00575	0·313	0·126	0·482	0·43	0·054	0·188	0·595	0·0163	0·0515
			0·509	0·067	0·122	0·50	0·042	0·111	0·672	0·0111	0·0234
			0·726	0·023	0·0129	0·612	0·0272	0·0451	0·765	0·0067	0·0085
			0·778	0·016	0·00615	0·723	0·0159	0·0151			
						0·844	0·0065	0·00247			

Frequency $H_z \rightarrow$ 0·99			4·07			8·13			16·4		
$(f\tau_c)$	L	$(f l_i^2/\alpha)$	$(f\tau_c)$	L	$(f l_i^2/\alpha)$	$(f\tau_c)$	L	$(f l_i^2/\alpha)$	$(f\tau_c)$	L	$(f l_i^2/\alpha)$
0·0446	0·154	10·5	0·0311	0·0895	12·6	0·0518	0·046	6·05	0·0525	0·0267	3·78
0·0857	0·121	6·0	0·117	0·0461	3·04	0·1165	0·0284	2·23	0·137	0·0171	1·52
0·1075	0·100	3·92	0·176	0·0340	1·62	0·223	0·0178	0·855	0·184	0·0149	1·15
0·164	0·0752	2·09	0·265	0·0225	0·690	0·328	0·0123	0·403	0·242	0·0120	0·740
0·214	0·0602	1·30	0·37	0·0156	0·327	0·43	0·00875	0·193	0·337	0·00872	0·389
0·284	0·0438	0·665	0·472	0·0109	0·158	0·523	0·00586	0·0906	0·479	0·00494	0·124
0·385	0·0295	0·293	0·600	0·00625	0·0515	0·596	0·0043	0·0485	0·579	0·00310	0·0486
0·496	0·0183	0·110	0·730	0·0032	0·0134	0·688	0·00263	0·0181	0·683	0·00192	0·0186
0·585	0·0135	0·0595	0·838	0·00137	0·00245	0·749	0·0018	0·00845	0·790	0·00089	0·004
0·68	0·0079	0·0201				0·870	0·0006	0·00095			
0·772	0·00444	0·00630									
0·833	0·00301	0·00289									
0·895	0·00099	0·000311									

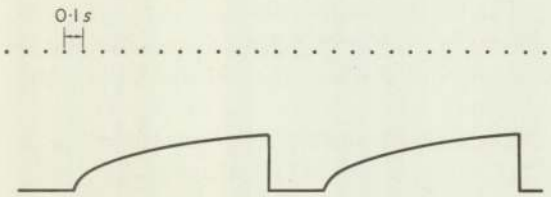

FIG. 6. Typical trace of ΔT_7

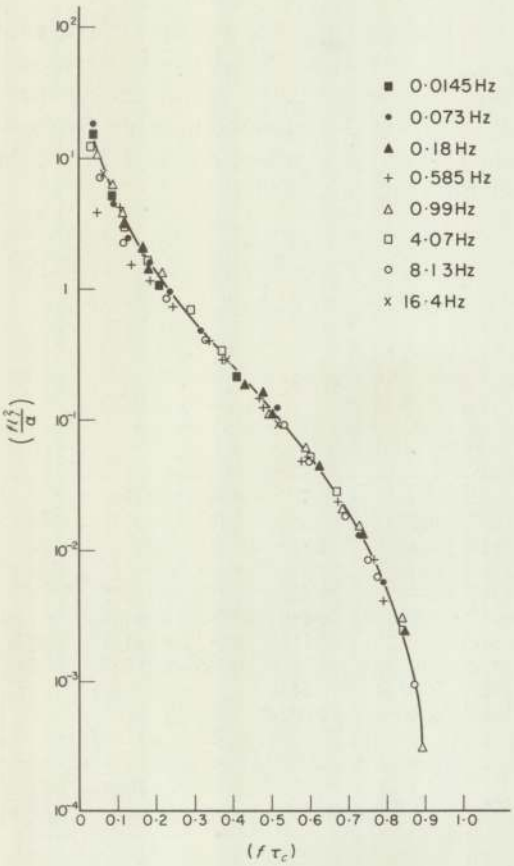

FIG. 7.

whence L tends to a value given by

$$L = \left(\frac{fl^2}{\alpha}\right)^{-\frac{1}{2}} \{g(f\tau_c)\}^{\frac{1}{2}}. \tag{21}$$

If the frequency of contact with a given system (of fixed l and α) is varied while $(f\tau_c)$ is maintained constant, then from equations (6) and (8), since L cannot be negative or exceed unity,

$$\frac{L}{1-L} = +(p/f)^{\frac{1}{2}} \tag{22}$$

where

$$p = \frac{\alpha \,.\, g(f\tau_c)}{l^2}, \tag{23}$$

giving

$$L = \frac{(p/f)^{\frac{1}{2}}}{1+(p/f)^{\frac{1}{2}}}. \tag{24}$$

Thus, as f increases so L falls, and at sufficiently large values of $(f\tau_c)$ i.e. small p, loss L of heat flow brought about by periodic interruption of heat flow will be small.

It should be emphasised that the analogue does not solve the partial differential equation (1) but only the finite-difference approximations to it, equations (9)–(16); which includes the boundary condition that the temperature at the hottest end of the bar is fixed i.e. $\Delta T_0 = 0$, equation (9). In practical cases the amplitude of temperature fluctuation within the rod will decay exponentially [6] with distance from the contact planes. At the lowest frequency investigated, 0·0145 Hz the amplitude at the hottest end of the bar would only amount to 2·2 per cent of that at the contact plane, thus approximating to the boundary condition closely.

Since a non-uniform division of the model Fig. 4(a) was employed it is difficult to estimate the error due to the finite-difference approximation. However, comparison of these results with some obtained using the division shown in Fig. 8 shows them to be in close agreement.

It is emphasised that the data obtained is applicable only to the case where both hot and cold members are of identical material and perfect contact and separation occurs at the plane of contact. Cases where the members are of different materials and where thermal contact resistance is present are being studied currently and will be dealt with in a later report.

Clearly the results suggest that in practical cases, at sufficiently high values of $(f\tau_c)$ and

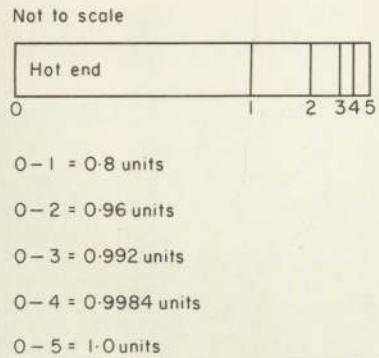

FIG. 8. Earlier division of model.

frequency thermal contact resistance at the contact plane will exert a more significant effect on heat flow than the periodic interruption at the contact plane.

ACKNOWLEDGEMENTS

The thanks of the authors are due to Dr. W. P. Mansfield, Director of Research, British Internal Combustion Engine Research Institute for suggesting the wider study currently being carried out by J. R. Howard and to Professor A. J. Ede, Head of the Department of Mechanical Engineering, University of Aston in Birmingham for his encouragement, help and, valuable criticism.

Finally we must express our gratitude to Dr. J. Barber of the Department of Mechanical Engineering, University of Newcastle upon Tyne for most painstaking and constructive criticism which led to the presentation of results in the present form.

REFERENCES

1. H. Y. WONG, A Survey of the thermal conductance of metallic contacts. Ministry of Technology Aeronautical Research Council Current Papers, C.P. No. 973. H.M.S.O. (1968).
2. H. ATKINS, Bibliography on thermal metallic contact conductance. N.A.S.A. Technical Memorandum TM X-53227. (15 April, 1965).
3. H. Y. WONG, Ph.D. Thesis No. 3011, University of Glasgow, Department of Aeronautics and Fluid Mechanics (1968).
4. H. GROBER, S. ERK and U. GRIGULL, *Fundamentals of Heat*, 3rd edn., pp. 133–136, equation 6.14. McGraw-Hill.
5. E. R. G. ECKERT and R. M. DRAKE, *Heat and Mass Transfer*, p. 106 Ex 4–7. McGraw-Hill, New York (1959).
6. E. R. G. ECKERT and R. M. DRAKE, *Heat and Mass Transfer* p. 102. McGraw-Hill, New York (1959).

APPENDIX

Consider Fig. 9, which shows the temperature distribution in the case where the hot and cold members are made of identical material of thermal conductivity k,

(i) their lengths are not equal

(ii) a thermal contact resistance $(1/h)$ exists at the plane of contact between hot and cold members. This introduces a discontinuity at the plane of contact.

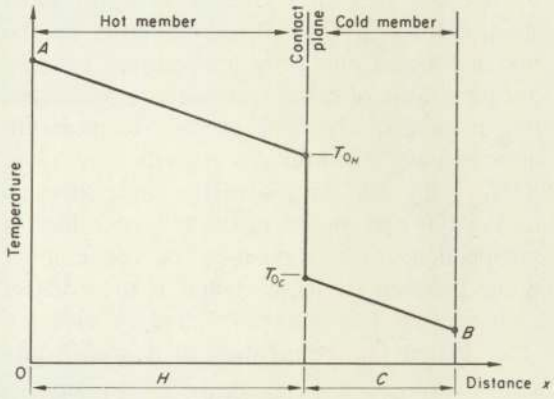

FIG. 9

(iii) the hot and cold members are permanently in contact.

Clearly the heat flux ϕ is given by

$$\phi = \frac{k(T_A - T_{0_H})}{H} = \frac{k(T_{0_C} - T_B)}{C} = h(T_{0_H} - T_{0_C}), \qquad (25)$$

which on eliminating T_{0_H} and T_{0_C} gives

$$\phi = \left\{\frac{T_A - T_B}{(1/k)(H + C) + (1/h)}\right\}. \qquad (26)$$

Thus, for given end temperatures T_A and T_B, overall length of the system $(H + C)$ and contact resistance $(1/h)$, the heat flux ϕ is independent of its position between the ends A and B.

Consider now the case where there is perfect thermal contact between the hot and cold

members when they are brought together and no heat transfer between the members when they are separated.

Figure 10 shows the temperature distribution when the members are meeting and parting at the plane of contact at a given frequency and ratio of contact time: periodic time ($f\tau_c$) and when quasi-steady conditions are reached.

The temperature in the immediate region of the plane of contact will vary with time but at some depth δ below the surface, the fluctuation of temperature will be negligible [5]. The shaded areas in Fig. 10 are bounded by the maximum and minimum temperature reached during a cycle of contact and separation of the two members. The time average temperature distribution however is given by line $ADT_{0_{Hav}}T_{0_{Cav}}EB$. This is of the same form as in Fig. 10 and hence again the heat flux is independent of the position of the contact plane between the ends A and B provided of course, that it is not positioned so close to A or B that the temperature at A and B fluctuates, thus invalidating our boundary condition of fixed temperatures at A and B. However, if we stipulated that the temperature at A and B were allowed to fluctuate but with a fixed time-average value, the heat flux ϕ would remain independent of the position of the contact plane over the entire distance between A and B.

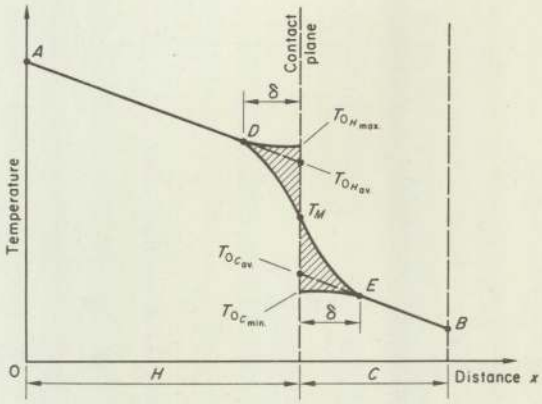

FIG. 10

ETUDE ANALOGIQUE DU TRANSPORT DE CHALEUR À TRAVERS DES SURFACES PÉRIODIQUEMENT EN CONTACT

Résumé—Un calculateur analogique a été employé pour déterminer l'effet de la fréquence et de la durée de contact par cycle sur le transport de chaleur à travers des surfaces qui se rejoignent et se séparent selon un cycle régulier. Les surfaces étaient constituées par des matériaux identiques et l'on a supposé que le contact et la séparation thermique étaient parfaits.

Les résultats montrent qu'à des fréquences élevées, le perte de vitesse de transfert de chaleur provenant de l'interruption du flux de chaleur, due à la séparation des surfaces, est faible et dépendant moins de la durée de contact par cycle qu'aux basses fréquences. La relation entre la diminution de la vitesse de transfert de chaleur, la fréquence et la durée de contact est montrée par une courbe unique.

EINE ANALOGIE-UNTERSUCHUNG DES WÄRMEDURCHGANGS DURCH PERIODISCH SICH BERÜHRENDE FLÄCHEN

Zusammenfassung—Mit Hilfe eines Analogrechners wurde der Einfluss von Frequenz und Dauer des Kontakts pro Periode auf den Wärmeübergang durch Flächen untersucht, die in regelmässiger Folge zusammengeführt und wieder getrennt werden.

Die Flächen waren aud gleichem Material, es wurde vollständiger thermischer Kontakt und vollständige Trennung vorausgesetzt.

Die Ergebnisse zeigen, dass bei hohen Frequenzen die Abnahme des Wärmeübergangs bei der Unterbrechnung des Wärmestroms durch Trennung der Flächen klein bleibt und die Kontaktdauer von geringerem Einfluss ist als bei kleinen Frequenzen. Der Zusammenhang zwischen Abnahme des Wärmeübergangs, Frequenz und Kontaktdauer wird durch eine einzige Kurve dargestellt.

АНАЛОГОВОЕ ИССЛЕДОВАНИЕ ТЕПЛООБМЕНА ЧЕРЕЗ ПЕРИОДИЧЕСКИ КОНТАКТНЫЕ ПОВЕРХНОСТИ

Аннотация—С помощью аналоговой вычислительной машины определялосъ влияние частоты и длительности контакта в течение цикла на перенос тепла через встречающиеся и расходящиеся в соответствии с релулярным циклом поверхности. Поверхности

изготовлены из идетичного материада и принято, что тепдовой контакт и разделение идеальные.

Результаты показывают, что при высоких частотах уменьшение теплового потока, возникающее из-за разделения поверхностей, невелико и меньше завсит от длительности контакта в течение цикла, чем при низких частотах. Соотношение между уменьшением теилового потока, частотой и длительностью контакта представлено одной кривой.

The Effect of Thermal Contact Resistance on Heat Transfer Between Periodically Contacting Surfaces

J. R. HOWARD[1] and A. E. SUTTON[2]

An analog-computer study is made of one-dimensional heat conduction through two bars whose axes are in line and whose adjacent ends make and break contact periodically. The work extends a previous study to take account of imperfect thermal contact at the contact interface. The effect of frequency and duration of contact are also discussed.

Nomenclature

f = frequency
$g(\ )$ = function of ( )
l = length of bar
l_i = length of bar material representing thermal resistance due to periodic interruptions of heat flow
Q = heat transfer rate (energy per unit time) under periodic contact conditions
Q_c = heat transfer rate (energy per unit time) under permanent contact conditions
t = time
T = temperature
x = distance
α = thermal diffusivity
λ = length of bar representing thermal contact resistance
τ_c = time surfaces are in contact per cycle
τ_0 = time surfaces are separated per cycle

Introduction

Heat transfer across the interface between two solids held permanently in contact has been the subject of much study. Various surveys of literature have been made [1–4],[3] and the subject continues to be studied.

The work in [5] described a one-dimensional heat transfer study along two identical bars whose axes are in line. The remote ends of the bars were at different, but fixed, temperatures and the adjacent ends were brought into contact and separated according to a continuous regular cycle. When the adjacent ends of the bars made contact, it was assumed that the thermal contact resistance was zero, and when they were separated there was no heat flow across the gap between the ends of the bars.

The foregoing work has been extended to examine the effect of finite thermal contact resistance at the interface when the bars make contact.

Formulation

An exact solution to the three-dimensional heat diffusion equation

$$\nabla^2 T = \frac{1}{\alpha}\frac{\partial T}{\partial t} \tag{1}$$

is not practical, due to the physical shape of the boundary at the contact interface and the numerous boundary conditions to be satisfied. Even when the surfaces are permanently in contact and the right-hand side of equation (1) is zero, e.g., see [6, 7], approximations had to be made.

An approximate representation is possible using the one-dimensional heat diffusion equation

$$\frac{\partial^2 T}{\partial l^2} = \frac{1}{\alpha}\frac{\partial T}{\partial t} \tag{2}$$

by assuming that during the period of contact the thermal contact resistance between the contact surfaces is due to a thin film whose thermal resistance is equal to the steady-state thermal contact resistance of the real surfaces. For simplicity, the heat capacity of the film is assumed to be negligible. A solution in the quasi-steady state is to be obtained.

Boundary and Initial Conditions. Since the bars are identical, events in only one bar, the hotter one, need be considered. The origin is taken at the hottest end of the bar, where the temperature is fixed at T_A. The temperature at the midpoint of the film is taken as zero, the length of bar as l, and half the thermal contact resistance equivalent to length λ of the bar material. The boundary conditions are then

1 at $x = 0$

$$T = T_A, \text{ at all times}$$

2(*a*) at $x = l$ during the contact period $0 < t < \tau_c$

$$\frac{\partial T}{\partial x} = -\frac{T}{\lambda}$$

2(*b*) at $x = l$ when the surfaces are separated $\tau_c < t < (\tau_0 + \tau_c)$

$$\frac{\partial T}{\partial x} = 0$$

Dimensional Analysis. The existence of an additional variable, namely thermal contact resistance characterised by a length λ of bar material, gives rise to a dimensionless group additional to the two quoted in [5]. If l_i is the length of bar material equivalent to the thermal resistance due to the periodic interruption of the heat flow, the groups become

$$\left(\frac{f l_i^2}{\alpha}\right) = g\left[(f\tau_c), \left(\frac{f\lambda^2}{\alpha}\right)\right] \tag{3}$$

for sufficiently large values of bar length l such that

$$\left(\frac{f l^2}{\alpha}\right) > 2.56\pi \tag{4}$$

see [5].

The inset at the top of Fig. 1 shows the time-average temperature distribution in the hotter bar when the surfaces are permanently in contact and when in the quasi steady state.

Simulation. Finite-difference approximations to the heat diffusion equation (2) and the boundary conditions were made, the mesh being identical to that used in [5]. The diagram of the circuit used will not be shown here as it differed from that described in [5] only at the section used to simulate the boundary condition at the contact interface.

Results and Discussion

The relationship between the dimensionless groups is shown plotted in Fig. 1, demonstrating the validity of equation (3).

Heat flow through the system may conveniently be expressed by the ratio Q/Q_c, where Q is the heat transfer rate under *periodic* contact conditions and Q_c is the heat transfer rate under *permanent* contact conditions with zero thermal contact resistance.

$$\frac{Q}{Q_c} = \frac{l}{l + \lambda + l_i} \tag{5}$$

Fig. 2, which is derived from equation (5) and Fig. 1 at a fixed frequency f and given diffusivity α, illustrates by example the importance of thermal contact resistance under periodic contact conditions.

[1] Department of Mechanical Engineering, University of Aston, Birmingham, England.
[2] Department of Mathematics, University of Aston, Birmingham, England.
[3] Numbers in brackets designate References at end of technical brief.

Contributed by the Heat Transfer Division of The American Society of Mechanical Engineers. Manuscript received by the Heat Transfer Division July 28, 1972.

A numerical method of solution shows extremely good agreement with these analog-computer results, showing that any errors due to the use of a nonuniform mesh for the finite-difference equations are small.

Conclusion

Thermal contact resistance between two periodically contacting surfaces can be the most significant factor in controlling the heat flow, particularly when the ratio of contact time/periodic time, $f\tau_c$, is high.

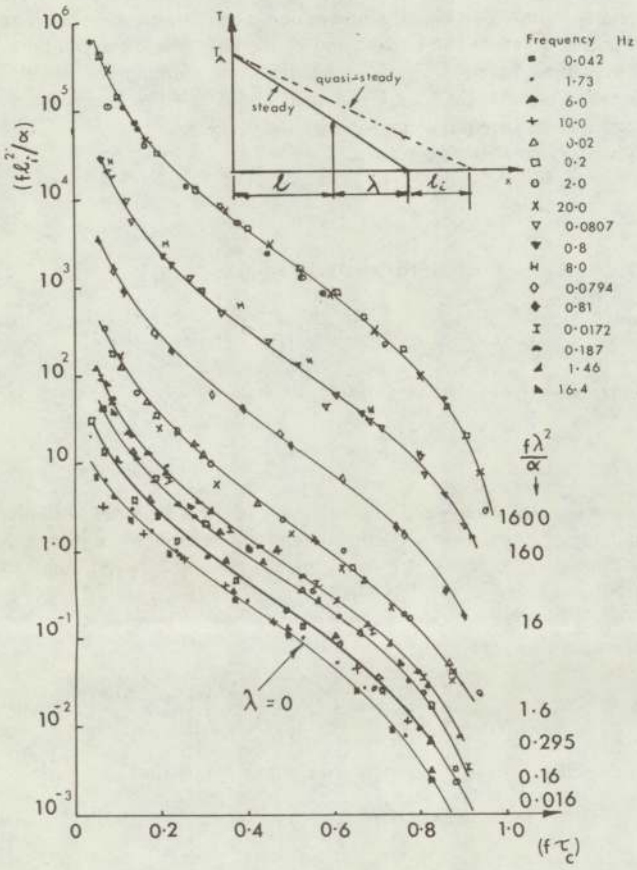

Fig. 1 Dimensionless plot of fl_i^2/α versus $f\tau_c$

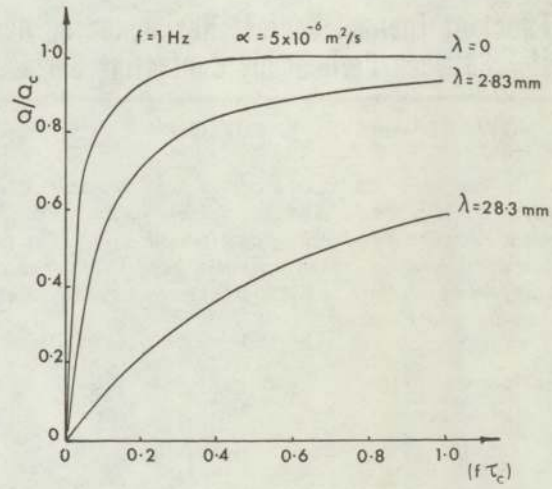

Fig. 2 Effect of contact time/periodic time on heat flow with various thermal contact resistances

Acknowledgments

We are grateful to our colleagues Prof. D. E. Elliott, N. Kerruish, and D. C. Hickson for their criticism and comments on this work.

References

1 Wong, H. Y., "A Survey of Thermal Conductance of Metallic Contacts," Ministry of Technology, Aeronautical Research Council Current Papers CP No. 973 HMSO, 1968.

2 Atkins, H., "Bibliography on Thermal Metallic Contact Conductance," NASA Technical Memorandum TMX-53227, Apr. 15, 1965.

3 Hseih, C. K., and Davis, F. E., "Bibliography on Thermal Contact Conductance," Purdue University Thermophysical Properties Research, AFML-TR-69-24, 1969.

4 Moore, C. J., Jr., Atkins, H., and Blum, H. A., "Subject Classification Bibliography for Thermal Contact Resistance Studies," ASME Paper No. 68-WA/HT-18.

5 Howard, J. R., and Sutton, A. E., "An Analogue Study of Heat Transfer Through Periodically Contacting Surfaces," *International Journal of Heat and Mass Transfer*, Vol. 13, 1970, pp. 173–183.

6 Fenech, H., and Rohsenow, W. M., "Prediction of Thermal Conductance of Metallic Surfaces in Contact," JOURNAL OF HEAT TRANSFER, TRANS. ASME, Series C, Vol. 85, No. 1, Feb. 1963, pp. 15–24.

7 Cetinkale, T. N., and Fishenden, M., "Thermal Conductance of Metallic Surfaces in Contact," General Discussion on Heat Transfer, *Proc. Inst. Mech. Engrs.*, London, Sept. 1951, pp. 271–275.

Reprinted from the August 1973
Journal of Heat Transfer

ADDENDUM

Solve

2. What do you understand by the concept 'thermal penetration coefficient? Evolve an expression for this parameter in terms of thermal conductivity, specific heat per unit volume and density. Why is a surface more comfortable to touch when its thermal penetration coefficient is small?

Dimensional analysis of the transient heat conduction equation suggests solutions in the usual nomenclature of the form

$$\frac{\theta}{\theta^*} = f\left(Fo, Bi, \frac{x}{\ell}\right)$$

Prove that when surface temperatures are specified the Biot number would not be present, that for a semi-infinite body the characteristic dimensionless ratio x/ℓ is inappropriate, and hence that $\frac{\theta}{\theta^*} = f\ (Fo)$ alone.

Using the substitution $\eta = \frac{1}{2\sqrt{Fo}}$ obtain a solution for the case of a sudden heating shock imposed upon the surface of a semi-infinite solid. Hence show that if the flat faces of two bodies (at temperatures T_1 and T_2) are brought together, the temperature of the interface becomes

$$\frac{T_1 \sqrt{k_1\ \rho_1\ c_{p1}} + T_2 \sqrt{k_2\ \rho_2\ c_{p2}}}{\sqrt{k_1\ \rho_1\ c_{p1}} + \sqrt{k_2\ \rho_2\ c_{p2}}}$$

where k, ρ and c_p have their usual meanings.

How would your analysis have to be modified due to the presence of roughness and curvature of the contacting surfaces?

The Gaussian error function,

$$G(z) = \frac{2}{\sqrt{\pi}} \int_0^z \exp\ (-z^2)\ dz$$

$$= \frac{2}{\sqrt{\pi}} \left(z - \frac{1}{1!}\ \frac{z^3}{3} + \frac{1}{2!}\ \frac{z^5}{5} - \frac{1}{3!}\ \frac{z^7}{7} + \ldots \right)$$

SOLUTION

Consider a semi-infinite solid see Fig. I initially at temperature T_i. Let the surface temperature at $x = 0$ be suddenly raised to temperature T_s, then it can be shown, see references (A,B) at the end of this addendum, that

$$\frac{T_s - T}{T_s - T_i} = \text{erf}\left\{\frac{1}{2\sqrt{Fo}}\right\} \qquad \text{(i)}$$

where Fourier number Fo is given by $\alpha t/x^2$.

The rate of heat passing through the surface at $x = 0$ is

$$\dot{Q} = -kA\left.\frac{\partial T}{\partial x}\right|_{x=0} = \frac{-kA}{2\sqrt{\alpha t}}(T_i - T_s)\frac{2}{\pi} \qquad \text{(ii)}$$

Thus the rate of penetration of the heat flow into the body at a given time t, for a given temperature difference $(T_i - T_s)$ depends on the value of $k/\sqrt{\alpha}$ $= \sqrt{k\rho c}$ for the body material. $k/\sqrt{\alpha}$ can be termed the "thermal penetration coefficient".

Conversely, if the above semi-infinite solid is heated at the surface $x = 0$ at steady rate $\dot{Q}$ then the temperature of the surface at $x = 0$ is given by

$$T_s - T_i = \frac{2\dot{Q}}{kA}\sqrt{\frac{\alpha t}{\pi}} \qquad \text{(iii)}$$

see reference (A page 256,). The temperature change of the surface at $x = 0$ at a given time t and heating rate $\dot{Q}$ is then dependent on the thermal penetration coefficient $k/\sqrt{\alpha}$. $= \sqrt{k\rho c}$

If the thermal penetration coefficient is small then, by equation (iii), the temperature change of the body will be high. Thus, if two bodies of dissimilar material at differing

temperatures T_1 and T_2 are brought into contact, the temperature at the contact interface will be given by (for proof see below)

$$\frac{T_2 - T_m}{T_m - T_1} = \frac{k_1}{\sqrt{\alpha_1}} \cdot \frac{\sqrt{\alpha_2}}{k_2} \qquad \text{(iv)}$$

this result explains the different sensation of warmth and coldness felt when touching objects of different materials at the same temperature. Since $k/\sqrt{\alpha}$ is much higher for metals than for wood, a piece of metal at, say, 288K, will feel colder to touch with the finger ~~at~~ of temperature 310K than a piece of wood at the same temperature 288K; in the case of wood, the interface temperature felt by the finger tip is closer to the finger temperature than when the finger touches the metal body.

Dimensional analysis of the transient heat conduction problem for a body of length l, of uniform initial temperature T_i, placed in an environment whose temperature is T_e suggests solutions of the form

$$\frac{T - T_e}{T_i - T_e} = f\left(Fo, Bi, \frac{x}{l}\right) \qquad \text{(v)}$$

where $Fo = \frac{\alpha t}{l^2}$, the Fourier number and $Bi = \frac{hl}{k}$, the Biot number with h = heat transfer coefficient between the surface of the body and the environment.

If the surface temperature were specified, the heat transfer coefficient h is irrelevant and the Biot number ceases to be a variable. For a semi-infinite body $l = \infty$ and x/l ceases to be a variable. Thus, when both the above conditions obtain, the Fourier number Fo will become $\alpha t/x^2$ and T_e will become the surface temperature T_s, so that

$$\frac{T - T_s}{T_i - T_s} = f\left(\frac{\alpha t}{x^2}\right) \qquad \text{(vi)}$$

Using the transformation

$$\eta = \frac{1}{2\sqrt{Fo}} = \frac{x}{2\sqrt{\alpha t}} \qquad \text{(vii)}$$

and

$$\frac{\theta}{\theta^*} = \frac{T - T_s}{T_i - T_s} \qquad \text{(viii)}$$

the heat diffusion equation

$$\frac{\partial T}{\partial t} = \alpha \frac{\partial^2 T}{\partial x^2} \qquad \text{(ix)}$$

becomes

$$\frac{d^2(\theta/\theta^*)}{d\eta^2} + 2\eta\frac{d(\theta/\theta^*)}{d\eta} = 0 \qquad \text{(x)}$$

The solution

$$\frac{\theta}{\theta^*} = \text{erf}\,(\eta) \qquad \text{(xi)}$$

satisfies the differential equation (x) and the boundary conditions which are

(a) $x = 0$ or $t = 0$, then $\eta = 0$ and $T = T_s$

(b) $t = 0$ or $x = \infty$, then $\eta = \infty$ and $T = T_i$

If two semi-infinite solids of differing materials having thermal conductivities k_1 and k_2 respectively and diffusivities α_1 and α_2 respectively and initial temperatures T_1 and T_2 respectively, are brought into perfect thermal contact with each other, then, referring to Fig. II, the contact interface at $x = 0$, will reach a common temperature T_m' instantaneously and the heat flux at the interface $x = 0$ in each body will be identical; hence

$$k_1 \left.\frac{\partial T_1}{\partial x_1}\right|_{x = 0} = -k_2 \left.\frac{\partial T_2}{\partial x_2}\right|_{x = 0} \qquad \text{(xii)}$$

Now

$$\left.\frac{\partial T}{\partial x}\right|_{x = 0} = \frac{\partial \eta}{\partial x} \cdot \frac{\partial T}{\partial \eta} = \frac{1}{2\sqrt{\alpha t}} \cdot \theta^* \cdot \frac{2}{\sqrt{\pi}} \qquad \text{(xiii)}$$

Hence

$$k_1 \, \theta_1^* \cdot \frac{1}{\sqrt{\pi \alpha_1 t}} = -k_2 \theta_2^* \frac{1}{\sqrt{\pi \alpha_2 t}} \qquad \text{(xiv)}$$

and since

$$\theta_1^* = T_1 - T_m' \qquad \text{(xv)}$$

and

$$\theta_2^* = T_2 - T_m' \qquad \text{(xvi)}$$

by substitution in equation (xiv) it follows that

$$\frac{T_1 - T_m'}{T_m' - T_2} = \frac{k_2}{\sqrt{\alpha_2}} \cdot \frac{\sqrt{\alpha_1}}{k_1} \qquad \text{(xvii)}$$

and since $\alpha = \frac{k}{\rho c}$

$$(T_1 - T_m) \; k_1 \rho_1 \; c_1 = (T_m - T_2) \; k_2 \rho_2 c_2 \qquad \text{(xviii)}$$

$$\therefore \; T_m = \frac{T_1 \sqrt{k_1 \rho_1 c_1} + T_2 \sqrt{k_2 \rho_2 c_2}}{\sqrt{k_1 \rho_1 c_1} + \sqrt{k_2 \rho_2 c_2}} \qquad \text{(xix)}$$

Thus, if the case where two bars of dissimilar materials are brought into periodic contact, the mean temperature of the interface would be as given by equation (xix).

Finally, if the surfaces in contact are rough or have curvature, the assumption of one-dimensional heat flow is invalid in the immediate neighbourhood of the contact interface and a solution of the heat diffusion equation in three dimensions would be required. An exact solution of this may not be practicable, however, for the boundary conditions involved. An approximate representation using the one-dimensional heat diffusion equation

is possible if a temperature drop $(T_{m_2} - T_{m_1})$ across the interface due to constriction of heat flow lines is assumed. Equation (xii) would then become

$$k_1 \frac{\partial T_1}{\partial x_1} = -k_2 \frac{\partial T_2}{\partial x_2} = h_c \left(T_{m_1} - T_{m_2}\right)$$

where h_c is the thermal contact conductance.

REFERENCES

(A) Jakob, Max. "Heat Transfer" Vol. I. Wiley, 1949, 253.

(B) Schneider, P.J. "Conduction Heat Transfer", Addison-Wesley, 1955, 240-242.

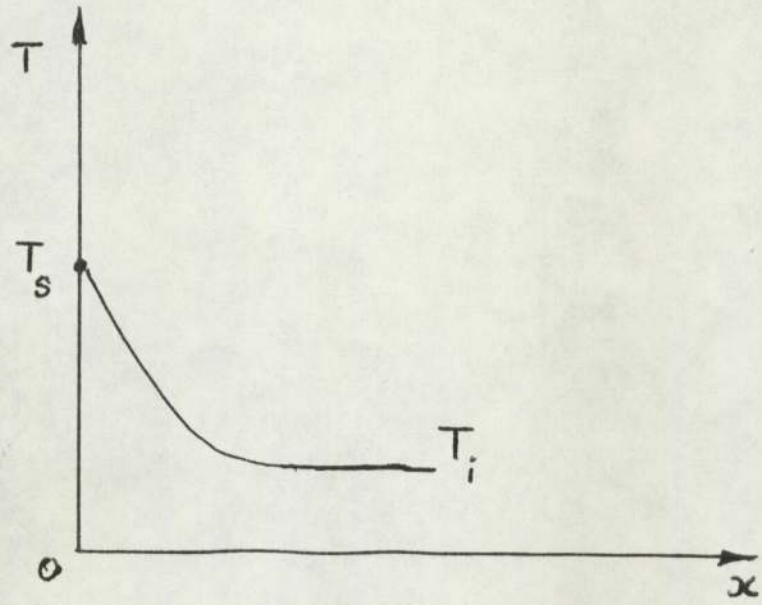

Fig I

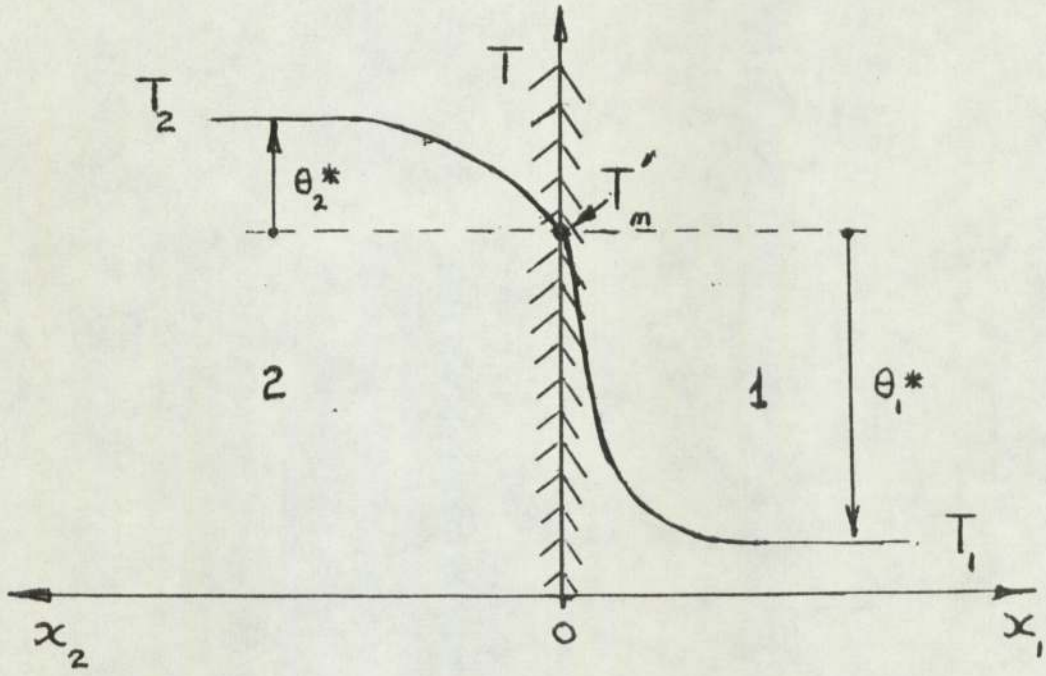

Fig II